UNIVERSIDAD DE GRANADA
INSTITUTO DE BIOTECNOLOGÍA

CONSEJO SUPERIOR DE INVESTIGACIONES CIENTÍFICAS

CHARACTERIZATION OF THE SPLICING REACTION OF THE *Sinorhizobium meliloti* RmInt1 GROUP II INTRON

ISABEL CHILLÓN GÁZQUEZ

TESIS DOCTORAL

2011

Editor: Editorial de la Universidad de Granada
Autor: Isabel Chillón Gázquez
D.L.: GR 4530-2011
ISBN: 978-84-694-6110-5

CHARACTERIZATION OF THE SPLICING REACTION OF THE *Sinorhizobium meliloti* RmInt1 GROUP II INTRON

Memoria que presenta la licenciada en Biología
Dña. Isabel Chillón Gázquez
como aspirante al grado de Doctor

Fdo: **Isabel Chillón Gázquez**

VºBº de los Directores de la Tesis Doctoral

Fdo: Dr. Nicolás Toro García
Doctor en Ciencias Biológicas
Profesor de Investigación del CSIC

Fdo: Dr. Francisco Martínez-Abarca Pastor
Doctor en Ciencias Biológicas
Investigador Científico del CSIC

Universidad de Granada
2011

Este trabajo de Tesis Doctoral ha sido realizado en el Departamento de Microbiología y Sistemas Simbióticos (Grupo de Ecología Genética de la Rizosfera) de la Estación Experimental del Zaidín (CSIC-Granada).

Para la realización del siguiente trabajo, la Lda. Isabel Chillón Gázquez fue financiada mediante las siguientes fuentes:

- Beca predoctoral I3P-CSIC-2006, de enero de 2007 a diciembre de 2010.
- Beca de movilidad para estancias breves del CSIC, disfrutada en el Departamento de Biofísica y Bioquímica Molecular de la Universidad de Yale (USA), bajo la dirección de la Profesora Anna Marie Pyle. Periodo: Abril-Junio 2010.

Parte de los resultados presentados en esta Tesis Doctoral han sido publicados en revistas internacionales o están en preparación:

Chillón I, Martínez-Abarca F and Toro N (2011) Splicing of the *Sinorhizobium meliloti* RmInt1 group II intron provides evidence of retroelement behavior. *Nucleic Acids Res* 39(3):1095-1104

Barrientos-Duran A, Chillon I, Martinez-Abarca F and Toro N (2011) Exon sequence requirements for excision *in vivo* of the bacterial group II intron RmInt1. *BMC Mol Biol* 12(1):24.

Chillón I, Fedorova O, Martínez-Abarca F, Pyle AM and Toro N (2011) *In vivo* and *in vitro* characterization of the splicing of RmInt1 group II intron. Implications of tertiary interactions in the ribozyme for the maintenance of the catalytic properties (In preparation).

Abstract

Group II introns are both auto-catalytic RNAs and retrotransposable elements. They were initially found in organellar genomes, and later in bacterial and archaeal genomes. Several data suggest that they are the ancestors of eukaryotic spliceosomal introns. They consist of a catalytically active intron RNA (ribozyme) and an optional intron-encoded protein (IEP), which assists the intron in the splicing and mobility processes. The secondary structure of the ribozyme consists of six helical domains radiating from a central wheel, which in turn interact to each other creating a complex tertiary networking. Group II introns are spliced via a lariat o linear intermediate, and can retrohome in cognate intronless target sites they recognized through base pairing.

RmInt1 is an efficient mobile intron found within the IS*Rm2011-2* insertion sequence in the symbiotic bacterium *Sinorhizobium meliloti*. This group II intron is excised, *in vivo* and *in vitro*, as both intron lariats and putative intron circles. However, until date, the complete splicing reaction *in vivo* remains to be elucidated. A *lac*Z reporter gene system, northern blotting and real-time reverse transcription were carried out to investigate RmInt1 splicing activity (Chapter 1 and 2). Splicing efficiency of 0.07 ± 0.02 % was recorded. These findings suggest that bacterial group II introns function more like retroelements than spliceosomal introns.

Previous studies on the *in vitro* self-splicing of RmInt1 intron showed an inefficient reaction characterized by the formation of unconventional side products. By testing different RmInt1-transcritp contexts and reaction conditions, we obtained a RmInt1-construction by eliminating an IBS1-like sequence present in the first 10 or 11 nucleotides of the 3' exon from the natural target IS*2011-2* insertion sequence (Chapter 4). The new construct prevented the formation of unusual truncated side products previously observed, producing an increment of the amplitude of the reaction.

Finally, we analyzed the effect of point mutations in conserved positions of the ribozyme of RmInt1 on the efficiency of first and second splicing steps *in vivo* and *in vitro* (Chapter 3 and 4). We identified the occurrence of tertiary interactions common to other group IIB introns, such as the γ-γ', EBS3-IBS3 and the non Watson-Crick interaction between first and penultimate nucleotides of the intron. In addition, we proved the existence of structural motifs conserved in group II introns as the triplex between domain

V and the nucleotides within the linker region J2/3. Mutations disrupting interaction between components of this motif resulted in the alteration of both steps of splicing *in vivo* and *in vitro*, which supports the occurrence of a unique active site catalyzing both steps of the splicing reaction.

Resumen

Los intrones del grupo II son ARNs autocatalíticos y elementos retrotransponibles. Fueron descubiertos inicialmente en los genomas de orgánulos, y más tarde en genomas bacterianos y de arqueas. Según diversos datos, se ha sugerido que podrían ser los antecesores de los intrones espliceosómicos eucarióticos. Constan de un componente de ARN que es activo catalíticamente (ribozima) y de una proteína codificada por el intrón (del inglés *I*ntron-*E*ncoded *P*rotein, IEP) que es opcional y asiste al intrón en los procesos de *splicing* y movilidad. La estructura secundaria de la ribozima consiste en seis dominios helicoidales que radian de una estructura central, y que contactan entre sí dando lugar a una compleja red de interacciones terciarias. Los intrones del grupo II se escinden mediante un intermediario en forma de lazo (*lariat*) o lineal, y pueden retrotransponerse (*retrohoming* o *homing)* en dianas apropiadas libres de intrón que son reconocidas mediante apareamiento de bases.

RmInt1 es un intrón móvil eficiente encontrado en el interior de la secuencia de inserción IS*Rm2011-2* de la bacteria simbiótica *Sinorhizobium meliloti*. Este intrón del grupo II se escinde, *in vivo* e *in vitro*, en forma de lazos y de círculos. Sin embargo, hasta la fecha, no se ha dilucidado el proceso completo de *splicing in vivo*. Con el fin de determinar la eficiencia del *splicing* de RmInt1, se elaboró un sistema informador basado en el gen *lac*Z y se realizaron ensayos de *Northern Blotting* y PCR cuantitativa (Capítulos 1 y 2). La eficiencia de *splicing* fue calculada en 0.07 ± 0.02 %. Estos resultados sugieren que los intrones bacterianos del grupo II funcionan de un modo más parecido a los retroelementos que a los intrones espliceosómicos.

Estudios previos sobre la reacción de *self-splicing* de RmInt1 mostraron que esta reacción, caracterizada por la aparición de co-productos no convencionales, es ineficiente. Mediante el análisis de diferentes transcritos de RmInt1 en diversos contextos y distintas condiciones de reacción, obtuvimos una construcción en la que se eliminó una secuencia parecida a IBS1 presente en los primeros 10 u 11 nucleótidos del exón 3' de la diana natural localizada en la secuencia de inserción IS*2011-2* (Capítulo 4). Esta nueva construcción soslayó la formación de productos truncados e inusuales observados previamente, lo que se tradujo en un incremento de la amplitud de la reacción.

Finalmente, analizamos los efectos de diversas mutaciones puntuales en posiciones conservadas de la ribozima de RmInt1 sobre la eficiencia del primer y segundo paso de la

reacción de *splicing in vivo* e *in vitro* (Capítulos 3 y 4). Así, identificamos la existencia de interacciones terciarias comunes a otros intrones del grupo II, tales como γ-γ', EBS3-IBS3 y la interacción no Watson-Crick entre el primer y el penúltimo nucleótidos del intrón. Además, probamos la existencia de motivos estructurales conservados en los intrones de grupo II como la triple hélice entre el dominio V y los nucleótidos de la región interdominios J2/3. Las mutaciones que interrumpen la interacción entre componentes de este motivo resultaron en la alteración de ambos pasos de la reacción de *splicing in vivo* e *in vitro*, lo que apoya la existencia de un único sitio activo que cataliza ambos pasos de la reacción de *splicing*.

Table of contents

Results

Chapter 1: Design of a reporter system for the quantification of exon ligation during the *in vivo* splicing of RmInt1 intron

Chapter 2: *In vivo* quantification of the *S.meliloti* RmInt1 group II intron splicing. Comparison with the *L.lactis* Ll.ltrB group IIA intron expressed in *E.coli*

Chapter 3: Effect of point mutations in conserved positions of the RmInt1 group II intron on the splicing reaction *in vivo*

List of figures

Introduction

Materials and Methods

Results

Chapter 1: Design of a reporter system for the quantification of exon ligation during the *in vivo* splicing of RmInt1 intron

Chapter 2: *In vivo* quantification of the *S.meliloti* RmInt1 group II intron splicing. Comparison with the *L.lactis* Ll.ltrB group IIA intron expressed in *E.coli*

Chapter 3: Effect of point mutations in conserved positions of the RmInt1 group II intron on the splicing reaction *in vivo*

Chapter 4: Self-splicing of RmInt1 group II intron: a qualitative, quantitative and mutational analysis

List of tables

Materials and Methods

Results

Chapter 2: *In vivo* quantification of the *S.meliloti* RmInt1 group II intron splicing. Comparison with the *L.lactis* Ll.ltrB group IIA intron expressed in *E.coli*

Chapter 3: Effect of point mutations in conserved positions of the RmInt1 group II intron on the splicing reaction *in vivo*

Chapter 4: Self-splicing of RmInt1 group II intron: a qualitative, quantitative and mutational analysis

INTRODUCTION

I.1 GENERAL FEATURES

Group II introns are one of the seven classes of natural ribozymes described to date (RNA molecules with catalytic activity), some of them showing capacity for self-splicing in the form of lariat RNA molecules (Peebles *et al.*, 1986) [for a review, see (Lehmann and Schmidt, 2003)]. They are also retroelements that encode reverse transcriptases (RTs) and can insert themselves into new localizations (Robart and Zimmerly, 2005). For these reasons, group II introns are thought to be the ancestors of nuclear spliceosomal introns and non-Long Terminal Repeat (LTR) retrotransposons (Sharp, 1985; Cech, 1986; Sharp, 1991; Cavalier-Smith, 2009; Koonin, 2009).

The concept of group II intron was created in 1982, when the sequences of several fugal mitochondrial introns were arranged into two unrelated families (Michel *et al.*, 1982). Until 1993, group II introns had been found only in precursor transcripts of essential organellar intron, encoding proteins, transfer RNAs or ribosomal RNAs (Michel *et al.*, 2009). Nevertheless, group II introns were then found in Cyanobacteria and Proteobacteria, two groups containing members considered to be the ancestors of chloroplasts and mitochondria, respectively (Ferat and Michel, 1993) and, subsequently, they were also described in Archeobacteria (Dai and Zimmerly, 2003).

Typically, group II introns consist of a conserved RNA structure and a RT ORF (optional). The RNA structure is organized in six domains, of which domain V is considered an essential part of the catalytic core (Pyle, 2010). The protein is commonly encoded in domain IV and forms RNP (ribonucleoprotein) particles with the RNA, serving as a splicing and mobility factor for the invasion of new DNA target sequences (Lambowitz and Zimmerly, 2010). These properties made group II introns suitable as biotechnological tools in which a group II intron is retargeted to insert into desired DNA by modifying the base pairing sequences in the intron RNA (Guo *et al.*, 2000; Zhuang *et al.*, 2009a). Finally, the RmInt1 intron, which deserves a special attention for being the subject of this work, is a IIB3 member of group II introns, found in the genome of the bacterium *Sinorhizobium meliloti* (Martínez-Abarca *et al.*, 1998), characterized by a low efficiency splicing but however a high mobility frequency.

I.2 STRUCTURAL ELEMENTS OF GROUP II INTRON RNA

Group II introns are characterized by a conserved secondary structure which varies in size from 100 nt up to about 3000 nt (Lehmann and Schmidt, 2003). The first model was established on the basis of a phylogenetic data comparison, looking for potential base pairings that had been preserved by evolution in spite of divergence in primary sequence (Michel *et al.*, 1982; Michel *et al.*, 1989). In fact, the only strongly conserved sequences are intron boundaries (GUGYG in the 5' exon junction and AY in the 3' counterpart), resembling those of spliceosomal introns (GU…AG) and few nucleotides dispersed in the rest of the structure (Michel and Ferat, 1995).

It is organized in six domains, DI-DVI, radiating from a central core. The structure is defined as a set of double helices resulted from Watson-Crick and Crick Wobble base pairs (Dunny and McKay, 1999; Lambowitz and Zimmerly, 2004) (Figure I1). According to differences in the RNA structure, three subclasses of group II introns: IIA, IIB and IIC, and further subdivisions: A1, A2, B1, B2 and B3 have been defined (See below) (Michel *et al.*, 1989; Toor *et al.*, 2001). The six domains fold into a catalytically active tertiary structure aided by a series of conserved motifs involved in long-range tertiary interactions. Some interactions involve Watson-Crick base pairs (α-α', β-β', γ-γ', δ-δ', ε-ε', IBS1-EBS1, IBS2-

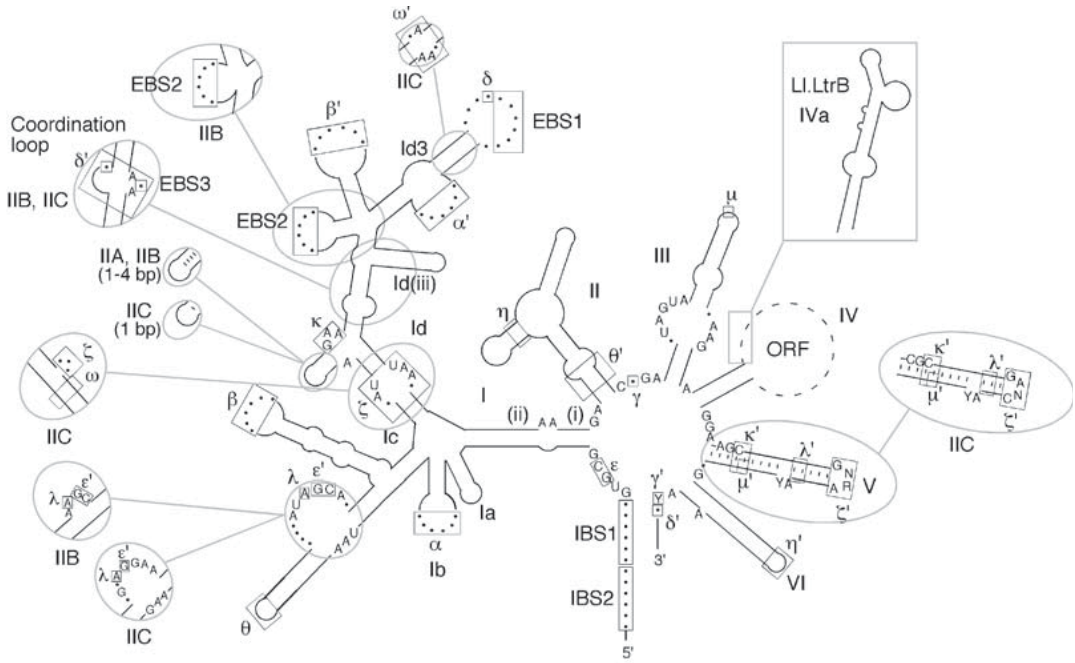

Figure I1. Group II intron RNA structure. The schematic structure of a IIA1 group II intron, with differences from IIB and IIC subgroups shown in circles. Tertiary interactions (Greek letters, EBSs and IBSs) are indicated in boxes. Adapted from Lambowitz and Zimmerly (2010).

EBS2 and IBS3-EBS3), whereas other are tetraloop-receptor interactions of known geometries (ζ-ζ', η-η' and θ-θ'), or other types of less defined non-Watson-Crick interactions (λ-λ', κ-κ' and μ-μ') (Dai *et al.*, 2008; Pyle, 2010).

Domain I (DI) is the largest domain and it is essential for catalysis, along with domain V (DV) (Fedorova and Zingler, 2007). Four conserved interactions linking DI with catalytic important sequences have been described (Figure I1): ζ-ζ' (Costa and Michel, 1995) and κ-κ' (Boudvillain and Pyle, 1998), which anchors DV binding face into the DI scaffold, so that orienting the latter properly in the active site and; ε-ε' (Jacquier and Michel, 1987) and λ-λ' (Boudvillain *et al.*, 2000), which form together a composite interaction involving DI, the 5'-splice site and the chemical face of DV, close to the catalytic triad, a critical trinucleotide for catalysis in group II introns. DI also establishes contacts with DII and DIII by means of θ-θ' (Costa *et al.*, 1997). Domain I is also indispensable for exonic substrate recognition. In classes IIA and IIB of group II introns, the tertiary interaction aimed to join the secondary structure of the intron with the 5'-splicin junction is mediated by the base-pairing between the two exon-binding sites 1 and 2 (EBS1 and EBS2), located in two distinct regions in the DI, and the two corresponding intron-binding sites 1 and 2 (IBS1-IBS2), located in the extremity of the 5'-exon, adjacent to each other (Figure I1) (Qin and Pyle, 1998). However, in class IIC introns, usually there is no EBS2/IBS2 interaction, instead recognizing an upstream transcriptional terminator motif important for the 5'-splice site definition (Fedorova and Zingler, 2007). The recognition of the 3'-splice site is mediated by an EBS3/IBS3 interaction in IIB and IIC subclasses, whereas a δ-δ' interaction is the counterpart for IIA introns (Costa *et al.*, 2000). Other internal tertiary interactions localized in DI, which are essential for the correct folding and stability of the intron are the α-α' interaction (Michel *et al.*, 1989), the less important β-β' interaction (Michel and Ferat, 1995) and the δ-δ' interaction for members of the class IIB introns, which facilitates the anchor of DI to the 5'-splice site and to the branching A sited in DVI, through the "coordination loop" (Figure I1) (Hamill and Pyle, 2006).

Domain II (DII) forms two essential long-range tertiary contacts with DI (θ-θ') (Costa *et al.*, 1997) and with DVI (η-η') (Chanfreau and Jacquier, 1996) (Figure I1). The η-η' interaction has been proposed to mediate a rearrangement of DVI between the first and the second splicing step aimed to approximate both ends of the intron and so intervening in the second splicing step efficiency(Lehmann and Schmidt, 2003). To the contrary, the θ-θ' interaction seems to be important for an efficient folding of the group II intron ribozyme molecule prior to the initiation of the self-splicing reaction (Costa *et al.*, 1997).

The linker region between DII and DIII, also known as J2/3, contains important positions for group II intron catalysis, especially the G588 and A589 (in the mitochondrial ai5γ intron of yeasts) proposed to be important in both the first and the second step of splicing (Chanfreau and Jacquier, 1996; Mikheeva *et al.*, 2000) and; the G587, which interacts with the last nucleotide of the intron by means the γ-γ' (Michel *et al.*, 1989). These positions have been also shown to be close to the active site during catalysis (de Lencastre *et al.*, 2005; de Lencastre and Pyle, 2008).

Domain III (DIII) is considered to function as a catalytic effector, since it enhances the chemical rate of group II-derived ribozyme constructs (Qin and Pyle, 1998; Fedorova and Zingler, 2007). DIII establishes a tertiary interaction with DV, the μ-μ' (Fedorova and Pyle, 2005) whereas the A-rich bulge in DIII also interacts, and potentially stabilizes the ε-ε' motif, bringing it closer to DV (Fedorova and Pyle, 2008).

Domain IV (DIV) is the region, in some group II introns, where it is located an open reading frame (ORF). Proteins codified by ORFs, also known as intron-encoded proteins (IEP), assist the intron during the folding and splicing *in vivo* due to its maturase activity and permit the invasion of DNA by its retrotransposase (RT) activity (Fedorova and Zingler, 2007). DIV also contains the primary binding site for these proteins (Wank *et al.*, 1999) and for other host-encoded splicing factor factors (Ostersetzer *et al.*, 2005; Fedorova and Zingler, 2007).

Domain V (DV) is, together with DI, absolutely required for catalysis in group II introns. It is divided in a "binding site", serving as a docking for other components of the intron interacting with DV and; a "chemical side", in which it is located the catalytic functionalities (Fedorova and Zingler, 2007). Interactions involving the binding site are the above described ζ-ζ' and κ-κ' whereas interactions involving the chemical face are the also mentioned λ-λ' and μ-μ'. It contains the catalytic triad, AGC, in the base of DV, in which G is an invariant residue critical for both *in vivo* and *in vitro* splicing (Koch *et al.*, 1992; Boulanger *et al.*, 1995; Peebles *et al.*, 1995). Another important catalytic motif is the bulge AC of DV. It has shown that the bulge AC establishes tertiary contacts with a conserve G (G588 in ai5γ intron) in the linker region J2/3 and with the fifth nucleotide of the intron (λ position), bring them together during catalysis (de Lencastre *et al.*, 2005; de Lencastre and Pyle, 2008; Michel *et al.*, 2009). It is also known that the AC bulge binds two metal ions within the core, which includes one with the AGC triad and another with the G288 (in the ai5γ intron) of J2/3, forming a metal ion binding platform that participates directly in chemical catalysis (Pyle, 2002; Toor *et al.*, 2009). The metal binding site is supported by a triple helical structure that results from binding of the conserved J2/3 region to an

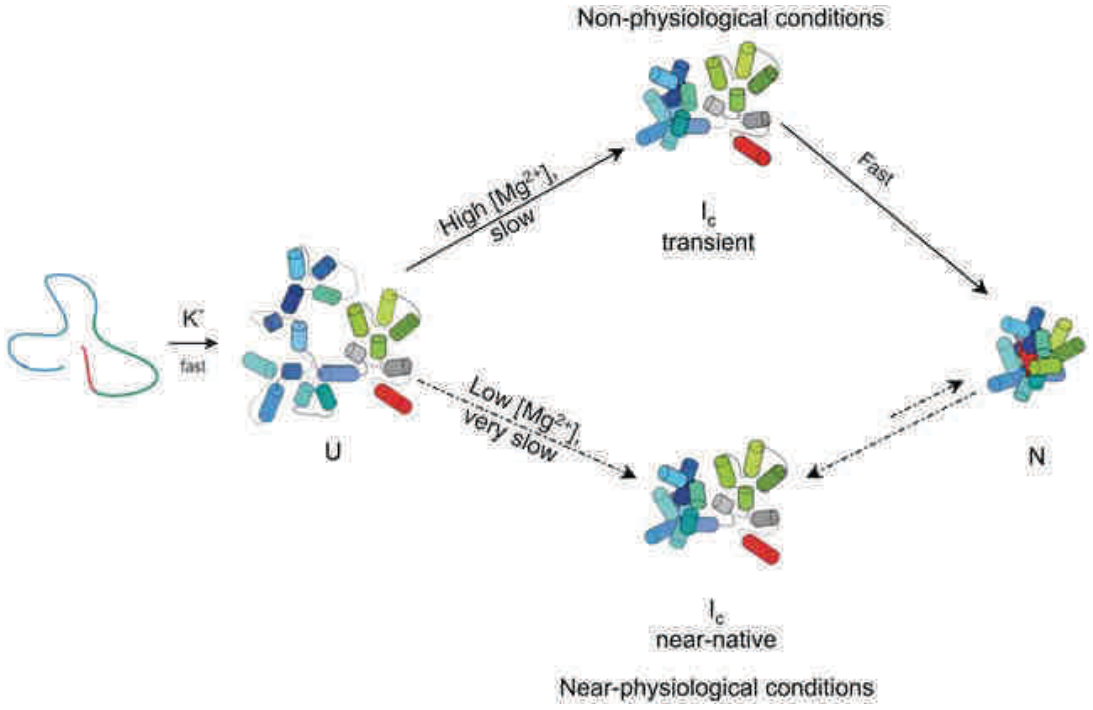

Figure I2. Folding pathways of ribozymes derived from the ai5γ group II intron under high-salt (top) and near-physiological (bottom) conditions. Adapted from Fedorova and Zingler (2007).

invariant region within the major groove of the DV lower stem (Keating *et al.*, 2010; Pyle, 2010).

Domain VI (DVI) contains a highly conserved bulged adenosine, which constitutes the branch point for lariat formation during splicing (Qin and Pyle, 1998). Other structural constraints determining the bulging point are the G-U wobble pairs flanking the bulged A, the length of the linker region between DV and DVI and the 4 bp basal stem of DVI (Qin and Pyle, 1998; Chu *et al.*, 2001; Fedorova and Zingler, 2007). DVI also takes part of the long-range interaction η-η', mentioned above, between the terminal loop of DVI and an internal helix of DII, reported to be important for transesterification at the 3'-splice site (Lehmann and Schmidt, 2003).

The six domains of group II introns need to fold into a correct native conformation in order to carry out the catalytic activity (Fedorova and Zingler, 2007). It has shown that this process occur *in vitro* through an apparent two-step mechanism, in which the folding of DI is a rate-limiting step and it constitutes an on-pathway intermediate (Swisher *et al.*, 2002; Su *et al.*, 2005; Waldsich and Pyle, 2008)(Figure I2) Once D1 has folded, catalytic Domains 3, 5 and 6 rapidly dock into respective receptor sites within the D1 scaffold, thereby completing the assembly of the intron (Pyle *et al.*, 2007).

Under near-physiological conditions (30 ºC and low Mg^{2+} concentration) a slow compact on-pathway folding intermediate (the near-native state) is formed(Fedorova *et al.*, 2007). Thus, the change to native state and the stabilization of the structure is achieved by the increment of Mg^{2+} concentration or the addition of a protein co-factor both *in vitro* (Dai *et al.*, 2008; Fedorova *et al.*, 2010) and *in vivo* (Liebeg *et al.*, 2010)(Figure I2).

Once the intron has folded up, the DV is found between the two halves of DI, joining them together by α-α' and β-β' tertiary interactions on one side, and with the DV, through the κ-κ' and ζ-ζ', on the other side (Dai *et al.*, 2008) (Figure I3). DIII is internalized, with contacts to DV and both halves of DI. The catalytic face of DV is oriented inward, where it interacts with the catalytically important elements J2/3, γ-γ', ε-ε' and the branch A. While the exon 5' binds EBS1 and EBS2 in the surface of the ribozyme, the exon junction penetrates internally into the active site (Dai *et al.*, 2008).

Group II introns show several types of structural variations. In organellar introns, it is frequently found degenerate introns, which show mispairs, insertions and deletions in DV and DVI or the absence of the bulged A (Lambowitz and Zimmerly, 2004). It is thought that the splicing of these introns require *trans*-acting RNAs or adjuvant proteins supplying the absence of RNA structures (Lambowitz and Zimmerly, 2004). Twintrons are

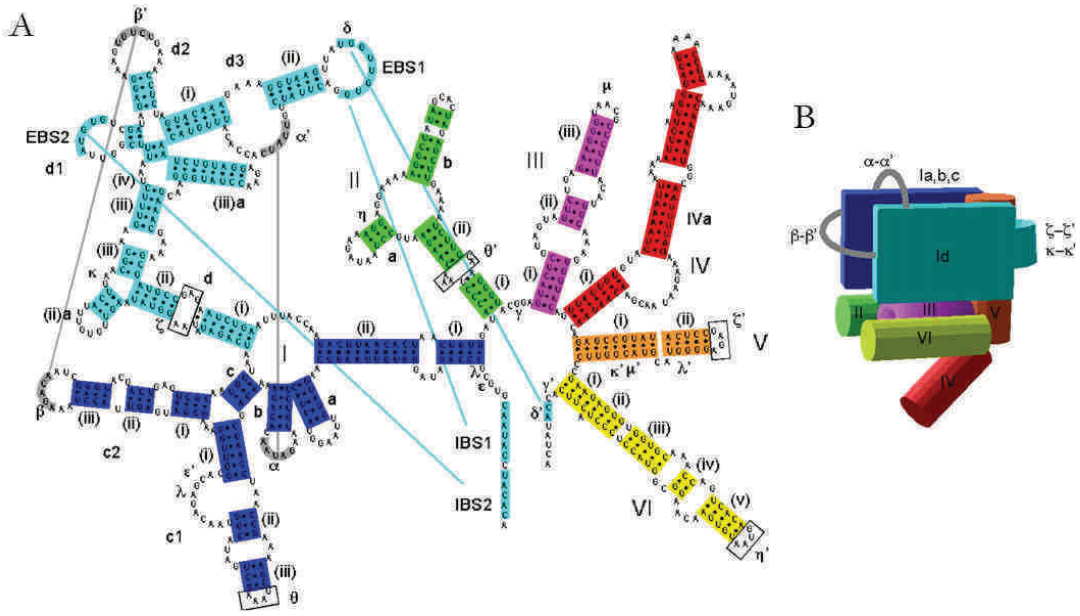

Figure I3. Three-dimensional model of Ll.ltrB-ΔORF Lariat RNA and Ligated exons. **A** Schematic of the secondary structure of the Ll.ltrB intron highlighting important tertiary interactions for the compaction of the intron structure. **B** Three-dimensional diagram of intron domains after folding of Ll.ltrB intron. Domains are colored as in A. Adapted from Dai *et al* (2008).

structures in which one intron has inserted into another; thus, if the outer intron interrupts essential structures of the inner intron, the former must be spliced first (Lambowitz and Zimmerly, 2010). *Trans*-splicing group II introns occurs when an intron has been split into two or more separate segments which must reassociate via tertiary interactions between domains in order to splice (Lambowitz and Zimmerly, 2010).

I.3 INTRON-ENCODED PROTEINS (IEPs) AND INTRON-RECRUITED MATURASES

Intron-encoded proteins (IEPs) are those proteins that have been acquired by introns, assisting them during its *in vivo* activity. They are about 2 kb in size and are, generally, encoded within intron DIV, outside the catalytic core (Lehmann and Schmidt, 2003). Functions associated with IEPs include RNA folding, acting as maturases that help the intron fold into a catalytically active structure; *in vivo* splicing, by stabilizing the active

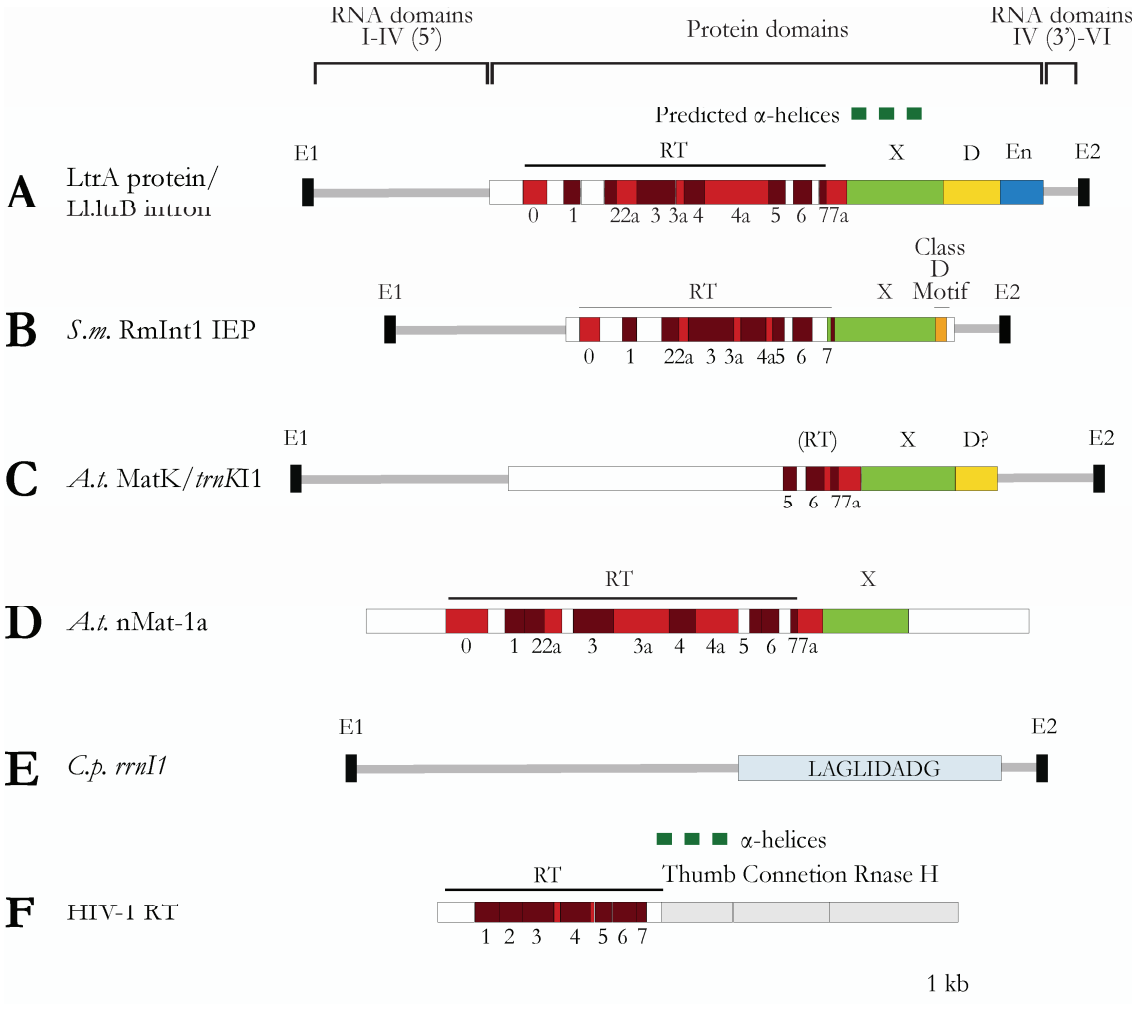

Figure I4. IEPs, host-encoded proteins and retrotransposons. **A** LtrA protein encoded by the *Lactococcus lactis* intron. **B** IEP encoded by the *Sinorhizobium meliloti* RmInt1 intron, which lacks the En domain. The "class D motif" is a conserved sequence that is required for splicing and mobility functions in lineage D IEPs. **C** Matk protein encoded by the *Arabidopsis thaliana trnK*I1intron. This protein only retains block RT5-RT7 of the RT domain and lack the En domain. **D** nMat-1a protein encoded by a nuclear gene in *Arabidopsis thaliana*. nMat-1 protein contains complete RT and X domains, but have mutations expected to inhibit RT activity. **E** LAGLIDADG protein encoded by *Cryphonectria parasititca rrn*I1 intron, which belongs to a familia of endonucleases typical of group I introns. **F** HIV-1 RT. Insertions between RT sequence block are denoted 2a, 3a, 4a and 7a. The locations of the predicted α-helices of characteristic thumb domains are shown above domain X. Adapted from Lambowitz and Zimmerly (2010).

structure and; retrohoming and retrotransposition through target-primed reverse transcription to insert introns into new DNA target genes (Fedorova and Zingler, 2007). All characterized IEPs are intron-specific factors, although closely related IEP's may have some cross-reactivity (Lambowitz and Zimmerly, 2004).

Group II intron IEPs consist of several domains: RT, reverse transcriptase; X, maturase; D, DNA binding and; En, endonuclease (Figure I4). The RT domain is comprised of seven conserved blocks common to all retroelements, which correspond to the palm and finger regions of the HIV-RT (Figure I4, F) (Lehmann and Schmidt, 2003). The RT5 contains the highly conserved sequence YADD, which is part of the RT active site (Lambowitz and Zimmerly, 2010). Moreover, group II introns and non-LTR-retrotransposons also harbor an amino-terminal extension (RT0) and insertions (Figure I4 A, light red blocks) between the RT sequence subdomains (Lambowitz and Zimmerly, 2010). The domain X is also known as "maturase" due to its essential role in the folding and splicing of the intron ribozyme. It is analogous to the thumb motif of HIV-RT, comprised of conserve sequences and three α-helices (Lambowitz and Zimmerly, 2010). Many IEPs, especially those of organellar intron, have lost some RT blocks required for retrotransposase activity, as that of *Arabidopsis thaliana trnK*I1 intron (Figure I4 C) or have accumulate mutations that also impair the RT activity, as the nuclear-encoded nMat proteins (Figure I4 D), both continuing to function in RNA splicing (Bonen and Vogel, 2001). The C-terminal region of IEPs is comprised of domains D and En. D is a DNA binding domain, characterized by the presence of a pair of cysteine residues which are part of a major class of zinc fingers and have been also proposed to play a critical role in maintaining the structure of the En domain, while a short region upstream would be responsible for DNA-binding (San Filippo and Lambowitz, 2002). The endonuclease domain (En) cleaves a target DNA strand to generate the primer for reverse transcription

(Lambowitz *et al.*, 2005; Marcaida *et al.*, 2010). It usually belongs to the H-N-H family, which contains a tight bound Mg^{2+} ion (San Filippo and Lambowitz, 2002). However, some fungal mitochondrial group II introns encode IEPs belonging to a family of DNA endonucleases with the conserved motif LAGLIDADG, typical of group I introns (Figure I4 E) (Toor and Zimmerly, 2002; Mullineux *et al.*, 2010). Many group II introns, particularly in bacteria, encode proteins lacking the En domain, and at least some are mobile, using alternate mechanisms for priming reverse transcription, as the RmInt1 intron of *Sinorhizobium meliloti* (Figure I4, B) (see above).

The IEP interacts with the intron RNA, producing ribonucleoprotein (RNP) particles. This interaction begins when the IEP binds unspliced precursor RNA, promoting its folding and splicing by stabilizing the catalytically active RNA structure (Lambowitz and Zimmerly, 2004). It is known, from studies on the bacterial LtrA protein coded in the Ll.ltrB intron form *Lactococcus lactis* that the IEP binds the intron in the form of a dimer, similar to HIV-1 and other RTs (Saldanha *et al.*, 1999; Rambo and Doudna, 2004). The IEP has a high-affinity binding site in the intron subdomain DVIa, a small stem-loop structure at the beginning of DIV that contains the Shine–Dalgarno (SD) and initiation codon at the beginning of the LtrA ORF (Figure I1), and makes additional contacts with conserved catalytic core regions, including parts of DI, DII, and DVI, which stabilize the active RNA structure (Lambowitz *et al.*, 2005). In the IEP, two regions have been identified to be required for the binding to the intron RNA: one corresponding to the N-terminal extension up to RT-0, which specifically binds the DIVa region and, a second, extending from RT-0 to RT-2 (Gu *et al.*, 2010). Another region, which extends to RT-3 to RT-4, seems to stabilize the protein or assist it during its folding, also contributing to splicing by binding other regions of the intron RNA in a DIVa-dependent manner (Gu *et al.*, 2010). Other regions, such as that extending from RT-2 to RT-3 and the X domain are presumably required for LtrA binding to core regions of the intron RNA (Gu *et al.*, 2010).

Some group II introns, especially those from mitochondria and chloroplast, lack ORFs and rely on host-encoded proteins to promote their splicing and homing processes and on chaperones to resolve stable inactive or intermediate structures that limit the rate of RNA folding (Lambowitz and Zimmerly, 2010). In general, group II intron splicing factor are proteins with additional cellular functions which can support splicing directly, interacting with specific regions of the RNA or indirectly, if they are involved in a generalized splicing mechanism (Solem *et al.*, 2009).

Host-encoded proteins known to assist chloroplast group II introns directly belong to a few families of proteins based on RNA-binding domains they contain: CRM (chloroplast RNA splicing and ribosome maduration), PPR (pentatricopeptide repeat), PORR (plant RNA recognition), OPR, ψ-uridine synthase, PTH (peptidyl-rRNA hydrolases), ribonuclease III or NAD binding (Lambowitz and Zimmerly, 2010). In these cases splicing factors play accessory roles without participating in catalysis directly. They may either stabilize the structure of the active intron ribozyme or assist in its proper folding to form the catalytically structure and avoid the formation of competing inactive folds (Stern *et al.*, 2010).

In mitochondrial group II introns, several host-encoded factors have been shown to participate in the splicing process: the MSS proteins (mitochondrial splicing system), specially Mss51, which is required for the splicing of the yeast aI5γ intron; MRF proteins (mitochondrial peptide chain release factor), which also participate in the termination of translation of mitochondrial proteins; NAM proteins (nuclear accomodation of mitochondria), some members of which have been shown to function in the maintenance of the stability of the intron-containing transcripts and; MRS (mitochondrial RNA splicing), which plays an essential role in mitochondrial Mg^{2+} homeostasis (Lehmann and Schmidt, 2003).

In addition to splicing factors, some host-encoded chaperones have been showed to be crucial for the correct RNA folding and splicing. Thus, the DEAD-box protein Mss116 from *Saccharomyces cerevisiae* is essential for the *in vivo* splicing of the group II intron ai5γ and sufficient alone to stimulate its self-splicing *in vitro* under near-physiological conditions (Fedorova and Zingler, 2007). Mss116 can be replaced *in vivo* and *in vitro* by other DEAD-box proteins that function in mitochondrial group I intron splicing, such as CYT-19 from *Neurospora crassa,* or by other DEAD-box proteins which do not usually function in splicing, such as Ded1p from *S.cerevisiae* or SrmB from *E.coli* (Lambowitz and Zimmerly, 2010). DEAD-box proteins can assist RNA folding through three major ways in an ATP-dependent manner: facilitating the collapse of the RNA, preventing or resolving misfolded structures or by stabilizing correctly folded structures (Solem *et al.*, 2009). Finally, it has been proposed that DEAD-box proteins can promote splicing in several ways: from the resolution of misfolded structures through its helicase activity to the stabilization of a correctly folded structure, both of them dependent on the ATP hydrolysis (Solem *et al.*, 2009).

I.4 GROUP II INTRON LINEAGES AND EVOLUTION

IEPs bind specifically to the intron RNA that encodes them. For that reason it is though that ribozymes and IEPs have coevolved, forming phylogenetic lineages (Toor *et al.*, 2001; Lambowitz and Zimmerly, 2010).

Phylogenetic analyses have identified eight lineages of group II introns IEPs: bacterial classes A-F, ML (mitochondrial-like) and CL (chloroplast-like) (Figure I5). Classes B, ML and CL all contain an En domain in their IEP, whereas classes C, D, E and F do not (Simon *et al.*, 2009). Each IEP lineage is associated with a RNA subgroup: ML with IIA, bacterial class C with IIC, CL with IIB1 and IIB2, bacterial class D with IIB3, bacterial class E with IIB5 and the remainder (bacterial A, B and F) with less typical IIB RNAs, (Toro *et al.*, 2007; Lambowitz and Zimmerly, 2010).

According to the RNA phylogenetic studies, IIA (mitochondrial-like) and IIC (class C) intron RNA structures are monophyletic groups, while IIB introns do not (chloroplast-like and bacterial classes) (Simon *et al.*, 2009). Moreover, according to the coevolution of the RNA and ORF, the IIA ribozyme structure has a relative recent origin compared with IIB, whereas the IIC RNAs would be the oldest (Toro *et al.*, 2007; Simon *et al.*, 2009).

The general correlation observed support the retroelement ancestor hypothesis, which predicts that the major RNA structural forms of group II introns developed through coevolution with the intron-encoded protein rather than as independent catalytic

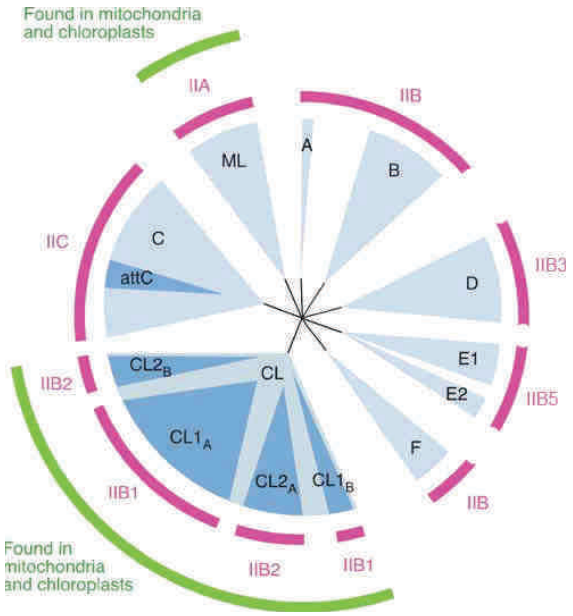

Figure I5. Group II intron lineages. The major lineages of group II intron IEPs are shown as blue sector. Sublineages are shown as darker blue sector within the major lineages. RNA structural subgroups that correspond to IEP lineages are shown in magenta. All group II intron IEP lineages and RNA types are found in bacteria. IEP lineages and RNA types also found in organelles are delineated in green (outer circle). Adapted from Lambowitz and Zimmerly (2010).

RNAs, and that most ORF-less introns are derivatives of ORF-containing introns (Toor *et al.*, 2001). However, CL subclasses of ORFs (CL1a, CL1B, CL2A and CL2B), which do not strictly correspond to the two RNA structural sustypes IIB1 and IIB2, are exception to this rule (Simon *et al.*, 2009).

I.5 THE MOBILITY OF GROUP II INTRONS

Group II introns are mobile elements that can spread within a genome or invade new genomes (Bonen and Vogel, 2001). The general mechanism consists on a process by which the intron RNA in the RNP particles uses its ribozyme activity to reverse splice into a DNA target site and is then reverse transcribed by the IEP (Lambowitz *et al.*, 2005). Two strategies are exploited for the movement, varying if the movement occurs into homologous sites (homing or retrohoming) or into ectopic sites (retrotransposition).

I.5.1 The homing (or retrohoming) process

Homing is initiated by the recognition of the DNA target site by the RNP. Target sites required for efficient homing were found to comprise 31 bp from positions -21 to +10 for yeast intron aI2, 35 bp from pos. -26 to +9 for the *L.lactis* Ll.ltrB intron and 25 bp from pos. -20 to +5 for the *S.meliloti* RmInt1 (Jiménez-Zurdo *et al.*, 2003; Lehmann and Schmidt, 2003). In the well-studied Ll.ltrB intron, the target sequence is mainly recognized by base-pairing with the RNA through the EBS2-IBS2 (-12 to -8 positions), EBS1-IBS1 (-6 to -1 positions) and δ-δ' (+1 to +3 positions) interactions (Toro *et al.*, 2007). Most of the interactions with the LtrA protein are in the distal 5'-exon region of the DNA target site (positions -23 to -14), with includes the critical bases T-23, G-21 and a-20.

Figure I6. Models of RT-mediated group II intron mobility. Schematic showing RNP composed of excised intron lariat RNA (orange line) and intron-encoded protein (grey oval), along with several possible mobility pathways. Exon sequences are indicated by dark green lines for donor gene, light green lines for homologous recipient gene and blue lines for ectopic site. After transcription of the donor gene and RNP assembly, movement can be into a homologous site by retrohoming (**A**, **B**, **C**) or into an ectopic site by retrotransposition (**D**). Retrohoming follow different pathways for mitochondrial (**A**), bacterial with En domain (**B**) or bacterial without En domain (**C**) group II intron. Adapted from Bonen and Vogel (2001).

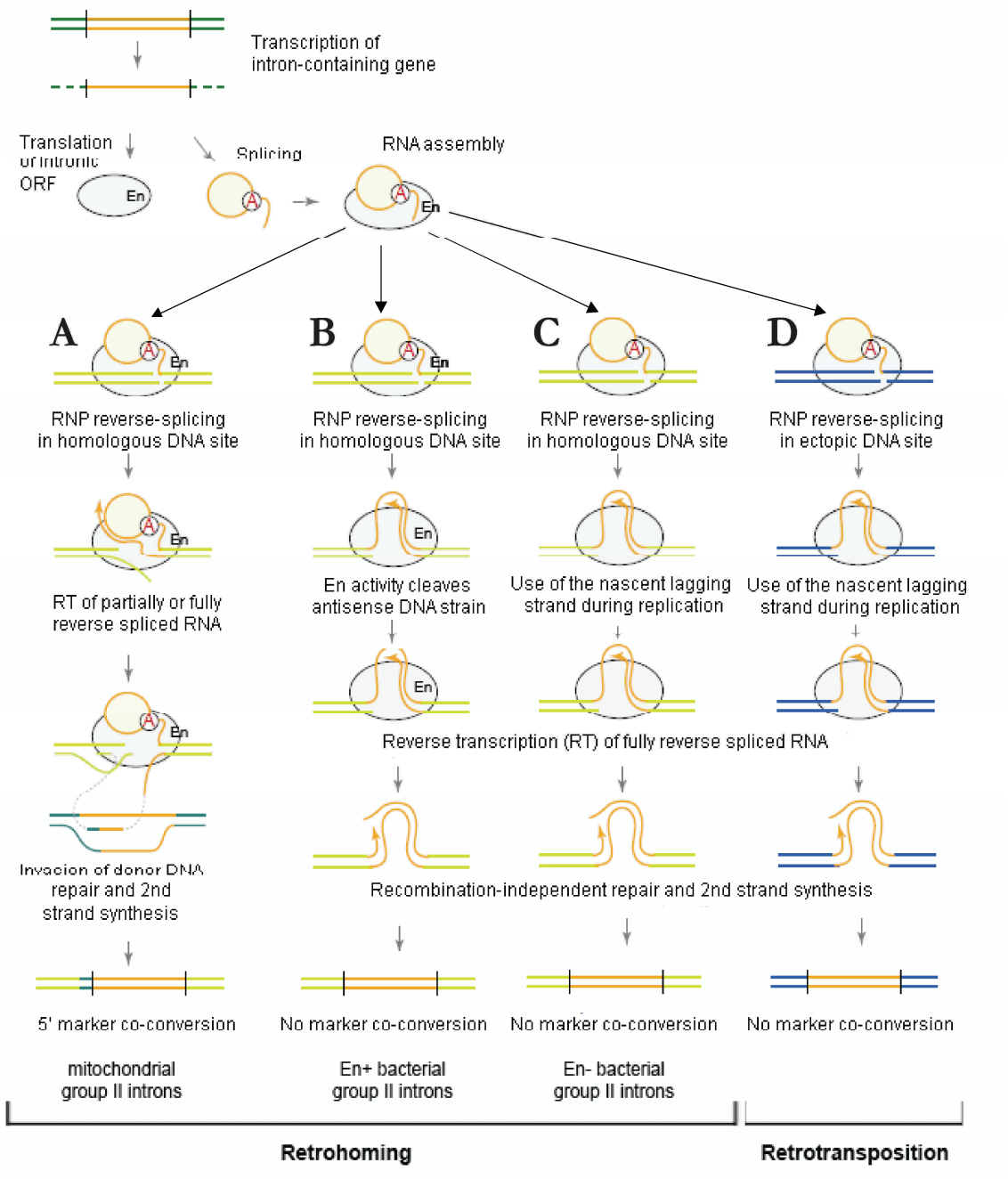

The model for *Ll.ltrB* retrohoming, through target DNA-primed reverse transcription (TPRT) is shown in the Figure I6 B. The process initiates when the lariat intron reverse-splices in the sense strand of the target site complete reverse splicing (CRS) (Cousineau *et al.*, 1998; Edgell *et al.*, 2000). The antisense strand is then recognized by the LtrA protein, although bases flanking the T+5 appear to make smaller contributions (Lambowitz *et al.*, 2005). The antisense strand is then cleaved by the endonuclease activity of the LtrA between positions +9 and +10, and the 3'- end of the cleaved antisense strand is then used as a primer for reverse transcription of the reverse-spliced intron RNA

(Cousineau *et al.*, 1998). After digestion of the RNA template, second strand synthesis could be primed by the 3'-end of the 5'-exon. Ligation of both strands completes the retrohoming event, which is RecA independent and occurs without co-conversion of the donor exons (Cousineau *et al.*, 1998). By contrast, retrohoming in yeasts is accompanied of co-conversion of upstream exon sequences, even the retrohoming initiates via complete or partial reverse splicing (PRS) (Figure I6 A) (Eickbush, 1999).

In group II introns lacking the endonuclease domain in the IEP, as the bacterial RmInt1 intron of *Sinorhizobium meliloti*, an En-independent retrohoming mechanism is used (Martínez-Abarca *et al.*, 2000) (see Section IX, below). In Ll.ltrB, this mechanism is also found in conditions in which second-strand cleavage is blocked by mutations in the endonuclease domain or DNA target site (Lambowitz and Zimmerly, 2004). Such mutations decreased the mobility frequency, which showed a replication dependence and strand bias, suggesting that a nascent leading strand at a DNA replication fork was used to primer reverse transcription (Lambowitz and Zimmerly, 2004). The preference for leading strands could reflect that, after reverse-splicing into double-stranded DNA, the intron RNP is positioned to use a leading strand primer directly (Lambowitz and Zimmerly, 2004). In Ll.ltrB intron retrohoming, some mobility also occurred in the opposite strand, but a lower frequency, whereas natural occurring group II intron that lack the En domain are preferentially found in the lagging strand (Lambowitz and Zimmerly, 2004). The latter bias could reflect that En- introns mainly reverse splice into single-stranded DNA after the passage of the replication fork, using then the lagging strand primers (Lambowitz and Zimmerly, 2004).

I.5.2 The retrotransposition process

Group II introns can also invade ectopic sites in their natural hosts at a low frequency (typically 10^{-4} to 10^{-5}), by a retrotransposition mechanism (Lambowitz and Zimmerly, 2004). The retrotransposition pathway studied in the bacterial Ll.ltrB intron occurs preferentially via DNA target site in the absence of homologous DNA recombination (Ichiyanagi *et al.*, 2002). Moreover, this process does not produce co-conversion of the 5'-exon, as observed in retrohoming (Figure I6). The IBS1 and δ' (for IIA introns)/IBS3 (for IIB introns) sequences in the target DNA match well the intron, whereas IBS2 shows only weak conservation (Cousineau *et al.*, 2000). Moreover, the positions -23 to -13 and +5 to +16, which are recognized by the LtrA moiety of the RNP particle, are only weakly conserved in the retrotransposition sites, which is consistent with a majority retrotransposition process independent of endonuclease activity (Cousineau *et*

al., 2000). In this process, the intron reverse-splices into transiently single-stranded DNA at a replication fork, followed by priming from a nascent lagging DNA strand. However, in *E.coli*, insertion occurs preferentially by an En-dependent manner, indicating that retrotransposition may be largely influenced by the host (Coros *et al.*, 2005).

I.5.3 Host-encoded proteins for mobility

Mobility of group II introns is influenced by cellular interactions, host factors and stress responses. In the initial steps of retrohoming, the group II intron recruits multiple host functions and enters the cellular replication and repair pathways (Smith *et al.*, 2005; Lambowitz and Zimmerly, 2010). Thus, after reverse transcription, the intron RNA must be removed for the synthesis of the second DNA strand using the cDNA as template, a process in which the *E.coli* RNAse H1 (*rnh*A) and the 5'-3' endonuclease activity of Pol I (*polA*) *are* involved (Smith *et al.*, 2005; Beauregard *et al.*, 2008). During the synthesis of the second DNA strand, it has been shown that the α-subunit of the polymerase Pol III and 3'-5' exonuclease ε proof-reading subunit of Pol III (*dnaQ*) are required in *E.coli*, helping the lower processive intron-encoded RT (Smith *et al.*, 2005; Beauregard *et al.*, 2008). In addition, the repair polymerases, Pol II (*polB*), Pol IV (*dinB*), and Pol V (*umuDC*) have a stimulatory effect on retrohoming in *E.coli*, participating in the repair of nicks on the DNA or in the DNA-RNA junction (Smith *et al.*, 2005; Beauregard *et al.*, 2008). 5'-3' ssDNA exonuclease RecJ is thought to participate resection of the 5' exon DNA, to allow the nascent cDNA to pair with the top strand, while the *E.coli* DNA ligase is required to seal the nicks produced after retrohoming (Beauregard *et al.*, 2008). Among factor inhibiting the retrohoming, both RNases (RNAse E, RNAse I and Exo III) and DNases are included, which may represent a cellular response against the group II intron mobility.

The retrohoming is also influences by global regulators and environmental factor. Two factors described, guanosine tetraphosphate (ppGpp) and cAMP, are of special interest (Beauregard *et al.*, 2008; Coros *et al.*, 2009). Polyphosphates accumulate when cells undergo amino acid starvation, while cAMP is activated under carbon source starvation, suggesting that these kinds of nutritional stresses can activate intron mobility (Coros *et al.*, 2009). In both cases, retrotransposition to ectopic sites was favored over retrohoming.

I.6 THE SPLICING OF GROUP II INTRONS

The splicing of group II introns was first described in 1980 in the mitochondria of yeast (Arnberg *et al.*, 1980; Halbreich *et al.*, 1980), when it was realized that group II introns accumulated as circular RNA species. Later, a self-splicing reaction was developed for the ai5γ and bI1 introns from the mitochondrial genome of the yeast *Saccharomyces cerevisiae*, showing that group II introns were able to splice autocatalytically in the form of RNA lariats, resembling those of spliceosomal introns (Peebles *et al.*, 1986; Schmelzer and Schweyen, 1986; van der Veen *et al.*, 1986). These latter experiments, which required unphysiologically high salt concentrations and temperatures, provided highlights on group II intron catalytic activity (Fedorova and Zingler, 2007).

I.6.1 The chemical mechanism of group II intron catalysis

The basic chemical reaction catalyzed by group II introns is the in-line, nucleophilic attack of an alcohol moiety or a water molecule on an activated phosphodiester linkage, resulting in release of a 3'-hydroxyl leaving group and a 5'-phosphate or new phosphodiester linkage (Figure I7) (Pyle, 2010).

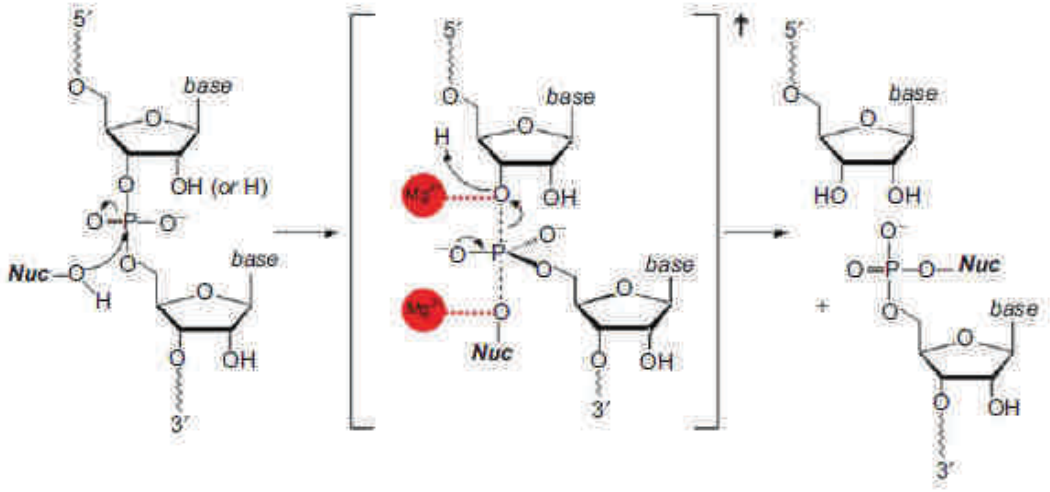

Figure I7. The chemical mechanism of catalysis by group II introns. Nuc can represent the 2'-OH group of the branch-site (for the first splicing step), the 3'-OH group of the 5'-exon (for the second splicing step) or the terminus of the intron (during circle formation), and it can also represent water (for the hydrolytic pathway). Note that the 2'-group on the departing sugar moiety can be a 2'-hydroxyl group (for RNA) or a 2'-hydrogen (for DNA), since both can be substrates of the intron RNA. Metal ions are indicated with red balls. Adapted from Pyle (2010).

Metal divalent ions are essential for the catalytic mechanism of group II introns. As protein phosphoester transferase enzymes, group II intron contain two metal ions within their active sites, helping to position the reactants, activate the nucleophile and stabilize the charge on the leaving group and phosphoryl group in the transition state (Gordon *et al.*, 2007). In particular, it has seen that one Mg^{2+} ion interacts with the 3' oxyanion leaving group during the first and second splicing steps, while a second one interacts with the nucleophile during the second exon-ligation step (Figure I7) (Gordon *et al.*, 2000; 2007). This is consistent with the group II intron crystal structure, which reveals that the catalytic triad and the bulge of DV, composing the active site, are proximal and coordinate two divalent metal ions to the scissile phosphate and the exon junction (Toor *et al.*, 2009). Additionally, it has been observed other metal ions within the core, including one that binds the G288 (of the ai5γ intron) of the J2/3 region and the bulge in DV, helping to link the active sites of the catalytic core (Toor *et al.*, 2009).

I.6.2 A single active-site for group II intron catalysis

The active-site of group II introns are composed of several elements, in addition to the well-known DV, which play important roles in catalysis and are positioned appropriately. These are the bulge and AGC triad regions of DV, the J2/3 linker region, the ε-ε' nucleotides and the coordination loop in DI (de Lencastre *et al.*, 2005; de Lencastre and Pyle, 2008). All of them are interconnected through long-range interactions, creating a network of tertiary contacts which compose the core of the catalytic properties (Figure I8).

It has been a major interest in elucidating the presence of either a unique or two active-sites catalyzing the first and second steps of the splicing reaction, which has been related with the precise identification of elements composing the catalytic core of group II introns.

It has been shown that certain functional groups at conserved positions of DV, such as the triad AGC in the base of the domain, are required for catalysis of both splicing steps, indicating the presence of a single active-site (Chanfreau and Jacquier, 1994). If this is true, then the active-site should rearrange its components to accommodate the successive substrates. In favor of the latter statement, it was shown the formation of the η-η' tertiary contact between DII and DVI was involved in a conformational change occurring before the second splicing step aimed to the displacement of the first-step product out of the active site (Chanfreau and Jacquier, 1996). More recently, it has been demonstrated that all reactants important for both steps of splicing are proximal before

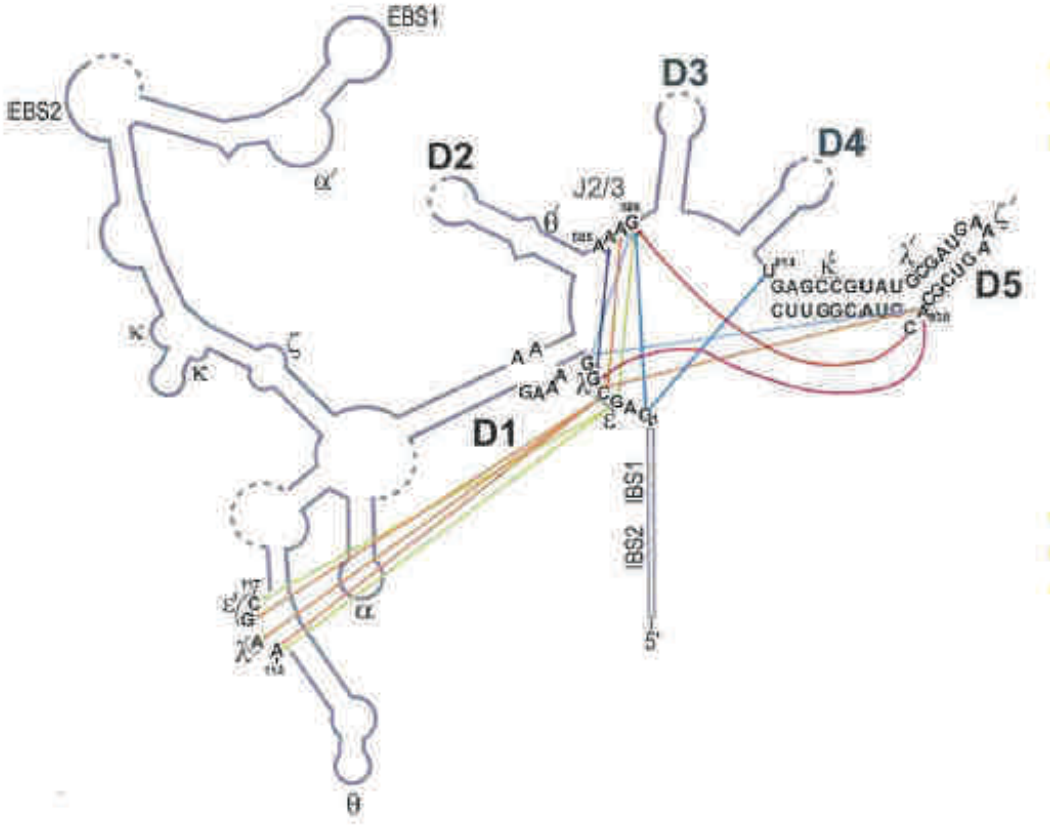

Figure I8. Three-dimensional organization of the catalytic core in group IIB introns. Lines represent cross-links observed for the ai5γ intron, which indicate that these elements are proximal before the first-step of splicing. Adapted from Lencastre and Pyle (2008).

the first step (de Lencastre *et al.*, 2005). Thus, the branch site, both exons, the catalytically essential regions of DV and J2/3, and ε-ε' are in close proximity before the first step of splicing occurs, which indicates the existence of a single active-site (de Lencastre *et al.*, 2005).

I.6.3 Definition of targets for activity

There are three targets or "reactants" that must be brought together before the initiation of the splicing reaction: the 5' and 3'-splice site (the substrates) and the branch-site (the nucleophile in the first step) (Pyle, 2008).

The 5' exon and the adjacent 5' splice site are mainly determined by the EBS-IBS interactions (EBS1-IBS1 and EBS2-IBS2), in which the sequences only need to co-vary and maintain the base-pairing, no existing sequence constraints. Then, the intron core specifically targets the phosphodiester junction between single and double stranded RNA (Pyle, 2008). In addition, the ε-ε' interaction, which occurs downstream of the 5' splice

junction, acts together with the EBS-IBS pairings to position correctly exon 1 and activate the appropriate phosphodiester bond (Jacquier and Jacquesson-Breuleux, 1991). These requirements are also true for the reverse splicing and the rest of reactions catalyzed by group II introns, in which the EBS1-IBS1 interaction has a major role for the definition of the 5'-splice site (Jacquier and Jacquesson-Breuleux, 1991; Michel and Ferat, 1995). By contrast, in group IIC introns, the 5'-splice site definition occurs through the EBS1-IBS1 interaction along with the recognition of transcription terminator stem-loop structures after which these group II introns insert (Toor *et al.*, 2006).

The 3'-splice site is determined by the contribution of several structural components. The γ-γ' interaction is important for the efficiency and precision of 3'-cleavage, particularly when some flexibility is introduced by the deletion of DVI (Jacquier and Jacquesson-Breuleux, 1991). It has also been observed that cryptic splice sites generated downstream in the 3' exon were at positions that allow the restoration of the stable wild-type pairing (Schmidt *et al.*, 1993). Moreover, in the group II intron *B.a.*I2 from *Bacillus anthracis*, an alternative splicing site is defined as a result of the presence of naturally occurring atypical structural motifs, in which the 3' splice site can be shifted as far away as four nucleotides from the wild-type site, thus restoring missing γ-γ' and EBS3-IBS3 pairings (Robart *et al.*, 2004). Another factor involved in the selection of the 3'-splice site is the length in the joining segment between DV and DVI [J(56)3], in which lengthening of the J(56)3 segment results in a reduced rate but with a correct branching, while shortening of the same produces an inefficient and inaccurate second splicing step (Boulanger *et al.*, 1996). In addition, the replacement of the first nucleotide of the 3' exon can result in a loss of fidelity and a downstream 3'-splice site selection (Su *et al.*, 2001), whereas mismatches incorporated at the EBS1/IBS1 terminus lead to a truncated interaction and a cleavage site occurring upstream the regular 3' splice site (Su *et al.*, 2001).

The two exon ends are brought together via three tertiary interactions: δ-δ', EBS1-IBS1 and EBS3-IBS3. While the δ' position is close to the EBS1 sequence in a loop of the D1 stem, the δ position is located in the coordination loop (see below) along with the EBS3 sequence. This tripartite interaction allows the approximation of DI to each of the intron flanking exons through the EBS-IBS interactions whereas the δ-δ' join both regions, and so both exon ends (Costa *et al.*, 2000).

The branch site, acting as the nucleophile in the splicing reaction, has been showed to be composed by the bulged adenosine along with the noncanonical pairs that flank the nucleophilic A and the polypurine sequence that anneals on the opposite strand (Chu *et al.*, 2001). The branch-site receptor for group IIB introns is found in a stem-loop structure

within intron DI, also containing nucleotides that participate in the δ-δ' and EBS3-IBS3 pairings that contribute to specification of both splice sites (Hamill and Pyle, 2006). The branch-site receptor, also known as coordination loop, positionates the nucleophilic adenosine to react with the 5'-splice site. Moreover, ζ-ζ' and κ-κ' interactions, which are separated from the coordination loop by a short helical stem of 6 base pairs, positionate the branch-site receptor close to major active-site components located in DV. This indicates that DV and branch-site receptor function together to place the nucleophile in the correct orientation for promoting catalysis (Hamill and Pyle, 2006). Finally, since branch-site receptor sequences are located next to EBS3-IBS3 and δ-δ' interactions, the branch site is brought into close proximity with both of the phosphodiester linkages that are cleaved during self-splicing (Hamill and Pyle, 2006).

I.6.4. Reactions catalyzed by group II intron RNAs

By employing the chemical reaction described above, group II intron can catalyze different reactions following diverse pathways (Figure I9):

a) Branching pathway

Group II intron splicing proceeds through two sequential transesterification reactions. In the first step, the 2' OH of the bulged adenosine in domain VI act as the nucleophile to attack the 5'-splice site, producing an intron lariat/3'-exon intermediate. In the second step, the 3' OH of the cleaved 5' exon, which remains tightly bound to the intron via IBS1 and IBS2 base-pairing interactions, is the nucleophile to attack the 3'-splice site, resulting in exon ligation and excision of an intron lariat RNA (Figure I9 A) (Lambowitz and Zimmerly, 2010). In group II intron self-splicing, the first step is typically rate-limiting, and the lariat/3'-exon intermediate is only detected under conditions inhibiting the second step (Pyle and Lambowitz, 2006).

Elimination of the bulging A leads to a predominance of linear intron forms (see below), although the global splicing efficiency is not affected (Chu *et al.*, 1998). Despite its importance, it seems that not only the bulging A is behind the branching process efficiency but lariat formation is in the base of several constraints, promoted by different substructures in RNA and DNA (Chu *et al.*, 1998). Thus, G-U base-pairings surrounding the bulging A also contribute to the splicing efficiency (Chu *et al.*, 1998), while the length of the segment joining DV to DVI has been reported to affect both the splicing and the accuracy of the 3' splice site (Boulanger *et al.*, 1996).

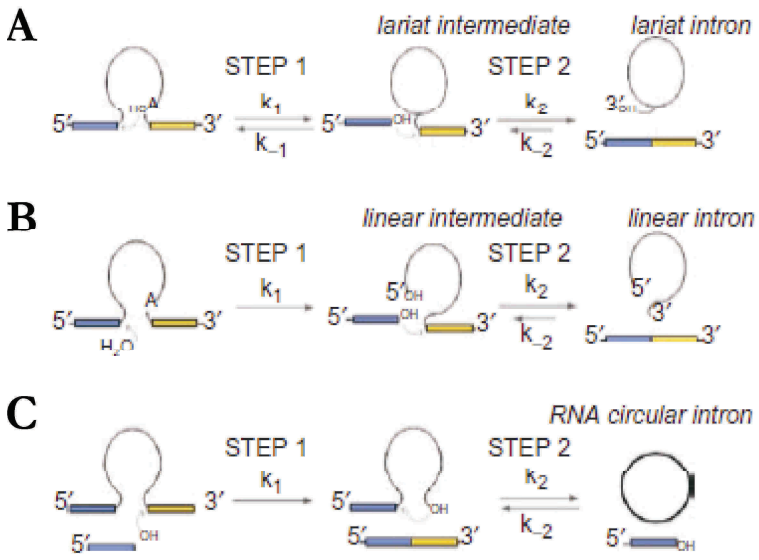

Figure I9. Three pathways for group II intron splicing and intron excision. **A** The branching pathway. **B** The hydrolytic pathway. **C** A possible circle formation pathway. 5'-exons are shown in blue and 3'-exons are shown in yellow. The intron is indicated by a thin black line. Adapted from Pyle (2010).

b) Hydrolytic splicing

This pathway involves the attack of a molecule of water as the nucleophile during the first step of splicing, while the second step proceeds as in the branching pathway, being the products of this reaction ligated exons and a linear intron (Figure I9 B) (Fedorova and Zingler, 2007; Pyle, 2010).

Although the branching pathway is more efficient in most *in vitro* studies, the hydrolytic route becomes dominant in the presence of KCl buffer (Jarrell *et al.*, 1988; Daniels *et al.*, 1996) and when the branch point is inactivated or deleted (Michel and Ferat, 1995; Pyle and Lambowitz, 2006). The hydrolytic pathway has been also observed *in vivo* for mutants blocking the branching pathway (Podar *et al.*, 1998) and for some chloroplast group II introns lacking the naturally occurring bulging A in domain VI (Vogel and Borner, 2002).

c) Excision as circles

Group II introns can also be excised as a true circle *in vitro* (Murray *et al.*, 2001; Molina-Sánchez *et al.*, 2006). The circle is created by the formation of a 2'-5'

phosphodiester bond that links the first residue of the intron to the last residue (Murray *et al.*, 2001). The 2'-5' linkage is generated when the 2' hydroxyl of the terminal nucleotide of the intron attacks the phosphodiester bond located at the 5' splice site (Murray *et al.*, 2001).

It has been suggested that circle formation is initiated by the attack of free 5'- exon molecules, which are the product of a spliced-exon reopening (SER) (Jarrell *et al.*, 1988). SER is a side-reaction catalyzed by linear and lariat group II introns in which the ligated exons are hydrolytically cleaved into free 5' and 3' exons (Figure I9 C)(Pyle, 2010).

d) Trans-splicing

Some organelle group II introns from chloroplasts and mitochondria of lower eukaryotes and plants are discontinuous, consisting of two or more segments encoded in different parts of the genome. Transcripts of these segments reassociate *in vivo* via tertiary interactions to form a functional intron, resulting in "trans-splicing" of the associated exons (Lambowitz and Zimmerly, 2004). Most fragmented group II introns are interrupted within DIV, with the IEP located either upstream or downstream the fragmentation site and some examples of fragmentation within DIII and tripartite group II introns have been also found (Lambowitz and Zimmerly, 2004).

Despite no discontinuous group II introns have been found in Prokaryotes, the Ll.LtrB intron from *L.lactis* shows the *in vivo* ability to splice *in trans* in a process dependent of the intron-encoded LtrA protein when fragmented at locations of various naturally occurring fragmentation sites (Belhocine *et al.*, 2007) or other locations not found in the nature (Belhocine *et al.*, 2008).

e) Reverse splicing

The splicing reaction can occur in the forward and reverse directions (Augustin *et al.*, 1990; Morl and Schmelzer, 1990). The reverse reaction is initiated by binding the free intron lariat via the EBS elements (EBS1, EBS2 and EBS3) located in DI with their counterparts IBSs (IBS1, IBS2 and IBS3) in the 5' exon region next to the exon ligation site (Lehmann and Schmidt, 2003). The 3'-OH of the intron attacks the exon ligation junction and the intron is integrated via two consecutive transesterifications, resulting in the original pre-RNA (Lehmann and Schmidt, 2003).

Excised linear introns are also able to carry out the reversal of the second splicing step, leading to the formation of intron/3'-exon intermediates. For the reversion of the first step, the energy of the 2'-5' phosphodiester bond not present in the linear molecule is

essential (Lehmann and Schmidt, 2003). Although this reaction was considered to be inefficient, it has been recently shown that linear introns can catalyze splicing efficiently and with high precision (Roitzsch and Pyle, 2009). Moreover, the reverse splicing occurs with similar rates for linear and lariat intron, but the majority of lariat intron molecules locks in a conformation deficient for reverse splicing, leading to the a prevalence of integrated linear intron intermediates (Roitzsch and Pyle, 2009).

I.7 GROUP II INTRONS AS BIOTECHNOLOGICAL TOOLS

Group II introns have a set of characteristics that make them suitable for their use as biotechnological tools (Toro *et al.*, 2007):

- They are mobile elements with the ability of integration into DNA target with high insertion frequency and specificity, by a homologous recombination-independent process;
- The recognition of DNA target is mediated by base-pairing of EBS-IBS sequences, which can be modified to change the target specificity;
- They can mobilize foreign genetic information inserted within the intron;
- Accessory functionalities are provided by the intron-encoded protein (IEP) or by conserved housekeeping genes, which allow its use in diverse background hosts.

In the basis on these properties, the Ll.ltrB group II intron from *L.lactis* was reprogrammed to insert into new target sequences, leading to a biotechnological tools known as "targetron" (Guo *et al.*, 2000). This tool has been used for conditional targeted gene disruption, in which the expression of the LtrA protein under an inducible promoter could lead to the expression of the interrupted gene (Guo *et al.*, 2000). Targetrons have also been developed for other bacterial group II introns, such as EcI5 of *E.coli* (Zhuang *et al.*, 2009a) and RmInt1 from *S.meliloti* (see below) (Garcia-Rodriguez *et al.*, 2011) and in eukaryotes (Mastroianni *et al.*, 2008; Zhuang *et al.*, 2009b). Introns integrated into the target DNA can be selected using a selectable marker, which can be coded in DIV after removal of the IEP sequence (Toro *et al.*, 2007). A development in this strategy is the retrotransposition-activated selectable marker (RAM), which includes a *td*I group I intron interrupting the selectable marker, so this can be only expressed if retrohoming occurs (Zhong *et al.*, 2003; Toro *et al.*, 2007).

Moreover, targetrons can be used to generate a targeted double-strand DNA break (resulted from partial reverse splicing and second-strand cleavage by the endonuclease

activity of the intron-encoded protein), that stimulates targeted DNA integration by homologous recombination, a favored mode of gene targeting in higher organisms (Karberg *et al.*, 2001; Lambowitz and Zimmerly, 2010).

I.8 THE *Sinorhizobium meliloti* RmInt1 GROUP II INTRON

RmInt1 was the first group II intron described in the family Rhizobiaceae. RmInt1 is a group IIB3 intron originally found by sequence analysis in the *Sinorhizobium meliloti* strain GR4, inserted within the insertion sequence IS*Rm2011-2* of the IS*630*-Tc1/IS*3* retroposon superfamily (Martínez-Abarca *et al.*, 1998). Later, it was shown that RmInt1 can be also associated to IS elements closely related to IS*Rm2011-2* and to the ectopic site of the *oxi1* gene with a 20-fold lower efficiency than into the homing site (Martínez-Abarca and Toro, 2000).

I.8.1 Intron-encoded protein (IEP) promoted mobility of RmInt1 intron

RmInt1 intron was found to possess an intron-encoded protein (IEP) within its DIV RNA structure, with homology to reverse transcriptases (Martínez-Abarca *et al.*, 1998). The RmInt1 IEP has a complete RT domain followed by a putative RNA-binding domain (domain X) associated with RNA splicing or maturase activity and an atypical C-terminal region which does not harbor the Zn motif characteristic of the endonuclease domain (En). However, RmInt1 has shown to be highly mobile *in vivo*, with a mechanism independent of endonuclease cleavage and homologous recombination (Martínez-Abarca *et al.*, 2000; Martínez-Abarca and Toro, 2000).

The conserved reverse transcriptase (RT) of the RmInt1 encoded-protein has been shown to be active *in vivo* and *in vitro* (Muñoz-Adelantado *et al.*, 2003). Like other group II intron IEPs, its function is completely abolished when replacing the conserved D230 and D231 residues with H230 and H231 of the active site in the RT domain, whereas binding to RNA and self-splicing promoting functions remain unaltered (Muñoz-Adelantado *et al.*, 2003).

The C-terminal region of the RmInt1 intron-encoded protein (IEP) has been found to be related to bacterial ORF class D (Molina-Sanchez *et al.*, 2010). Thus, the C-tail of the RmInt1 IEP, located in a predicted α-helical region, contributes to the maturase

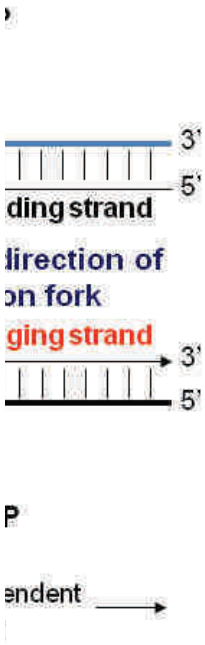

is linked to DNA
emplate for lagging
ion of the inserted
dependently of the
ed DNA. Adapted

function of the reverse transcriptase domain of the protein, whereas a region located downstream of the former and also taking part of the α-helix, contains conserved residues specifically required for the insertion of intron RNA into DNA targets in the leading strand of the replication fork (Molina-Sanchez *et al.*, 2010). These novel characteristics may have evolved to facilitate the mobility of ORF-less introns by using either leading or lagging-oriented DNA targets (Molina-Sanchez *et al.*, 2010).

Like other group II intron, RmInt1 is able to reverse-spliced into single-stranded and double-stranded DNA target sites (Muñoz-Adelantado *et al.*, 2003), using two distinct mechanisms depending on the orientation of the target site relative to the direction of DNA replication (Martínez-Abarca *et al.*, 2004). A major pathway implies the insertion of intron RNA into single-stranded DNA once the replication fork has passed the DNA target and before use of the nascent lagging DNA strand as a primer (Martínez-Abarca *et al.*, 2004), similarly as ectopic transposition of group II introns (Figure I10 A). The minor retrohoming pathway involves reverse splicing into either double-stranded DNA or

transiently single-stranded DNA target sites. Mechanisms for priming include random non-specific opposite strand nicks, a nascent leading strand or de novo initiation priming (Figure I10 B) (Martínez-Abarca *et al.*, 2004).

Retrohoming in RmInt1 is very efficient, with all recipient cells undergoing homing event (100 % homing frequency) and up to 50 % of the recipient targets are invaded (Martínez-Abarca *et al.*, 2004). The sequence requirements for efficient RmInt1 homing *in vivo* have been deciphered, showing that a DNA fragment extending from position -20 to +5, relative to the intron insertion site, supports the homing efficiency (Figure I11) (Jiménez-Zurdo *et al.*, 2003). This segment includes the IBS1 and IBS1 sequences, extending from positions -13 to -9 and -7 to -1, respectively, in the 5' exon, with a spacing of one nucleotide that it is not essential. In the 3' exon, the IBS3, corresponding to the first nucleotide, is also required. 2nt 5' upstream the IBS2 are sufficient to support homing, although wild-type levels also require the segment extending from -16 to -20 positions, being the -15 nucleotide highly conserved (Jiménez-Zurdo *et al.*, 2003). This constraint seems to rely on a novel pairing generated by shifting the IBS2 sequence from -15 to -18, which has been observed to be conserved in all published sequences (Costa *et al.*, 2006b). The 3' distal exon extends 4 nt downstream from IBS3 and only the G+4 is compulsory required (Jiménez-Zurdo *et al.*, 2003).

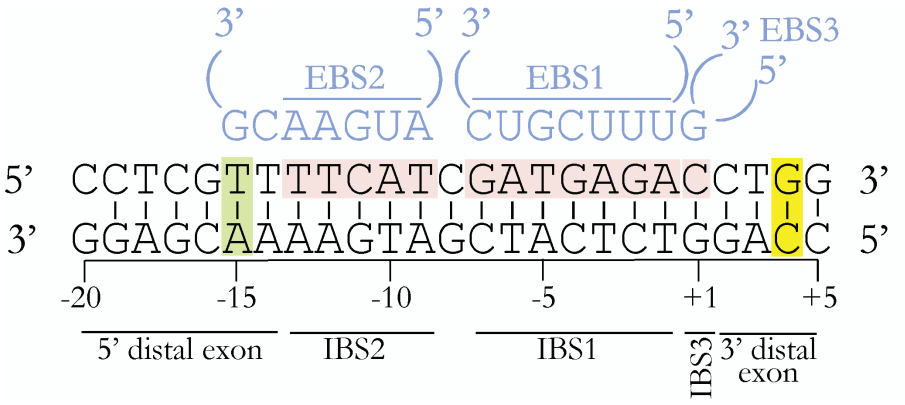

Figure I11. DNA target site recognition by RmInt1group II intron. The most critical positions conserved in 5' and 3' distal exons are indicated by green and yellow shadowing, respectively. The IBS regions recognized by base-pairing of the intron RNA's EBS sequences are shaded in pink. Adapted from Jiménez-Zurdo *et al* (2003) and Lambowitz and Zimmerly (2004).

Likewise other group II introns, such as Ll.ltrB from *L.lactis* and ai5γ from *S.cerevisiae,* RmInt1 can be retargeted at high frequency in genes present in plasmids or as single copies in the chromosome of *E.coli* (Garcia-Rodriguez *et al.*, 2011). Potential targets were selected to retain only critical nucleotide residues T-15, C+1 and G+4, whereas the

intron was engineered in order to EBS/IBS base pairings occur. Targeting frequencies of the retargeted introns varied from 0.02 % for the gene *ompT2* to 30 % for *trxB1* (Garcia-Rodriguez *et al.*, 2011). In addition, the retrohoming efficiency in *E.coli* is lower than in its natural host, and in the former, RmInt1 mobility is higher at 28 ºC than at 37 ºC, suggesting that host factors may play an important role in the process (Garcia-Rodriguez *et al.*, 2011).

I.8.2 Splicing of the RmInt1 intron

The *in vivo* splicing of RmInt1 was firstly assessed by RT-PCR in *E.coli* and *S.meliloti*, showing that the intron is able to splice from the transposase gene of the IS*2011-2* where it is inserted, and that this process it is dependent of the maturase protein encoded in DIV (Martínez-Abarca *et al.*, 1998; Martínez-Abarca *et al.*, 2000).

The wild-type RmInt1 intron efficiently excises from its precursor ARN in a lariat form (Muñoz-Adelantado *et al.*, 2003). Mutations in the conserved YADD motif to YAHH in the RT domain just produce a slight reduction, showing that the RT activity is not required for splicing. However, the truncation of the RT domain or the disruption in the catalytically critical conserved pairing AGC-GUU of the DV completely abolish the excision capacity (Muñoz-Adelantado *et al.*, 2003). In addition, RmInt1 is able to excise as circles *in vivo*, even in not mobile mutant intron-derivatives, indicating that intron dimers arranged head-to-tail are not generated (Molina-Sánchez *et al.*, 2006). It has been also shown that the maturase domain of the IEP is required for the formation of both RNA circle and intron lariat *in vivo* and that it controls in some way the balance of intron excision as lariat or intron circles (Molina-Sánchez *et al.*, 2006).

The excision of the RmInt1, through the branching pathway or in the form or circles, has been shown to be regulated by the branch-point and the coordination loop structures (Molina Sanchez *et al.*, 2011). Mutations in the branch-point prevent branching, producing an enrichment on the circular form, whereas mutation in the coordination loop do not abolish the formation of lariat intron, unlike other group II introns, which show a similar phenotype when both structures are altered (Molina Sanchez *et al.*, 2011). Moreover, the mutation in the EBS3 position (G to C) results in a great accumulation of circular and head-to-tail intron molecules, resulted from circularization of the intron and the formation of intron dimers, respectively (Molina Sanchez *et al.*, 2011).

The exon sequence requirements for RmInt1 excision *in vivo* have been elucidated, showing that the EBS1-IBS1 interaction is required and sufficient for RmInt1 excision and that, in contrast to the critical positions of the EBS-IBS interactions in the DNA target, neither the distal 5´exon region, the IBS2-EBS2, the putative IBS2*-EBS2, the IBS3-EBS3 pairings nor the distal 3' exon region are required for intron excision (Barrientos-Durán *et al.*, 2011).

RmInt1 intron self-splices *in vitro* in the absence of the intron-encoded protein when incubated under permissive conditions (Costa *et al.*, 2006a). However, the reaction is very inefficient, which show low reactivity and reaction rates. In addition, unconventional products truncated in the 3'-exon accumulate along with the expected ones, a fact resulting from the presence of a IBS1-like sequence in the 3'-exon better matching the authentic IBS1 sequence in the 5'-exon (Costa *et al.*, 2006a).

I.8.3 Dispersion and evolution of the RmInt1 intron

The ectopic retrotransposition to novel (ectopic) sites is considered a key mechanism by which group II introns have dispersed in the nature. The RmInt1 intron has been shown to invade the *oxi*1 gene independently of recombinase in its natural bacterial population (Martínez-Abarca and Toro, 2000; Muñoz-Adelantado *et al.*, 2001). However, the RmInt1 intron propagates into the *S.meliloti* genome primary by retrohoming upon acquisition by conjugative transfer, invading unoccupied RmInt1 homing sites in the genome of some *S.meliloti* strains with high efficiency (Nisa-Martínez *et al.*, 2007). According with previous results (Martínez-Abarca *et al.*, 2004), the homing sites located on the template for the lagging strand synthesis are the first to be invaded by the intron, although the available homing sites on the leading strand template are eventually occupied (Nisa-Martínez *et al.*, 2007). Once the homing sites are saturated, retrotransposition could contribute to further intron dispersion (Nisa-Martínez *et al.*, 2007).

The RmInt1 intron is also present in other *Sinorhizobium* and rhizobia species (Fernandez-Lopez *et al.*, 2005). The intron-homing sites in these species are also IS elements of the IS*2011-2* group, as in *S.meliloti*, although ectopic sites of insertion have been observed as well (Fernandez-Lopez *et al.*, 2005). RmInt1 is present predominantly in the genus *Sinorhizobium*, where vertical inheritance seems to occur from a common ancestor. In other rhizobia species, the intron only appears as fragmented copies, which show the existence of a horizontal transfer among closely related strains and species with a possible lost in some of them (Fernandez-Lopez *et al.*, 2005). Then, the RmInt1 intron is

able to propagate by vertical and lateral transfer, retrohoming or ectopic transposition, and show that they tend to evolve into fragmented introns, mechanisms underlying the origin of eukaryotic spliceosomal introns (Fernandez-Lopez *et al.*, 2005).

OBJECTIVES

On the basis of the previous knowledge of the RmInt1 group II intron biology, our goal is to deepen in the study of the molecular processes involved in the *in vivo* and *in vitro* splicing of the *Sinorhizobium meliloti* RmInt1 intron.

This general objective will be developed through the following specific aims:

1. Creation of a reporter system for the quantitative assessment of the *in vivo* splicing of the RmInt1 intron.
2. Quantitative determination of the complete splicing reaction (intron excision and exon ligation) efficiency *in vivo* of the RmInt1 intron in its natural host *Sinorhizobium meliloti* and in the heterologous host *Escherichia coli*.
3. Improvement on the efficiency of the *in vitro* self-splicing reaction of RmInt1. Quantitative analysis of the reaction rates, products and pathways in different RmInt1-transcript contexts.

Study of the effects on the first and second splicing step efficiency of point mutations in the ribozyme of RmInt1 intron previously reported to be part of conserved tertiary interactions involved in the maintenance of the RNA intron structure and function.

MATERIALS AND METHODS

M.1 BACTERIAL STRAINS

Bacterial strains used in this work are described in Table M1.

TABLE M1. Bacterial strains used in this work.

Bacterial Strain	Characteristics	Reference
Sinorhizobium meliloti RMO17	RmInt1 intronless strain. *Nod*$^+$, *Fix*$^+$.	Villadas *et al*, 1995
Escherichia coli DH5α	F$^-$, ø80d*lacZ*ΔM15, Δ(*lacZYA-argF*)U169, *deo*R, *recA*1, *endA*1, *hsd*R17(rK$^-$, mK$^+$), *phoA*, *supE*44, λ–, *thi*-1, *gyrA*96, *relA*1	Bethesda Research Lab
E.coli HB101	*supE*44, Δ(*mcrC-mrr*), *recA*13, *ara*-14, *proA*2, *lacY*1, *galK*2, *rpsL*20, *xyl*-5, *mtl*-1, *leuB*6, *thi*-1	Promega Corporation

M.2 BACTERIAL CULTURES

M.2.1 Culture media

E.coli strain was grown in Luria-Bertani (LB) broth (Sambrook *et al.*, 1989): NaCl 5 g/l, tryptone 10 g/l and yeast extract 5 g/l, made with desionized water (MQ water) and adjusted to pH 7. Solid medium was supplemented with 1.6% w/v agar. It was sterilized by autoclaving at 120 ºC for 20 minutes.

The selective solid culture medium of coliform bacteria Endo Agar (Difco) was used for the detection of contaminant *E.coli* cells in *S.meliloti* trans-conjugants. It was made with 51 g/l of powder in MQ water, heating to dissolve and sterilizing by autoclaving at 120 ºC for 20 minutes.

S.meliloti strain was grown in TY medium (Beringer, 1974): $CaCl_2 \cdot 2H_2O$ 0.9 g/l, tryptone 5 g/l and yeast extract 3 g/l, prepared with MQ water and adjusted to pH 7. Solid medium was supplemented with 1.6% w/v agar. It was sterilized by autoclaving at 120 ºC for 20 minutes.

S.meliloti trans-conjugants were grown in minimal medium (Robertsen *et al.* 1981: K_2HPO_4 0.3 g/l, KH_2PO_4 0.3 g/l, $CaCl_2$ 0.05 g/l, $MgSO_4 \cdot 7H_2O$ 0.15 g/l, $FeCl_3$ 0.006 g/l,

NaCl 0.05 g/l, sodium glutamate 1.1 g/l, mannitol 10g/l, biotin 0.0002 g/l and calcium pantothenate 0.0001 g/l. Solid medium was supplemented with 1.6% w/v agar. It was sterilized by autoclaving at 120 ºC for 20 minutes.

M.2.2 Antibiotics

Antibiotics were made as 100X stock solutions in MQ water (Km, Ap) and filter sterilized through 0.2 μm membrane Minisart® NML (Sartorius). Tetracycline and Ampicillin were used at 10 g/l and 200 g/l final concentration, respectively, for both *E.coli* and *S.meliloti*. Kanamycin was used at a final concentration of 180 g/l for *S.meliloti* and of 50 g/l for *E.coli*.

M.2.3 Growth conditions and storage

S. meliloti was routinely grown at 28ºC in shaker at 190 rpm, having a generation time of 2.5 h, approximately. *E.coli* was grown at 37ºC in the same conditions as above, with a generation time of 30 min.

Bacterial cultures grown until late exponential growth phase were deposited in cryotubes with added 20% (v/v) final concentration glycerol and preserved at -80 ºC for long-term storage.

M.3 PLASMIDS AND CLONING VECTORS

M.3.1 Commercial plasmids and vectors

TABLE M2. Plasmids and vectors used in this work

Name	Characteristics	Reference
pGEM-T easy	Vector for the cloning of PCR products. High copy number. 3015 bp. Ampicillin resistant. Recombinant cloned identified by color screening.	Promega
pRK2013	Helper plasmid. RK2 derivative. Replicon ColE1. Kanamycin resistant. Used for *trans*-complementation during mobilization of plasmids in tri-parental conjugations.	(Figurski and Helinski, 1979)

pBB0.6	Receptor plasmid in homing assays. pBBR1MS-2 derivative (Kovach *et al.*, 1995). 5820 bp. Kanamycin resistant. Comprised of the -175/+466 of the RmInt1 target site of IS*Rm2011-2*.	(Martinez-Abarca *et al.*, 2000)
pBBΔ129	Derivative of pBB0.6, where a region of 129 bp (-125/+4) in the IS*Rm2011-2* has been deleted.	(Martinez-Abarca *et al.*, 2000)
pKG0IEP	Plasmid producing constitutively the intron-encoded protein (IEP) for *trans*-complementation in splicing. 6533 bp. Kanamycin resistant.	(Muñoz-Adelantado *et al.*, 2003)
pMP220	Broad-host range transcriptional fusion vector. Precursor of pICG plasmids. It contain a multicloning site sequence, a Shine-Dalgarno sequence from the *E.coli* CAT gene and the β-galactosidase *lac*Z gene of *E.coli*. 10.5 Kb. Tetracycline resistant.	(Spaink *et al.*, 1987)
pKG2.5	Intron construct used as a donor in homing assays. Flanking exons of -174/+466 bp. 7859 bp. Kanamycin resistant.	(Martinez-Abarca *et al.*, 2000)
pKG2.5DV-CGA	Splicing defective intron construct. Derivative of pKG2.5. 7859 bp. Kanamycin resistant.	(Muñoz-Adelantado *et al.*, 2003)
pKGEMA4	IEP-ΔORF intron construct, from which most nucleotides of the ORF has been deleted. Flanking exons of -20/+5 bp. 7318 bp. Kanamycin resistant.	(Nisa-Martínez *et al.*, 2007)
pKGEMA4DV	Splicing defective intron construct. Derivative of pKGEMA4. 7859 bp. Kanamycin resistant.	(Nisa-Martínez *et al.*, 2007)
pLM1	ΔORF intron construct under T7 promoter. Template for *in vitro* transcription. pUC derivative. Flanking exons of -15/+146 bp. Ampicillin resistant.	(Costa *et al.*, 2006)
pLI1	Contains the Ll.ltrB intron and flanking exons (-58/+38) cloned behind the phage T7 promoter in the expression vector pET-11a. 8477 bp. Ampicillin resistant.	(Matsuura *et al.*, 1997)

M.3.2 *pICG plasmid series*

pICG plasmids are derivative of pMP220 (Spaink *et al.*, 1987), to which the pSyn promoter (Giacomini *et al.*, 1994) has been cloned upstream from the *lac*Z gene and the ribosome binding site, to ensure strong constitutive expression. In addition, the *Bln*I and polylinker *Bam*HI sites have been removed (Figure M1).

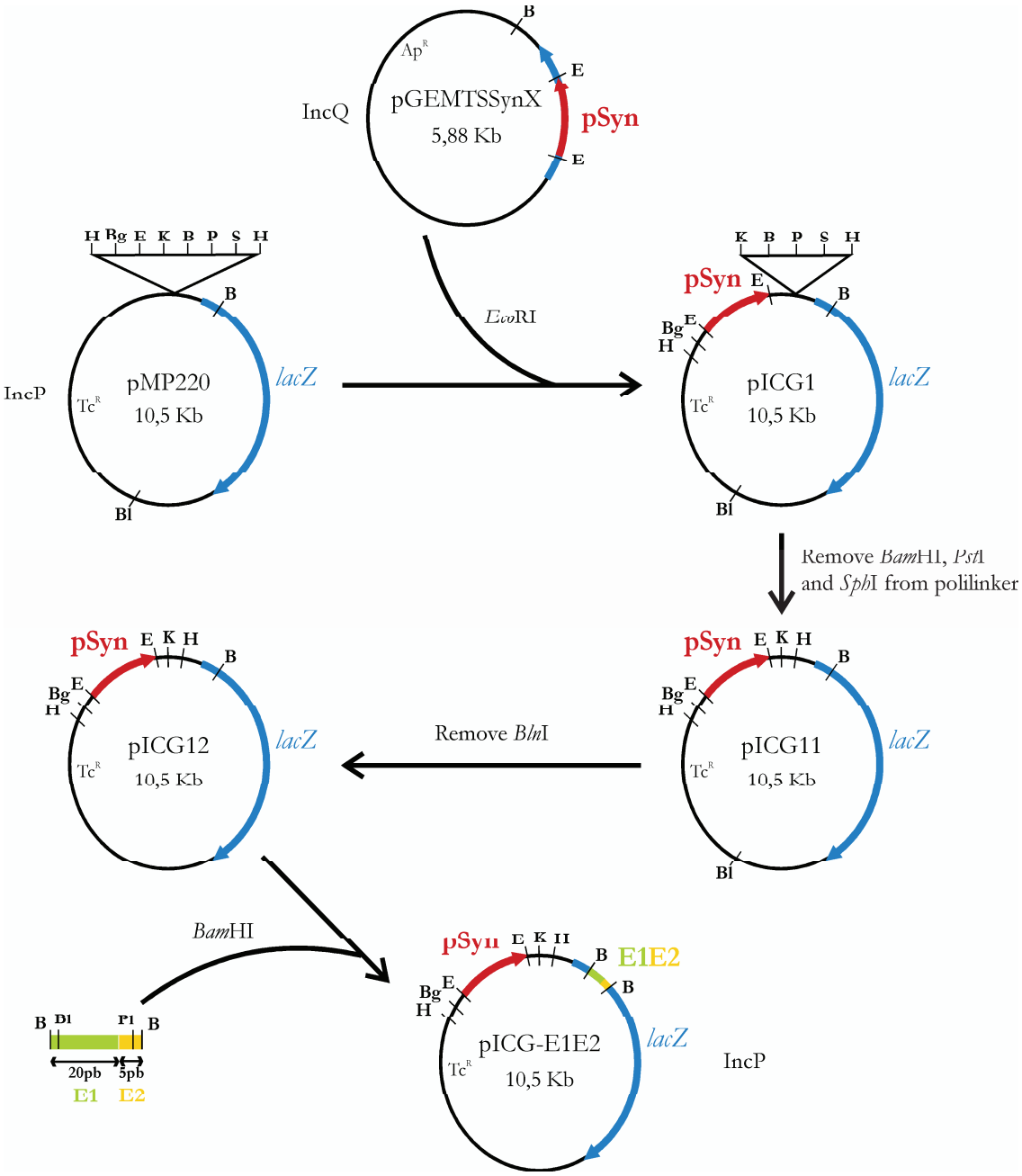

Figure M1. Construction of broad host range expression vector pICG-E1E2. **A** The pSyn promoter (Giacomini *et al.*, 1994) from pGEMTSSynX was cloned in the *Eco*RI cloning site in the polylinker of pMP220. *Bam*HI, *Pst*I and *Sph*I were first removed of the polylinker by digestion with *Kpn*I and *Sph*I, treated with T4 DNA-polymerase (Roche) and auto-ligated with T4 DNA ligase (Roche). After removal of *Bln*I by digestion and filling in with Klenow fragment of DNA

polymerase I, a fragment containing the minimal RmInt1 target site (20 bp of the 5´exon (E1) and 5 bp of the 3´exon (E2)) (Nisa-Martínez *et al.*, 2007) from the IS*Rm2011-2* insertion sequence and flanked by *Bam*HI restriction sequences was inserted into the *Bam*HI site of the *lac*Z gene to create pICG-E1E2. Tc^R and Ap^R indicate resistance markers. Plasmids and polylinkers have not been drawn to scale. H, *Hind*III; Bg, *Bgl*II; E, *Eco*RI; K, *Kpn*I; B, *Bam*HI; P, *Pst*I; S, *Sph*I; Bl, *Bln*I; Pl, *Plm*I. **B** Schematic diagram of the nucleotide sequence of the *lac*Z mRNA in pICG-E1E2 and the ligated exons resulting from RmInt1 splicing, presented with the corresponding amino-acid sequence. This region consists of 42 nucleotides, including 25 nucleotides corresponding to the IS*Rm2011-2* flanking exons and 17 corresponding to the additional *Pml*I, *Bln*I and *Bam*HI cloning sites linked in-frame to the *lac*Z gene. Upper case letters indicate the *lac*Z sequence, whereas lower case letter indicate the exon flanking sequences. Additional amino acids due to the addition of nucleotides to the residual *lac*Z remaining after intron excision are identified by asterisks. A vertical arrow indicates the site of intron insertion (wt or □ ORF) in the intron-containing constructs.

pICG-E1E2 contains 25 nucleotides corresponding to the intron flanking exons (20 bp of the 5´exon (E1) and 5 bp of the 3´exon (E2))(Nisa-Martínez *et al.*, 2007) from the IS*Rm2011-2* insertion sequence inserted into the *Bam*HI site of the *lac*Z gene (Figure M1 B). pICG-WT contains the wild-type RmInt1 intron, generated *in vivo* by the invasion of pICG-E1E2 by the RmInt1 intron from pKG2.5 (Martínez-Abarca *et al.*, 2000). pICG-DV contains a variant of the intron with a mutation in catalytic domain V, obtained from pKG2.5D5-CGA (Muñoz-Adelantado *et al.*, 2003) (Figure M2 A).

The construct used to produce the IEP protein in *trans* was pKGIEP (Muñoz-Adelantado *et al.*, 2003) (Figure M2 B). The series of constructs in *trans* generated in this study are ΔORF constructs (Nisa-Martínez *et al.*, 2007), from which most of the intron ORF has been deleted. pICG-ΔORF was constructed by ligating the 0.8 kb *Pml*I/*Bln*I fragment of pKGMA4 between the corresponding sites of pICG-E1E2. pICGΔORFDV contains the ΔORF fragment with a mutation in the catalytic domain, as in pKG2.5D5-CGA (Muñoz-Adelantado *et al.*, 2003), inserted between the *Pml*I and *Bln*I restriction sites (Figure M2 B).

The plasmids in the *cis* series are also based on ΔORF constructs, with the sequence encoding the IEP protein located upstream from the 5´exon on the same plasmid (Figure M2 C). This IEP sequence was obtained by amplification from pKGIEP, with the primers 5'-GGGGAGTACTGGAAACAGGATGACTTCGGA and 5'-GGGGGCATGCTCAGGTAAACGTGTTCGTTCC, and was inserted between the *Sca*I and *Sph*I sites added to the polylinker of pICG-E1E2, pICG-ΔORF and pICG-ΔORFDV, to give pICG-IEP-E1E2 (without intron), pICG-IEP-ΔORF (intron ΔORF) and pICG-IEP-ΔORFDV (CGA-mutated intron), respectively (Figure M2 C).

No se puede mostrar la imagen. Puede que su equipo no tenga suficiente memoria para abrir la imagen o que ésta esté dañada. Reinicie el equipo y, a continuación, abra el archivo de nuevo. Si sigue apareciendo la x roja, puede que tenga que borrar la imagen e insertarla de nuevo.

Figure M2. Construction of pICG plasmids from pICG-E1E2. **A** The intron donor plasmid pKG2.5 (Martínez-Abarca *et al.*, 2000) was mobilized to a *S.meliloti* RMO17 strain carrying the intronless construct pICG-E1E2, invading the later and creating pICG-WT. The fragment ΔORFDV from the splicing-defective pKG2.5DV plasmid (Muñoz-Adelantado *et al.*, 2003) was amplified and cloned in the *Bln*I and *Pml*I sites of pICG-E1E2. **B** pKGMA4 and pKGEMA4DV plasmids were used to construct pICG-ΔORF and pICG-ΔORFDV plasmids, respectively, in which the fragment containing the ΔORF or the ΔORFDV sequences was cloned into the *Bln*I and *Pml*I sites of pICG-E1E2. **C** The transient plasmid pICG-ScaSph was created by introducing a mutated *Kpn*I-*Kpn*I oligonucleotide into the *Kpn*I site of the pICG-ΔORF plasmid, thus inactivating this site and adding new *Sca*I, *Kpn*I and *Sph*I sites to the polylinker. The pICG-ScaSph plasmid was subsequently used to create the pICG-IEP-ΔORF plasmid in which the IEP fragment from pKGIEP0 was amplified and cloned in the *Sca*I-*Sph*I sites. The ΔORFDV fragment from pIGMA4DV and the flanking-exon oligonucleotide were exchanged with the ΔORF fragment to create pICG-IEP-ΔORFDV and pICG-IEP-E1E2, respectively. Plasmids and polylinkers have not been drawn to scale. H, *Himd*III; Bg, *Bgl*II; E, *Eco*RI; K, *Kpn*I; B, *Bam*HI; P, *Pst*I; S, *Sph*I; Bl, *Bln*I; Pl, *Plm*I, Sc, *Sca*I.

The plasmids of the ter series contain a synthetic Rho-independent transcription terminator (Kingsford *et al.*, 2007) (Figure M3). In these constructs, oligonucleotides 5'-GATCCCCTAGGTGAAAAAACGACAAAGCAGCACTGATTACAGTGCTGCTTTT TTTATCCCTGTG and 5'-GATCCACAGGGATAAAAAAAGCAGCACTGTAATCAGTGCTGCTTTGTCGTTT TTTCACCTAGGG were annealed and ligated downstream from the intron-flanking exons, into the *Bln*I/*Bam*HI sites of pICG-E1E2, pICG-ΔORF and pICG-ΔORFDV, generating pICGTer-E1E2 (without intron), pICGTer-ΔORF (intron ΔORF) and pICGTer-ΔORFDV (CGA mutated intron), respectively.

pICG plasmids expressing the *Lactococcus lactis* Ll.ltrB intron derived from pICG12 and pLI1 (Matsuura *et al.*, 1997). pICG-Ll.ltrB (Ll.ltrB intron in sense orientation) and pICG-Ll.ltrBA (in antisense orientation) were constructed by using primers 11P_ltrBE1 (5'- GGGGGATCCAGGTGGCGAATA) and 12PR_ltrBE2 (5-GGGGGATCCTTGCCAGTATAAAGATTC) to amplify a 2.6 kb region of pLI1, which was then cloned in the *Bam*HI site of pICG12. The resulting constructions were confirmed by sequencing and both orientation of the insert were selected by restriction analysis. pICG-*ltr*B contained a 96-nucleotide sequence of ligated *ltrB* exons 1 and 2, extending from 58 nucleotides upstream to 38 nucleotides downstream of the intron insertion site, cloned in the *Bam*HI site of pICG-E1E2. The insert was generated from cDNA of reverse transcribed pLI1 RNA by PCR with the primers 11P_ltrBE1 and 12PR_ltrBE2.

pICG plasmid series containing mutations in the ribozyme of RmInt1 intron derived from pICG-ΔORF plasmid via site-directed mutagenesis. Mutations located in the termini of the intron sequence was incorporated into one of the primer used in the PCR

reaction (Scharf *et al.*, 1986). Mismatched and overlapping primers were used when mutations were located anywhere else along the intron length (Higuchi *et al.*, 1988). In that case, two primary PCR reactions produced two overlapping DNA fragments, which were subsequently mixed, serving as templates for the secondary reamplification using only the outermost two of the four primers used in the primary PCR reaction. The recombined PCR product was then cloned in *Pml*I-*Bln*I sites of pICG-E1E2 or pICGTer -E1E2 plasmids. Recombinant plasmids were sequenced in order to verify constructions. A summary of mutant constructions and the primers used are listed in Table M3.

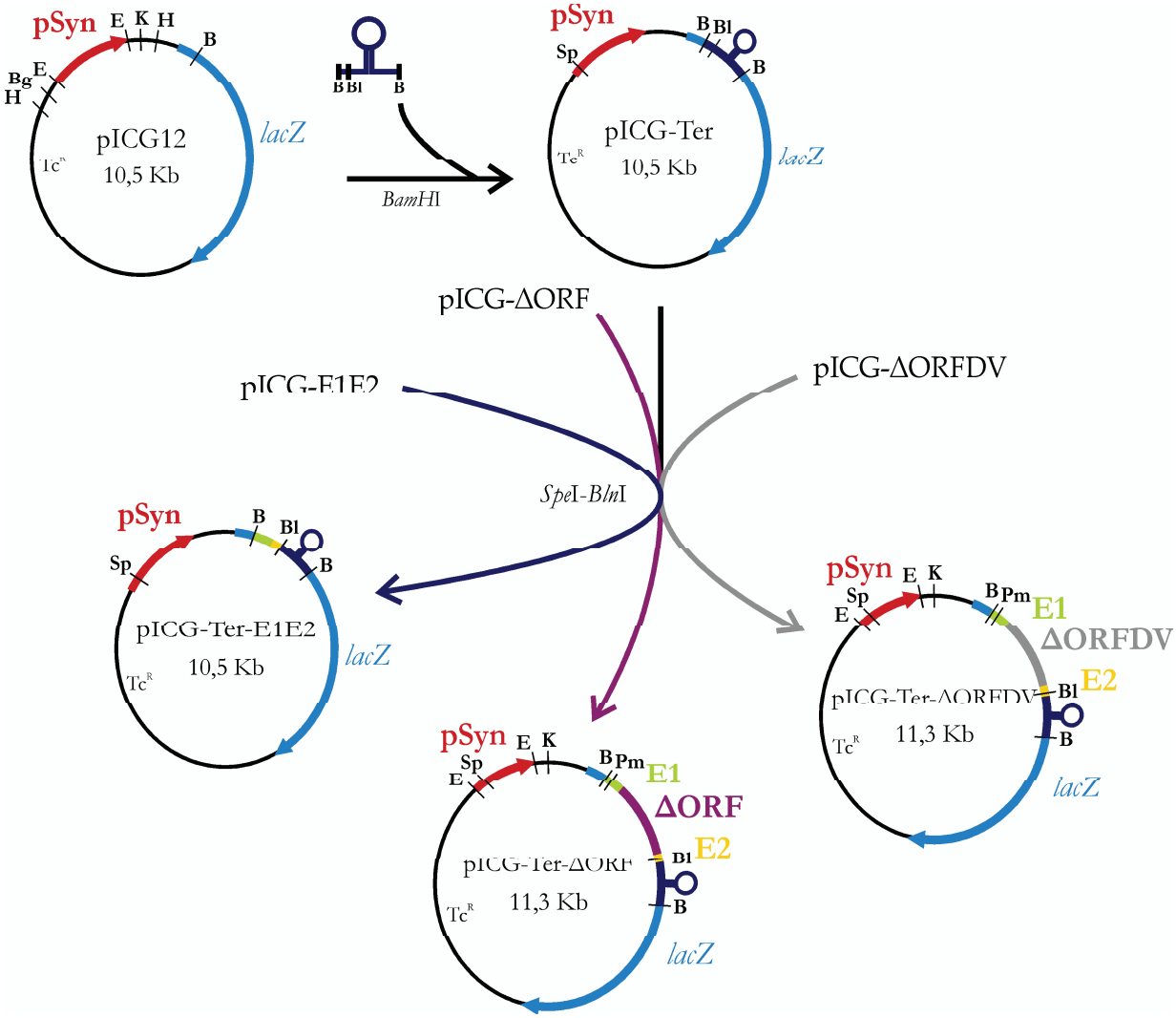

Figure M3. Construction of pICG-Ter series plasmids from pICG-E1E2. The synthetic Rho-independent transcription terminator (Kingsford *et al.*, 2007) was introduced in the *Bam*HI sites of pICG-E1E2, replacing the 25nt intron flanking exon fragment and creating the pICGTer plasmid. The *Spe*I-*Bln*I fragment of the later was exchanged with pICG-E1E2, pICG-ΔORF and pICG-ΔORFDV, resulting in pICGTer-E1E2, pICGTer-ΔORF and pICGTer-ΔORFDV, respectively. Plasmids and polylinkers have not been drawn to scale. B, *Bam*HI; Bl, *Bln*I; Pl, *Plm*I, Sp, *Spe*I

TABLE M3. Primers used for the construction of mutants in the ribozyme of RmInt1 intron

Mutant	Template	PCR Primer[1]	Sequence
C1883A	pICG-ΔORF	5Q_CAT	TGTACCTATAACCAGACCGTTCAG
		22PR_C1883A	CCCCTAGGCCAGGGTTGAGTAGG
C1883G	pICG-ΔORF	5Q_CAT	TGTACCTATAACCAGACCGTTCAG
		23PR_C1883G	CCCCTAGGCCAGGGCTGAGTAGG
C1883T	pICG-ΔORF	5Q_CAT	TGTACCTATAACCAGACCGTTCAG
		24PR_C1883T	CCCCTAGGCCAGGGATGAGTAGG
ΔGA	pICG-ΔORF	**5Q_CAT**	TGTACCTATAACCAGACCGTTCAG
		4OR_ΔGA	TACGGGGCGACGCCCCAGTCTCCTGCATC
		4O_ΔGA	GACTGGGGCGTCGCCCCGTATGAGCGTCGAGG
		6QR_LACZ	GATGTGCTGCAAGGCGATT
Δγ	pICG-ΔORF	**5Q_CAT**	TGTACCTATAACCAGACCGTTCAG
		5OR_Δgamma	TACGGGGCGATCGCCCCAGTCTCCTGCATC
		5O_Δgamma	GACTGGGGCGATCGCCCCGTATGAGCGTCGAGG
		6QR_LACZ	GATGTGCTGCAAGGCGATT
Δγ-GEBS3C	pICG-GEBS3C	**5Q_CAT**	TGTACCTATAACCAGACCGTTCAG
		5OR_Δgamma	TACGGGGCGATCGCCCCAGTCTCCTGCATC
		5O_Δgamma	GACTGGGGCGATCGCCCCGTATGAGCGTCGAGG
		6QR_LACZ	GATGTGCTGCAAGGCGATT

[1] Bold letters indicate outer primers used in secondary PCR reaction.

M.3.3 Other described pICG and pICGTer plasmids

TABLE M4. Described pICG and pICGTer plasmids used in this work

Name	Characteristics	Reference
GγC	Position G452 mutated to C. Disrupts γ-γ' interaction.	(Molina Sanchez *et al.*, 2011)
Cγ'G	Position C1884 mutated to G. Disrupts γ-γ' interaction.	
GγCγ'G	Double mutation G452 to C and C1884 to C. Restoration of γ-γ' interaction.	
GEBS3C	Position G329 mutated to C. Disrupts EBS3-IBS3 interaction.	

M.3.4 pLM plasmid series

pLM plasmids were derivative of pLM1 (Costa *et al.*, 2006). To create pLM-WT, primers 5Q_CAT and 27PR_lacZtranscript (5'-GGAGATCTCATATGACTGTTGGGAAGGGCGA) were used to amplify a 1009 bp fragment of pICG-ΔORF, which was then cloned in *Cla*I-*Bam*HI sites of pLM1.

Mutant pLM-derivative plasmids were generated by cutting and cloning a *Cla*I-*Bam*HI fragment from mutated pICG plasmids in pLM-WT.

M.4 NUCLEIC ACIDS EXTRACTION

M.4.1 Plasmid DNA extraction by magnesium salts

This procedure, based on that of Studier (Studier, 1991), was used for rapid plasmid extraction from *E.coli* cultures. An overnight-grown culture of *E.coli* was collected in 1.5 ml microcentrifuge tubes and centrifuged at 13000 rpm for 2 min. The supernatant was removed by aspiration and the pellet suspended in 100 µl of MQ water. To this suspension it was added NaOH 0.1 M, EDTA 10 mM and 2% SDS and mixed immediately by vortexing. Tubes were heated for 2 min in a boiling water-bath. 50 µl of 1 M $MgCl_2$ was mixed in by vortexing and the tube was placed on ice for 2 min. The precipitate was pelleted by centrifuging for 1 min. 50 µl of 5 M potassium acetate was mixed into the supernatant in the same tube by brief vortexing and the tube was again placed on ice for 2 min. After centrifuging another 5 min at 13000 rpm, the supernatant was removed to a new tube containing 0.6 ml of 100% (v/v) ethanol, mixed by vortexing and placed on ice for 5 min. The tube was centrifuged for 5 min, the supernatant removed by aspiration, and 0.2 ml of 70% (v/v) ethanol was added, centrifuged for 5 min and removed by aspiration. Residual solvent was removed under vacuum for 5 to 10 min and the pellet dissolved in a 0.2mg/ml of an RNAse solution.

M.4.2 Plasmid DNA extraction by alkaline lysis

This method was routinely used for plasmid DNA extraction from *S.meliloti.* It is based on the modified procedure of Sambrook (Birnboim and Doly, 1979; Ish-Horowicz and Burke, 1981; Sambrook *et al.*, 1989). 3 ml of a saturated culture of *S.meliloti* was harvested in 1.5 ml microcentrifuge tubes and washed with 200 µl of 0.1% sarkosyl (made

in TE). Cell were resuspended in 100 µl of 50mM glucose, 25mM Tris pH 8.0 and 10mM EDTA and incubated for 5 min at room temperature. 200 µl of 0.2N NaOH and 1% SDS were added, mixed gently and put on ice for 5 min. 150 µl of precooled 5M KOAc pH 4.8 was added, mixed gently, and after 5 min on ice, samples were centrifuged for 1 min. The supernatant was then extracted with phenol-chloroform and reconstituted in a 0.2mg/ml of an RNAse solution.

M.4.3 Total RNA extraction

This procedure, used for isolation of RNA from both *S.meliloti* and *E.coli* cultures, is based on the method described by (Cabanes *et al.*, 2000). The bacterial pellet from a culture from *S.meliloti* or *E.coli* (optical density at 600 nm = 0.6) was resuspended and incubated for 10 min at 65°C in 2 ml of prewarmed lysis solution (1.4% SDS, 4 mM EDTA and 0.4 mg/ml Proteinase K solution). Proteins were removed by adding 150 µl of NaCl (5 M) at 4 °C for 10 min. After centrifugation, the nucleic acids present in the supernatant were precipitated by adding 1 ml of ethanol (100%). The pellet was resuspended in 85 µl of MQ water and digested with 50 units of RNase-free DNase I. The RNA was first extracted with 1 volume of phenol (pH 4.5)/chloroform/isoamyl alcohol (25:24:1) and then with 1 volume of chloroform/isoamyl alcohol (24:1). Finally, the RNA was precipitated with 3 volumes of ethanol (100%) and 75 mM NaOAc (pH 5.2). The RNA pellet was washed with 70% ethanol, dried, and resuspended in 20 µl of nuclease-free water.

M.5 CLONING AND ENZYMATIC MANIPULATION OF DNA

M.5.1 DNA digestion with restriction endonucleases

DNA was digested directly with commercially available restriction endonucleases according to the manufacturer's recommendations (New England Biolabs). Typically, each microgram (µg) of DNA was digested in the presence of 5 units of enzymes and 1X reaction buffer, in a volume ranged from 10 µl (analytical digestion) to 50 µl (preparative digestion). When a double digestion was performed, reaction conditions were selected to ensure being amenable to any two restriction enzymes.

M.5.2 Conversion of protruding to blunt-ended restriction fragments

For converting a 5' overhang to blunt end, a method based on (Wartell and Reznikoff, 1980) and modified by (Sambrook *et al.*, 1989) was employed using the klenow fragment of *E.coli* DNA polymerase I (Roche). 0.5-1 μg of DNA restriction fragments were incubated for 15-30 min at 22ºC with a mix of 1X filling buffer (500 mM Tris pH 7.5, 100 mM $MgCl_2$, 10 mM DTT,5 00 μg/ml BSA), 1mM of each dNTP and 1U of Klenow Enzyme (Roche) in a volume of 10μl. Then, the enzyme was inactivated by heating at 70ºC for 5 min.

DNA fragments with protruding 3' ends were blunt-ended using the 3'-5' exonuclease activity of bacteriophage T4 DNA polymerase (Sambrook *et al.*, 1989). A mix of 1X incubation buffer (10 mM Tris-HCl 50 mM NaCl, 10 mM $MgCl_2$, 1 mM Dithiothreitol) supplemented with 100 μg/ml Bovine Serum Albumin and 100 μM dNTPs and 1U of T4 DNA Polymerase I (New England Biolabs) were added to 0.5-1 μg of DNA fragments, and incubated 5 min at 37ºC. The reaction was stopped by adding EDTA to a final concentration of 10 mM.

M.5.3 Dephosphorilation of DNA fragments

Terminal phosphate groups from restriction endonuclease digested DNA were removed by incubation in the presence of calf intestinal alkaline phosphatase (CIP). Typically, 5-10 μg of DNA from a restriction digest was added directly to a reaction containing 1X capping buffer and 2 units of CIP (Roche) in a total volume of 50 μl. This reaction was incubated at 37 ºC for 30 min, supplemented with a further 2 units CIP, and incubated at 37 ºC for an additional 30 min. The reaction was terminated by adding a mix of 1% SDS in STE 1X buffer (100 mM NaCl, 1mM Tris-Cl pH 8 and 1 mM EDTA) and heating at 75ºC for 15 min. Then, the DNA was extracted with phenol/chloroform.

M.5.4 Nucleic Acids Purification

The cleanup of DNA fragments from enzymatic reactions was carried out by the commercial kits QIAquick PCR Purification Kit (Qiagen) and Illustra GFX PCR DNA and Gel Band Purification Kit (GE Healthcare) or by phenol-chloroform extraction.

In the phenol-chloroform extraction, the DNA to be purified was extracted with an equal volume of phenol/chloroform/isoamyl alcohol (25:24:1) and centrifuged for 5

minutes. The aqueous phase was transferred to a fresh tube and extracted with chloroform/isoamyl alcohol (24:1), then centrifuged for 5 minutes. The supernatant was transferred to a fresh tube and precipitated with 3 volumes of 100% ethanol and 0.1X volume of 3M sodium acetate pH 5.2 for 5 minutes. The DNA was precipitated at -80ºC for at least one hour and then pelleted by centrifugation for 15 minutes. The pellet sas washed with 70% EtOH, dried, and resuspended in an appropriate solvent.

For extraction of ¨DNA fragments from agarose gels in TAE (Tris acetate/EDTA) buffer, the commercial kits Perfectprep Gel Cleanup (Eppendorf) and Illustra GFX PCR DNA and Gel Band Purification Kit (GE Healthcare) were used.

M.5.5 Ligation of DNA fragments

Restriction endonuclease digested or blunt end DNA was typically ligated into a vector backbone using the T4 DNA ligase (Engler and Richardson, 1983). Ligations were performed in a 10 µl reaction volume at 14-16ºC for up to 24 h in the presence of 1 x ligase buffer and 1 U T4 DNA ligase (Roche). To calculate the appropriate amount of insert to include in the ligation reaction, the following equation was used:

$$\frac{(ng\ of\ vector) \cdot (Kb\ size\ of\ insert)}{Kb\ size\ of\ vector} \cdot (insert{:}\ vector\ molar\ ratio) = ng\ of\ insert$$

M.6 BACTERIAL TRANSFORMATION AND CONJUGATION

M.6.1 Competent *E.coli* cells and transformation

Bacterial cells were made competent according to the rubidium chloride method of Rodríguez and Tait (1983). A culture of *E.coli* was grown until the OD_{600} reached 0.4. Cells were pelleted by centrifugation at 6000 rpm for 10 min at 4ºC. The cell pellet was resuspended in 30 ml of pre-chilled TFB1 solution [Composition: 30mM potassium acetate, 10mM CaCl2, 50mM $MnCl_2$, 100mM RbCl, 15% glycerol. pH adjusted to 5.8 with 1M acetic acid. Filter sterilized and stored at 4ºC]. The resuspended cells were incubated on ice for 15 minutes at 4°C and centrifuged again at 6000 rpm for 10 min at 4ºC. The cells was resuspended in 4 ml of ice-cold TBFII solution [Composition: 100mM MOPS (pH 6.5), 5mM $CaCl_2$, 10mM RbCl, 15% glycerol. pH adjusted to 6.5 with 1M KOH. Filter

sterilized and stored at 4ºC]. Cells were dispensed in aliquiots, quick frozen in liquid nitrogen and stored at – 80 ºC.

For transforming reaction, 50-500 ng of plasmid DNA or ligated DNA fragments were added to a 100 µl aliquot of competent cells and incubated for 30 min. Tubes were transferred from ice to a 42°C water bath, heat-shocked for 2 min and place on ice immediately to cool for 5 minutes. 1ml of LB medium was added and incubated for 1 hour at 37ºC with shaking (~150 rpm). 100-200 µl of the transformation mix was plated and onto selection plates and incubated overnight at 37ºC.

M.6.2 Plasmid conjugation between *E.coli* and *S.meliloti* strains

Plasmids were mobilized from *E.coli* to *S.meliloti* strain by tri-parental conjugation, using the helper plasmid pRK2013 (Ditta *et al.*, 1980) for *trans*-complementation. A loopful of bacteria from each fresh plate was mixedtogether on a TY plaque without antibiotics and incubated at 28ºC for 12-16 hours. The mix was then streaked onto MM medium with the appropriate antibiotics and incubated until the appearance of *S.meliloti trans*-conjugants colonies (2-3 days). A test of coliform-contaminant colonies were carried out in parallel onto Endo-Agar medium.

M.7 DNA AMPLIFICATION

M.7.1 The Polymerase Chain Reaction (PCR)

Typically, PCR reactions were performed in a final volumen of 25 µl reaction including 10-100 ng of template DNA, 10 pmol of each specific primer, 0.1 mM of each dNTP, 1X reaction buffer and 2 U of DNA polymerase. The DNA polymerases used were AccuPrime Taq DNA Polymerase High Fidelity (Invitrogen), Pfu DNA Polimerasa (Biotools) and Phusion High-Fidelity DNA Polymerase (Finnzymes). Each set of reactions included a negative control consisting of all the reagents but the DNA was replaced with MQ water.

PCR amplifications were performed with an Eppendorf Mastercycler termal cycler. PCR conditions varied depending on the annealing primer temperature. A typical reaction consisted of a denaturing cycle at 94ºC for 5 min, followed by 30 cycles: 30 s at 94 ºC for

denaturation, 30 s at 60 ºC for primer annealing and 30 s at 72ºC for the extension of the polymerase. A final extension step at 72 ºC for 10 min was also performed.

Amplified products were resolved on a 0.8 % agarose gel in TAE buffer and stained with ethidium bromide or RedGel (Biotium, Inc) or purified for later use.

M.7.2 Quantitative real-time RT-PCR

Real-time PCR is bases on the procedure described by (Higuchi *et al.*, 1993). Primers were designed with Primer 3 software (http://fokker.wi.mit.edu/primer3) (Rozen and Skaletsky, 2000) and examined for possible secondary structures with the mfold program (http://www.bioinfo.rpi.edu/applications/mfold) (Zuker, 2003). *lac*Z1 region, RmInt1 intron and ligated β-galactosidase gene *lac*Z were amplified from the pICG-WT plasmid. The sequences of the primers used are summarized in Table M5.

TABLE M5. Primers used in real-time qRT-PCR

Primer	Sequence
1Q_CAT	CAGGAGCTAAGGAAGCTAAAATGG
2QR_CAT	AGGCCGTAATATCCAGCTGAAC
3Q_RIB1	GCGTAAAGCTGCGTGAATGAT
4QR_RIB1	TCCTCGGAGGGTTCACTTT
5Q_CAT	TGTACCTATAACCAGACCGTTCAG
6QR_LACZ	GATGTGCTGCAAGGCGATT

The amplification efficiencies of all the primers were determined with serial ten-fold dilutions of the recombinant pICG-E1E2 and pICG-WT plasmids (Figure M4).

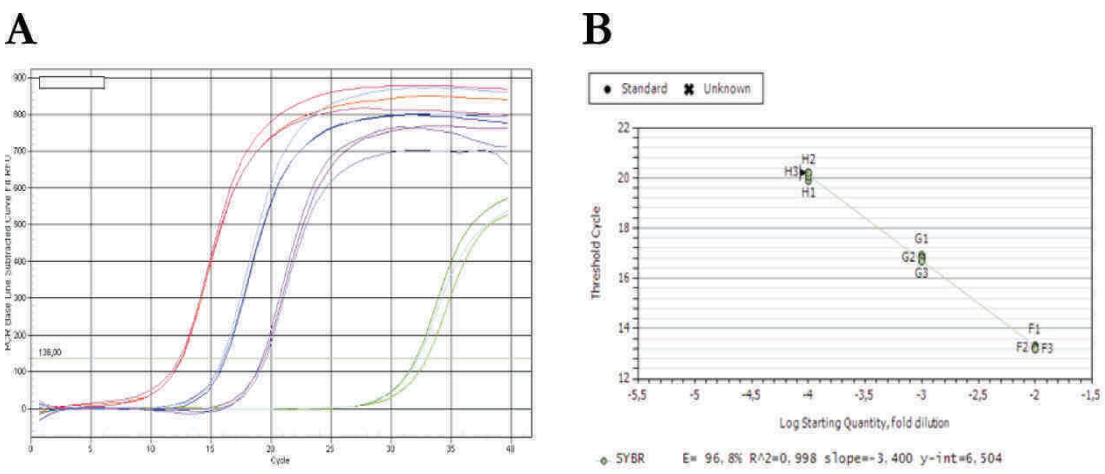

Figure M4. Generation of a standard curve to assess reaction optimization. **A** The standard curve was generated from plasmid DNA of pICG-E1E2 by using primers 1 and 2 and a 10-fold dilution on the iCycler iQ® real-time system. Each dilution was assayed in triplicate. **B** The standard curve generated from plasmid DNA using primers 1 and 2. The C_T is plotted against the log of the starting quantity of template for each dilution. The equation for the regression line and the r value are shown below the graph. The calculated amplification efficiency was 96.8%.

PCR efficiency was high, at 94 to 97.7%, with a high degree of linearity (Pearson correlation coefficient r) (Table M6).

TABLE M6. Real-time PCR assay characteristics

Parameter	Assay value for indicated region		
	*lacZ*1	RmInt1	*lacZ*
PCR efficiency (%)	96.8	103.6	103.8
Melting temp (ºC)	63.5	62.5	63.0
Amplicon length (pb)	149	178	194

The optimal annealing temperature was assessed by testing a range of annealing temperatures above and below the calculated Tm of the primers (Figure M5).

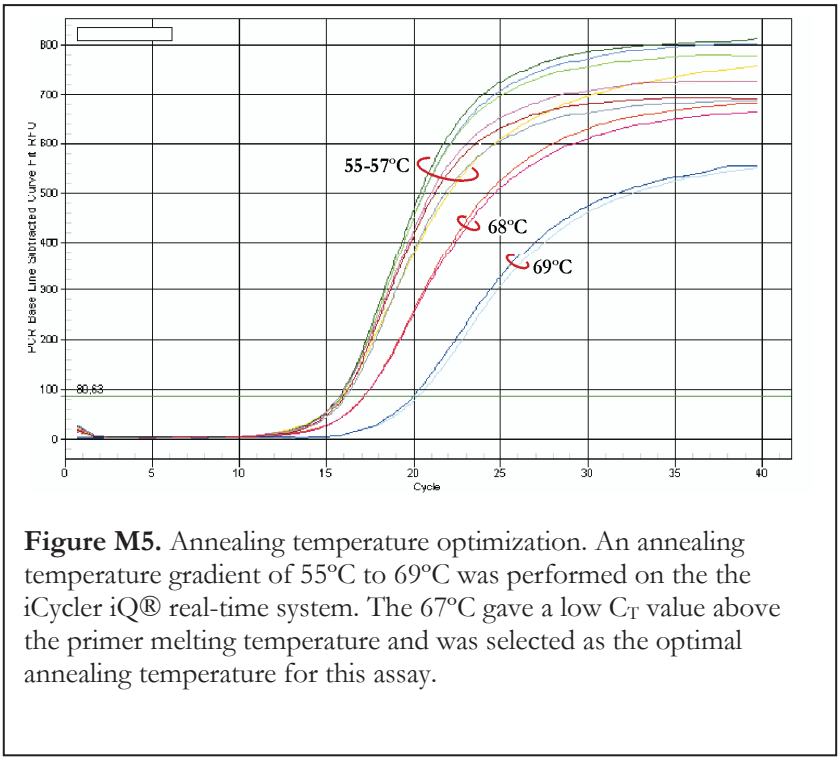

Figure M5. Annealing temperature optimization. An annealing temperature gradient of 55ºC to 69ºC was performed on the the iCycler iQ® real-time system. The 67ºC gave a low C_T value above the primer melting temperature and was selected as the optimal annealing temperature for this assay.

We carried out qRT-PCR on the iCycler System (Bio-Rad). Each reaction was run in triplicate and contained 5 µl of cDNA template (equivalent to 500 ng total RNA), 0.5 mM dNTP, 5 pmol of each oligonucleotide primer, 7.5 mM $MgCl_2$, 2.5 µl of a 1:10,000 dilution of SYBR Green, 2.3 µl of reaction buffer and 0.5 U of Platinum *Taq* DNA Polymerase (Invitrogen), with the final volume made up to 23 µl with DEPC water. The PCR cycling conditions were as follows: hot start, with heating at 94°C for 3 min, followed by 40 cycles of denaturation at 94ºC for 30 s, annealing at 67ºC for 30 s, and extension at 72ºC for 15 s. A melting curve analysis was performed in all PCR runs, to check the identity of the PCR product obtained. Controls without a template were also included. Three independent RNA preparations from each strain were tested.

Absolute mRNA levels were determined, whereas relative quantification was carried out for splicing, based on the $2^{-\Delta\Delta_{CT}}$ method (Livak and Schmittgen, 2001). Differences in relative expression were identified by carrying out Student's t test. Levene's test was used to check that the variances were equal.

M.8 ELECTROFORESIS

M.8.1 Non-denaturing agarose gel electroforesis

Plasmid DNA, PCR products o restriction DNA fragments were resolved by 0.8-2 % agarose gel electrophoresis in TAE buffer (Tris-HCl 40 mM, EDTA Na_2 2 mM, glacial acetic acid 0,1142%(v/v)). 5 µL of PCR product or 2 µL of plasmid DNA or restriction DNA fragments were mixed with 2 µL of loading dye (Orange G 0.50%(w/v), EDTA Na_2 0.01M and 50% Glycerol) and pipetted into the wells. 300 ng of DNA ladder (*Himd*II digested Φ29 phago or *Himd*III and *Eco*RI digested phago λ) was used to determine the size of the PCR products. Gels were stained with ethidium bromide (1 mg/ml) or 2% RedGel (Biotium, Inc). The stained gel was visualised under UV light in a Bio-Rad Gel Doc 2000 transilluminator. Images were captured, cropped, and printed with Gel Doc software version 4.3.1.

M.8.2 Denaturing agarose gel electroforesis

Total RNA was resolved by 1.4 % agarose gel electrophoresis in MOPS buffer (3-(N-morpholino)propanesulfonic acid) and 0.05 % (v/v) formaldehyde. 1 µl of total RNA

was mixed with 4 µl of MQ water and 2 µl of a solution of 1% RedGel (Biotium, Inc) in loading dye [1.8% sucrose, 1X TBE (Tris-borate EDTA, pH 8.3), 0.018% xylene cyanol, 36% (v/v) formamide and 25 mM EDTA]. The gel was visualised under UV light in a Bio-Rad Gel Doc 2000 transilluminator. Images were captured, cropped, and printed with Gel Doc software version 4.3.1.

M.8.3 Denaturing polyacrylamide gel electroforesis

Single stranded nucleic acids were resolved by 8 M urea 5-6 % bisacrylamide (Acribis 40%, acrilamyde:bisacrylamide (29:1), Amresco) gels in TBE buffer (Tris-HCl 0,089 M pH 8, Boric Acid 0,089 M and EDTA 0,002 M). For every 100 ml of gel casting solution, 40 µl of TEMED and 0.6 ml of freshly prepared 10 % Ammonium Persulfate were added. Samples were mixed with 2X loading dye [1.8% sucrose, 1X TBE (Tris-borate EDTA, pH 8.3), 0.018% xylene cyanol, 36% (v/v) formamide and 25 mM EDTA]. The gel was run in a vertical electrophoresis system in TBE buffer at 20-45 W. Gels were dried in a *Gel Dryer® 583* (Bio-Rad) and exposed in phosphorus plates (*Imagin Plate 2040*, Fujifilm). The image was captured after 24-48 hours with the laser scanning system *Personal Molecular Imager® FX* and edited with the software *Quantity One®* Bio-Rad).

M.9 NUCLEIC ACIDS HYBRIDIZATION

M.9.1 DNA-DNA Hybridization (Southern Blotting)

This procedure, based on that of (Southern, 1975; Southern, 1979), was used in mobility assays of RmInt1 intron. DNA restriction fragments were separated in a 0.8 % agarose gel at 20-35 V for 17-20 hours. For partial fragmentation of large DNA fragment prior to transfer, the gel was left under UV light for 30 min. DNA was blotted onto a 20X SSC (1xSSC: NaCl 150 mM, sodium citrate 15 mM, pH 7,0) prewet nylon filter (Biodine) by means of a denaturing (NaOH) vacuum system (VacuGene® de Pharmacia).

Membranes were hybridized with a digoxigenin-11-dUTP-labelled probe (0.1M) that was diluted down to 60 ng DNA/ml in prehybridization buffer [5xSSC, 0.1% sarkosyl, 0.02%SDS, 50% formamide and 2% blocking reagent (Roche)]. The membrane was incubated in a hybridization oven *Hybridiser HB-1D* (Techne) at 42ºC for 20-24 h.

The membrane was soaked twice for 5 minutes each with 50 ml of 0.1 % (w/v) 2X SSC/SDS at room temperature, followed by soaking twice for 15 min each with 0.1 % (w/v) 0.1X SSC/SDS at 68ºC and finally, soaking with washing buffer for 5 min at room temperature [0,3% Tween-20 in buffer 1 (0.1 M malic acid, 0.15 M NaCl, pH 7,5)].

After washing, the membrane was blocked with buffer 2 [1% (p/v) Blocking Reagent in buffer 1] for 30 min at room temperature and incubated with a 1:10000 dilution of an anti-digoxigenin-AP (Roche) antibody-conjugate for 30 min. To remove unbound antibody-conjugate, the membrane was washed twice for 15 min with washing buffer and equilibrated with buffer 3 [0.1 M Tris-HCl, 0.1 M NaCl, 50 mM $MgCl_2$ pH 9,5]. The chemiluminescent CSPD substrate (Roche) was diluted in buffer 3 and incubated with the blot for 5 min at room temperature. The blot was tranferred onto a plastic report cover and incubated for 15 min at 37ºC. Finally, the membrane was exposed to film for 4-5 hours (short exposition) or 18-20 (long exposition).

M.9.2 RNA-DNA hibridization (Northern Blotting)

This technique, described sby (Alwine *et al.*, 1979), was used for the *in vitro* analysis of splicing products. 5 μg of *S.meliloti* total cellular RNA was subjected to electrophoresis in a denaturing 6% polyacrylamide gel (8M urea) and blotted onto a nylon filter (Biodine) in a TE 77 PWR Semi-Dry (GE Healthcare) transfer unit according to the manufacturer's recommendations. The membrane was baked at 80ªC for 1 hour.

Probes used in Northern hydridization (Table M7) were radiolabeled in a final volume of 10 μl containing 75 pmol of the oligonucleotide, 20 μCi of [γ-^{32}P]ATP (3000 Ci/mmol; 10 μCi/μl; PerkinElmer) and 10 U of T4 polynucleotide (New England Biolabs), at 37ºC, for 2 h, and the labeling mixture was then passed through Sephadex G-25 columns (GE Healthcare) for probe purification. The membrane was hybridized with about 20,000 cpm of probe/ml overnight at 42ºC.

TABLE M7. Probes used in Northern Blotting assay

Probe	Localization	Sequence
1Q_CAT	5' exon	CAGGAGCTAAGGAAGCTAAAATGG
3Q_RIB1	Intron	GCGTAAAGCTGCGTGAATGAT

	Transcription	GATCCACAGGGATAAAAAAAGCAGCACT
3OR_ter	terminator	GTAATCAGTGCTGCTTTGTCGTTTTTTCA
	(3' exon)	CCTAGGG

The blot was washed by soaking three-fold for 15 min each with 100 ml of 2X SSC/0.1% SDS, 1X SSC/0.1% SDS and 0.1X SSC/0.1% SDS at 42ºC. Finally, the blot was placed against a phosphor screen, for visualization of the bands with the Personal Molecular Imager FX scanner and Quantity One software (BioRad).

M.10 MOBILITY ASSAY (HOMING) OF RmInt1 INTRON

In vivo homing efficiency of RmInt1 intron from pICG plasmids was determined by the double-plasmid assay in *S.meliloti* strain RMO17 using pICG-WT as donor plasmids and pBB0.6 (bearing the intron target sequence) or pBBΔ129 (negative control lacking the intron target sequence) (Martínez-Abarca *et al.*, 2000) as recipient plasmids. *Trans*-conjugants were selected in minimal medium supplemented with antibiotics and the plasmid DNA extracted, digested with *Xba*I restriction enzyme and resolved in a non-denaturing 0.8 % agarose gel. DNA fragments were then transferred to a nylon membrane.

Mobility events were assessed by DNA hybridization analysis carried out using PCR-amplified probes. Primers used in the PCR reaction are listed in Table M7.

TABLE M8. Primers used to amplify probe oligonucleotides

Primer	Sequence	Probe	Ref.
2011-b1	TGGACGAAGACGAACATGG	3' exon of *IS*2011-2 (+3,+466 positions)	(Martínez-Abarca *et al.*, 2000)
2011-b2	TTGAAGTAGGCTGCGCATT		
ε1	GTGAGCGTCGGATGAAAC	RmInt1 intron (147-594 positions)	
18R.0	ACGTTTCTCAATTCGAAACG		

The homing efficiency was calculated as the percentage of the ratio of homing product to the addition of homing product and non-invaded recipient plasmid, following formulas:

$$Homing\ efficiency = \frac{Invaded\ recipient\ plasmid}{Invaded\ recipient\ p. + non - invaded\ recipient\ p.} x100$$

Images were edited with the software *Quantity One* Bio-Rad).

M.11 β-GALACTOSIDASE ASSAY

This assay was used for the determination of the expression level of the ligated β-galactosidase gene *lac*Z in pICG constructs. β-galactosidase assays were performed as described by Miller (Miller, 1972). Briefly, overnight cultures of *E. coli* grown at 28ºC and 37ºC and of *S. meliloti* grown at 28ºC were diluted 1:50 in fresh LB and TY medium, respectively, and incubated until the cultures reached the exponential growth phase (OD_{600} = 0.6). Cultures were then cooled on ice for 20 minutes and bacterial density was recorded by measuring optical density at 600 nm. We then added aliquots of 10 µl to 300 µl of bacteria to the assay Z buffer containing 60 mM Na_2HPO_4, 40 mM NaH_2PO_4, 10 mM KCl, 1 mM $MgSO_4$ and 50 mM β-mercaptoethanol and adjusted the pH to 7. We added 50 µl of chloroform and 25 µl of 0.1% SDS to the sample-buffer mixture, which we then vortexed for 30 seconds. The samples were incubated at 28ºC for 5 minutes and the reaction was then started by adding 0.2 ml of o-nitrophenyl-β-D-galactopyraniside (ONPG) (4 mg/ml) (Fluka). The reaction was allowed to proceed for 10 minutes and was then stopped, by adding 0.5ml of a 1 M Na_2CO_3 solution. Samples were centrifuged for two minutes to eliminate cell debris and absorbance was recorded at 420 nm. The results are expressed in Miller units, following formulas:

$$\beta - Galactosidase\ Activity\ (U) = \frac{1000 \times DO_{420}}{t \times V \times OD_{600}}$$

where *t* is the reaction time expressed in minutes and *V* is the volumen of reaction expressed in milliliters.

M.12 PRIMER EXTENSION ASSAY

This procedure was initially described by (Boorstein and Craig, 1989) and later modified by (Marques *et al.*, 1993) was used for the detection of the excised intron products derived of the splicing reaction. The primer annealing mixture contained 20 mg

of total RNA in 10 mM Pipes (pH 7.5), 400 mM NaCl and 0.2 pmol (300,000 cpm) of (5'-^{32}P)-labeled primer P, complementary to nucleotides 90 to 87 of the RmInt1 intron sequence (TGA AAG CCG ATC CCG GAG). The mixture (10 μl) was first heated at 85 ºC for five minutes, then incubated at 60 ºC for three minutes and cooled slowly to 44 ºC. Extension reactions were started by adding 40 ml of 50 mM Tris–HCl (pH 8.0), 60 mM NaCl, 10 mM DTT, 6 mM magnesium acetate, 1 mM each of all four dNTPs, 60 mg/ml of actinomycin D (Sigma), two units of RNaseOUT (Invitrogen) and seven units of AMV RT (Roche). Reaction mixtures were incubated at 44 ºC for 60 minutes. The reaction was stopped by adding 5 ml of 3 M sodium acetate (pH 5.2) and 150 ml of cold ethanol. Half of each sample was analyzed on a denaturing (8 M urea) 6% (w/v) polyacrylamide gel.

M13. *IN VITRO* SPLICING ASSAYS

M.13.1 RNA synthesis and purification

The LT1 transcript (911 nt)(see Figure R3.3) was synthesized from plasmid pLM1 (see Section M3.3 and Figure R3.3), after digesting with *Bam*HI restriction enzyme. The LT2 transcript (908 nt)(see Figure R3.3) was synthesized from pLM2 (see Section M3.3 and Figure R3.3) linearized with *Nde*I restriction enzyme, while the ST2 transcript (775 nt) (see Figure R3.3) was synthesized from the same plasmid linearized with *Bam*HI enzyme (see Section M3.3 and Figure R3.3).

T7 RNA polymerase transcriptions were performed in presence of 4μg of linearized plasmid, 1X transcription buffer [10X transcription buffer: 1M $MgCl_2$, 1M Tris-HCl pH7.5, 2M spermidine, 1M DTT], 0.96mM ATP, 0.96mM CTP, 0.96mM UTP, 0.064mM GTP, 50 μCi of [α-^{32}P]GTP (3000 Ci/mmol; 10 mCi/ml; PerkinElmer), 10mM DTT, 80 U of RNAseOUT (Invitrogen) and 3 μl of T7 RNA polymerase in a final volume of 50 μl (Pyle and Green, 1994) (See Section M.X). Transcription was stopped after 1.5 hours at 37ºC by adding an equal volume of gel loading dye (10 M urea, 0.1% (w/v) xylene cyanol and bromophenol blue dyes, 40 mM Tris (pH 7.5), 8.3% (w/v) sucrose, and 0.83 mM EDTA, final concentrations) and then loading directly on a 5% (w/v) denaturing (7M urea) polyacrylamide gel.

Following electrophoresis, the band was visualized by autoradiography for ten minutes, excised from the gel, and eluted for 3 hours in elution buffer (0.3M NaCl, 10mM MOPS pH6, 1Mm EDTA, final concentrations). RNA was then isolated by ethanol precipitation of the eluate (three volumes of 100% ethanol and 40μg of Glycogen

(Roche)). The RNA was dried and resuspended in 30µl of RNA storage buffer (10mM MOPS pH6, 1mM EDTA, final concentrations).

M.13.2 *S*elf-splicing reaction

The splicing reactions were performed using a total volume of 40 µl. The precursor RNA (150000 to 300000 cpm) was preincubated in 80 mM MOPS buffer pH 7.5 at 95°C for one minute. The RNA sample was then allowed to cool to reaction temperature before combining with 500mM KCl or 500mM $(NH_4)_2SO_4$ (final concentrations) monovalent salts. Reactions were initiated by adding 100mM $MgCl_2$ (final concentration) and incubated at 42 ºC (for KCl-containing reactions) or 50 ºC (for $(NH_4)_2SO_4$-containing reactions).

To perform timecourses, aliquots (1–2 µl) were removed at the indicated timepoints, added to quench buffer (1.8% sucrose, 1X TBE (Tris-borate EDTA, pH 8.3), 0.018% xylene cyanol dye, 36% (v/v) formamide, and 25 mM EDTA) and placed on ice to stop the reaction. Samples were then loaded onto a 5% denaturing polyacrylamide gel and products were resolved by electrophoresis. The gels were dried and exposed to phosphorus plates (Imaging Plate *2040*, Fujifilm). The image was captured after 24-48 hours with the laser scanning system Personal Molecular Imager FX and quantified with the software Quantity One (Bio-Rad).

In preparative-scale self-splicing reactions for product isolation, the total volume of transcript synthesized were loaded onto a preparative (0.750 mm thick) 5% denaturing polyacrylamide gel and products were resolved by electrophoresis. The wet gel was exposed in phosphorus plates for 10-15 minutes, after which they were scanned. The captured image was used as a template for cutting bands which were eluted for 3 hours in elution buffer (0.3M NaCl, 10mM MOPS pH6, 1Mm EDTA) and ethanol precipitated (three volumes of 100% ethanol and 40µg of Glycogen (Roche)). The RNA was dried and resuspended in an appropriate volume of RNA storage buffer (10mM MOPS pH6, 1mM EDTA).

M.13.3 Identification of splicing products by DNAzyme treatment

Purified self-splicing product RNA was combined with DNAzyme (about 40 µM final concentration) (Table M8), heated at 95 ºC for 2 min for denaturation and then placed on ice for 5 min. The reaction was initiated by adding the reaction buffer [5X: 250 mM $MgCl_2$, 750 mM NaCl, 200 mM Tris-HCl pH8] and incubating at 37 ºC for 2 hours.

The reaction stopped by adding an equal volume of quench buffer (1.8% sucrose, 1X TBE (Tris-borate EDTA, pH 8.3), 0.018% xylene cyanol dye, 36% (v/v) formamide, and 25 mM EDTA). Samples were resolved by PAGE and the gel dried and exposed for 24-48 hours in phosphorus plates (Imaging Plate 2040, Fujifilm). The image was revealed by the laser scanning system Personal Molecular Imager FX and quantified with the software Quantity One (Bio-Rad).

TABLE M9. Sequences of DNAzymes used in this work

DNAzyme	Sequence[1]
DZ1	5' – gttcatgttgaa GGCTAGCTACAACGA tccttccgtgc
DZ2	5' – cgttcataacga GGCTAGCTACAACGA gcgtcctcg
DZ3	5' – gtgaaagccta GGCTAGCTACAACGA gtccaactcac
DZ4	5' – ctgcatcggta GGCTAGCTACAACGA tctcgccttg
DZ5	5' – ctctcgcagaa GGCTAGCTACAACGA ggtgcgtgaa
DZ6	5' – gaggagtttca GGCTAGCTACAACGA cagccggc

[1] Upper-case letters indicate the catalytic core; lower-case letters indicate left and right base-pairing arms.

M.13.4 Quantitative analysis of splicing reactions

Individual bands on autoradiographic images were quantified with the software Quantity One (Bio-Rad). Counts from a nearby blanck position on the same lane were substracted as an internal measure of background RNA degradation at each timepoint. The resulted adjusted bands were normalized for decreasing counts with respect to precursor at time t=0. Finally, the relative fractions of precursor and products were calculated and corrected for the guanidine-content of each species.

Fractions of precursor and products were plotted against time. The rate constant of the overall reaction (k_I) was calculated from the decrease of precursor, which follows a single exponential behavior, incorporating the next expression into the Kaleidagraph program (Abelbeck Software):

(1) $$[Pr]_t = [Pr]_0 \cdot e^{-k_I t}$$

where: $[Pr]_t$ is the amount of precursor molecules at any time (t); $[Pr]_0$ is the amount of precursor molecules at time t=0 and; k_T is the total rate of reaction.

In time courses carried out in KCl, where a unique population of molecules reacted through hydrolytic pathway (see Section R3.5, Scheme 4), equation (1) was enough for deciphering the hydrolytic rate constant. However, in times courses carried out in $(NH_4)_2SO_4$ buffer, where both branching and hydrolytic pathways are observed, branching (k_{br}) and hydrolytic (k_{hy}) rates were extracted using a parallel kinetic model for simultaneous branching and hydrolysis reactions. First, fractions of lariat and linear products were determined from the fit of product evolution, following the equations (2) and (3):

(2) $$[PLin]_t = [Pr]_0 \cdot f_{hy}(1 - e^{-k_t t})$$

(3) $$[PLar]_t = [Pr]_0 \cdot f_{br}(1 - e^{-k_t t})$$

where: $[PLin]_t$ is the total amount of molecules that proceeds from hydrolytic pathway at any time (t); [PLar]t is the total amount of molecules that proceeds from branching pathway at any time (t); f_{hy} is the fraction of linear products and; f_{br} is the fraction of lariat products. Second, the hydrolytic (k_{hy}) and branching (k_{br}) rates were solved from equations (4) and (5):

(4) $$k_{hy} = \frac{f_{hy}}{f_{hy}+f_{br}} \cdot k_T$$

(5) $$k_{br} = \frac{f_{br}}{f_{hy}+f_{br}} \cdot k_T$$

where: k_{hy} is the individual rate of hydrolytic pathway; k_{br} is the individual rate of branching pathway and where $k_T = k_{hy} + k_{br}$. It is also correct that $f_{hy} + f_{br} = 1$, but it is more accurate to use individual values for f in the denominator of equation (4) and (5) and not assume that reactions go to completion. The parallel model was verified by the fact that k_T value obtained from either product evolution or substrate decay were nearby the same, and that the sum of f_{hy} and f_{br} approached 1.

In order to dissect the branching and hydrolytic pathways under $(NH_4)_2SO_4$ buffer, and calculate all the rate constants, data were fit to equations, which varied depending on the transcript used. In LT1 transcripts (see Section R3.5, Scheme 1), which all products emerged independently and simultaneously from the precursor, following parallel first-order kinetics, the equations that described this reaction were:

(6) $$[Pr]_t = [Pr]_0 \cdot e^{-(k_1+k_2+k_3)t}$$

(7) $$[ILar - E2*]_t = [Pr]_0 \cdot \frac{k_1}{k_1+k_2+k_3} \cdot \left[1 - e^{-(k_1+k_2+k_3)}\right] =$$

$$= [Pr]_0 \cdot f_{ILar-E2*} \cdot \left[1 - e^{-(k_1+k_2+k_3)}\right]$$

(8) $$[ILar]_t = [Pr]_0 \cdot \frac{k_2}{k_1+k_2+k_3} \cdot \left[1 - e^{-(k_1+k_2+k_3)}\right] =$$

$$= [Pr]_0 \cdot f_{ILar} \cdot \left[1 - e^{-(k_1+k_2+k_3)}\right]$$

(9) $$[PLin]_t = [Pr]_0 \cdot \frac{k_3}{k_1+k_2+k_3} \cdot \left[1 - e^{-(k_1+k_2+k_3)}\right] =$$

$$= [Pr]_0 \cdot f_{PLin} \cdot \left[1 - e^{-(k_1+k_2+k_3)}\right]$$

where $[Pr]_t$, $[Ilar\text{-}E2*]_t$, $[Ilar]_t$ and $[PLin]_t$ represent the amount of molecules of the precursor, lariat/3'-exon intermediate, intron lariat and linear products at any time, respectively; k_i, each rate constant indicated in Scheme 1 and f_i, the fraction of molecules reacting in each pathway.

In LT2 transcripts (see Section R3.5, Scheme 2), which followed a parallel-sequential kinetic model, the equations that described this reaction were:

(10) $$[Pr]_t = [Pr]_0 \cdot e^{-(k_1+k_3)t}$$

(11) $$[ILar - E2]_t = [Pr]_0 \cdot \frac{k_1}{k_2-(k_1+k_3)} \cdot \left[e^{-(k_1+k_3)t} - e^{-k_2 t}\right]$$

(12) $$[ILin]_t = [Pr]_0 \cdot \frac{k_3}{k_1+k_3} \cdot \left[1 - e^{-(k_1+k_3)}\right]$$

(13) $$[ILar]_t = [Pr]_0[1 - [Pr]_t - [ILar - E2]_t - [ILar]_t]$$

where $[Pr]_t$, $[Ilar\text{-}E2]_t$, $[Ilar]_t$ and $[ILin]_t$ represent the amount of molecules of the precursor, lariat/3'-exon intermediate, lariat intron and linear intron at any time, respectively and; k_i, each rate constant indicated in Scheme 2.

In ST2 transcripts (see Section R3.5, Scheme 3), which followed a parallel-sequential kinetic model, the equations that described this reaction were:

(14) $$[Pr]_t = [Pr]_0 \cdot e^{-(k_1+k_4)t}$$

(15) $$[ILar - E2]_t = [Pr]_0 \cdot \frac{k_1}{(k_2+k_3)-(k_1+k_4)} \cdot \left[e^{-(k_1+k_4)t} - e^{-(k_2+k_3)t}\right]$$

(16) $$[ILar]_t = [Pr]_0 \cdot \frac{k_1}{k_3-(k_1+k_4)} \cdot \left[e^{-(k_1+k_4)t} - e^{-k_3 t}\right] - [ILar - E2]_t$$

(17) $$[Unk]_t = [Pr]_0 \cdot \frac{k_1}{k_2-(k_1+k_4)} \cdot \left[e^{-(k_1+k_4)t} - e^{-k_2 t}\right] - [ILar - E2]_t$$

(18) $$[ILin - E2]_t = [Pr]_0 \cdot \frac{k_4}{k_5-(k_1+k_4)} \cdot \left[e^{-(k_1+k_4)t} - e^{-k_5 t}\right]$$

(19) $$[ILin]_t=[Pr]_0[1 - [Pr]_t - [ILar - E2]_t - [ILar]_t] - [Unk]_t - [ILin - E2]_t$$

where $[Pr]_t$, $[Ilar\text{-}E2]_t$, $[Ilar]_t$, $[Ilin\text{-}E2]_t$, $[ILin]_t$ and $[Unk]_t$ represent the amount of molecules of the precursor, lariat/3'-exon intermediate, lariat intron, linear/3'-exon intermediate , linear intron and an unknown covalently circular RNA (see section R3.3 for a description) at any time, respectively and; k_i, each rate constant indicated in Scheme 3.

In order to dissect the hydrolytic pathway under KCl buffer, and calculate all the rate constants, data from LT1 (see Section R3.5, Scheme 4) and LT2 (see Section R3.5, Scheme 5) were fit to first order single exponential equations:

(20) $$[Pr]_t = [Pr]_0 \cdot e^{-k_4 t}$$

(21) $$[PLin]_t/[ILin]_t = [Pr]_0 \cdot (1 - e^{-k_4 t})$$

where $[Pr]_t$, $[PLin]_t$ and $[ILin]$ represent the amount of molecules of the precursor, total products reacting through the hydrolytic pathway and the intron linear at any time, respectively and; k_4, the global rate constant of the hydrolytic reaction, as shown in Schemes 4 and 5.

In ST2 transcripts (see Section R3.5, Scheme 6), which followed a parallel-sequential kinetic model, the equations that described this reaction were:

(22) $$[Pr]_t = [Pr]_0 \cdot e^{-(k_4+k_6)t}$$

(23) $$[ILin - E2]_t = [Pr]_0 \cdot \frac{k_4}{k_5-(k_4+k_6)} \cdot \left[e^{-(k_4+k_6)t} - e^{-k_5 t}\right]$$

(24) $$[ILin]_t = [Pr]_0[1 - [Pr]_t - [ILar - E2]_t]$$

where $[Pr]_t$, $[Ilin\text{-}E2]_t$ and $[ILin]_t$ represent the amount of molecules of the precursor, linear/3'-exon intermediate and linear intron at any time, respectively and; k_i, each rate constant indicated in Scheme 6.

All the rate constants calculated were also verified by an independent fitting by nonlinear least-squares regression using the Dynafit software (Biokin). The variation coefficients associated to rate constants were less than 10 % in all cases, and the values differed in less than 1.5-fold from those calculated from equations above.

RESULTS

CHAPTER 1

CHAPTER 1: DESIGN OF A REPORTER SYSTEM FOR THE QUANTIFICATION OF EXON LIGATION DURING THE IN VIVO SPLICING OF RMINT1 INTRON

R1.1 BACKGROUND

Traditionally, the study of the *in vivo* splicing of RmInt1 has been focused on the detection of the excised form of the intron (Muñoz-Adelantado *et al.*, 2003; Molina-Sánchez *et al.*, 2006; Nisa-Martínez *et al.*, 2007; Molina-Sanchez *et al.*, 2010). This fact has led up to a major development of tools aimed to fulfill this goal while resting attention to approaches pointing to the detection of ligated exons as a measure of splicing efficiency.

Until date, plasmid systems used in the study of the *in vivo* splicing of RmInt1 intron were derivatives of the broad-host-range vector pBBR1MCS, a vector compatible with IncP, IncQ and IncW group plasmids, as well as with ColE1- and P15a-based replicons (Kovach *et al.*, 1994; Kovach *et al.*, 1995). In order to obtain plasmids that constitutively expressed a functional RmInt1, intron derivatives containing the kanamycin promoter from pKG10 plasmid (M. J. Soto, unpublished results), were constructed: pKG2.5 and its derivatives (Martínez-Abarca *et al.*, 2000), containing the full-length intron and; pKGEMA4 and its derivatives, based on ΔORF constructs complemented with the *I*ntron *E*ncoded *P*rotein (IEP) located upstream or downstream of its ribozyme counterpart (Nisa-Martínez *et al.*, 2007). Furthermore, in the construction of pKGEMA4, the context of long exons flanking the RmInt1 intron (-175/+466) from the insertion sequence IS*2011-2* was replaced with a variant of short exons (-20/+5), shown to allow efficient homing of RmInt1 into DNA *in vivo* (Jiménez-Zurdo *et al.*, 2003; Nisa-Martínez *et al.*, 2007) and because long exons has been postulated to promote inactivation of group II ribozyme constructs (Nolte *et al.*, 1998; Costa *et al.*, 2006a).

To evaluate the exon ligation extent during the *in vivo* splicing of RmInt1 intron, a new plasmid vector carrying a reporter system to monitor the splicing events was needed. For that reason, the pICG series of plasmids were created.

R1.2 DESIGN OF A GENETIC ASSAY BASED ON A *lacZ* GENE REPORTER SYSTEM FOR THE EVALUATION OF THE RmInt1 GROUP II INTRON SPLICING EFFICIENCY

We developed a splicing reporter system by linking the splicing of RmInt1 to the constitutive expression of the *lac*Z gene in pICG plasmids. Previous studies with reporter genes have been carried out for other group II introns, like the *L.lactis* Ll.ltrB expressed in *E.coli* (Singh *et al.*, 2002) and group I introns (Mercure *et al.*, 1997; Hong *et al.*, 2008). Other

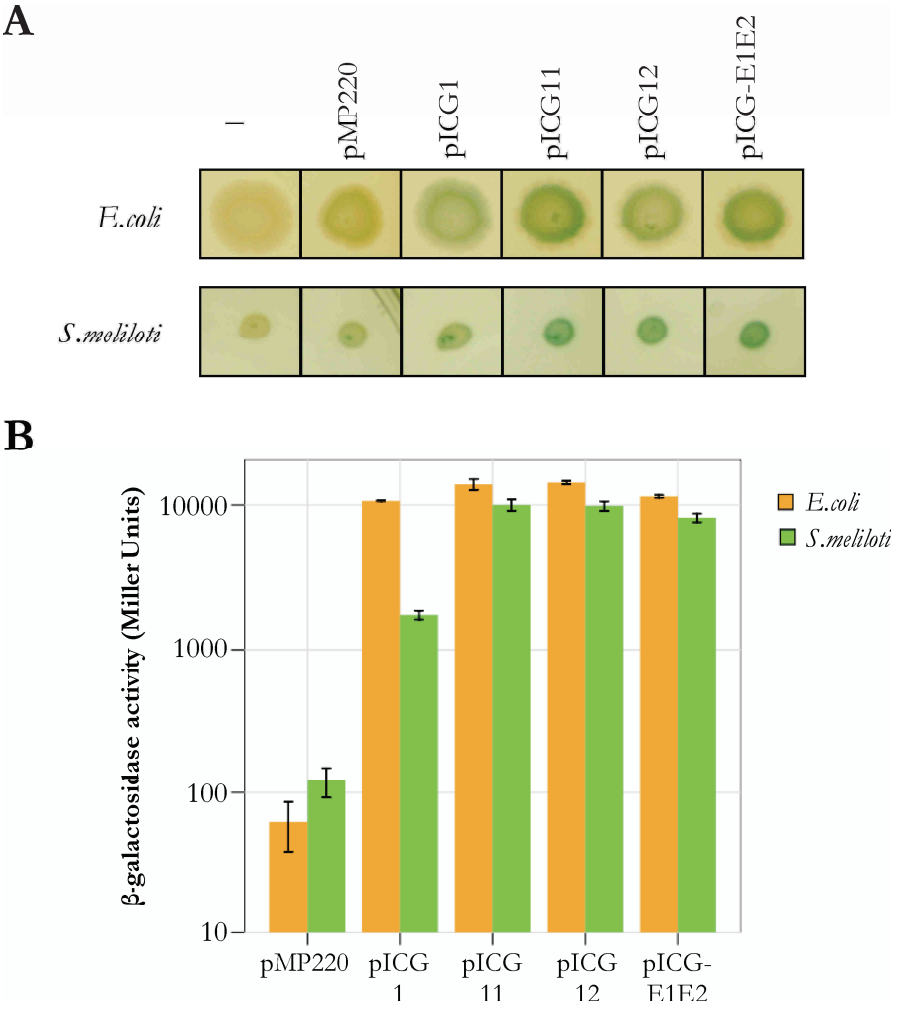

Figure R1.1. β-Galactosidase activity of *lacZ* gene in pICG constructs carrying the pSyn promoter. **A** On-plate blue-white discrimination of constructions expressing β-galactosidase protein. Cells from saturated cultures of *E.coli* and *S.meliloti* strains were plated on LB and TY medium, respectively, containing X-Gal (40 mg/l). *E.coli* DH5α and *S.meliloti* RMO17 cultures harboring no plasmid were used as *lac*⁻ controls. **B** Miller assay of the intronless construct pICG-E1E2 and its precursors. Cultures were grown until exponential-phase and assayed for β-galactosidase activity by adding ONPG (ortho-Nitrophenyl-β-galactoside) (see Material and Methods). *E.coli* DH5α and *S.meliloti* RMO17 cultures were used as background measures of β-galactosidase activity. Error bars represent the standard error of the mean.

screenable markers, such as the GFP gene, have also been used in other group II introns (Cui *et al.*, 2004; Rawsthorne *et al.*, 2006; Gu *et al.*, 2010).

pICG plasmids are derivative of pMP220, an Inc-P broad host range transcriptional fusion vector, designed to measure transcriptional activity as β-galactosidase activity starting from a promoter cloned in the multicloning site (Spaink *et al.*, 1987) (See Figure M1, Material and Methods). pMP220 contains the *E.coli lacZ* gene, which constitutes the reporter marker, lacking the *lac* promoter and operator. Moreover, the *lacZ*

gene derived of the pMP220 vector was devoid of the first eight codons, which are not essential for enzymatic activity (Casadaban *et al.*, 1980); instead, 57 amino-acid residues of the fragment containing the ribosome binding site derived of the chloramphenicol acetyl transferase gene (CAT) were added in the 5' end of the *lac*Z gene to ensure a efficient translation of transcripts (Spaink *et al.*, 1987). The use of pMP220 as the basis for the pICG system allowed us, on the one hand, the analysis of the splicing of RmInt1 in its natural host, *S.meliloti,* as well as in *E.coli*, due to its wide-ranging specificity of DNA replication initiation at origin and; on the other hand, because it could coexist with pBBR1MCS-derived plasmids (Kovach *et al.*, 1994; Kovach *et al.*, 1995) in *E.coli* and *S.meliloti* or with pBR322-derived plasmids (Bolivar, 1978) in *E.coli*, allowing assays of complementation *in trans.*

pICG1 was constructed by cloning the synthetic promoter pSyn (Giacomini *et al.*, 1994) in the polylinker of pMP220. This promoter presented a consensus in the region from -50 to +5 with respect to the putative *tsp* (transcription start point) (+1) from known *E.coli* promoter sequences. Besides, the -35 (TTGACA) and -10 (TATAAT) regions were

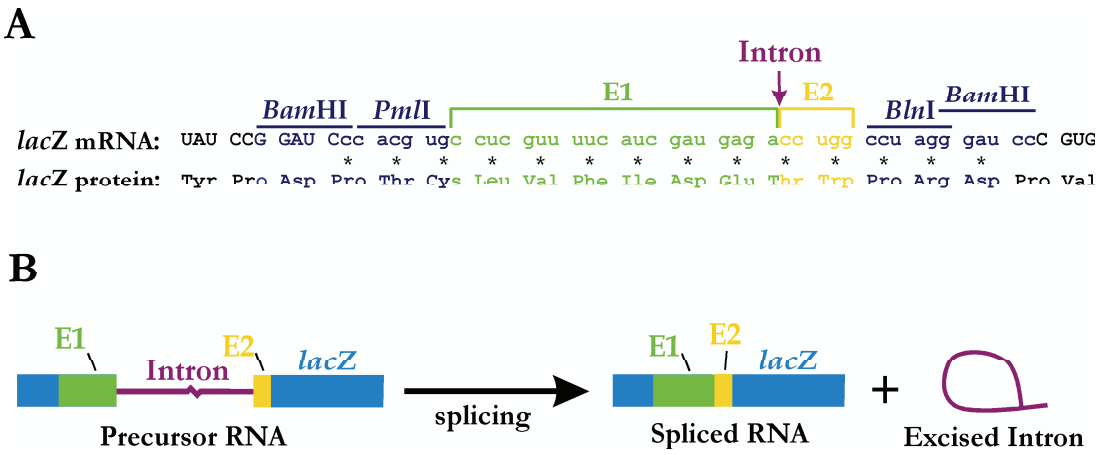

Figure R1.2. Strategy used in the construction of a genetic assay for the splicing of RmInt1 linked to the expression of β-galactosidase protein. **A** Schematic diagram of the nucleotide sequence of the *lac*Z mRNA in pICG-E1E2 and the ligated exons resulting from RmInt1 splicing, presented with the corresponding amino-acid sequence. This region consists of 42 nucleotides, including 25 nucleotides corresponding to the IS*m2011-2* flanking exons and 17 corresponding to the additional *Pml*I, *Bln*I and *Bam*HI cloning sites linked in-frame to the *lac*Z gene. Upper case letters indicate the *lac*Z sequence, whereas lower case letter indicate the exon flanking sequences and restriction sites added. Additional amino acids due to the addition of nucleotides to the residual *lac*Z remaining after intron excision are identified by asterisks. A vertical arrow indicates the site of intron insertion in the intron-containing constructs. **B** A diagram showing splicing of RmInt1 intron linked to the expression of β-galactosidase. Intron splicing leads to the synthesis of a β-galactosidase protein with a short extension (14 amino-acid residues) corresponding to the ligated exons, whereas, in the absence of splicing, translation is terminated due to the presence of multiple stop codons within the intron, giving a *lac*- phenotype.

separated by 17 nt, reported to be the optimal distance (de Boer *et al.*, 1983; Giacomini *et al.*, 1994). pICG1 displayed a constitutive and strong β-galactosidase activity in *E.coli* strain (10680 ± 60 Miller Units), in agreement with previous assays with this promoter (Giacomini *et al.*, 1994), which was 180-fold the activity shown by pMP220 devoid of promoter (Figure R1.1). However, pICG1 expressed in *S.meliloti* host presented an 84% reduction in β-galactosidase activity with respect to the same construction expressed in *E.coli*, which is clearly perceptible in the XGal-based colorimetric assay on plate (Figure R1.1 A). This decrease is not well understood, since other related constructions (pICG11 and pICG12, see below), also expressed in *S.meliloti*, showed a similar level of activity than pICG1 expressed in *E.coli*.

pICG11 and pICG12 were removed of repeated *Bln*I and *Bam*HI restriction sites located in the polylinker and after *lac*Z gene, respectively, aimed to keep only one copy of each for cloning purposes. These modifications resulted in an increase in the β-galactosidase activity both in *E.coli* and in *S.meliloti* host (Figure R1.1 B), although no changes were introduced in the *lac*Z gene. However, it is probably that length or sequence modifications in the polilynker could provoke an enhancement of the transcription or translation rates. Again, the β-galactosidase activity was about 1.4-fold greater in *E.coli* than in *S.meliloti*, in both cases.

pICG-E1E2 was the result of the inclusion of the minimal flanking exon sequences (-20/+5 nt length) from the *ISRm2011-2* insertion sequence in the unique *Bam*HI site of pICG12. This intron context has been shown to improve the efficiency of RmInt1 splicing both *in vivo* (Nisa-Martínez *et al.*, 2007) and *in vitro* (Costa *et al.*, 2006a; Costa *et al.*, 2006b). It is not easy to insert intron RNA into reporter genes, because group II intron splicing requires base-pairing between the intron sequences EBS1, EBS2 and EBS3 located in DI and the 5' and 3'-exon sequences IBS1, IBS2 and IBS3 (EBS and IBS indicate exon-binding and intron-binding sites, respectively). We solved this problem by introducing the flanking exon sequences from the *ISRm2011-2* insertion sequence in frame with codon 58 of the *lac*Z gene, making a transcriptional and translational *lac*Z fusion (Figure R1.2 A). The resulting *lac*Z gene was increased by 42 base pairs which corresponded with a short extension of 14 amino-acid residues when translated (Figure R1.2 B), giving a fusion β-galactosidase protein with high hydrolase activity (Fig R1.1 B). Although a significant reduction in activity was revealed from the Miller assay in pICG-E1E2 construction with respect to pICG12 (about 20 % less β-galactosidase activity both in *E.coli* and *S.meliloti*, likely due to the elongation of the N-terminal end of the protein), the level of expression was about 8000 Miller Units, so it was considered to be active enough for being the basis for the rest of pICG constructs (Fig R1.1 B).

A

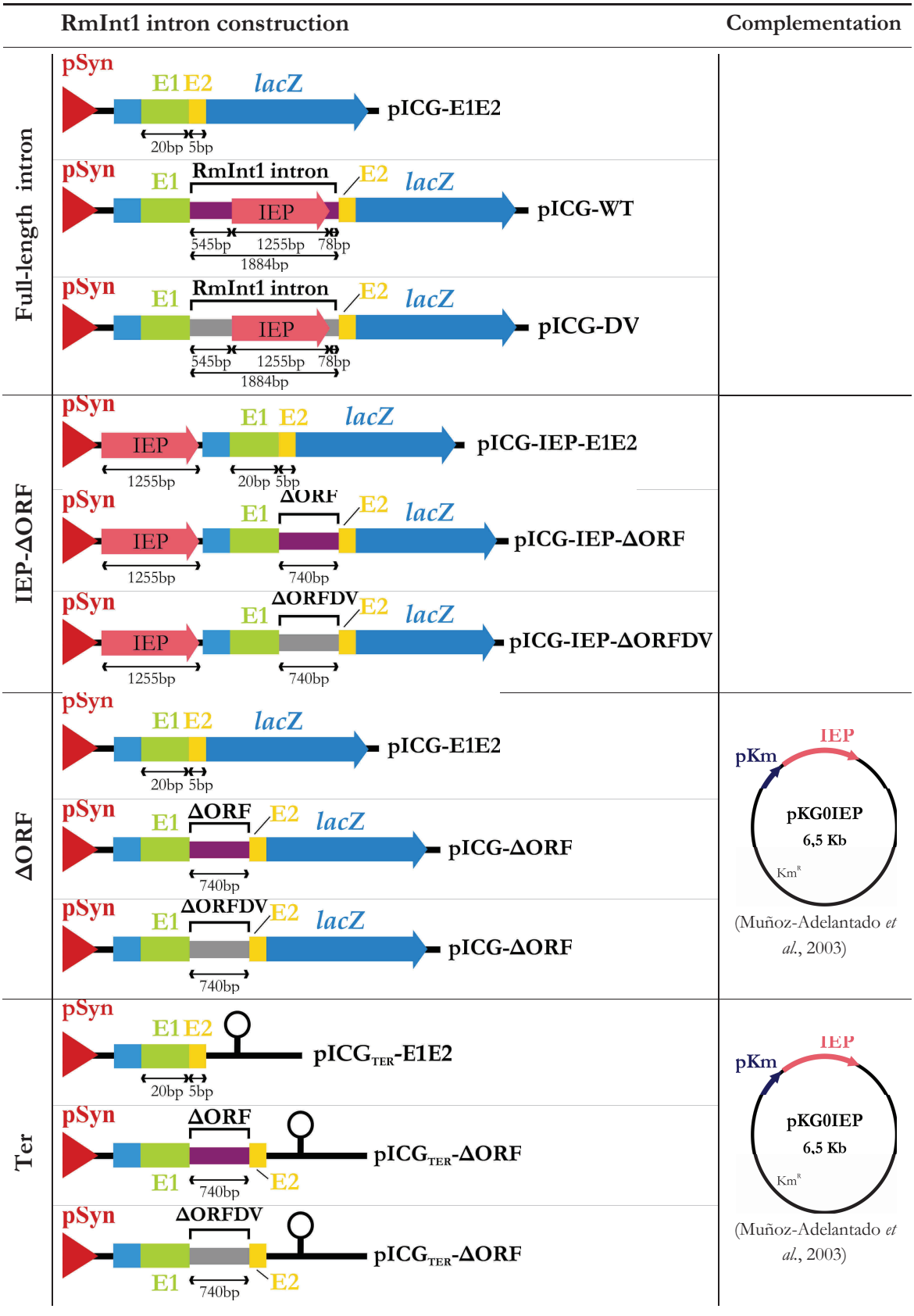
RmInt1 intron construction
Complementation
Full-length intron
IEP-ΔORF
ΔORF
Ter
pSyn
E1
E2
lacZ
IEP
RmInt1 intron
ΔORF
ΔORFDV
pICG-E1E2
pICG-WT
pICG-DV
pICG-IEP-E1E2
pICG-IEP-ΔORF
pICG-IEP-ΔORFDV
pICG-ΔORF
pICG$_{TER}$-E1E2
pICG$_{TER}$-ΔORF
20bp
5bp
545bp
1255bp
78bp
1884bp
740bp
pKm
pKG0IEP
6,5 Kb
Km^R
(Muñoz-Adelantado *et al.*, 2003)

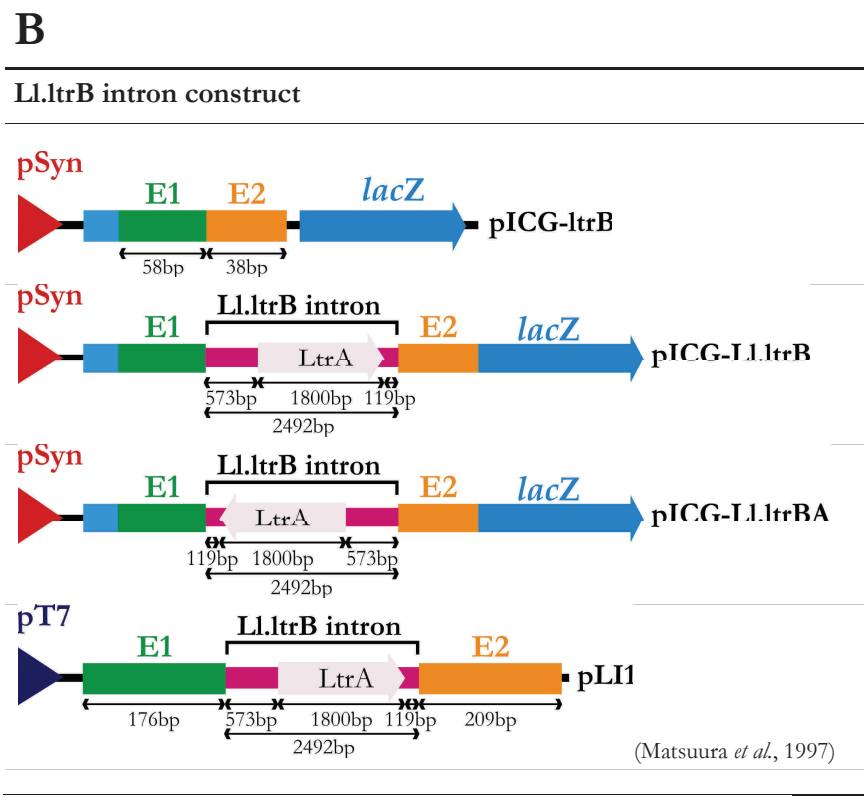

Figure R1.3. Constructions used in the *in vivo* splicing analysis of *S.meliloti* RmInt1 and *L.lactis* Ll.ltrB group II introns. **A** Schematic diagram of RmInt1 intron-based constructions in the pICG system. Four intron constructions were created, each belonging to a series of plasmids: the wild-type construct, pICG-WT, in the full-length intron series, contains the full-length RmInt1 intron (1.9 kb) with the protein encoded by a sequence in DIV; pICG-IEP-ΔORF, in the IEP-ΔORF series, and pICG-ΔORF, in the ΔORF series, that contain a 0.74 kb intron in which the IEP is either encoded by a sequence just upstream from the 5'-exon/*lacZ* sequence or constitutively produced from a compatible pKGIEP plasmid, respectively. As a control for the ligated exons expected from the constructs described above, an intron-less construct, pICG-E1E2, consisting of the RmInt1 short flanking exons fused in frame with the *lacZ* gene, was used in which the IEP was either encoded by a sequence in the *cis* position (pICG-IEP-E1E2) or by a sequence in *trans* (pICG-E1E2+IEP), from compatible pKGIEP plasmids. As a negative control in these splicing assays, plasmids containing splicing-defective mutants, with a mutation in the critical conserved AGC-GUU pairing of intron RNA domain V (GUU converted to CGA) were generated. These constructs were named pICGDV, pICG-IEP-ΔORFDV and pICG-ΔORFDV+IEP, for the corresponding full-length intron, and for the 0.74 kb intron with the IEP sequence expressed in *cis* and in *trans*, respectively. **B** Schematic diagram of Ll.ltrB intron-based constructions. All Ll.ltrB constructions are based in the full-length intron, with the LtrA protein encoded by a sequence in the RNA DIV. pICG-Ll.ltrB is the wild-type intron in the pICG system, with the Ll.ltrB intron cloned in sense with respect to the promoter orientation, allowing RNA and LtrA protein to express. As a control for the ligated exons of the above construction, the intronless construct, pICG-*ltr*B, where the intron flanking exons fused in-phase with the *lacZ* gene, was used. As a negative control of splicing, pICG-Ll.ltrBA, harboring an wild-type Ll.ltrB intron cloned in antisense with respect to the promoter pSyn, was used. The pLI1 construction (Matsuura *et al.*, 1997), carrying the wild-type Ll.ltrB intron under the inducible T7 promoter, was used as a control of expression and as a PCR template for cloning. The red and blue arrow-head represents the pSyn and T7 promoters, respectively. The two flanking exons (E1 and E2), the RmInt1 or Ll.ltrB introns, and the intron-encoded protein genes are indicated. The *lacZ* gene is indicated as a blue arrow. The transcription terminator is represented by a stem-loop hairpin in thick black lines.

The first RmInt1 intron construction in the pICG reporter system, the wild-type construct, pICG-WT, contained the full-length RmInt1 intron (1.9 kb) with the protein encoded by a sequence in DIV (Figure R1.3). This construction was the result of the invasion of the intronless construct, pICG-E1E2, with the RmInt1 intron expressed from the donor intron construction pKG-2.5 (Figure M2, See Materials and Methods). pICG-WT could potentially express both the intron RNA and the IEP protein, producing active RNP particles.

We carried out double-plasmid mobility assays to check that the pICG-WT plasmid was fully active. The pICG-WT plasmid harboring the RmInt1 intron was transferred to the RMO17 strain (an intron-less *S. meliloti* strain) by conjugation, together with the acceptor construct pBB0.6+ containing the RmInt1 homing site (-175/+466) (Figure R1.4, lane 3). As negative control, pBBΔ129, a recipient construct lacking the homing site, was used (laness 2, 4) (Martínez-Abarca *et al.*, 2000). The recipient plasmids pBB0.6 and pBBΔ129, not conjugated with the donor plasmid pICG-WT, were also assayed (lanes 1, 2). We analyzed the invasion of the recipient plasmids, pBB0.6 and pBBΔ129, by Southern Blotting Hybridizations by using an IS*Rm2011-2* exon 2 and an intron probes (Figure R1.4). Plasmid analysis for the transconjugants showed that almost 100% of the recipient plasmids were invaded by the RmInt1 intron (lane 3, exon 2 and intron probes). In contrast, the negative control (lane 4) and the recipient plasmids not complemented with the donor constructions (lanes 1 and 2) only hybridized with the exon 2 specific probe, and did not exhibit any hybridization signal with the intron specific probe.

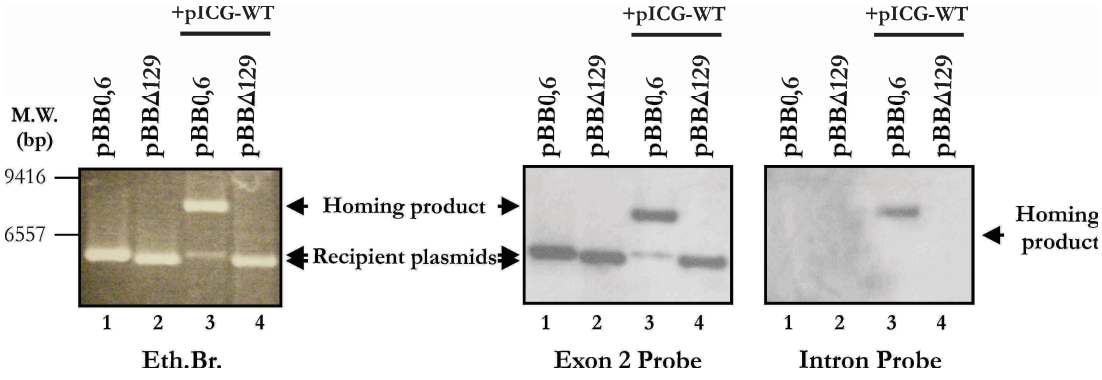

Figure R1.4. Homing assay of wild-type RmInt1 in the pICG reporter system. For homing assays, plasmid pools from RMO17 cells harbouring donor (pICG-WT) and recipient (pBB0.6) plasmids were blotted onto a nylon membrane and analyzed by Southern hybridization with DNA probes specific to the insertion sequence ISRm2011-2 (Exon 2 Probe, middle panel) and RmInt1 intron (Intron Probe, right panel). Recipient plasmid pBBΔ129 was used as negative control in the assays (lane 5) along with recipient plasmids pBB0.6 and pBBΔ129 not complemented with the donor construction (lanes 2 and 3).

A splicing defective construction, pICG-DV, was used as a negative control of the full-length wild-type pICG-WT plasmid in splicing analysis. This construction derived from pKG2.5-DV, which has a mutation in the critical conserved pairing AGC-GUU of intron RNA domain V (GUU → CGA) (Muñoz-Adelantado *et al.*, 2003) (Figure R1.3, Figure M2, see Materials and Methods).

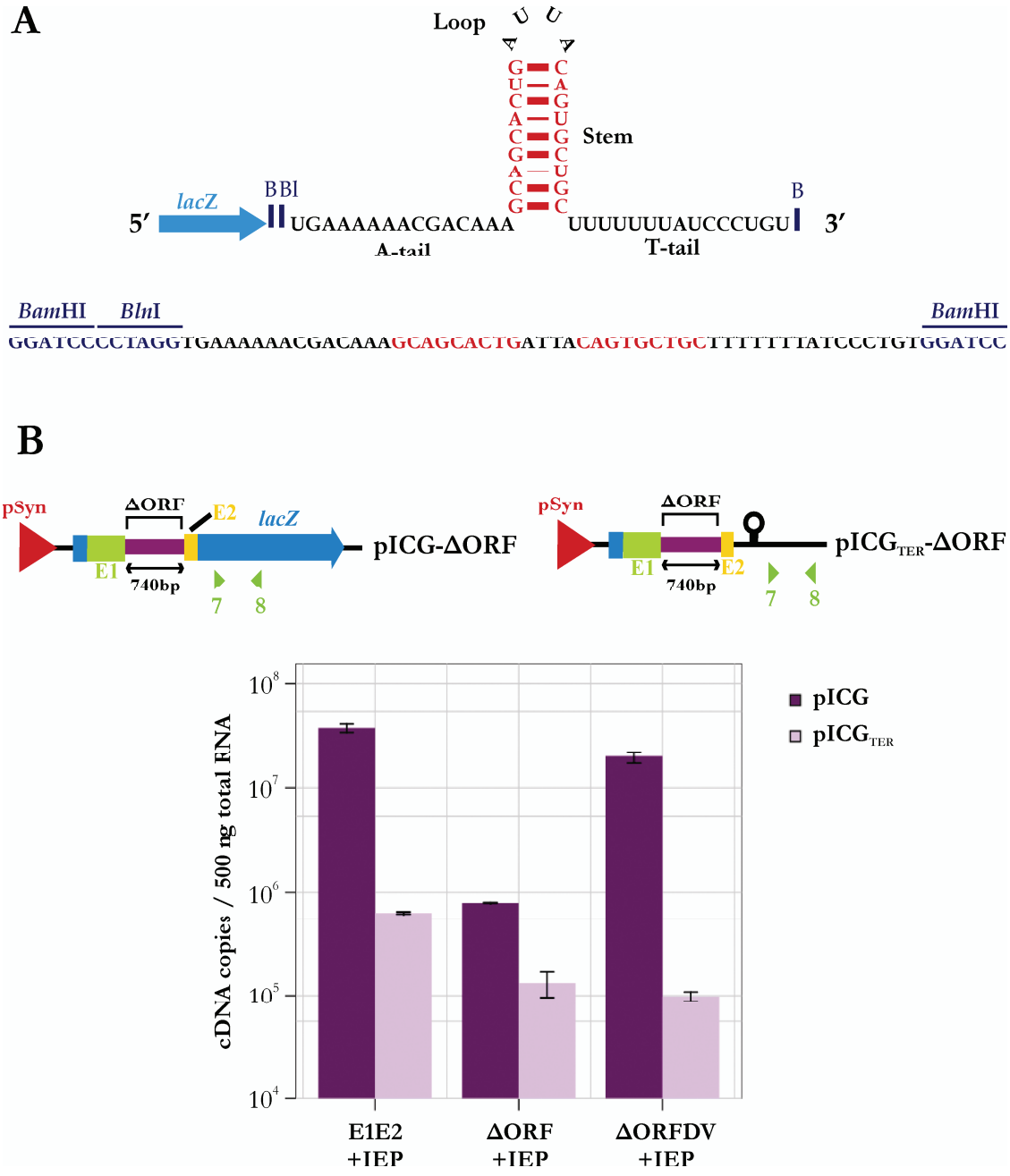

Figure R1.5. Characteristics and effect of the transcription terminator in pICG constructs. **A** Schematic of the transcription motif added to the pICG-ΔORF constructs in the *ter* series of plasmids. The terminator consists of a short stem-loop hairpin surrounded by 15 bases rich in adenine nucleotides on the 5' end of the motif, called the "A-tail" and 15 bases rich in thymine nucleotides on the 3' side called the "T-tail" (Adapted from Kingsford *et al* (2007). Below, the DNA sequence of the synthetic transcription terminator. Restriction sites added to the ends of the oligonucleotide are indicated. The motif was introduced in the unique *Bam*HI restriction site in pICG12. Nucleotides of the stem are highlighted in red. **B** Quantitative analysis of the effect of the transcription terminator in the expression of *lac*Z gene in pICG-ΔORF and pICG$_{TER}$-ΔORF constructs in *S.meliloti* by real-time RT-PCR. The map of the *lac*Z region of pICG-ΔORF and pICG$_{TER}$-ΔORF are depicted on the top. Green arrows under the map indicate the primers used in the real-time RT-PCR assay to amplify the *lac*Z gene (pICG-ΔORF construct, left) or the region located after the transcription terminator (pICG$_{TER}$-ΔORF construct, right). Error bars represent the standard error of the mean.

pICG-ΔORF contained a 0.74 kb intron whereas the IEP protein was constitutively produced from a compatible pKGIEP plasmid (the *trans* position, as described in Muñoz-Adelantado *et al* (2003)) (Figure R1.3) as previously carried out for Ll.ltrB group II intron *in vivo* (Matsuura *et al*., 1997; Cousineau *et al*., 1998; Mohr *et al*., 2000; Cui *et al*., 2004; Watanabe and Lambowitz, 2004). The IEP produced *in trans* could potentially bind to the intron RNA domain IV, similarly as in Ll.ltrB intron (Wank *et al*., 1999; Matsuura *et al*., 2001; Singh *et al*., 2002; Noah and Lambowitz, 2003), promoting splicing of the RNA in the ΔORF construct. The negative control was comprised of a splicing defective construction, pICG-ΔORFDV, derived of pKGEMA4-DV.

pICG-IEP-ΔORF also contained a 0.74 kb intron in which the IEP was encoded by a sequence just upstream from the 5'-exon/*lac*Z sequence (referred to as the *cis* position; Figure R1.3) (Nisa-Martínez *et al*., 2007). This intron construct was derived of pKGMA4, along with its splicing defective counterpart, pICG-IEP-ΔORF, derived from pKGEMA4-DV, also impaired in the catalytic triad AGC of intron RNA domain V.

As a control for the ligated exons expected from the constructs described above, an intron-less construct, pICG-E1E2, consisting of the RmInt1 short flanking exons fused in frame with the *lac*Z gene, was used in which the IEP was either encoded by a sequence in the *cis* position (pICG-IEP-E1E2) or by a sequence in *trans* (pICG-E1E2+IEP), from compatible pKGIEP plasmids.

In order to get transcripts of a defined size, with homogenized 3' ends of RNA precursor, for being analyzed on Northern Blotting assays as discrete bands, an intron ΔORF derivative construct was created in which the expression of the *lac*Z gene was interrupted by the introduction of a transcription terminator (Figure R1.5, Figure R1.3). The rho-independent synthetic transcription terminator was based on that designed by

Kigsford *et al* (2007), which accomplished the requirements for intrinsic termination (Rosenberg and Court, 1979). It was constituted by a short, low-energy hairpin followed downstream by a stretch of thymine nucleotides (which are transcribed into uracils). On the 5' side there was another stretch of adenine nucleotides, because the same sequence can function as a terminator on both strands (Kingsford *et al.*, 2007) (Figure R1.5 A and B). No other recently described parameters were analyzed, such as the effect of the DNA downstream sequences (Nudler and Gottesman, 2002; Martinez-Trujillo *et al.*, 2010).

To test the termination efficiency *in vivo*, the level of mRNA amplified in ΔORF constructions with and without terminator was compared (Figure R1.5 C). The termination efficiency varied from about 83 % in the intron construct to about 99.5 % in the splicing defective construction. This meant that RNA polymerase significantly paused at the hairpin, giving the chance to the destabilization of the rU-dA RNA-DNA hybrid, which has an unusually weak base-paired structure, and so terminating the transcription.

R1.4 INTRODUCTION OF THE *Lactococcus lactis* Ll.ltrB INTRON IN THE REPORTER SYSTEM OF pICG PLASMIDS

Since it has been reported that the comparison of values obtained from independent Miller assays may lead to inaccurate results, unless all experimental parameters are standardized (Giacomini *et al.*, 1992), we performed a direct comparison of *L.lactis* Ll.ltrB intron and *S.meliloti* RmInt1 intron by introducing the Ll.ltrB intron in the reporter *lac*Z gene of pICG plasmids, as previously performed (Giacomini *et al.*, 1994). Since Ll.ltrB intron is the most studied bacterial group II intron (Dunny and McKay, 1999; Klein and Dunny, 2002), many aspects of its molecular biology and *in vivo* behavior have been elucidated, enabling us to determine key aspects of the RmInt1 behavior.

Traditionally, Ll.ltrB intron has been studied in *L.lactis* within the *ltrB* relaxase gene in the natural context of the 48-kb conjugative element pRS01 (Mills *et al.*, 1996; Chen *et al.*, 2005). The copy number of pRS01 is less than 1 molecule per cell, and it likely integrates reversibly into the chromosome (Chen *et al.*, 2005). In *E.coli*, several Ll.ltrB-containing plasmids were used for the splicing analysis of Ll.ltrB. Some of them are pLI1, a pET-11a derivative which expressed the wild-type full-length intron with long flanking exons (-176/+209) under the T7 promoter (Matsuura *et al.*, 1997); pLE12-ΔORF, a pLE12-derivative (Mills *et al.*, 1996), deleted of the intron-encoded LtrA protein coding region (Matsuura *et al.*, 1997) or; the wild-type intron in the pALG1 series with minimal

flanking exons (-58/+38), the full-length construct pALG1 and the ΔORF-intron construct pALG2, both containing *ltrB*/GFP fusions (Cui *et al.*, 2004).

pICG-Ll.ltrB contained the wild-type Ll.ltrB intron and short flanking exons (-58/+38) (Cui *et al.*, 2004), cloned in sense orientation with respect to the promoter, so that this construct could potentially express both the intron RNA and the LtrA ORF, the latter with its own promoter sequence within the intron (Zhou *et al.*, 2000) and Shine–Dalgarno-like sequence for translation (Matsuura *et al.*, 1997). For comparing, pLI1 plasmid, in which Ll.ltrB intron is expressed under the inducible T7 promoter in *E.coli*, was used in the splicing assays (see Chapter 2).

For negative control of splicing, an Ll.ltrB construction in antisense orientation with respect to the direction of DNA replication was used. As not being expressed the LtrA protein, no splicing events were predicted to occur. As a control for the ligated exons, the construction pICG-*ltr*B, which contained the sequence of ligated *ltrB* flanking exons 1 and 2 (-58/+38), was used.

R1.5 POTENTIAL OF THE pICG REPORTER SYSTEM IN THE STUDY OF THE BIOLOGY OF *S.meliloti*

In this work, pICG reporter system will be use in the analysis of splicing of the RmInt1 intron. Nevertheless, due to its characteristics, it could be useful for many other purposes:

- The intronless construct pICG-E1E2 contains the minimal target site for RmInt1 insertion. Conjugated along with a compatible intron donor construct, pICG-E1E2 can participate as a recipient plasmid in homing assays. Moreover, by using *Xba*I restriction sites, located on both sides of the *lacZ* gene, a 3.5 kb band harboring the inserted intron is released, suitable for Southern Blotting hybridizations with an exon 2 probe.
- It could be used in plant-based infection experiments for the localization of *S.meliloti* bacteria on nodules due to the constitutive expression of the reporter gene *lacZ*.
- Under the pSyn promoter, the *lacZ* cassette can be replaced by digestion with *Bam*HI and *Nhe*I restriction enzymes with another reporter gene. The RmInt1

target site could be introduced later in the *Bam*HI site, bearing in mind not to impair the phase.

- Furthermore, other intronic elements could be potentially introduced in the *Bam*HI site of *lac*Z gene, as the rybozime DIV for studying its interaction with the IEP protein as previously reported (Singh *et al.*, 2002; Gu *et al.*, 2010).

CHAPTER 2

IN VIVO QUANTIFICATION OF THE *S.MELILOTI* RMINT1 GROUP II INTRON SPLICING. COMPARISON WITH THE *L.LACTIS* LL.LTRB GROUP IIA INTRON EXPRESSED IN *E.COLI*

R.2.1 BACKGROUND

Since the discover of the first bacterial group II intron (Ferat and Michel, 1993), more than 30 full-length group II introns 9 partial group II introns had been identified in Eubacteria by 2002 (Dai *et al.*, 2003) and about 20 more in Archaebacteria (Dai and Zimmerly, 2003). Most of these introns were identified through sequence analysis in microbial genome sequencing projects or directly through genome database searches (Dai and Zimmerly, 2002). However, only a minority of bacterial group II introns have been unequivocally shown to be functional or to undergo splicing *in vivo*: Ll.ltrB from *Lactococcus lactis* ML3 (Mills *et al.*, 1996) and a group II intron similar to Ll.ltrB identified in the sex factor from *L. lactis* 712 (Shearman *et al.*, 1996); the *Sinorhizobium meliloti* RmInt1 (Martínez-Abarca *et al.*, 1998); B.a.I1 and B.a.I2 from *Bacillus anthracis* (Robart *et al.*, 2004); a *Clostridium difficile* intron (Roberts *et al.*, 2001) and the Avi.groEL intron from *Azotobacter vinelandii,* which inserts within the termination codon of the essential *groEL* gene (Adamidi *et al.*, 2003; Ferat *et al.*, 2003).

While organellar group II introns are frequently located in essential genes (e.g. NAD dehydrogenase, ribulose-bisphosphate carboxylase, cytochrome oxidase), which require efficient transcription and splicing (Dai *et al.*, 2003), nearly all bacterial group II introns are associated with mobile DNAs or even they are located outside genes, as those of bacterial class C, which insert exclusively after terminator structures. As far, no bacterial group II introns have yet been found in highly conserved or housekeeping genes. It is therefore possible that many of these bacterial group II introns are transcribed only weakly, if at all, in the cell.

RmInt1 splicing has been investigated principally by analyzing excised intron products. These analyses have shown that the maturase (X domain), including the conserved C-terminal tail of the IEP, is required for splicing (Molina-Sanchez *et al.*, 2010). The excised intron products have been characterized in detail and shown to consist mostly of lariat forms, but with some putative circular forms (Molina-Sánchez *et al.*, 2006). Exon junction products have been detected *in vivo* only in RT-PCR assays (Martínez-Abarca *et al.*, 1998; Martínez-Abarca and Toro, 2000). Moreover, *in vitro,* it has been shown that exon ligation is unusually inefficient for RmInt1 (Costa *et al.*, 2006a), partly because nucleotides 5 to 11 of the 3' exon match the EBS1 5'-exon-binding site much better than the authentic IBS1 sequence in the 5' exon (Costa *et al.*, 2006b). For the reasons exposed above, we rationalized to develop an accurate study of the whole splicing reaction of RmInt1 group II intron. To achieve this purpose, we made use of the new context of pICG plasmid

system for analyzing all the products obtained in the splicing reaction, including excised intron and ligated exons, *in vivo*.

R.2.2 THE *IN VIVO* EXCISION OF RmInt1

RmInt1 excision products were assessed by carrying out primer extension analysis on pICG constructs (Figure R2.1), as previously described for other plasmid constructs (Muñoz-Adelantado *et al.*, 2003; Molina-Sánchez *et al.*, 2006; Nisa-Martínez *et al.*, 2007). In these assays, the excised lariat intron RNA (L) is detected as an extension product of 97 nt, together with larger bands derived from unspliced precursor RNA molecules (Pr) (Figure R2.1 B). In *S. meliloti*, the expected 97 nt product was obtained from constructs containing the RmInt1 intron (lanes 2, 5 and 8), whereas no band was obtained from intron-less constructs (lanes 1, 4 and 7) or from splicing-defective constructs with a mutation in DV of the intron (lanes 3, 6 and 9). RmInt1-ΔORF intron excision was three times more efficient when IEP was expressed in *trans* (lane 8) than when expressed in *cis* (lane 5), being almost as efficient as that observed with the wild-type intron construct (lane 2). This result contrasts with those for the Ll.ltrB intron, for which ΔORF intron splicing occurred at wild-type levels when the IEP sequence was expressed in *cis,* but at much lower levels expressed in *trans* from a separate plasmid (Cui *et al.*, 2004). We analyzed the pICG constructs in *E. coli*, and found that the amount of excision product obtained was 95% lower than that obtained in *S. meliloti* for constructs containing RmInt1 intron (lanes 11, 14 and 17). No band was observed for intron-less (lanes 10, 13 and 16) and splicing-defective (lanes 12, 15 and 18) constructs, as expected. Thus, the efficiency of RmInt1 excision depends on the bacterial host.

Figure R2.1 *In vivo* excision of the RmInt1 intron in *S. meliloti* and *E. coli*. **A** Primer extension assays were performed on total RNA extracted from *S. meliloti* (lanes 1-9) and *E. coli* (lanes 10-18) harboring the indicated constructs. RNA was reverse-transcribed with a ^{32}P [γ-ATP] 5'-labeled primer complementary to the first 97 nt of RmInt1. The products were analyzed by electrophoresis in a denaturing 6% polyacrylamide gel, which was dried and quantified with a PhosphorImager. The major cDNA product (97 nt, indicated with a dot) for the wild-type and ΔORF constructs (lanes 2, 5, 8, 11, 14 and 17) corresponds to the excised intron RNA. Larger products derived from unspliced precursor RNAs were also detected (110 and 126 nt). As negative controls, we used DV mutant intron constructs (lanes 3, 6, 9, 12, 15 and 18) and intron-less constructs (E1E2, Lanes 1, 4, 7, 10, 13 and 16). **B** Schematic diagram of primer extension on linear unspliced precursors and excised intron lariats, showing the expected extension products. The bulged A in DVI is also indicated.

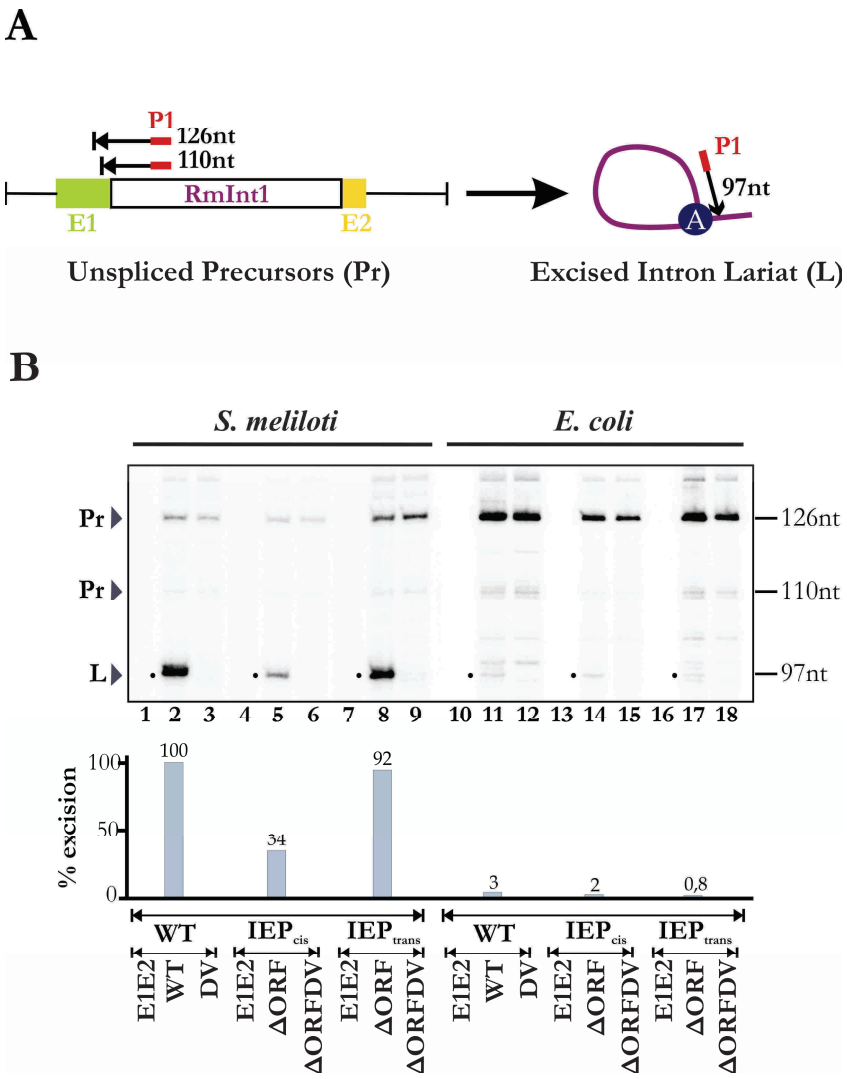

R.2.3 RmInt1 SPLICING IN *S. meliloti*

The splicing products of the RmInt1 intron were analyzed in *S. meliloti*-host RNA samples, in which *in vivo* excision was the most efficient (Figure R2.1).

First, we attempted to detect the cDNA from ligated exon RNAs with a primer extension assay from an exon 2 primer (primer P2; Figure R2.2 A, B). The positive control, the intronless construct pICG-E1E2 (Figure R2.2 B; lane 1), showed a cDNA triplet when extended from the primer P2. The longest 5' exon end corresponds to the predicted start site at the pSyn promoter of pICG plasmid (Giacomini *et al.*, 1994), whereas the other 5' ends were empirically determined to be 19 nt and 29 nt shorther than the longest one, respectively, and may reflect the creation of a new transcription start site (Figure R2.2 B). However, neither in the full-length wild-type construct, pICG-WT (lane

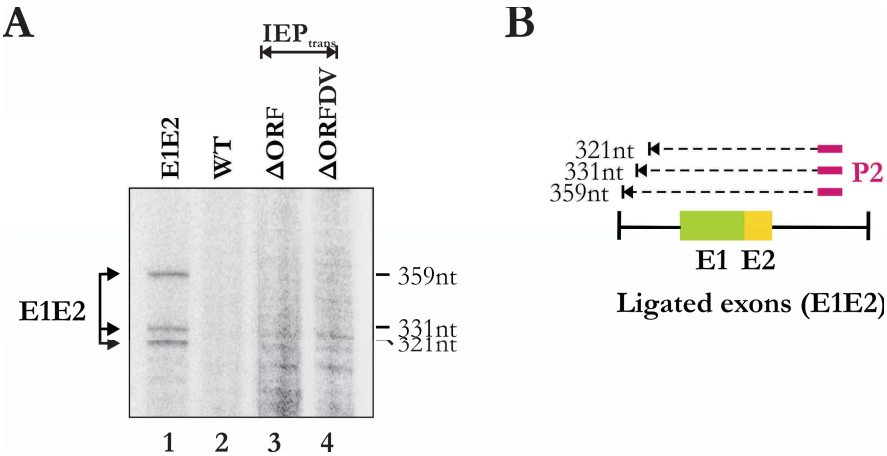

Figure R2.2 Attempt of detection of ligated exons in the RmInt1 splicing. **A** RNAs from pICG plasmids expressed in *S.meliloti* was extracted and reverse transcribed with exon 2-specific primer P2. The cDNA bands, of lengths indicated to the right of each panel, correspond to ligated exons (E1E2), which are shown as a triplet in the intronless construct pICG-E1E2 (lane 1). No bands were detected in the intron-containing constructs, neither for the wild-type (lane 2) nor for the RmInt1-ΔORF intron construct (lane 3). The splicing defective construction pICG-ΔORFDV was used as negative control. **B** Schematic of RNAs and cDNAs products. RNA is depicted as a solid line and cDNAs as broken lines. Exons are represented as green (E1) and yellow (E2) boxes.

2), nor in the ΔORF construct, pICG-ΔORF + IEP (lane 3), ligated exons could be detected. As a negative control, the splicing defective construction pICG-ΔORFDV + IEP, was used (lane 4).

We also analyzed the splicing products of the RmInt1 intron by carrying out northern blotting (Figure R2.3). In this approach, the RmInt1-ΔORF intron was used, due to its shorter size respect to full-length constructions. In addition, we introduced an intrinsic transcription terminator (pICG$_{TER}$ constructions, see Materials and Methods and Chapter 1) into the constructs, for the identification of RNA precursors of a precise size (Figure R1.5, Figure R2.3 B, lanes 1-6). As control for this element, we included constructs without the Rho-independent transcription terminator (lanes 7-9). A set of negative control samples, in which the IEP was absent, was used to identify the precursors and transcript forms. Precursor accumulated only for constructs containing the transcription terminator (lanes 2, 3, 5 and 6). The precursor was resolved as a triplet, because transcription is initiated by the Syn promoter at three different positions, as explained above. The lower intensity of the precursor band for intron-bearing constructs (lanes 2, 3, 5 and 6) than for intron-less constructs (lanes 1 and 4, left and right panel) probably reflects a lower efficiency of the RNA polymerase with longer templates and a greater susceptibility of the larger precursor RNA to nucleolytic degradation. Nevertheless, no traces of ligated exons were observed with the ΔORF construct complemented with the

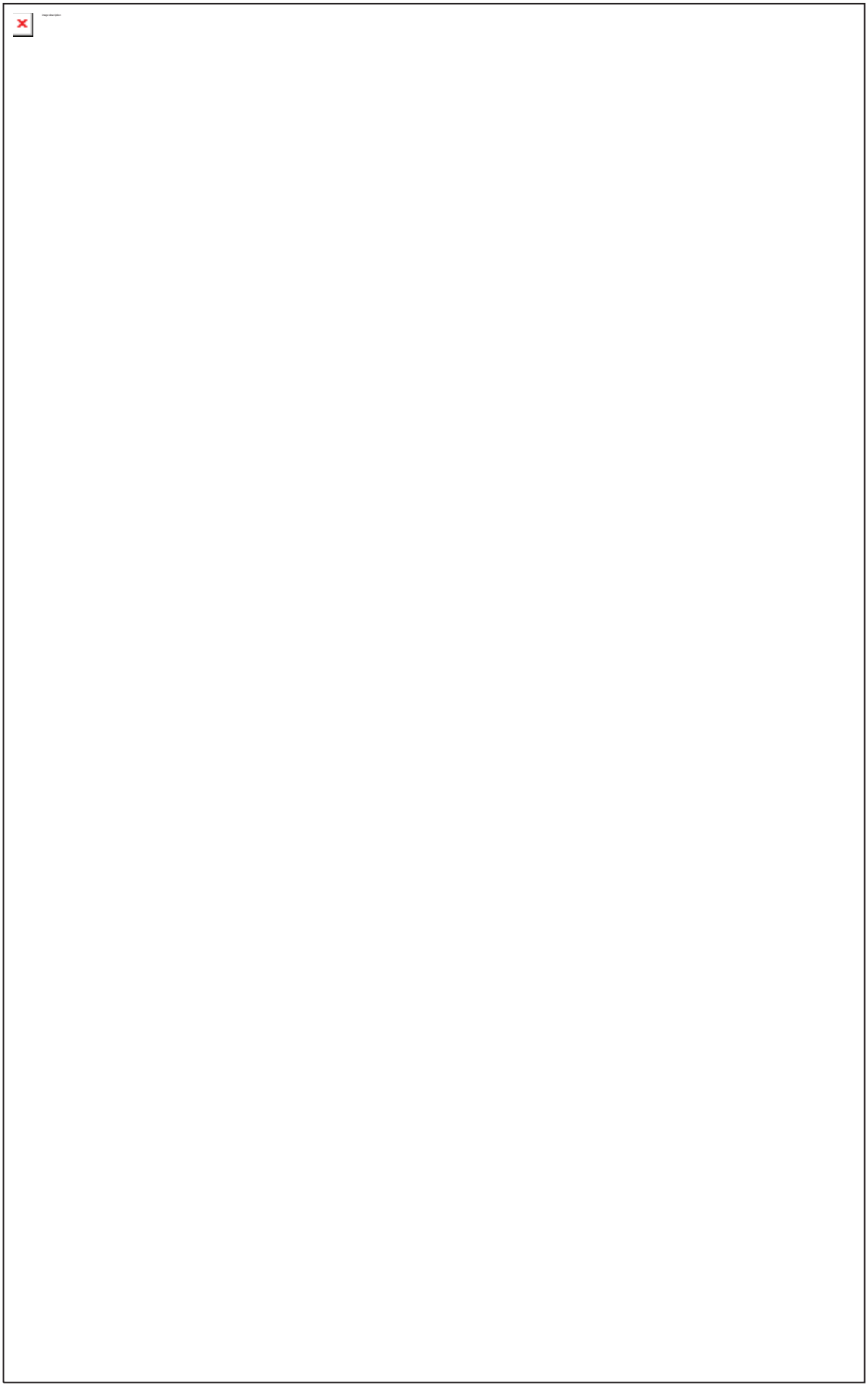

Figure R2.3 RmInt1 splicing products in *S. meliloti*. **A** Schematic diagram showing the splicing products identified with the various probes used. The 5' and 3' exon probes hybridize to the precursor RNA and ligated exons, whereas the intron probe hybridizes to the precursor RNA, excised lariat intron and broken lariat intron. Exons are depicted in green (E1) and yellow (E2), the intron is shown as a solid black line with a circle indicating the bulging adenosine in DVI, the transcription terminator is a stem-loop hairpin and the probes are represented by a bold red line. The pSyn promoter includes three origins of transcription, generating three bands for the precursor or ligated exons, the size of which is indicated. **B** Northern blot hybridizations were performed with 5 μg of total RNA extracted from *S. meliloti* harboring the indicated pICG plasmids with (lanes 1-6; ter series) and without (lanes 7-9) the Rho-independent transcription terminator and complemented (lanes 4-9) or not (lanes 1-3) with the IEP *in trans*. The splicing products detected are indicated to the right of the panels. Three bands corresponding to the expected ligated exons are visible only in bacteria containing intron-less constructs of the ter series (Ter-E1E2; lanes 1, 4). Excised and broken lariat bands are detectable only in samples containing ΔORF constructs complemented with IEP (lanes 5 and 8). Other bands corresponding to nonspecific cleavage or cross-hybridization products of about 600 nt are indicated (x).

IEP (lane 5, left and right panel). Lariat intron forms were also observed for RmInt1 constructs (lanes 5 and 8, middle panel). Their electrophoretic mobility was low due to their three-dimensional configuration. The absence of ligated exons cannot be accounted for by the accumulation of intermediates of the splicing reaction steps, as no lariat-3' exon intermediates were observed, as shown by the lack of bands on hybridization with 3' exon probe (lanes 5 and 8, right panel). Further, a 740 nt band was shown, probably corresponding to a broken lariat form because it was detected only with the intron probe for constructs containing ΔORF complemented with the IEP in *trans* (lanes 5 and 8, middle panel), with no bands detected for the intron-less (lanes 1, 4 and 7, middle panel) and DV mutant (lanes 3, 6 and 9) constructs. The other bands observed on hybridization with the 3' exon probe correspond to nonspecific cleavage products (lanes 2, 3, 5 and 6, right panel, x products). Our results provide direct evidence that RmInt1 splicing in *S. meliloti* is inefficient, with the accumulation of the intron lariat not accompanied by the accumulation of ligated exons.

R.2.4 QUANTITATIVE ANALYSIS OF RmInt1 EXPRESSION AND SPLICING

No ligated exons were detected on northern blotting. We therefore used a reporter gene system to determine the extent to which exon ligation occurred during RmInt1 splicing *in vivo*. In this system, intron excision is linked to *lacZ* gene expression. Quantification was carried out in *S. meliloti* at its growth temperature (28ºC) and in *E. coli* at

37ºC and 28ºC (Table R2.1). The intron-less construct of each plasmid series was used to test the system and the reaction conditions. With these constructs, β-galactosidase activity ranged from about 4000 Miller units in the *cis* series in *S. meliloti* to 15000 Miller units in the wild-type series in *E. coli* grown at 37ºC, demonstrating an effect of temperature on the enzymatic activity of β-galactosidase in *E. coli*. However, constructs harboring introns had very low levels of activity (from 5 to 20 Miller units) in both *S. meliloti* and *E. coli* and, in most cases, activity levels were similar to those obtained with the splicing-defective DV mutant. Thus, there are presumably too few ligated exons for quantification by this enzymatic method.

TABLE R2.1. RmInt1 intron splicing measured as β-galactosidase activity

Construction	β-galactosidase activity (U) ± SEM [a]		
	E. coli		*S. meliloti*
	37ºC	28ºC	28ºC
Wild-type series			
E1E2	15000 ± 300	10300 ± 300	6580 ± 20
WT	18 ± 1	14.1 ± 0.8	5 ± 1
DV	16.9 ± 0.3	12 ± 1	7.5 ± 0.3
IEP *trans* series			
E1E2	13600 ± 400	10300 ± 300	8400 ± 300
ΔORF	20.4 ± 0.6	19 ± 1	14.4 ± 0.3
ΔORF DV	24 ± 2	22 ± 1	21.3 ± 1.3
IEP *cis* series			
E1E2	9900 ± 200	5700 ± 200	3980 ± 70
ΔORF	18.4 ± 0.6	15.3 ± 0.9	12 ± 1
ΔORFDV	18.6 ± 0.3	17.9 ± 1.1	15.1 ± 0.9

[a] β-galactosidase activity is expressed in Miller Units as described in the Materials and Methods

We developed a quantitative real-time reverse transcription-PCR (qRT-PCR) assay, to quantify the ligated exons generated by intron splicing and to analyze RmInt1 and *lac*Z transcript levels in the context of pICG plasmids, as previously carried out for Ll.ltrB in *L. lactis* (Chen *et al.*, 2005). Absolute quantification was used to determine mRNA levels in the wild-type series of plasmids. Three primer pairs were used to amplify *lac*Z1, RmInt1 intron and ligated β-galactosidase gene *lac*Z produced as a consequence of the splicing of RmInt1 (Figure R2.4 and Table M.5, see Materials and Methods). All transcripts displayed constitutively high levels of expression (Figure R2.4 B). The amount of *lac*Z1 mRNA

(primer pair 1-2), which represents total mRNA transcribed, was almost constant in all samples. The RmInt1 intron mRNA (primer pair 3-4) is produced only from constructs harboring the intron (pICG-WT and DV), both excised and being part of the precursor mRNA. RmInt1 mRNA levels were highest, due to accumulation of the more stable lariat form of the intron. The ligated β-galactosidase gene *lac*Z transcripts (primer pair 5-6) are produced by intron excision and ligation of the 5' and 3'exons containing lacZ1 and *lac*Z2 fragments. To avoid amplification of precursor molecules by primers 5-6, the extension step in the qRT-PCR was reduced until ligated exons were the unique product detected (see Material and Methods). The mRNA for the intron-less construct pICG-E1E2 amplified by primers 5-6 was produced at almost the same level as that for the *lac*Z1, and it constituted the positive control for exon ligation. In contrast, the intron-containing construct pICG-WT generated three orders of magnitude less mRNA than pICG-E1E2 and 15 times as much mRNA as the splicing defective pICG-DV construct, which gave no distinct amplicon even if PCR was carried out over 40 cycles (Figure R2.4 B).

We investigated the splicing efficiency of RmInt1 in *S. meliloti*, by calculating the ratio of the ligated *lac*Z gene mRNA to *lac*Z1 mRNA for pICG-WT and pICG-DV, normalizing the value obtained with respect to the intron-less exon-ligated control and

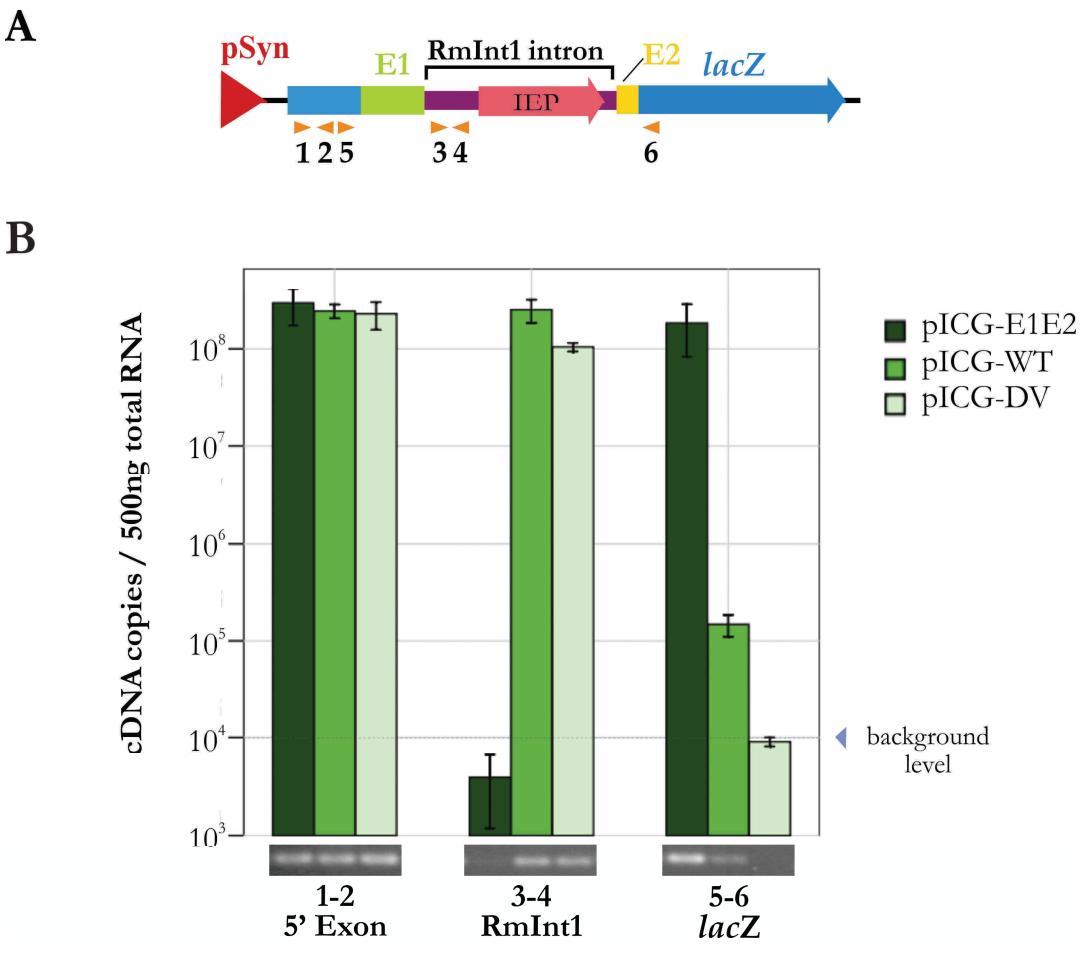

Figure R2.4. Quantitative analysis of RmInt1 in *S. meliloti*. **A** Map of the *lac*Z region of pICG-WT. The RmInt1 intron with the IEP (pink arrow) encoded in DIV and minimal flanking sequences from the *ISRm2011-2* insertion sequence (E1 and E2) (green and yellow boxes, respectively) are located in the *lac*Z gene (blue arrow). The interrupted *lac*Z gene is shown as *lac*Z1 and *lac*Z2 exons. Arrows under the map indicate the primers used in the real-time RT-PCR assay. Primer pair 1-2 was used to amplify the *lac*Z1; primers 3-4 were used to amplify the RmInt1 intron and primers 5-6 were used to amplify the ligated β-galactosidase gene *lac*Z. **B** Total RNA was isolated from *S. meliloti* containing the wild-type intron pICG-WT, the intron-less construct pICG-E1E2 and the splicing-defective mutant pICG-DV. The levels of *lac*Z1 (1-2), RmInt1 intron (3-4) and ligated β-galactosidase gene *lac*Z (5-6) mRNA were determined by an absolute quantification method. Each measurement is the mean of at least three independent RNA preparations. A 40 cycle end-point RT-PCR was carried out, analyzed by an electrophoresis in a 0.8% agarose gel and observed under UV light. A photograph of the revealed cDNA bands corresponding to each sample are depicted under the graphic bars. Note that no distinct bands are detected in lanes with an expression lower than the background level in qRT-PCR.

expressing the result as a percentage. We compared the splicing efficiency of RmInt1 in *S. meliloti* with that in *E. coli* (Table R2.2). The splicing efficiency of RmInt1 was very low in *S. meliloti,* at 0.07 ± 0.02%, but was nonetheless 4.5 times higher than that in *E. coli*, confirming that the intron was more functional in its natural host.

TABLE R2.2. RmInt1 and Ll.ltrB splicing activity in *S.meliloti* and *E.coli* measured by relative quantification in qRT-PCR

Strain and construction	% splicing ± error[a]
S.meliloti RmInt1	
E1E2	100
WT	0.07 ± 0.02
DV	0.002 ± 0.002
E.coli RmInt1	
E1E2	100
WT	0.016 ± 0.006
DV	0.004 ± 0.002
E.coli Ll.ltrB	
*ltr*B	100
Ll.ltrB	0.23 ± 0.05
Ll.ltrBA	0.001 ± 0.001

[a] The percentage of RmInt1 splicing is defined by the following equation: $2^{-\Delta\Delta CT}$ where ΔΔCT = ΔCT (mRNA amplified by 5–6 primer pair) - ΔCT (mRNA amplified by 1–2 primer pair) expressed as a percentage related to each ligated-exon construction. The error is calculated applying the formula: $2^{-\Delta\Delta CT} \cdot \ln 2 \cdot \Sigma SE$

R.2.5 ANALYSIS OF THE *L.lactis* Ll.ltrB INTRON SPLICING IN *E.coliI* AND *S. meliloti*

We made use of the Ll.ltrB-containing pICG constructs to analyze the splicing level of the Ll.ltrB intron in the context of the *lac*Z reporter system and to compare it with that of RmInt1, carried out in *E.coli* and *S.meliloti* hosts and under different temperature conditions.

A primer extension assay was carried out to determine whether the Ll.ltrB intron, expressed in *E.coli*, was excised in the pICG system (Figure R2.5). We performed cDNA synthesis by using a primer complementary to the Ll.ltrB intron. A cDNA band, corresponding to the excised product (L) was detected as an extension product of 92 nt in the intron-harboring construct, pICG-Ll.ltrB (lane 2), while no band was detected in the construction in which the intron was inserted in antisense orientation with respect to the promoter (pICG-Ll.ltrBA, lane 1). For comparison, it was included the pLI1 construct (Matsuura *et al.*, 1997), expressed in *E.coli* under the T7 promoter and analyzed after 3 hours of induction with IPTG (lane 3). Compared to pICG-Ll.ltrB, whose excised lariat band was barely detectable, a strong signal, belonging to pLI1, was identify. The contrast in the detection level of excised intron lariat forms when the Ll.ltrB intron is expressed either in the pICG vector, under the constitutive promoter pSyn or in the pLI1 plasmid, under the inducible promoter T7, may represent a key factor for the detection of the spliced forms produced during the splicing process.

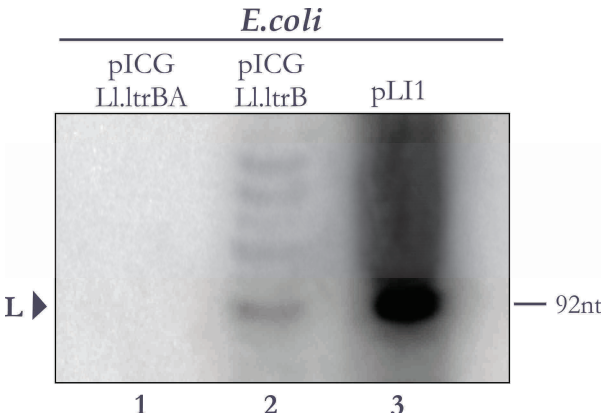

Figure R2.5. *In vivo* excision of Ll.ltrB intron in *E.coli*. Primer extension analysis was performed on total RNA extracted from pICG plasmids pICG-Ll.ltrBA (lane 1) and pICG-Ll.ltrB (lane2) expressed in *E.coli* cultures until exponential phase of growth and from pLI1 plasmid (Matsuura *et al.*, 1997), after 3 hours of induction with IPTG (lane 3). RNA was reverse-transcribed from a primer complementary to the intron. cDNA bands, of 92 nt length, correspond to the excised intron lariat. No bands were detected in pICG-Ll.ltrBA, in which the intron was inserted in antisense orientation with respect to the promoter.

A quantitative evaluation of the splicing level in the Ll.ltrB constructs was carried out by the determination of the β-galactosidase activity in strains of *E.coli* and *S.meliloti* carrying the intronless construct pICG-*ltr*B, the full-length wild-type intron construction pICG-Ll.ltrB and the negative control, pICG-Ll.ltrBA.

We evaluated the impact of temperature in the splicing of Ll.ltrB in *E.coli* (Figure R2.6, left panel). Three different temperatures: 37ºC, 28ºC and 24ºC was assayed. In its natural host, *L.lactis,* the Ll.ltrB intron encounters various temperatures, from low temperatures as 24ºC to higher ones as 37ºC (Chen *et al.*, 2005), which may influence the ability of Ll.ltrB to splice in a variable environment. In the heterologous host *E.coli*, the optimal growing temperature is 37ºC, although it was forced to grow as well at 28ºC and 24ºC. At 37ºC, the β-galactosidase activity measured in *E.coli* cultures in pICG-*ltr*B was about 12000 U Miller, in the order of magnitude as pICG-E1E2 (Table R2.1). Nonetheless, the level of activity in the intron-carrying construct pICG-Ll.ltrB (4 ± 1) was under the background, as determined by the β-galactosidase activity of pICG-Ll.ltrBA (14 ± 2), in the same way as observed for RmInt1. When the activity was determined from a culture of *E,coli* grown at 28ºC, the level of expression of the lacZ gene in the positive control, pICG-*ltr*B, dropped until ~5000 U Miller although, surprisingly, the activity in pICG-Ll.ltrB increased 4.5-fold respect to that observed at 37ºC and above 3.5-fold above the background level (Figure R2.6, left panel). The splicing efficiency calculated for Ll.ltrB expressed at 28ºC was (0.39 ± 0.05) % respect to that of ligated-exon construction (100 %). The β-galactosidase activity was also determined in cultures grown at 24ºC, showing again a decrease in *ltr*B expression accompanied by a 2-fold increase in the activity of the Ll.ltrB intron construct with respect to that assayed at 28ºC. The result was a net raise of splicing efficiency, which was calculated to be (0.89 ± 0.04) %. The expression level was also assayed in *S.meliloti* cultures harboring the Ll.ltrB intron grown at 28ºC, the optimal temperature for the growth of this strain (Figure R2.6, right panel). As previously observed for RmInt1, the expression of the intron construction was similar to the negative control, not allowing any quantification of the splicing activity.

We performed real-time quantitative RT-PCR on samples of *E.coli* carrying Ll.ltrB constructs grown at 28ºC as described above (also see Materials and Methods). The splicing efficiency was calculated normalizing with respect to the intron-less exon-ligated control and expressing the result as a percentage (Table R2.2). The splicing efficiency of Ll.ltrB in the pICG context was quantified at (0.23 ± 0.05) %, significantly higher than the negative control (0.001 ± 0.001) %. This value was in agreement with that obtained from

Figure R2.6. Quantitative analysis of Ll.ltrB intron in *E.coli* and *S.meliloti* hosts. Expression of the *lac*Z gene in pICG constructs harboring the Ll.ltrB intron was measured by a β-galactosidase assay (Miller, 1972) both in *E.coli* (left panel) and *S.meliloti* (right panel) cultures, grown until exponential phase. Expression in *E.coli* was assessed at three different temperatures: 37ºC, 28ºC and 24ºC. The expression of the negative control construction, pICG-Ll.ltrBA, determines the background level for each temperature assayed. The evaluation of the β-galactosidase activity in *S.meliloti* was only performed at 28ºC. Miller Units are indicated in the graphic in logarithmic scale.

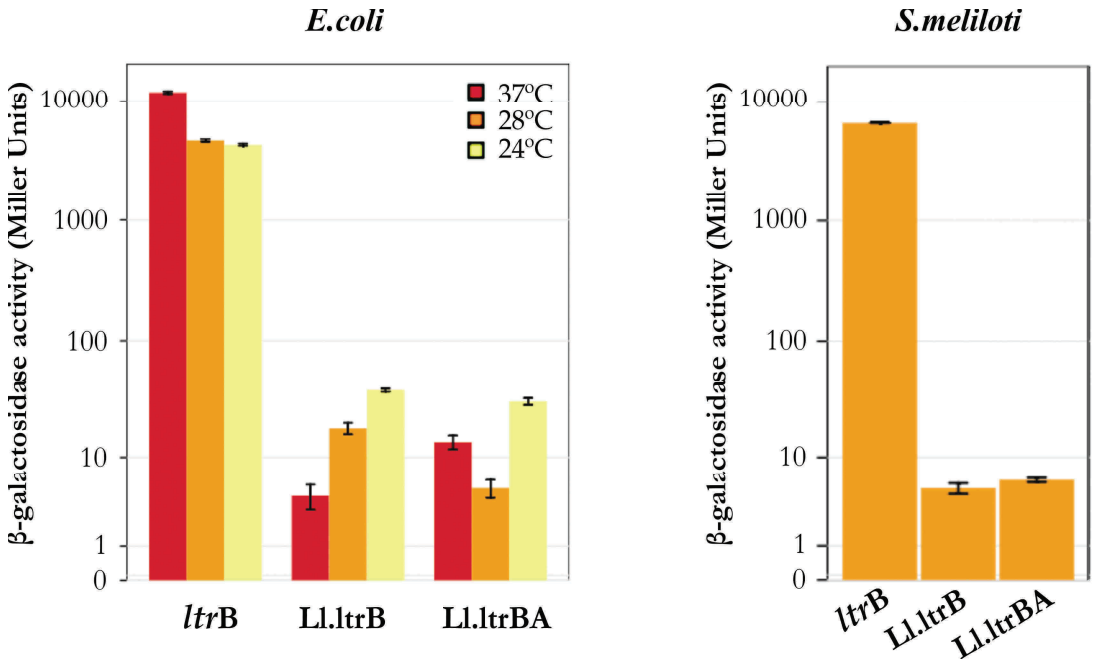

the Miller assay and it was about 3-fold higher than RmInt1 splicing efficiency in *S.meliloti* and about 14-fold higher if measured in an *E.coli* culture.

R.2.6 DISCUSSION

The *in vivo* splicing of group II introns has been studied in detail for a small number of well known group II introns, such as Ll.ltrB from *L. lactis* and aI5γ from *S. cerevisiae* (Arnberg *et al.*, 1980; Hensgens *et al.*, 1983; Domdey *et al.*, 1984; Peebles *et al.*, 1993; Boulanger *et al.*, 1996; Mills *et al.*, 1996; Podar *et al.*, 1998; Cui *et al.*, 2004; Yao *et al.*, 2006; Belhocine *et al.*, 2007). In most cases, these analyses were limited to the detection of the spliced form of the intron, with very few studies considering the detection (Matsuura *et al.*, 1997) or quantification (Chen *et al.*, 2005) of ligated exon forms. In this study, we analyzed the splicing of the bacterial group II intron RmInt1, including intron excision and exon ligation, in *S. meliloti* and in *E. coli,* by northern blotting, β-galactosidase assays and qRT-PCR approaches, and compared it with the *L.lactis* Ll.ltrB intron in *E.coli*. We show that the splicing of a group II intron naturally located into an insertion sequence (IS*Rm2011-2*) interrupting the transposase gene is almost completely abolished, but this intron retains its invasion capacity.

Assays of RmInt1 excision efficiency in the pICG system showed similar rates of excision for the wild-type construct and the construct in which the IEP sequence was

present *in trans* on a separate plasmid. These findings contrast with those for LtrA in *E. coli,* for which lower levels of excision were reported in *trans* (Cui *et al.*, 2004). As the plasmid carrying the IEP sequence in *trans* is present at a higher copy number than the IEP sequence in *cis*, the larger amount of protein produced in the *trans* system may rapidly become available for the binding of intron RNA, preventing degradation of the precursor RNA. RmInt1 in a *cis* position upstream from the 5' exon was excised less efficiently, probably due to the larger distance to the promoter and the higher probability of the RNA polymerase releasing the RNA chain or dissociating from the DNA template. By contrast, RmInt1 excision in *E. coli* was 95% less efficient than excision of the intron from the wild-type construct in *S. meliloti*, suggesting that host factors may play an important role in the splicing reaction, probably during ribozyme folding, as previously reported for other group II introns (Smith *et al.*, 2005; Beauregard *et al.*, 2008).

The analysis of RmInt1 splicing products *in vivo* in *S. meliloti* confirmed that lariat form accumulates in the splicing process and that this product is free of lariat-3' exon reaction intermediates. However, ligated exons forms, more susceptible to cell degradation and thus less prone to accumulate, were not detected. The absence of ligated exon forms contrasts with the *in vivo* detection of exon ligation during splicing of the lactococcal group II intron Ll.ltrB in *E. coli* (Cui *et al.*, 2004), which suggests that splicing of RmInt1 may be very inefficient. The lower level of accumulation of splicing products from constructs harboring a transcription terminator may be due to higher rates of RNA polymerase dissociation from short templates with a high degree of secondary structure than from templates lacking terminator sequences. We also detected a 740 nt intron band, probably corresponding to a broken lariat form. Linear group II introns have been reported to occur *in vivo* (Vogel and Borner, 2002), but this form is produced predominantly during *in vitro* splicing reactions (Daniels *et al.*, 1996) or as a consequence of branch-site mutations *in vivo* (Podar *et al.*, 1998).

The absence of ligated exons on northern blots led us to use more sensitive approaches for monitoring this product of intron RNA splicing. Nevertheless, the level of exon ligation observed for RmInt1 intron, in Miller units, was below background levels. Quantitative real-time qRT-PCR assays enabled us to analyze RmInt1 and *lac*Z mRNA levels and the intron splicing efficiency. Large amounts of *lac*Z1 and RmInt1 RNA were produced, but ligated *lac*Z gene produced three orders of magnitude less RNA, demonstrating the strong effect of RmInt1 on the genes it interrupts. We found that RmInt1 was very inefficiently spliced *in vivo* in *S. meliloti* (0.07 ± 0.02%) and in *E. coli* (0.016 ± 0.006%).

The *L.lactis* Gram-positive bacterium Ll.ltrB group II intron has been extensively studied for its splicing activity. Since it was initially reported in its natural host *L.lactis* (Mills *et al.*, 1996; Shearman *et al.*, 1996), diverse methods have been used for the detection of the excised form as well as the ligated exons of Ll.ltrB *in vivo* (Matsuura *et al.*, 1997; Cui *et al.*, 2004; Klein *et al.*, 2004; Chen *et al.*, 2005) both in *L.lactis* and the heterologous host *E.coli.* Here, we inserted the Ll.ltrB intron in the reported system pICG for comparing the splicing abilities of both introns expressed under the same conditions.

First, we confirmed that Ll.ltrB was efficiently excised from pICG plasmids and compared it with pLI1, previously used by Matsuura *et al* (1997), observing that the expression under the inducible promoter T7 in pLI1 was several orders of magnitude higher. This finding may be the responsible for the accumulation of a big amount of intron mRNAs in the cell, allowing the detection of splicing reaction products which are in low numbers.

The study of Ll.ltrB intron in the *lacZ* context in *E.coli* revealed an splicing efficiency of Ll.ltrB ranged from (0.23 ± 0.05) %, as measured by qRT-PCR at 28ºC to (0.89 ± 0.04) %, as reported by β-galactosidase activity analysis in a culture grown at 24ºC. These values were 3.2 to 13-fold higher than those of *S.meliloti.* In addition, a previous work on Ll.ltrB intron expressed in its natural host *L.lactis* (Chen *et al.*, 2005) reported splicing efficiencies 85 to 315 times more efficient than that for RmInt1 in *S. meliloti,* probably due to the assistant of specific host-encoded proteins of *L.lactis* recruited to ensure the intron function. In that work, it was also postulated that temperature stress had no significant effects on expression and splicing of Ll.ltrB. Consistent with Yao *et al* (2006), who reported an inherent temperature sensitivity of the splicing reaction of Ll.ltrB expressed in *E.coli*, we have observed a decrease in the expression of Ll.ltrB when the temperature rises from 24ºC or 28ºC to 37ºC. Probably, this controversy could be the result of the influence of cell physiology and environmental conditions on the intron splicing. On the one hand, the changing dairy environment of *L.lactis* may influence that the host better resists temperature and other stresses while, in the other hand, a constant environment as that of *E.coli* could explain why this host is more sensitive to temperature variations.

Considered together, our results suggest that the splicing of RmInt1 in its natural host *S. meliloti*, where it interrupts the transposase of IS*Rm2011-2*, is much less efficient than that of other described bacterial group II introns, as Ll.ltrB. However, this inefficiency does not lead to defects in intron mobility, since a small amount of excised intron remains stable and accumulates, likely because of its association with the IEP,

forming ribonucleoprotein particles. In fact, this intron has been shown to spread well in *S. meliloti* (Martínez-Abarca *et al.*, 2000; Martínez-Abarca and Toro, 2000; Nisa-Martínez *et al.*, 2007). In contrast, the minimal quantities of ligated exons produced during the splicing process are more likely to be susceptible to cell degradation, giving little chance of transposase translation. According to this, it could be of interest the use of strong inducible promoters as that of T7, using T7 RNA polymerase introduced via a λDE3 lysogen or from a separate plasmid (Guo *et al.*, 2000; Karberg *et al.*, 2001) to increase the steady-state level of a significant cross section of transcripts (Carpousis, 2007). Another possibility it could be the use of an overexpressed RraA protein (*r*egulator of *r*ibonuclease *a*ctivity A), that binds to RNase E and inhibits RNase E endonucleolytic cleavages without interacting with substrate RNAs (Lee *et al.*, 2003). Nevertheless, this option is only available for strains containing a functional ortholog of *E. coli* RraA, not found in *S.meliloti.*

Finally, our findings support the postulated differentiation between bacterial and organellar group II introns (Dai and Zimmerly, 2002). In agreement with that, RmInt1 have many characteristic features attributed to bacterial group II introns. Its low splicing efficiency, as described above, occurs along with its localization in the insertion sequence IS*Rm2011-2* which, in turn, is located outside of any gene. In addition, although RmInt1 splicing efficiency is very low, its invasion capacity is high, helped by the presence of a reverse-transcriptase codified in the ribozyme DIV, because survival of group II introns in bacteria appears to rely on constant movement (Dai and Zimmerly, 2002). According with that, RmInt1 provides evidence of retroelement behavior, while its intronic character is less prominent.

CHAPTER 3

EFFECT OF POINT MUTATIONS IN CONSERVED POSITIONS OF THE RMINT1 GROUP II INTRON ON THE SPLICING REACTION *IN VIVO*

R.3.1 BACKGROUND

Splicing efficiency of group II introns located in bacterial genomes has been reported to be less efficient than that of those placed in organellar genomes of eukaryotic organisms (Dai and Zimmerly, 2002). The *in vivo* splicing of RmInt1 intron even shows a lower efficiency than that of other bacterial introns (See Chapter 1). However, it seems that there is no uncoupling between the two steps of splicing, since no traces of accumulation of intron intermediates of reaction has been observed (See Chapter 2, Figure R2.3).

The six domains of group II introns fold into a catalytically active structure following well-known conserved long-range tertiary interactions identified by phylogenetic covariation and biochemical analyses (Michel *et al.*, 1989; Lehmann and Schmidt, 2003; Fedorova and Zingler, 2007; Dai *et al.*, 2008). These include those involving Watson-Crick base pairs (α-α', β-β', γ-γ', δ-δ', ε-ε', IBS1-EBS1, IBS2-EBS2, and IBS3-EBS3), tetraloop-receptor interactions of known geometries (ζ-ζ', η-η', and θ-θ'), and other of less defined geometries (λ-λ', ϰ-ϰ', and μ-μ'). Recently, the use of site-specific cross-linkers to the establishment of distance constraints and the evolution of crystallography techniques have allow a more complex panorama of tertiary interactions (Toor *et al.*, 2009; Keating *et al.*, 2010; Pyle, 2010). Of these tertiary interactions, those involving 1) the conserved linker sequence between domain II and III (J2/3), which have been previously reported to interact with the catalytic domain V and to affect one or both splicing steps (Jacquier and Michel, 1990; Bar-Shalom and Moore, 2000; Mikheeva *et al.*, 2000; de Lencastre *et al.*, 2005; Keating *et al.*, 2010) and; 2) the 3'-intron boundary and the intron/3'-exon EBS3-IBS3 interaction, previously reported to inhibit the second step of the splicing reaction (Chanfreau and Jacquier, 1993; Costa *et al.*, 2000; Molina Sanchez *et al.*, 2011) were of our interest.

Compared to *in vitro* investigations, only few reports show data from *in vivo* studies using site-directed intron mutations. In the mitochondrial yeast aI5γ intron, *in vivo* splicing has been analyzed using ribozyme mutants affected in the conserved first nucleotide G1 (Peebles *et al.*, 1993), in selected positions of the catalytic DV (Boulanger *et al.*, 1995; Schmidt *et al.*, 1996) and in the length of the joining segment between domains 5 and 6 (Boulanger *et al.*, 1996). The *in vivo* studies were also extended to the *Scenedesmus obliquus* algae mitochondrial rI1 group II intron, where complete deletion of domains V and VI and substitutions of the first intron nucleotide and γ-γ' base pair were analyzed (Hollander and Kuck, 1999a; 1999b). A comprehensive study of mutations retaining mobility *in vivo*

were also developed for the bacterial Ll.ltrB intron from *Lactococcus lactis* (D'Souza and Zhong, 2002).

In this chapter, we studied the effect on the splicing of the RmInt1 group II intron of point mutations in positions in the intron ribozyme previously reported to be part of conserved tertiary interactions in ai5γ, Ll.ltrB and *Oceanobacillus iheyensis* group II introns (Dai *et al.*, 2008; de Lencastre and Pyle, 2008; Toor *et al.*, 2009; Toor *et al.*, 2010). Through the analysis of the effect of these mutations on the first and second splicing steps, we identified long-range interactions occurring in the RmInt1 tertiary structure which are common to other group II introns and deepened the understanding of the structural constraints involved in the intrinsic low efficiency displayed by RmInt1 intron.

R.3.2 MAP OF POINT MUTATIONS INTRODUCED IN THE RIBOZYME OF RmInt1 INTRON

Using site-directed mutagenesis (See section M.X, Materials and Methods), point mutations (substitutions and deletions), were introduced in the ribozyme of RmInt1 intron (Figure R3.1). All mutated intron positions have been shown previously to be part of conserved tertiary interactions during the *in vivo* and/or *in vitro* splicing of yeast and bacterial group II introns. The wild-type intron and its mutant derivatives were inserted in the pICG system for the *in vivo* splicing analysis.

We introduced a triple mutation in positions G1840, U1841 and U1842 which base pair with the conserved catalytic triad A1811, G1812 and C1843, located in the stem 1 of domain V and disrupting the Watson-Crick base pair (DV-CGA mutant) (Figure R3.1, violet box). Related mutations affecting the catalytic domain V has also been reported *in vitro* and *in vivo* (Jarrell *et al.*, 1988; Koch *et al.*, 1992; Dib-Hajj *et al.*, 1993; Boulanger *et al.*, 1995; Peebles *et al.*, 1995). Three mutations where introduced in J2/3 region. We deleted the conserved nucleotides G453 and A454 as previously reported by Mikheeva *et al* (2000) (J2/3-ΔGA mutant) (Figure R3.1, orange box). In addition, we assayed two mutations in the nucleotide G452, which is part of the conserved tertiary interaction γ-γ' with the C1884 position: its deletion (Δγ mutant) and its substitution by a C (GγC mutant) (Molina Sanchez *et al.*, 2011), disrupting the long-range interaction (Figure R3.1, blue box). On the other hand, the C1884 mutated to a G (Cγ'G mutant) (Molina Sanchez *et al.*, 2011) was assayed, which also disrupted the Watson-Crick interaction. A double G452C C1884G, restoring the γ-γ' base pair, was used as well (GγC-Cγ'G mutant) (Figure R3.1, blue box)

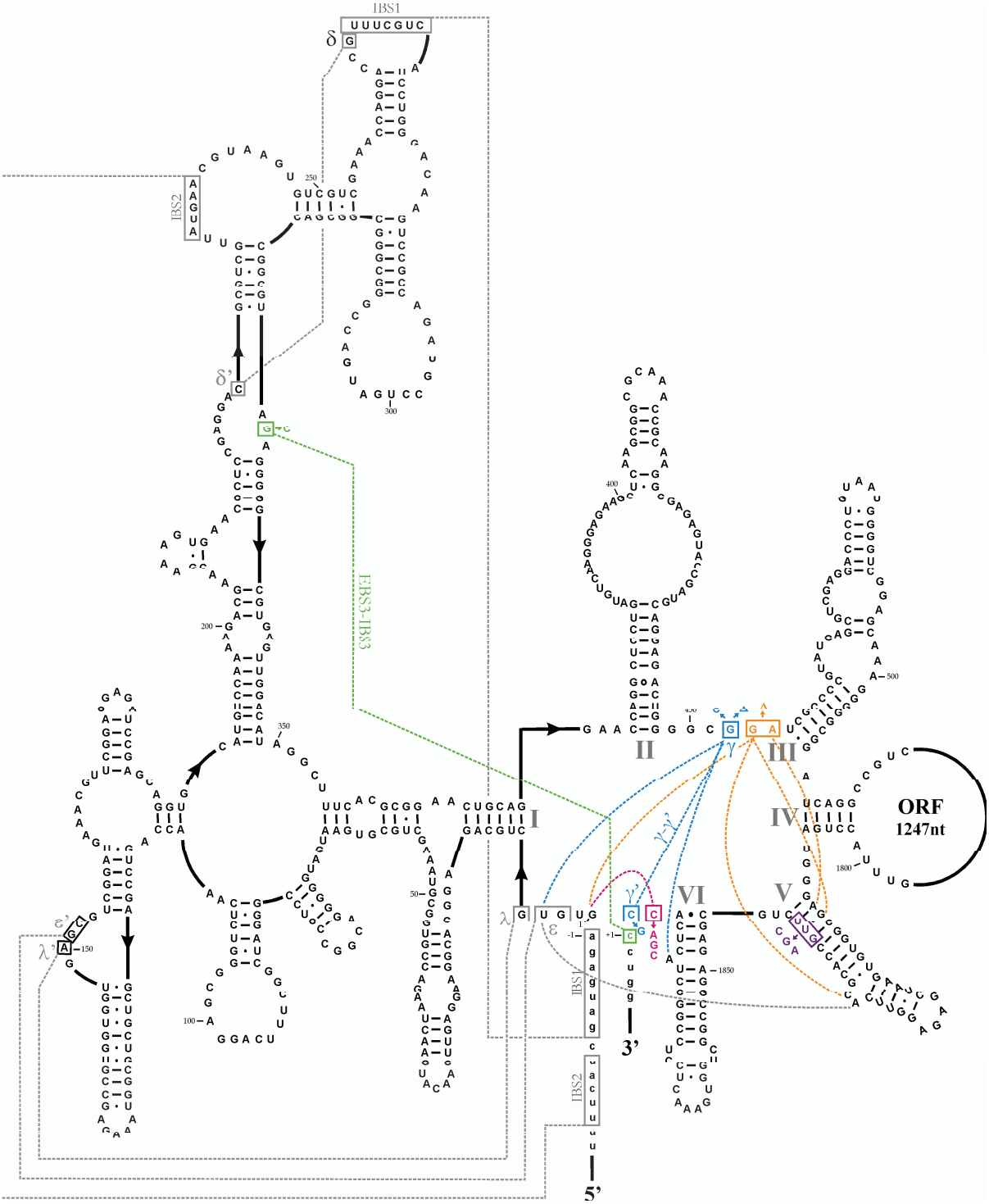

Figure R3.1. Diagram of point mutations and deletions of the ΔORF RmInt1 group II intron flanked by short exons (-20/+5). The mutation in the C+1 position was introduced in the full-length intron flanked by long exons (-146/+466). The RmInt1 intron sequence is indicated by upper-case letters; the exonic sequences are indicated by lower-case letters. Point mutations are indicated by an arrow follow by the new nucleotide. Deletions are represented by a Δ symbol. Interactions in which mutated position participate include conserved described interactions (Michel *et al.*, 1989; Jacquier and Michel, 1990; Chanfreau and Jacquier, 1993; Boulanger *et al.*, 1995; Costa *et al.*, 2000) and those obtained from crosslinks and/or crystal structure determinations described for ai5γ (de Lencastre *et al.*, 2005; de Lencastre and Pyle, 2008) *O.i.* (Toor *et al.*, 2008a; 2008b; Keating *et al.*, 2010) and Ll.ltrB (Dai *et al.*, 2008) introns.

(Molina Sanchez *et al.*, 2011). Mutations of the γ-γ' base pair have been previously described for the yeast ai5γ and the ascomycete *Podospora anserina* group II intron *in vitro* (Jacquier and Michel, 1990; Schmidt *et al.*, 1993) and for *S.meliloti* RmInt1 and *Chlamydomonas reinhardtii* rI1 *in vivo* (Hollander and Kuck, 1999a; Hollander and Kuck, 1999b; Molina Sanchez *et al.*, 2011). In the 3' boundary, the penultimate position C1883 was mutated to the other three bases (C to A, G and U) as previously assayed (Chanfreau and Jacquier, 1993) (C1883A, C1883G and C1883U mutants, respectively) (Figure R3.1, pink box). Finally, position G329 of the intron and C+1, located in the 3'-exon, were mutated to C and A, respectively (GEBS3C and C+1A mutants, respectively) (Figure R3.1, green box) (Molina Sanchez *et al.*, 2011). These positions, which are part of the conserved tertiary interaction EBS3-IBS3 observed in group IIB introns, has been analyzed both *in vitro* (Costa *et al.*, 2000) as *in vivo* (Robart *et al.*, 2004; Molina Sanchez *et al.*, 2011).

R.3.3 QUANTITATIVE ANALYSIS OF SPLICING EFFICIENCY IN WILD-TYPE AND MUTANT RmInt1 INTRON

We use the pICG reported system to accurately and quantitatively evaluate the splicing efficiency through the measurement of ligated exons in the wild-type and mutant RmInt1 intron constructions.

A relative quantification was used to determine the splicing efficiency of mutant derivatives related to wild-type RmInt1 intron construct (Table R3.1). The majority of mutants were severely affected in the splicing efficiency *in vivo,* showing less than 5 % splicing activity. These include DV-CGA, J2/3ΔGA, Δγ, Δγ+GEBS3C, GγC, Cγ'G and GEBS3C. GγC-Cγ'G and C1883G mutants showed between 15-20 % splicing activity. These data shed light on the importance of such positions in the splicing *in vivo.* Mutants in the penultimate position of the intron C1883A and C1883U were moderately affected, displaying splicing activities of 70 and 40 %, respectively. Finally, the relative activity of the C+1A mutant was similar to the wild-type allele, indicating that this position is not important for the *in vivo* splicing.

Note, however, that the splicing activity depends on the ability of the wild-type and mutant introns to efficiently and accurately go through the first and second steps of the splicing reaction and join the exons of the gene interrupted by the intron. Thus, effects observed in the splicing of mutant intron variants are the result of the addition of the defects added in each step of the reaction and, then, splicing efficiency values give no

information whether the first or second splicing steps were affected. As a consequence, it was necessary to compare with data of excision and accumulation of intron intermediates to figure out the effect of each mutation in the complete splicing reaction.

TABLE R3.1. RmInt1 splicing activity[a] in ΔORF and ΔORF mutant constructs expressed in *S.meliloti*[b]

Construction	% splicing ± error[c]
ΔORF	100
DV-CGA	1.2 ± 0.3
J2/3ΔGA	2 ± 2
Δγ	0.016 ± 0.007
Δγ+GEBS3C	1.3 ± 0.1
GγC	0.43 ± 0.09
GγC-Cγ'G	15 ± 3
Cγ'G	1.2 ± 0.2
C1883A	70 ± 30
C1883G	19 ± 3
C1883U	40 ± 10
GEBS3C	4 ± 1
C+1A	98 ±1

[a] Activity measured by relative quantification of a qRT-PCR assay.

[b] All mutants were introduced in the ΔORF construct and co-expressed *in trans* with the IEP protein, with the exception of the C+1A mutation, which was introduced in the full-length long-exon RmInt1 intron context.

[c] RmInt1 splicing is defined by the following equation: $2^{-\Delta\Delta CT}$ where ΔΔCT = ΔCT (mutant ΔORF) - ΔCT (ΔORF). ΔCT (mutant ΔORF) = CT (mutant ΔORF mRNA amplified by 5-6 primers) – CT (mutant ΔORF mRNA amplified by 16S_Fw-16S_Rv2 primers). ΔCT (ΔORF) = CT (ΔORF mRNA amplified by 5-6 primers) – CT (ΔORF mRNA amplified by 16S_Fw-16S_Rv2 primers). The result is expressed as a percentage related to ΔORF construct. The error is calculated applying the formula: $2^{-\Delta\Delta CT} \cdot \ln 2 \cdot \Sigma SE$.

R.3.4 QUANTIFICATION OF THE FIRST STEP OF THE *IN VIVO* SPLICING IN WILD-TYPE AND MUTANT RmInt1 INTRON DERIVATIVES

The first step of the splicing reaction *in vivo* was determined by the efficiency at which the intron excises from the precursor RNA. In order to accurately quantify excised intron products during the *in vivo* splicing both wild-type and mutant RmInt1 introns were subjected to primer extension assays (Figure R3.2). As previously assessed in Chapter 2, the excised lariat intron RNA (L) was detected as an extension product of 97 nt together with larger bands (not shown) derived from the 330-nt unspliced precursor (Pr) (Figure R3.2 A). The wild-type intron (lane 1) produced a strong intron band, which was quantified (see Materials and Methods and Figure R3.2 legend). The extension products of mutant-intron derivatives were also quantified and normalized to that of wild-type, giving relative excision efficiency values (Figure R3.2 B).

The most affected mutants in the excision capacity were DV-CGA (lane 2) and Δγ+GEBS3C (lane 5), with relative excision efficiencies of 3 and 7 %, respectively. They

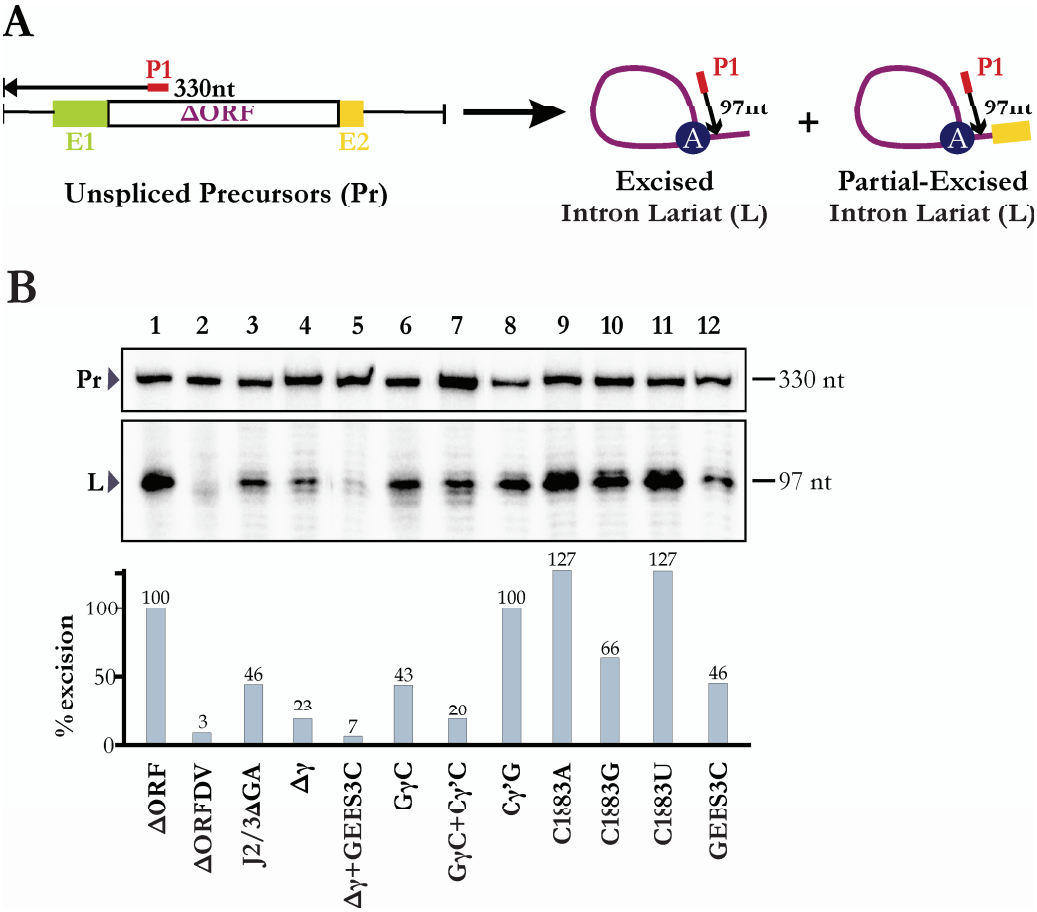

Figure R3.2. *In vivo* excision of the wild-type and mutant ΔORF intron in *S. meliloti*. **A** Schematic diagram of primer extension on linear unspliced precursor and excised and partial-excised intron lariats, showing the expected extension products derived from pICG plasmids. The bulged A in DVI is also indicated. **B** Primer extension assays were performed on total RNA extracted from *S. meliloti* harboring either the wild-type ΔORF (lane 1) or the mutant intron constructions (lanes 2-12) complemented with the IEP *in trans*. RNA was reverse-transcribed with a ^{32}P [γ-ATP] 5'-labeled primer complementary to the first 97 nt of RmInt1 ribozyme. The products were analyzed by electrophoresis in a denaturing 6% polyacrylamide gel, which was dried and quantified with a PhosphorImager. The major cDNA product of 97 nt corresponds to the excised intron RNA. Transcription was started from three different points, giving a strong unspliced precursor of 330 nt, characteristic of pICG plasmid, which were used as a loading control. Excision efficiency was calculated as the ratio of the intensity of the 97 nt product to that of the transcription start point, related to wild-type ΔORF construct (lane 1) and expressed as a percentage.

were followed by Δγ (lane 4) and GγC-Cγ'G (lane 7), with excision efficiencies of 23 and 20 % respectively. Mutants J2/3ΔGA (lane 3) and GEBS3C (lane 46) showing 46 % excision efficiency and GγC (lane 6) with 43 %, were moderately affected. By contrast, C1883G (lane 10) presented a low decrease in the excision efficiency, whereas Cγ'G (lane 8), C1883A (lane 9) and C1833U (lane 11) showed a wilt-type phenotype.

Considered together, it was observed that mutations primarily affecting the first step of the RmInt1 splicing reaction *in vivo* are located in the catalytic domain V, in the J2/3 region and in the EBS3 position in the coordination loop of the ribozyme. By contrast, mutations located in the 3'-intron boundary produced no decrease in the intron excision capacity. Note, however, that the measure of the first step of splicing makes no difference between partial and full-excised intron forms, then requiring the determination of the extent at which the intron is completely excised from the flanking exons (*vide infra*).

R3.5 OVERVIEW OF THE COMPLETE SPLICING REACTION OF MUTANT-DERIVATIVES AND WILD-TYPE RmInt1 ΔORF INTRON IN *S.meliloti*

In vivo splicing products from *S.meliloti* cultures harboring mutant-derivatives and wild-type ΔORF RmInt1 intron were tested by RNA gel blot analysis. Figure R3.3 shows northern hybridizations of various intron mutants with the intron-specific probe (left panel). For comparison, all filters were rehybridized with a probe specific for the 3'-exon of pICG plasmids (right panel). The ΔORF wild-type strain (lane 1) was used as a control.

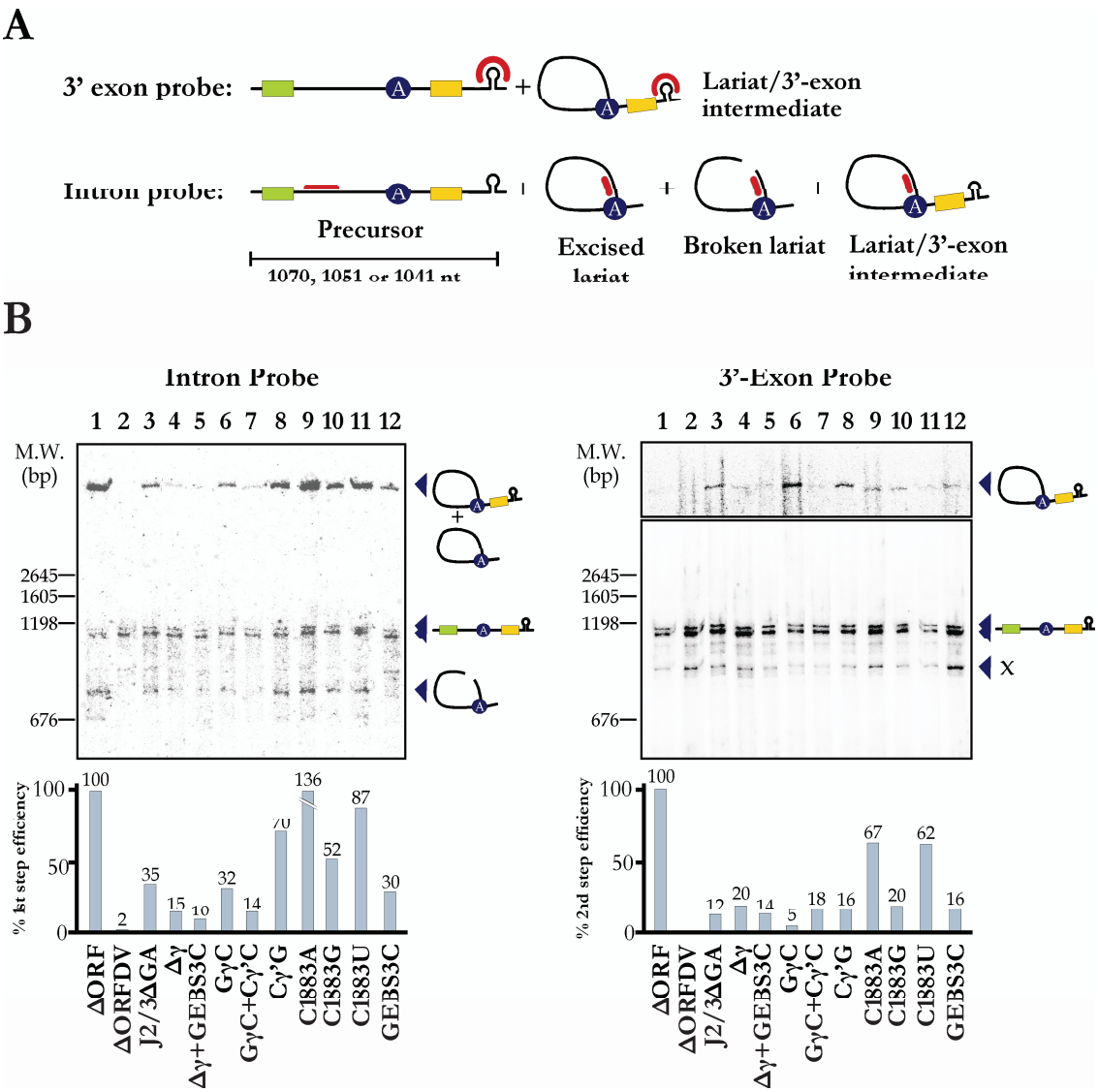

Figure R3.2. *In vivo* excision of the wild-type and mutant ΔORF intron in *S. meliloti*. **A** Schematic diagram of primer extension on linear unspliced precursor and excised and partial-excised intron lariats, showing the expected extension products derived from pICG plasmids. The bulged A in DVI is also indicated. **B** Primer extension assays were performed on total RNA extracted from *S. meliloti* harboring either the wild-type ΔORF (lane 1) or the mutant intron constructions (lanes 2-12) complemented with the IEP *in trans*. RNA was reverse-transcribed with a ^{32}P [γ-ATP] 5'-labeled primer complementary to the first 97 nt of RmInt1 ribozyme. The products were analyzed by electrophoresis in a denaturing 6% polyacrylamide gel, which was dried and quantified with a PhosphorImager. The major cDNA product of 97 nt corresponds to the excised intron RNA. Transcription was started from three different points, giving a strong unspliced precursor of 330 nt, characteristic of pICG plasmid, which were used as a loading control. Excision efficiency was calculated as the ratio of the intensity of the 97 nt product to that of the transcription start point, related to wild-type ΔORF construct (lane 1) and expressed as a percentage.

Intron mutations resulted in alterations of splicing activity *in vivo* in a variable extent. Intron mutants with altered positions located in DV, the J2/3 region and the EBS3 position in the coordination loop (lanes 2-7 and 13) showed intron probe hybridization signals lesser than 35 % related to wild-type ΔORF construct (lane 1) (left panel). Of them, the DV-CGA (lane 2) was the most affected, with barely detectable hybridization signal. It was followed by the double mutant Δγ+GEBS3C (lane 5), Δγ (lane 4) and the double mutant GγC-Cγ'G (lane 7), restoring the γ-γ' base pair, which showed intron hybridization signals lesser than 15 %. In the contrary, mutants affected in the 3'-intron boundary (lanes 8-11) showed intron signals higher than 50 % related to wild-type (lane 1). Of those, the least affected mutant was C1883A (lane 9), which displayed a strong intron signal, higher of that of wild-type intron (lane 1).

The accumulation of intermediate products of reaction was used as a rough measurement of the second splicing step efficiency, as observed when the filter was hybridized with a 3'-exon-specific probe (right panel). As expected, the wild-type intron (lane 1) did not show any 3'-exon signal and then, no reaction intermediate accumulation. Alterations in the G453 position, the J2/3ΔGA (lane 3) and GγC (lane 6) mutants, displayed a marked 3'-exon probe signal compared with that of intron probe, indicating an important accumulation of lariat/3'-exon. Particularly striking was the latter, which presented a 95 % decrease in the second splicing step with respect to the wild-type intron. The rest of mutant-intron derivatives resulted in a second splicing step efficiency lesser than 20 %, with the exception of those with altered penultimate position of the intron C1883A and C1883 U (lanes 9 and 11, respectively) were moderately affected in the second splicing step, as indicated the intensity of the 3'-signal probe. Note that both lariat intron and lariat/3'-exon intermediate products co-migrated, so just one lower-migrating band could be observed in samples accumulating reaction intermediates when hybridized with the intron probe.

From the analysis of data from Northern Blotting hybridization, we can conclude that mutations located in DV, the J2/3 region and the EBS3 position in the coordination loop, all affected the first splicing step in some extent. By contrast, mutations altering positions involved in the establishment of the conserved interaction γ-γ', the EBS3 nucleotide and the penultimate nucleotide of the intron, was all affected in the second step of the splicing reaction.

R.3.6 DISCUSSION

Here, we have elaborated a map of RmInt1 intron mutations affecting the first, second or both splicing steps based on the disruption of tertiary interactions established between conserved positions on the ribozyme.

We introduced a triple mutation in positions G1840, U1841 and U1842 which base pair with the conserved catalytic triad A1811, G1812 and C1843, located in the stem 1 of domain V. The mutation, disrupting the Watson-Crick base pair, strongly reduced the splicing efficiency *in vivo* (of which, at least the first step was affected, although we were not able to determine the effect of the second step). Boulanger *et al* (1995) previously assayed these mutations in the *in vivo* splicing of the ai5γ intron, showing an asymmetry of mutational effects in DV stem 1. Particularly, they found that A2, G3 and C4 (referred to the first position of DV) were essential for splicing *in vivo*, whereas U33, U32 and G31, base pairing with them, tolerated well the introduction of mutations. These results were also observed for the ai5γ intron *in vitro* (Peebles *et al.*, 1995). This made sense in the perspective of structure, since it has been shown that only the conserved 5'-AGC-3' nucleotides (and not their pairing partners) form hydrogen bonds with nucleotides of the J2/3 region and the AC bulge in DV, constituting a triple helix (triplex) which is essential for splicing catalysis (Toor *et al.*, 2008a; Toor *et al.*, 2009; Keating *et al.*, 2010). However, the simultaneous introduction of mutations in the RmInt1 DV and the loose of three base pairs could have an additive and deleterious effect on the splicing reaction which could explain how mutations in the opposite strand of that containing the conserved 5'-AGC-3' nucleotides, also produces a strong reduction in splicing efficiency.

The deletion of the dinucleotide G453 A454, located in the J2/3 region, produced an effect in both first and second steps of the splicing reaction, being the latter the most accused. Previously, Mikheeva *et al* (2000) reported a profound negative effect on the second step of splicing *in vitro*, but little effect on the first step, according with Chanfreau and Jacquier (1996), which observed a strong and specific effect on the second splicing step when they modified the adenosine residue. However, mutations in the same position resulted in affectation of both steps of splicing (Chanfreau and Jacquier, 1996). Despite its importance in the second splicing step repeatedly observed, the effect on the first step of splicing is supported by the crystallographic results recently obtained. In these, the position G288 (G453 for RmInt1 intron) of the J2/3 region has been shown to take part of the triple interaction with the G359 U384 base pair (G1812 U1841 in RmInt1 intron) and the C289 (equivalent to the A454) in the triple interaction with the C358 G385 (equivalent to the A1811 U1842) of the catalytic triad 5'-AGC-3' in DV (Keating *et al.*,

2010). In addition, the G588 (in ai5γ intron) has been previously observed to crosslink with the first nucleotide of the intron, which indicates its role in the approximation of the catalytic core to the 5'-splice site (Hamill and Pyle, 2006; de Lencastre and Pyle, 2008). Moreover, since the fact that a mutation located in the catalytic core affect both steps of splicing, is in accordance with results suggesting the occurrence of an unique active-site catalyzing both first and second steps of the splicing reaction (Chanfreau and Jacquier, 1994; de Lencastre *et al.*, 2005).

We also observed that mutations or deletions in the G452 (γ position) and mutations in the C1884 (γ' position) disrupting the conserved γ-γ' interaction resulted in a pronounced alteration of the second splicing step, accordingly with previous *in vivo* and *in vitro* studies. Thus, a complete loss of exon-exon ligation was observed for the rI1 intron from *S.obliquus* algae after disruption of the wild-type AγUγ' base pair when expressed *in vivo* in *E.coli* and in chloroplasts from *Chlamydomonas reinhardtii* (Hollander and Kuck, 1999a; 1999b). *In vitro,* it has also been shown that the γ-γ' base pairing is essential for an efficient second splicing step (Jacquier and Michel, 1990; Jacquier and Jacquesson-Breuleux, 1991). However, unlike the studies above, the double mutation restoring the γ-γ' base-pair did not eliminated defects on the second splicing step. Moreover, a decrease in the efficiency for 5' cleavage when the G452 was mutated, independent of the γ-γ' interaction, was observed both in single and double mutants restoring the base pair, whereas mutation in the C1884 showed a wild-type phenotype for the first step of splicing, in agreement with previous assays *in vivo* on the RmInt1 intron (Molina Sanchez *et al.*, 2011). These results can be explained on the base of crystallographic experiments on the *O.i.* group II intron. In those, it was showed that the γ nucleotide is located near the domain V bulge, positioning the 3' splice site for catalysis of the exon junction (Toor *et al.*, 2008c). In addition, as mentioned above, it has been establish the existence of a single active-site catalyzing both steps of splicing (Chanfreau and Jacquier, 1994; de Lencastre *et al.*, 2005). We proposed that the γ-γ' interaction is important for the second splicing step, as shown by the fact that mutations in the γ' position disrupting the γ-γ' base pair specifically affect the second step of splicing reaction. However, we think that mutations in the catalytic core have a predominant character in the RmInt1 intron, and so, when the γ position is mutated, both steps of splicing is altered, independently of the integrity of the γ-γ' interaction.

Mutations in the penultimate position of the intron resulted in a specific but slight affectation of the second step of the splicing reaction. The less tolerated base change was the C to G, which resulted in a 50 % reduction in the first step and an 80 % decrease in the second step of splicing. Mutations of the C1884 position to A and U resulted in a wild-

type phenotype. This result partially agrees with previous data obtained from the ai5γ intron (Chanfreau and Jacquier, 1993), in which the penultimate position is an A. According with this study, the substitution to a G strongly reduced the second splicing step as well as to a U, unlike that observed for the RmInt1 intron. Interestingly, we have found that the wild-type phenotype is kept both A and C nucleotides in the penultimate position of the intron. This position has been shown to interact with the first nucleotide of the intron, approximating the exon ends, which occurs after the lariat formation, through a non Watson-Crick interaction, as confirmed by the absence of compensatory substitutions (Chanfreau and Jacquier, 1993).

The substitution of the EBS3 position (G329) in the coordination loop resulted in a moderate effect in the first and second splicing steps, whereas the mutation of the first nucleotide of the 3'-exon showed a wild-type splicing efficiency level. This effect on the first step splicing has been recently reported by Molina-Sánchez and colleges (Molina Sanchez *et al.*, 2011), who proposed that this observation could be the result of the increase in the reversibility of the first step (and so the reduction of excision product) due to the impairment in the second step, thus preventing the reaction to proceeds until completion. On the other hand, the wild-type splicing efficiency produced by the mutation in the first nucleotide of the 3' exon is in agreement with the observation that the 3' exon could be minimized to a single monophosphate group, not being determinant in the second transesterification reaction during splicing neither the nature nor the sequence composition of that (Müller *et al.*, 1991). Moreover, in agreement with our results, it has been previously reported that the coordination loop spatially organizes all reactants involved in both steps of group II intron self-splicing *in vitro* (Costa *et al.*, 2000; Hamill and Pyle, 2006). The role of the EBS3 in the coordination loop on the approximation of exon ends and the interaction with the DV has been elucidated through the analysis of the structure. Thus, the 5' and 3' exons are brought together and recognized by EBS1 and EBS3 motifs (interacting with the IBS1 motif in 5' exon and IBS3 nucleotide in 3' exon, respectively), which are joined through the δ-δ' interaction (Toor *et al.*, 2008b); on the other hand, the coordination loop interacts with the ϰ motif, which in turn, forms a binding interface within the noncatalytic face of DV (Toor *et al.*, 2010). This arrangement presents then the scissile phosphate to the active site in DV, carrying on both steps of splicing, which are coordinated within the active site.

Taking all together, our data show that disruption of interactions in which components of the catalytic core are included affected both steps of splicing, supporting that a unique catalytic site carries out both splicing steps. In the contrary, interactions

promoting the approximation of exons but not included in the catalytic core exclusively affected the second splicing step.

Moreover, the analysis of mutations affecting conserved positions in the ribozyme has allowed us a deeper understanding of tertiary interactions in the RmInt1 group II intron, which in turn could give us the clues needed for the improvement of the splicing efficiency and the use of RmInt1 as a biotechnological tool.

CHAPTER 4

Self-splicing of RmInt1 group II intron: a qualitative, quantitative and mutational analysis

R.4.1 BACKGROUND

Some group II introns can catalyze their own splicing *in vitro* (self-splicing reaction *in vitro*), in a manner independent of protein assistance, though under non-physiological conditions such as high concentrations of monovalent salts (Lambowitz and Zimmerly, 2010). As occurring *in vivo*, self-splicing can occur via a branching pathway by means of two sequential transesterification reactions. In the first step, the 2' OH of the branchpoint adenosine in DVI acts as the nucleophile to attack the 5'-splice site, producing an intron lariat-3' exon intermediate. In the second step, the 3' OH of the cleaved 5' exon is the nucleophile and attacks the 3'-splice site, resulting in exon ligation and excision of an intron lariat RNA (Figure R4.1 A) (van der Veen *et al.*, 1986). A hydrolytic pathway, in which the first step of splicing involves the use of a water molecule or a hydroxyl ion as the nucleophile, may also occur both *in vitro* and *in vivo* (Figure R4.1 B) (Jarrell *et al.*, 1988b).

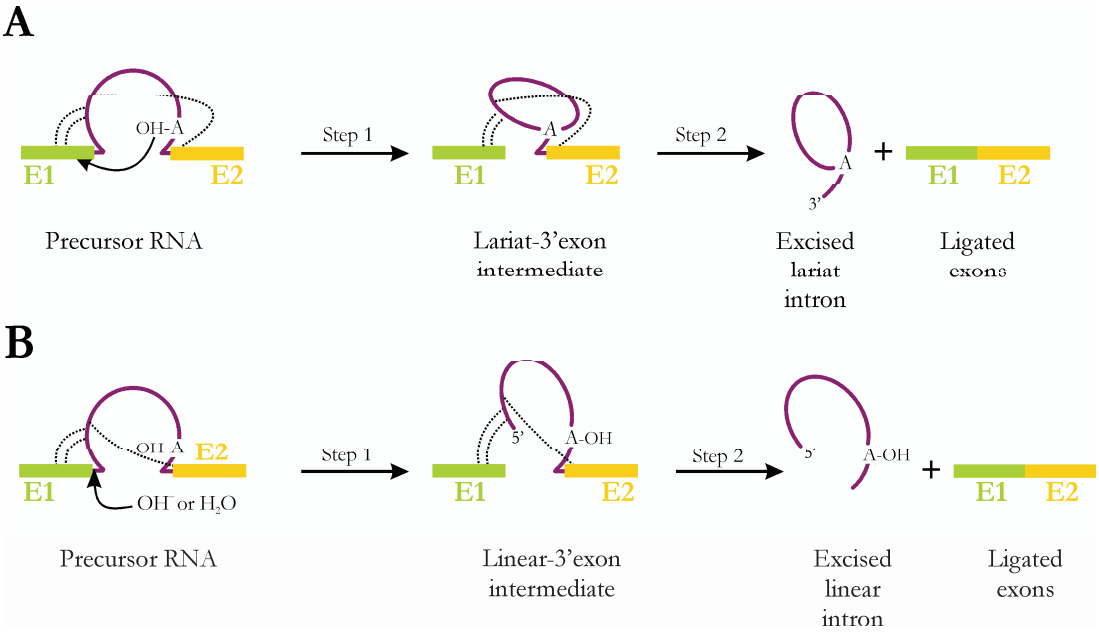

Figure R4.1. Schematic representation of the observed reactions during *in vitro* self-splicing of group II introns. All reaction products can be observed in high resolution polyacrylamide gels under a particular set of reaction conditions. **A** Schematic of the branching pathway. It is the predominant pathway observed in the presence of high concentrations of ammonium salts. The first step of splicing proceeds through a branch-point attack on the 5'-splice site, followed by a second attack of the 5'-exon on the 3'-splice site. The reaction leads to the formation of a lariat intron molecule, along with ligated exons. **B** Schematic of the hydrolytic pathway. It is the predominant pathway observed in the presence of high concentrations of KCl. In this route, the first step of splicing is mediated by a water molecule or a hydroxide ion on the 5'-splice site. After the second step of splicing, it results in the formation of a linear intron molecule and ligated exons. Adapted from Daniels *et al.* (1996).

These two pathways are sensitive to ionic conditions, in such way that, by varying the monovalent cation in the reaction mixture, one can force the ribozyme to prefer one reaction pathway over the other (Fedorova *et al.*, 2002). In the presence of ammonium salts, the branching pathway is predominant, leading to an intron excision as lariats (Peebles *et al.*, 1986; van der Veen *et al.*, 1986; van der Veen *et al.*, 1987; Jarrell *et al.*, 1988b; Bachl and Schmelzer, 1990; Daniels *et al.*, 1996; Zingler *et al.*, 2010). In this case, $(NH_4)_2SO_4$ at high concentration causes the highest increment of lariat with respect linear intron whereas in other monovalent salts as NH_4Cl, LiCl or NaCl is less prominent (Jarrell *et al.*, 1988b; Peebles *et al.*, 1993; Daniels *et al.*, 1996). In the presence of KCl buffer, the predominant route is the hydrolytic one, with linear intron as the main excised intron form (Jarrell *et al.*, 1988b; Peebles *et al.*, 1993; Daniels *et al.*, 1996; Zingler *et al.*, 2010).

To date a myriad of self-splicing assays have been performed in the well-studied aI5γ intron from *S.cereviasiae* mitochondria (Kwakman *et al.*, 1989; Koch *et al.*, 1992; Su *et al.*, 2001) and in other group II introns such as the first intron of the mitochondrial gene coding for cytochrome oxidase subunit I (COI I1) of *Podospora anserina* (Schmidt *et al.*, 1990), the aI1 intron of the mitochondrial *cox*I gene of *S.cerevisiae* (Hebbar *et al.*, 1992), the bacterial Ll.ltrB intron from *Lactococcus lactis* (Matsuura *et al.*, 1997) or that of the mitochondrial *rns* gene of the filamentous fungus *Leptographium truncatum* (Mullineux *et al.*, 2010). In general, these studies can be carried out through two major approaches: either studying self-splicing in an intron containing all intronic domains and flanking exons or dissecting the intron into several individual constructs (Fedorova *et al.*, 2002). Advantage of the first is the possibility of getting a global understanding of the overall reaction, observing the accumulation of each product and studying the effect of varying reaction conditions (Jarrell *et al.*, 1988b; Daniels *et al.*, 1996; Fedorova *et al.*, 2002). The second approach offers the means for dissecting the splicing process in individual reactions which can be readily characterized (Chin and Pyle, 1995; Fedorova *et al.*, 2002).

The bacterial group II intron RmInt1 has been also subjected to *in vitro* self-splicing analysis (Costa *et al.*, 2006a; 2006b). In these studies, constructs containing the ΔORF RmInt1 intron along with its flanked exons were assayed in $(NH_4)_2SO_4$ as well as in KCl buffers, showing a predominant lariat and linear intron formation, respectively (Figure R4.2 A). The 5' exons in these constructs were trimmed to its last 20 and 15 nucleotides, although the latter (pLM1) was shown to react better, with a first-order rate constant for conversion of precursor RNA into products of about 0.1 min^{-1} at 45 ºC and a fraction of reactive precursor molecules of 0.30 (Costa *et al.*, 2006a). Unlike other group II introns studied, self-splicing in RmInt1 led to the accumulation of lariat-3' exon intermediate,

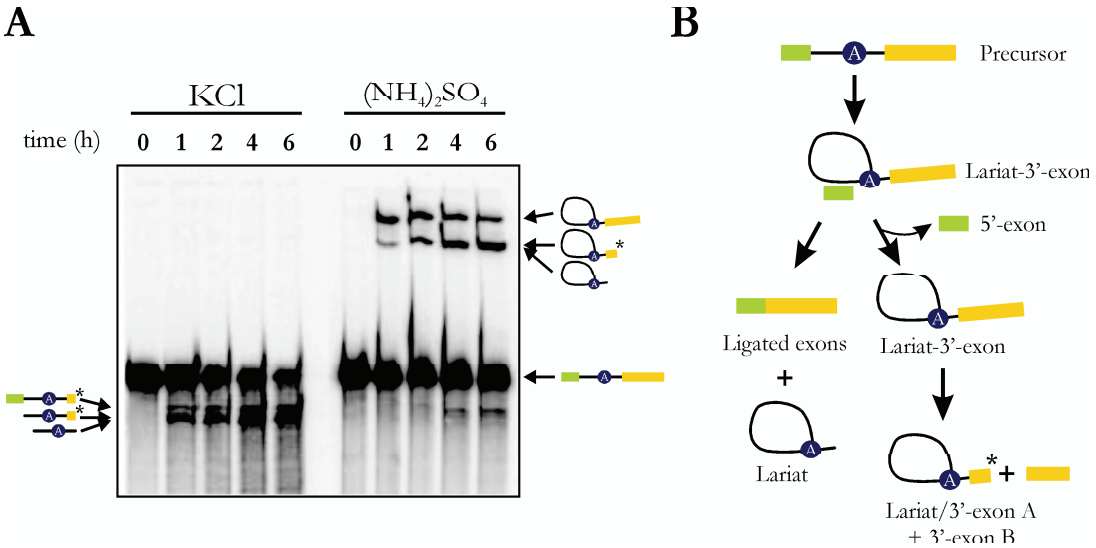

Figure R4.2. Self-splicing of pLM1 (ΔORF RmInt1 construct) at 45ºC (Costa *et al.*, 2006). **A** ^{32}P[α-UTP] radiolabelled precursor molecules were subjected to a self-splicing reaction in the presence of KCl (left side of the panel) or $(NH_4)_2SO_4$ (right side of the panel) buffer salts, respectively. Products were analyzed after separation by denaturing PAGE. On the far left and right, representations of products identified are shown. Products generated by cleavage at positions +10 or +11 of the 3' exons (IBS1* sequence; see the text for explanation) are marked with an asterisk. KCl buffer is 1 M KCl, 40 mM Tris-Cl pH 7.5, 100 mM $MgCl_2$, 1 mM Na_2EDTA. $(NH_4)_2SO_4$ buffer is 1 M $(NH_4)_2SO_4$, 40 mM Tris-Cl pH 7.5, 50 mM $MgCl_2$. **B** Proposed pathway framework for reactions of the ΔORF RmInt1 intron expressed from pLM1 plasmid under ammonium salt buffer. The intron is depicted as a black line; the branchpoint adenosine is market as a white A into a blue circle and; the exons are green (5') and yellow (3') boxes.

which predominated for at least 2 first hours of reaction, resulting in an unusually inefficient exon ligation. Moreover, an unexpected truncated lariat/3'-exon intermediate, with only 10 or 11 nucleotides in its 3'-exon, was found (Figure R4.2 A). This aberrant product was suggested to be a result of the ribozyme-promoted cleavage 3' of the sequence GACGAA or GACGAAG (hereafter designated as IBS1*), located in the 3'-exon, which matched better the EBS1 (UUUCGUC) sequence sited in the DI of the ribozyme than the authentic IBS1 (GAUGAGA)sequence in the 5' exon (Costa *et al.*, 2006a). This situation was explained as two parallel pathways competing for the lariat/3'-exon intermediate to yield the canonical lariat and ligated exons as well as the lariat/3'-truncated-exon plus a smaller 3' exon not ligated to 5' exon (Figure R4.2 B).

Based on the previous studies, our research had the following goals: (1) to improve the efficiency of the *in vitro* self-splicing reaction of RmInt1, and thus prevent the formation of unexpected products by testing different RmInt1-transcript contexts and reaction conditions (2) to elucidate the molecular mechanisms involved in the low splicing

efficiency displayed by RmIn1 intron *in vitro*, for which we introduced point mutations at conserved positions of the ribozyme in order to analyze their influence on the splicing reaction.

R.4.2 CONSTRUCTS FOR SELF-SPLICING ASSAYS

The pLM1 construct used in the ΔORF RmInt1 self-splicing assays by Costa *et al* (2006a; 2006b) is shown in Figure R4.3. In this RNA, RmInt1 5' exon was trimmed to its last 15 nucleotides, because it has been previously shown that long 5' exons can inhibit group II intron ribozyme self-splicing reactions (Nolte *et al.*, 1998). pLM1 contained a long 3' exon of 146 bp, similar to the previously studied ai5γ intron constructs (Daniels *et al.*, 1996), resulting in a 911 nt LT1 transcript synthesized from the T7 promoter (Figure R4.3 A). Interestingly, the 3' exon of pLM1, which was derived from the natural RmInt1 flanking exon of the IS*Rm2011*-2, carried an IBS1* sequence in its 5 to 10 or 11 first nucleotides. As mentioned above, it competes for the intron binding with the authentic IBS1 sequence (Figure R4.3 B) (Costa *et al.*, 2006a). As a result, a hydrolytic cleavage at this position occurred and truncated products appeared during self-splicing (Figure R4.2).

A pLM1-derivative pLM2 construct was created to circumvent problems associated with cross-interactions produced between the intron and the 3' exon in pLM1 plasmid. Similar to constructs used *in vivo,* we trimmed the RmInt1 3' exon of the IS*Rm2011*-2 to its first 5 nucleotides CCTGG to which a 128 bp fragment from the *E.coli lacZ* gene was added (Figure R4.3 B). The pLM2 plasmid was linearized by either *Nde*I or *Bam*HI restriction enzymes, which allowed us to synthesize two alternative transcripts. *Nde*I digest resulted in a 908 nt LT2 transcript (LT2), which no longer contained the IBS1* sequence. We predicted that the new 3'-exon would not be involved in novel tertiary contacts and it would potentially eliminate the kinetic trap caused by IBS1* sequence. *Bam*HI digest resulted in a smaller 775 nt ST2 transcript. This transcript keeps the EBS3-IBS3 tertiary interaction, while exons are long enough to resolve the precursor from the excised linear intron on a gel. Thus we could assay a transcript similar in length to RNAs produced for the *in vivo* splicing analysis.

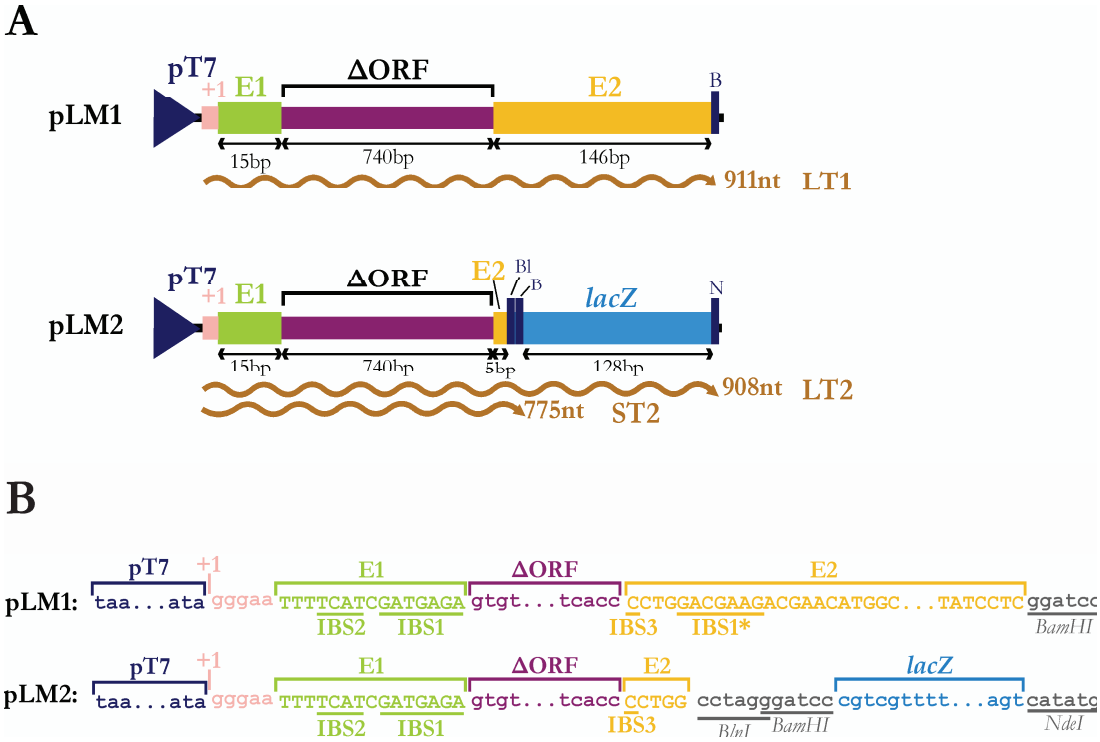

Figure R4.3. Constructs for RmInt1 self-splicing analysis. **A** Schematic diagram of RmInt1 intron-based constructions shown along with the RNA transcripts generated (below, wavy lines) after treatment with the restriction enzymes indicated. All the pLM constructs, derivative of pUC19 plasmid, contain the last 15 nucleotides of the RmInt1 5' exon (E1, green box) and the ΔORF RmInt1 intron (purple heave line), following the T7 promoter (blue arrow head) and a short transcription start sequence recognized by T7 polymerase (in a pink box). The 3' region in the pLM1 plasmid (Costa *et al.*, 2006) (yellow box) is comprised of 146 bp of the RmInt1 3' exon corresponding to the sequence of the IS*Rm2011-2* (E2, yellow box) and the *Bam*HI (B) restriction site, which allows the generation of 911 bp LT1 transcript by the T7 RNA polymerase from the T7 promoter. The 3' region in the pLM2 plasmid (yellow and blue boxes) is comprised of 5 bp of the RmInt1 3' exon (E2, yellow box) and 145 bp of the *lacZ* gene (positions 42-169) flanked by *Bln*I (Bl) and *Bam*HI (B) sites on the left and *Nde*I (N) site on the right (blue box). Two RNA transcripts can be synthesized from the T7 promoter in pLM2 plasmid: the 908 nt LT2, after *Nde*I digestion and the 775 nt ST2, after *Bam*HI digestion. **B** Detail of the pLM plasmids highlighting relevant sequences of the intron flanking exons. Different regions are colored according to elements in A. IBS elements and restriction sites are indicated.

R.4.3 OPTIMIZATION OF REACTION CONDITIONS

Prior to qualitatively and quantitatively study the kinetic behavior of RmInt1 intron splicing in these three constructs, we tested some reaction conditions previously used for *in vitro* aI5γ intron self-splicing (Daniels *et al.*, 1996; Fedorova *et al.*, 2007). We chose ST2 transcript because short exons transcripts has been reported to react with a higher rate

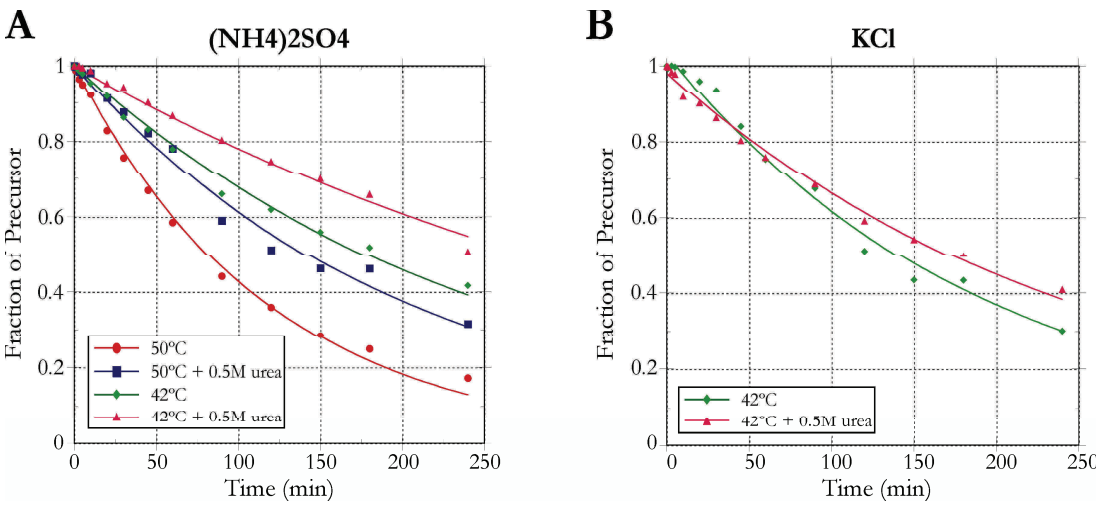

Figure 4.4. Optimization of RmInt1 self-splicing reaction conditions. Timecourses with ST2 transcript at different reaction conditions were carried out both in $(NH_4)_2SO_4$ buffer, predominantly promoting branched molecules and KCl buffer, mainly giving rise to linear molecules. Representative datasets of precursor disappearance were plotted against time. The data were fit to a single exponential. **A** Optimization of self-splicing of ST2 in $(NH_4)_2SO_4$ buffer varying the temperature reaction and the composition of salts. In all cases, $(NH_4)_2SO_4$ buffer contained 500 mM $(NH_4)_2SO_4$, 100 mM $MgCl_2$ and 80 mM MOPS (pH 7.5). Rate constants obtained from at least two independent experiments are (0.0027 ± 0.0003) min^{-1} for ST2 splicing adding 500 mM urea at 42 ºC; (0.0039 ± 0.0001) min^{-1} for ST2 splicing at 42 ºC; (0.006 ± 0.001) min^{-1} for ST2 splicing adding 500 mM urea at 50 ºC and; (0,0081 ± 0.0002) min^{-1} for ST2 splicing at 50 ºC. **B** Optimization of self-splicing of ST2 in KCl buffer varying the composition of salts. In all cases, KCl buffer contained 500 mM KCl, 100 mM $MgCl_2$ and 80 mM Mops (pH 7.5). Rate constants obtained from at least two independent experiments are (0.005 ± 0.001) min^{-1} for ST2 splicing adding 500 mM urea at 42 ºC and (0.0054 ± 0.0006) min^{-1} for ST2 splicing at 42 ºC

constant (Zingler *et al.*, 2010). All reaction were carried out at high monovalent and Mg^{2+}salt concentrations, since an unbalance in favor of the former has been observed to result in an inhibitory effect (Daniels *et al.*, 1996).

In ammonium sulfate buffer (500 mM $(NH_4)_2SO_4$, 100 mM $MgCl_2$ and 80 mM MOPS pH 7.5), we first conducted self-splicing reactions at 42 ºC, as described for the aI5γ intron (Daniels *et al.*, 1996; Chu *et al.*, 1998; Chu *et al.*, 2001; Zingler *et al.*, 2010) (Figure R4.4 A, green line). The apparent first order rate constant of this reaction was (0.00391 ± 0.00006) min^{-1}. One of possible reasons for such a slow reaction is misfolding of the precursor RNA. Therefore we attempted to alleviate this potential problem by using subdenaturing urea concentrations (0.5 M final concentration) in our splicing reactions (Fedorova *et al.*, 2007). However, we observed a decrease in the global rate constant which

was (0.00249 ± 0.00006) min^{-1} (Figure R4.4 A, pink line), which suggests partial unfolding of the RNA structure. We also observed that precursor did not react completely after long timepoints (not shown). In order to increase the amplitude of reaction, we raised the temperature from 42 ºC to 50 ºC, which resulted in almost complete disappearance of the precursor and two-fold increase of the reaction rate (0.0085 ± 0.0002) min^{-1} (Figure R4.4 A, red line). Again, the addition of urea resulted in a reduction in the observed rate constant, which was (0.0049 ± 0.0002) min^{-1} (Figure R4.4 A, blue line). We, therefore, chose to carry out the kinetic analysis of ammonium sulfate self-splicing reactions at 50 ºC in the absence of urea.

In potassium chloride buffer (500 mM KCl, 100 mM $MgCl_2$ and 80 mM MOPS pH 7.5), self-splicing reactions were tested at 42 ºC in the presence or in the absence of urea (Figure R4.4 B) (Jacquier and Rosbash, 1986b; Jarrell *et al.*, 1988b; Daniels *et al.*, 1996). A preliminary test performed at 50 ºC (not shown) resulted in a vast degradation at long timepoints, therefore we chose not to use these conditions. At 42 ºC, the apparent reaction rate was (0.0051 ± 0.0002) min^{-1}. Like in ammonium sulfate buffer, addition of subdenaturing urea concentrations resulted in a decrease in the rate constant, which was (0.0039 ± 0.0001) min^{-1}. Therefore, the kinetic analysis was performed at 42 ºC without the addition of urea.

R.4.4 QUALITATIVE ANALYSIS OF BRANCHING AND HYDROLYTIC SELF-SPLICING PATHWAYS OF RmInt1 INTRON

We then analyzed products obtained in course of branching and hydrolytic self-splicing pathways for different RmInt1 intron transcripts. For this purpose, reaction timecourses of LT1, LT2 and ST2 transcripts were carried out in the presence of high concentration of monovalent salts and the products were examined by PAGE (Figure R4.5). The branching pathway was induced by adding a $(NH_4)_2SO_4$ buffer to the reaction mixture (Figure R4.5 A) while the hydrolytic route was forced by adding a KCl buffer (Figure R4.5 B). Although not being favored, the hydrolytic pathway also occurred in the presence of ammonium salts (Figure R4.5 A).

In the presence of $(NH_4)_2SO_4$ buffer, LT1 gave rise to a comparable pattern of products than those observed by Costa *et al* (2006a) (Figure R4.2), despite some changes in the composition of reaction buffer (see Materials and Methods and legends of Figures

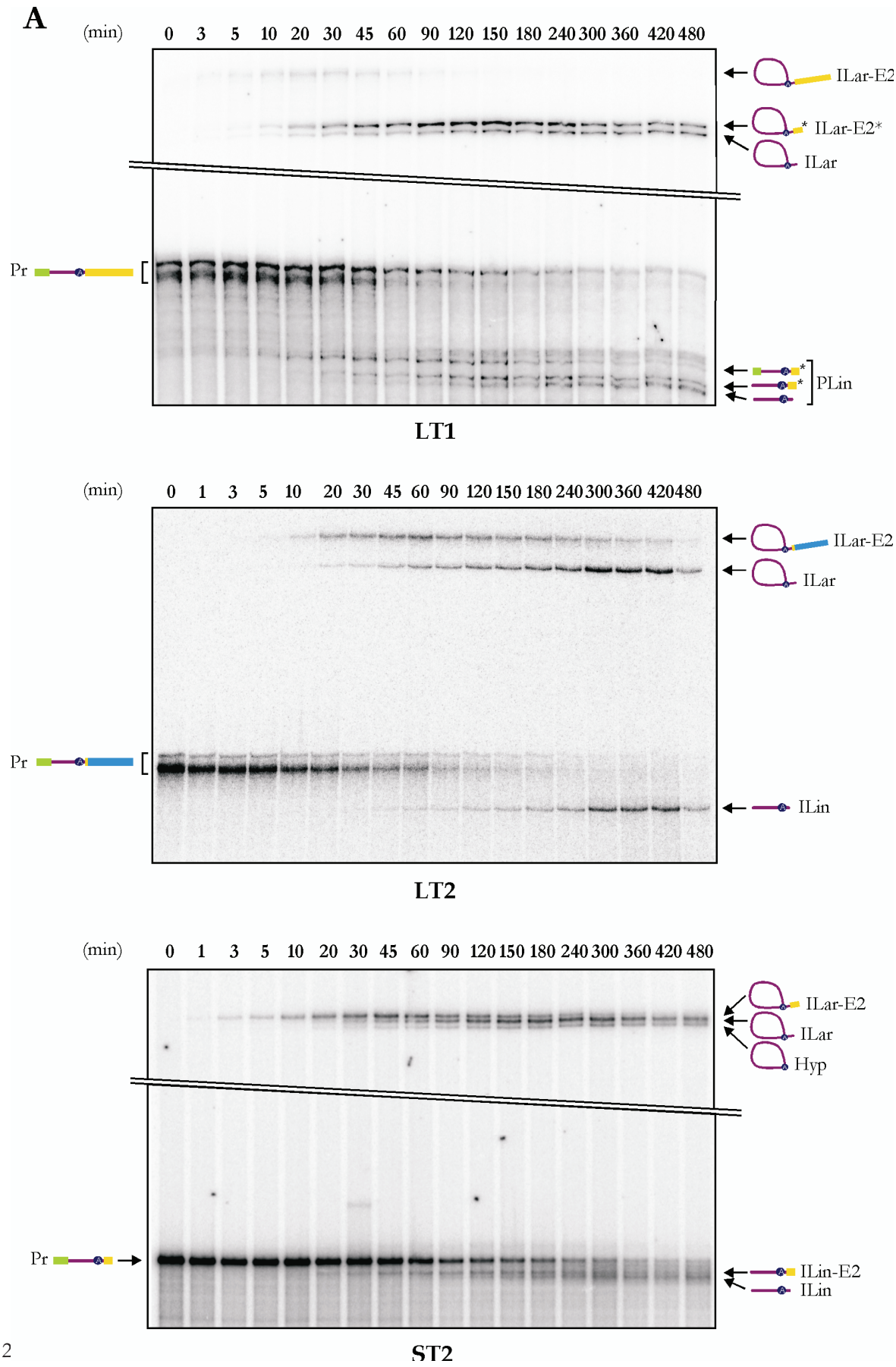
A
(min)
0 3 5 10 20 30 45 60 90 120 150 180 240 300 360 420 480
ILar-E2
* ILar-E2*
ILar
Pr
PLin
LT1
(min)
0 1 3 5 10 20 30 45 60 90 120 150 180 240 300 360 420 480
ILar-E2
ILar
Pr
ILin
LT2
(min)
0 1 3 5 10 20 30 45 60 90 120 150 180 240 300 360 420 480
ILar-E2
ILar
Hyp
Pr
ILin-E2
ILin
ST2

B

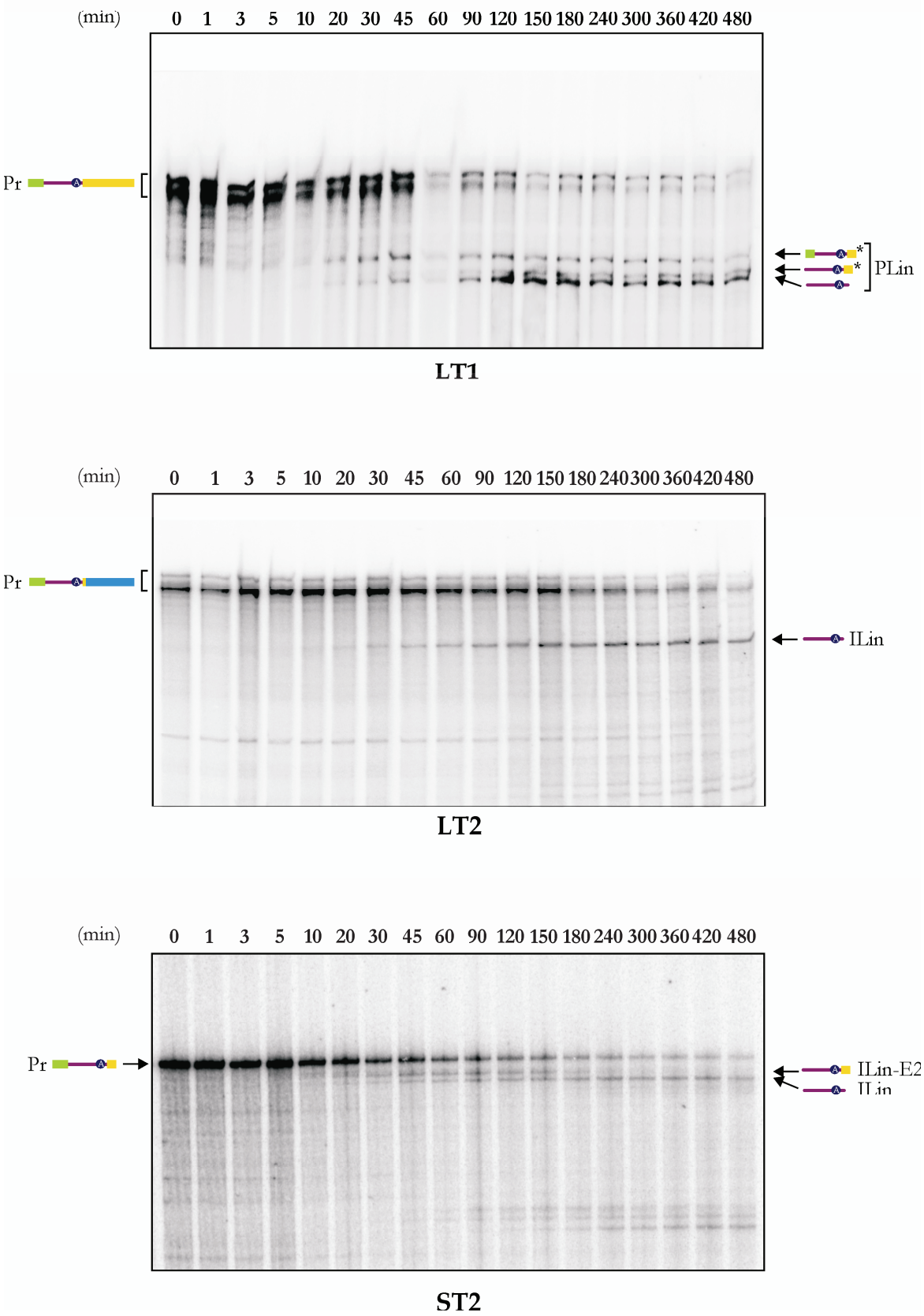
(min)
0 1 3 5 10 20 30 45 60 90 120 150 180 240 300 360 420 480
Pr
PLin
LT1
(min)
0 1 3 5 10 20 30 45 60 90 120 150 180 240 300 360 420 480
Pr
ILin
LT2
(min)
0 1 3 5 10 20 30 45 60 90 120 150 180 240 300 360 420 480
Pr
ILin-E2
ILin
ST2

Figure R4.5 Self-splicing of ΔORF RmInt1 from pLM constructs. Each sample, containing about 3 nM of ^{32}P [α-GTP] labelled precursor was subjected to self-splicing reactions in the presence of high concentrations of monovalent salts prior to be analyzed in a high resolution polyacrilamyde gel. On the far left and far right of autoradiograph panels are tentative interpretations of the various bands observed following color codes as in Fig R3.3. Upper panels represent self-splicing reactions from LT1 transcript; middle panels, those from LT2 transcript and; lower panels, those from ST2 transcript. **A** Self-splicing reactions carried out in the presence of $(NH_4)_2SO_4$ buffer at 50 °C. The reaction buffer contained 500 mM $(NH_4)_2SO_4$, 100 mM $MgCl_2$ and 80 mM MOPS (pH 7.5). **B** Self-splicing reactions carried out in the presence of KCl buffer at 42 °C. KCl buffer is 500 mM KCl, 100 mM $MgCl_2$ and 80 mM Mops (pH 7.5). Pr is precursor RNA; ILar-E2 is intron-lariat/3'-exon intermediate; ILar-E2* is the intron-lariat/3'-exon intermediate cleaved at the IBS1* sequence; ILar is the intron lariat; PLin is the complete set of linear products; ILin is the linear intron; Hyp is an hypothetical intron-derived product.

R4.2 A and R4.4 A). Low-migrating (presumably) branched molecules were predominant, especially those assumed to be lariat intron and lariat-intron/IBS1*-truncated-3'-exon (Figure R4.5 A, upper panel). The band corresponding to a lariat-intron/complete-3'-exon was barely detectable, disappearing completely at 150 minutes of reaction. Linear products were also observed. Of these, three were predominant over a background of linear products probably caused by RNA degradation. We hypothesized that these linear products are an IBS1*-truncated precursor, an IBS1*-truncated linear-intron intermediate and a linear intron form, as previously reported by Costa *et al* (2006a). However, unlike in previously published observations, precursor reacted to completion. In LT2 transcript, self-splicing timecourse revealed a smaller number of discrete product bands (Figure R4.5 A, middle panel). Early in time, a low-migrating band, probably a branched intermediate was observed, which then gave rise to a branched smaller-sized lariat molecule. A unique linear band, which accumulated over time, was also detected (Figure R4.5 A). Precursor, which reacted completely, was accompanied by a less intense lower-migrating linear band, probably because the transcript is a mixture of two species. In timecourses conducted with ST2 transcript (Figure R4.5 A, lower panel), the precursor reacted almost to completion, giving rise, via the branching pathway, to two low-migrating bands assumed to be lariat/3'exon intermediate and lariat intron, respectively. Along with these, a third product, deriving apparently from the intermediate/3'-lariat form, was observed. Alternatively, by the hydrolytic pathway, two linear bands were observed, the first one originated from the precursor and interpreted to be a linear intermediate, and the second, a likely linear intron.

Consistent with previously published data (Costa 2006a), in KCl buffer the LT1 transcript gave rise to three linear bands, previously identified as an IBS1*-truncated

precursor, a linear-intron/IBS1*-truncated-3'-exon intermediate and a linear intron form (Figure R4.5 B, upper panel). In timecourses from the LT2 transcript, a prominent product band, assumed to be a linear intron, accumulated over time as precursor reacted; however, no other linear intermediate product was observed. Finally, the reaction of the ST2 transcript resulted, first, in a transient linear band of a slightly smaller size than the precursor that, in turn, produced two smaller linear bands interpreted to be a linear intermediate and a linear intron form, respectively.

R.4.5 CHARACTERIZATION OF SELF-SPLICING PRODUCTS BY DNAZYME CLEAVAGE

DNAzymes, also known as deoxyribozymes, are catalytically active DNA molecules that cleave RNA (Silverman, 2005). DNAzymes were first identified through *in vitro* selection in 1994 (Breaker and Joyce, 1994). The mechanism of RNA cleavage by DNAzymes involves the attack of an RNA 2'-hydroxyl group on the adjacent phosphodiester linkage in the presence of Mg^{2+} or other divalent ions, resulting in 2',3'-cyclic phosphate and 5'-hydroxyl RNA termini (Figure R4.6 A) (Pyle *et al.*, 2000; Silverman, 2005). The DNAzyme in the 10-23 family, which has been used in this work, is comprised of a small catalytic core flanked by two arms that base pair with RNA (9-14 nucleotides depending on the sequence) (Figure R4.6 A) (Santoro and Joyce, 1997) [see Silverman (2005) for a comprehensive study of different DNAzyme families]. They can cleave any 5'-purine-pyrimidine-3' linkage (5'-RY-3') in the RNA sequence, although a uridine is preferred rather than a cytidine (Pyle *et al.*, 2000). DNAzymes can be used for excision of small fragments of RNA from a larger parent RNA in order to study the fragment in detail (Pyle *et al.*, 2000) or for linearization of circular molecules.

In this study, DNAzymes were used for the generation of a pattern of fragments characteristic of each RNA molecule, as in a restriction analysis. Through the comparison of motifs we carried out a preliminary identification of forms produced during self-splicing, which was the previous step to the quantitative analysis of reaction rates.

R.4.5.1 Design of DNAzymes for splicing product analysis

Six DNAzymes were designed taking into account cleavage site preferences. Cleavage sires were interspersed in the sequence, in order to get as many different cleavage

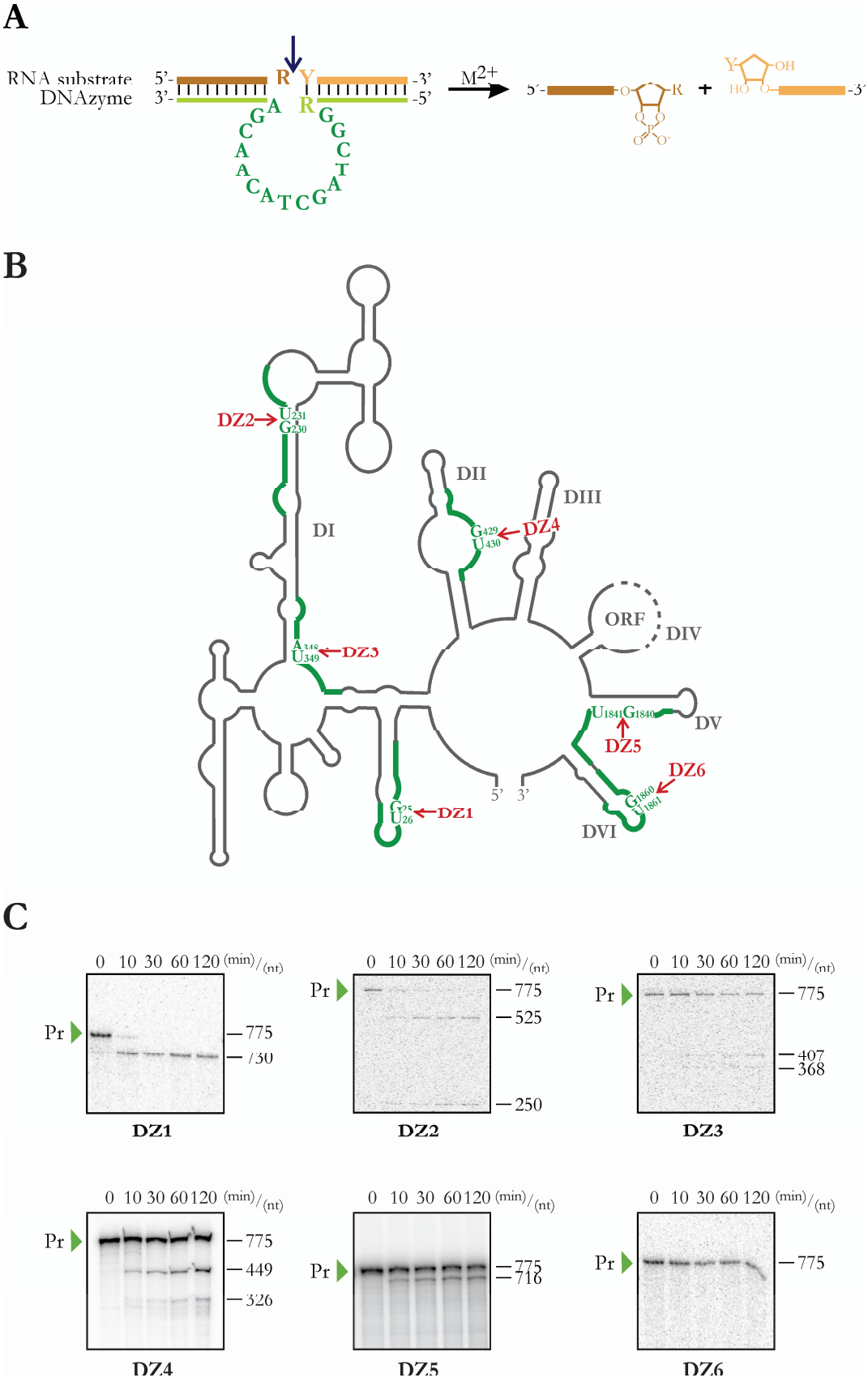
A
RNA substrate
DNAzyme
5'-
3'-
-3'
-5'
R
Y
M2+
OH
HO
B
DZ2
U231
G230
DII
DIII
DI
G429
U430
DZ4
ORF
DIV
DZ3
U1841
G1840
DV
DZ5
DZ6
5'
3'
G75
U26
DZ1
DVI
C
0 10 30 60 120 (min)/(nt)
Pr
775
750
525
250
407
368
449
326
716
DZ1
DZ2
DZ3
DZ4
DZ5
DZ6

Figure R4.6. DNAzymes for the analysis of self-splicing products. **A** Schematic representation of a DNAzyme with the 10-23 motif (Santoro and Joyce, 1997). It is comprised of two arms (light green) with a duplex stability of 10-12 kcal/mol (9-14 nt depending on the sequence) base paired to the RNA substrate (orange). The catalytic core is denoted by a green uppercase-letter loop. The arrow indicates the DNAzyme cleavage site produced between an unpaired purine nucleotide (R) and a pyrimidine (Y) in the RNA substrate in the presence of a divalent metal ion cofactor (M^{2+}). The cleavage results in 2',3'-cyclic phosphate and 5'-hydroxyl temini in the 5' and 3' RNA products, respectively. **B** Schematic of RmInt1 intron RNA showing the cleavage sites of designed DNAzymes on the molecule. DNAzymes DZ1, DZ2 and DZ3 were designed to cut the RNA domain I, whereas other three, DZ4, DZ5 and DZ6, recognized regions in domains II, V and VI, respectively. Base-paired regions of DNAzymes in the RNA substrate are denoted by bold lines in green. The cleavage site is indicated by a red arrow between the uppercase letter nucleotides (green) in the RNA substrate. **C** Cleavage efficiency of designed DNAzymes. ^{32}P [α-GTP] labelled precursor from the ST2 transcript (775 nt) was combined with an excess of DNAzyme, heated at 95 ºC to denature RNA and DNA and added to a magnesium salt buffer (see Material and Methods). Aliquots were taken out at selected timepoints and cleavage products were resolved by denaturing polyacrylamide gel electrophoresis (PAGE). Precursor RNA is indicated by a green arrowhead on the left of each panel, while sizes of precursor and cleavage products are shown on the right of each panel.

patterns as possible. (Figure R4.6 B; see Table MX.X in Materials and Methods for DNAzyme sequences). Three DNAzymes (DZ) were located in the domain I of the ribozyme: DZ1, cleaving between nucleotides G25 and U26 of RmInt1 intron; DZ2, between G230 and U231 and; DZ3, between A348 and U349. Other three DNAzyme cleavage sites were located in domains II, V and VI, respectively: DZ4 cleaved between G429 and U430; DZ5 between G1840 and U1841 and; DZ6, between G1860 and U1861.

The cleavage efficiency of these DNAzymes was determined using ST2 transcript as a substrate, which was chosen because of its small size and the appropriate range of fragments produced (Figure R4.6 C). Cleavage efficiency of DZ1, calculated as the reaction extent after 2 hours of incubation at 37 ºC in the presence of a magnesium salt (see Material and Methods for reaction conditions) was 98.5 %, which is the best among all DNAzymes tested. Two fragments of 730 nt (Figure R4.5 C, upper left panel) and 45 nt (not shown in the image) were obtained. DZ2 exhibited 89.2 % efficiency and produced two fragments of 525 nt and 250 nt (Figure R4.5 C, upper middle panel). DZ3, with a 45.5 % of cleavage efficiency, gave rise to two fragments of similar size, 407 and 368 nt. The DZ4 cut the ST2 transcript with an efficiency of 40.3 %, resulting in RNA fragments of 449 and 326 nt length. DZ5 showed a 20.2 % of cleavage efficiency and produced a large fragment of 716 nt and a smaller one of 59 nt in the ST2 molecule (not shown). Finally, DZ6 did not cleave the ST2 transcript at all, probably because the base pairing region is rich in GC and then hard to denature and access. Two DNAzymes, DZ1 and DZ2, were

classified as fast cutters (Pyle *et al.*, 2000), because they were able to almost completely cleave the RNA substrate in the first 10 minutes of reaction. In contrast, DZ3, DZ4 and DZ5 were considered as slow cutters, producing less than 50 % cleavage after 2 hours.

We chose to use DZ1 and DZ4 for the characterization of self-splicing products. DZ1, due to its ability to process the RNA substrate with a very high efficiency, was used to linearize circular forms (i.e. covalently closed molecules). DZ4, which yielded less than 50 % cleavage, was chosen because, in combination with DZ1, the intron and other splicing forms were divided into two fragments in a range of lengths appropriated to be accurately resolved by PAGE.

R.4.52 Self-splicing product characterization

Self-splicing products generated by two-hour preparative reactions of LT1, LT2 and ST2 transcripts were gel-extracted and reacted with DZ1, DZ4 or a combination of both (Figure R4.7). Precursor, undigested and partially digested products were used as size controls. LT1 self-splicing bands cut with DNAzymes were identified taking into account self-splicing product analysis previously reported for RmInt1 intron (Costa *et al.*, 2006a). According to this, probable unusual intermediate products were detected, in which the truncated 3' exon was attached to lariat (Figure R4.6 A, ILar-E2*, as part of band labeled as *a*, or linear intron (ILin-E2*, as part of band *b*. Lariat (ILar) and linear (ILin) intron bands were co-purified with lariat/3'-truncated-exon (ILar-E2*) and linear/3'-truncated-exon (ILin-E2*) bands, respectively. We could not isolate the lariat/3'-full-exon described in Costa's work, although we strongly believe it corresponds to the low-migrating band observed in time course gels (Figure R4.5 A, upper panel) but almost completely reacted after 2 hours.

In LT2 transcript, three self-splicing product bands, with the corresponding precursor, were isolated and preliminary characterized by DNAzyme digestion (Figure R4.7 B; bands *a*, *b* and *c*). The lariat intron (ILar) likely corresponded to band *b*, since it was linearized when treated with DZ1 (giving a 740 nt band) and divided into two fragments of about 404 and 336 nt when digested with a mix of DZ1 and DZ4, which were the sizes expected after this treatment. The lariat/3'-exon intermediate (ILar-E2) was isolated as band *a*. In this case, the linearized band had nearby the same mobility as the precursor while, as a result of the treatment with a DZ1/DZ4 mix, the band released a 404 nt fragment common with lariat intron plus an additional fragment of lower mobility,

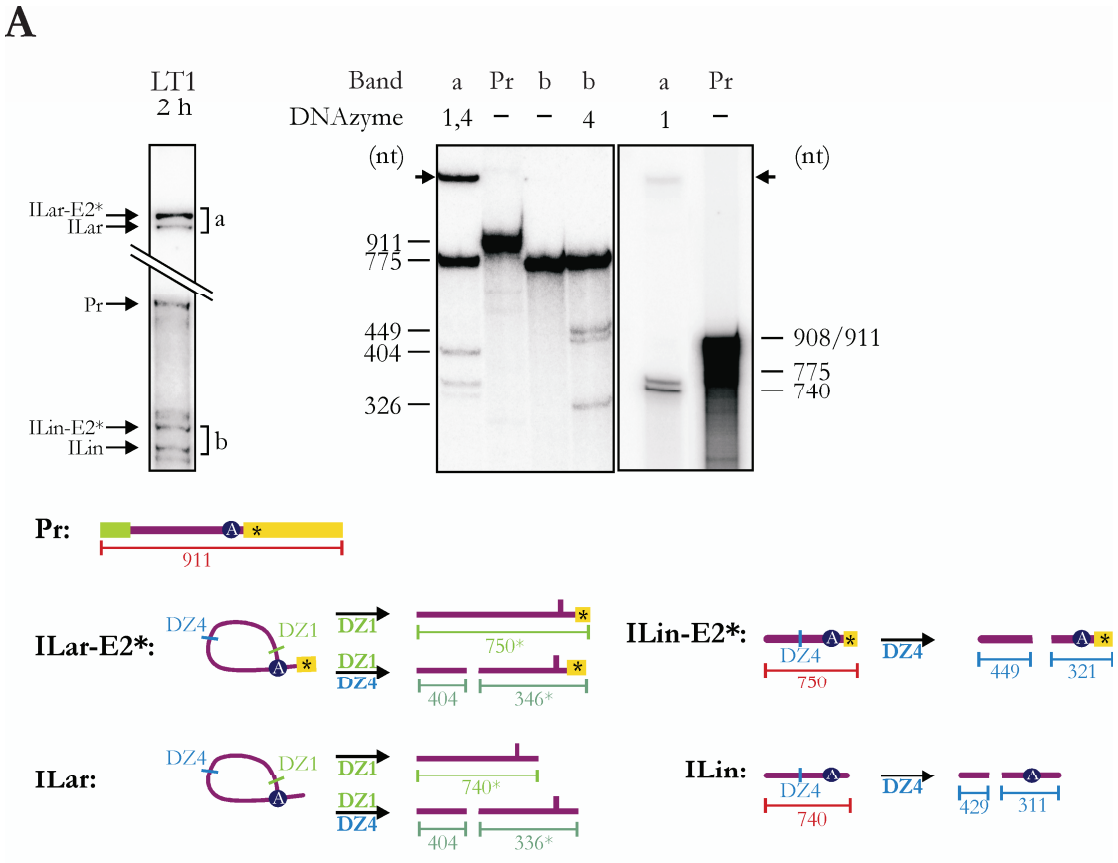
A
LT1
2 h
ILar-E2*
ILar
a
Pr
ILin-E2*
ILin
b
Band a Pr b b a Pr
DNAzyme 1,4 – – 4 1 –
(nt)
911
775
449
404
326
908/911
775
740
Pr:
911
ILar-E2*:
DZ4
DZ1
DZ1
DZ1
DZ4
750*
404
346*
ILin-E2*:
DZ4
750
DZ4
449
321
ILar:
DZ4
DZ1
DZ1
DZ1
DZ4
740*
404
336*
ILin:
DZ4
740
DZ4
429
311

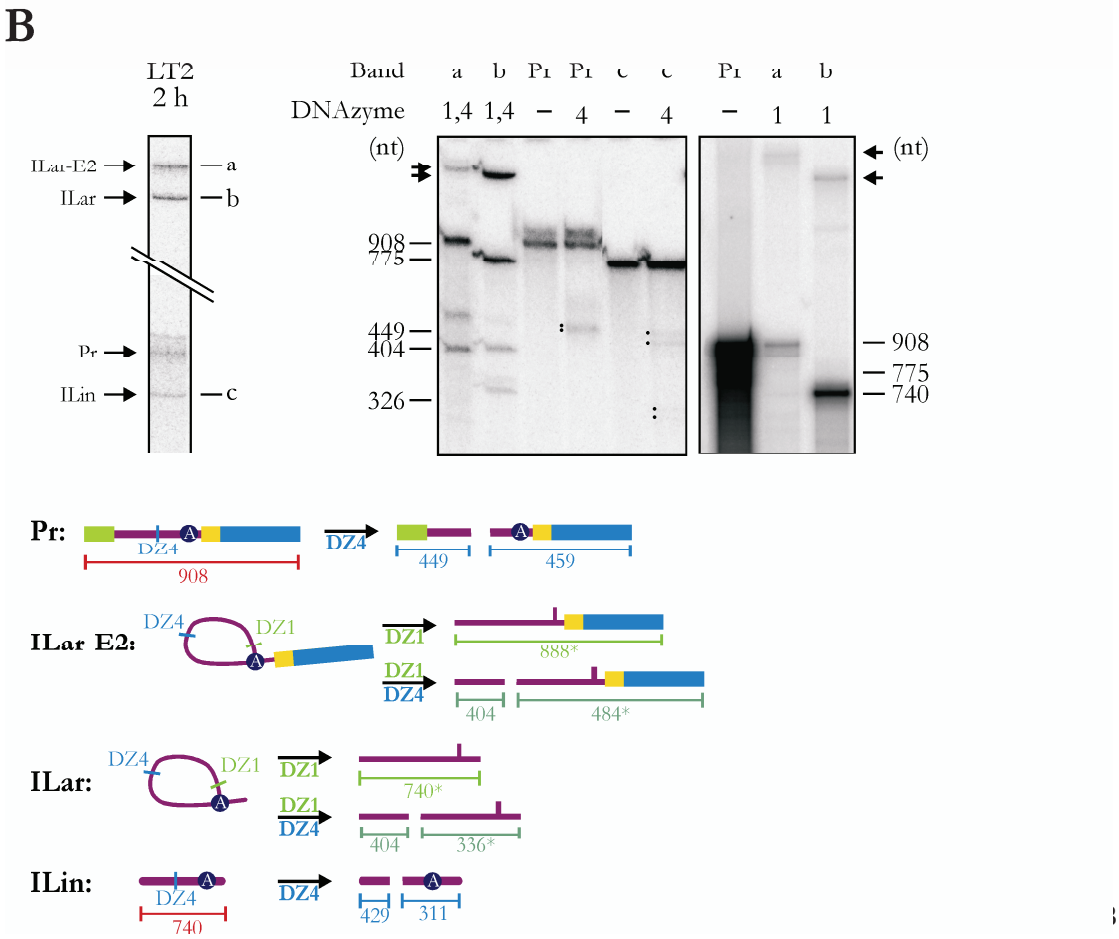
B
LT2
2 h
ILar-E2
ILar
a
b
Pr
ILin
c
Band a b P1 P1 c c P1 a b
DNAzyme 1,4 1,4 – 4 – 4 – 1 1
(nt)
908
775
449
404
326
908
775
740
Pr:
DZ4
908
DZ4
449
459
ILar-E2:
DZ4
DZ1
DZ1
DZ1
DZ4
888*
404
484*
ILar:
DZ4
DZ1
DZ1
DZ1
DZ4
740*
404
336*
ILin:
DZ4
740
DZ4
429
311

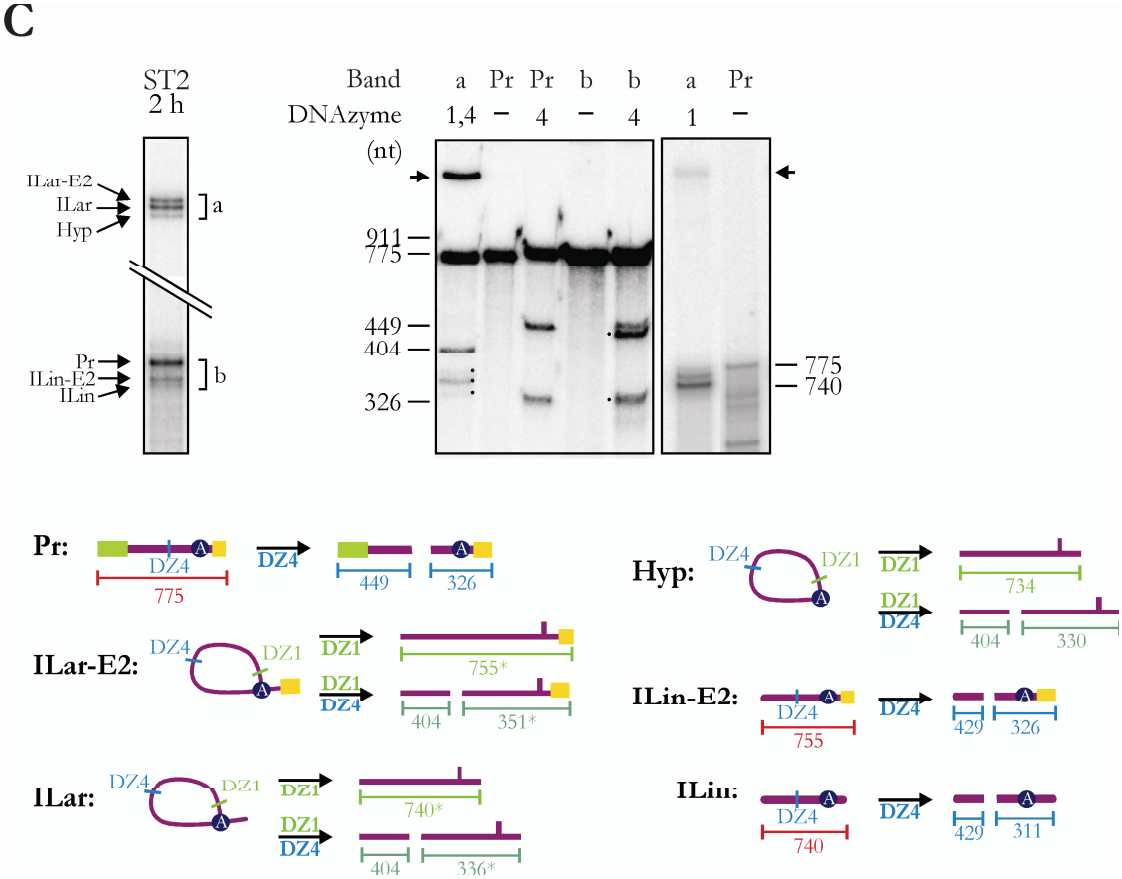

Figure 4.7. Identification of RmInt1 self-splicing products by DNAzyme treatment. ^{32}P [α-GTP] labelled LT1 (A), LT2 (B) and ST2 (C) transcripts were subjected to a preparative-scale self-splicing reaction for 2 hours in $(NH_4)_2SO_4$ buffer at 50 °C (see Materials and Methods). Products of self-splicing were purified by PAGE, eluted from the gel and cleaved with the DNAzymes indicated. In upper left panels, details of the self-splicing products at 2 hours of reaction are shown. The precursor and main products are indicated on the left while the corresponding isolated band are indicated with lower-case letters on the right. The cleavage products after DNAzyme treatment are shown in the upper right panels, along with known molecular sizes indicated on the left. Arrows indicate undigested remaining products. Below, schematic interpretations of the self-splicing products are displayed, indicating DNAzyme cleavage sites and the various fragments produced. Asterisks indicate branched products which can have a retarded migration. The color code and abbreviations are those specified in Fig R3.3 and R3.4, respectively.

which could be that expected of 484 nt. The band *c* was preliminary identified as the linear intron (ILin), since it gave rise to two products of sizes similar to the expected 429 and 311 nt after DZ4 cleavage. Besides, we noted that two bands close to the previous ones were detected, giving two doublets, which probably were due to degradation occurred after product isolation. There was no evidence of the presence of a linear/3'-exon intermediate (ILin-E2).

The ST2 transcript yielded self-splicing products of closed related sizes more difficult to resolve in a preparative gel. For that reason, branched and linear products were extracted as two single bands (*a* and *b*, respectively) and subjected to DNAzyme cleavage (Figure R4.7 C). Branched molecules included three products observed in time-course gels, which probably were the lariat/3'exon intermediate (ILar-E2), lariat intron (ILar) and a hypothetical intron-derived band (Hyp). After DZ1 and DZ4 digestion, a 404 nt fragment common to the three products was produced, along with three smaller bands, which could be those of 351, 336 and 330 nt, respectively, expected to obtain after digestion of the branching products above. Since linear products were partly contaminated by the slower migrating precursor, these were more difficult to characterize. Two cleavage fragments of about 326 and 311 nt were obtained, which could correspond to the expected linear intron (ILin) and linear/3'-exon intermediate (ILin-E2) forms, along with a fragment of about 429 nt, probably derived from both products after DZ4 cleavage.

R4.6 KINETIC ANALYSIS OF BRANCHING AND HYDROLYTIC SELF-SPLICING PATHWAYS WITH HIGH CONCENTRATIONS OF MONOVALENT ION

Once the self-splicing products formed via branching and hydrolytic pathways were identified, we analyzed their evolution over time under the best reaction conditions, determining their rate constants and amplitudes for the three classes of transcripts (see above). With the data collected, we put them all together to establish the best context of expression and reaction conditions for further *in vitro* studies of RmInt1 intron.

In order to determine the reaction rates, we first described each model by a differential equation and found an exact analytical solution for each equation (not shown). Then, the models (equations) were fitted to the experimental data using nonlinear regression to obtain estimates of parameters using the software packages Kaleidagraph (Abelbeck Software) and DynaFit (Kiokin Ltd). In complex reaction pathways, a simplification was introduced for the estimation of k_{br} and k_{hy}, in which all products proceeding from the branching and the hydrolytic pathways, respectively, were added together. For a detailed description of this approach and the equations used, refer to Materials and Methods (Section M.13.4).

R.4.6.1 Kinetics of self-splicing in the LT1 transcript

Self-splicing reactions of LT1 transcript under $(NH_4)_2SO_4$ buffer at 50 ºC (Figure R4.8 A, left panel) are described by the model shown in Figure R4.2 B. Notably, we do not observe the accumulation of any products containing intron and full-length 3'-exon, which are the intermediates formed after the first step of each reaction. This indicates that for all three pathways (branching, hydrolysis and exon truncation) the second steps are much faster than the first steps. Thus, the first steps are rate-limiting for all three reactions. Therefore we are determining rate constants only for the first steps of all respective reactions and the kinetic model can be simplified as illustrated in Scheme 1:

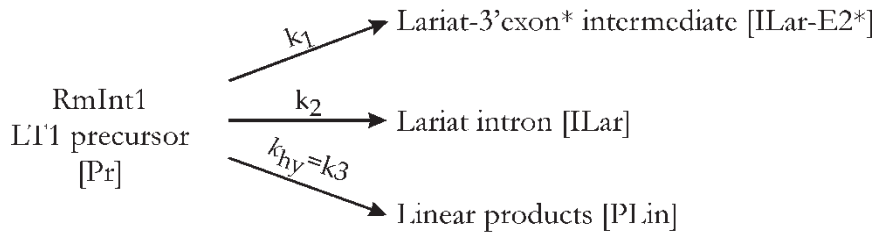

Scheme 1

where $k_{br} = k_1 + k_2$ and $k_T = k_1 + k_2 + k_3$. All products are considered to evolve simultaneously and independently from precursor, so the sum of product fractions (f_{br} and f_{hy}) will equal 1.

The overall k_T value of the reaction was 0.020 min^{-1} (note that standard errors for all rates are provided in Table R4.1), which was two-fold higher than that previously reported for RmInt1 intron (0.01min^{-1}) (Costa *et al.*, 2006a). The fraction of reactive

Figure R4.8. Kinetic analysis of RmInt1 self-splicing under high concentrations of monovalent ions. Splicing reactions were performed in the presence of either 500 mM $(NH_4)_2SO_4$ buffer (A) or 500mM KCl buffer (B). Experimental data for the decrease in precursor RNA and the evolution of products from Figure R3.4 were plotted and fit using DinaFit (BioKin Ltd). Models describing reactions in $(NH_4)_2SO_4$ buffer were fitted to equation (6) to (9) for LT1, (10) to (13) for LT2 and (14) to (19) for ST2 (see Materials and Methods). Models describing reactions in KCl buffer were fitted to equation (20) and (21) for LT1 and LT2, and to equations (22) to (24) for ST2 (see Materials and Methods). All reactions proceeded to completion at long times (8-9 hours), but the significant amount of RNA degradation that occurred after four hours of reaction prevented quantitative analysis after that time in the majority of samples. Reaction rates and product constants are summarized in Table R3.1. Pr is precursor RNA; ILar-E2 is intron-lariat/3'-exon intermediate; ILar-E2* is the intron-lariat/3'-exon intermediate cleaved at the IBS1* sequence; ILar is the intron lariat; PLin is the complete set of linear products; ILin is the linear intron; Hyp is an hypothetical intron-derived product.

A LT1

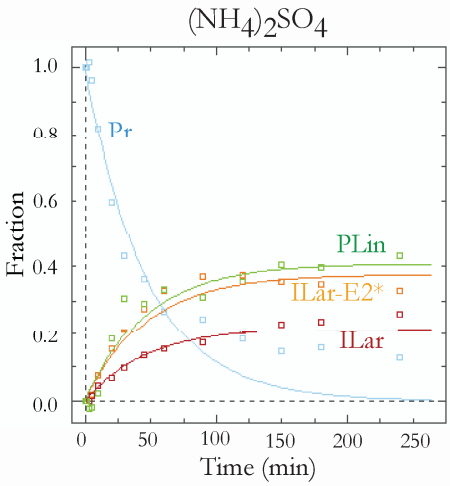

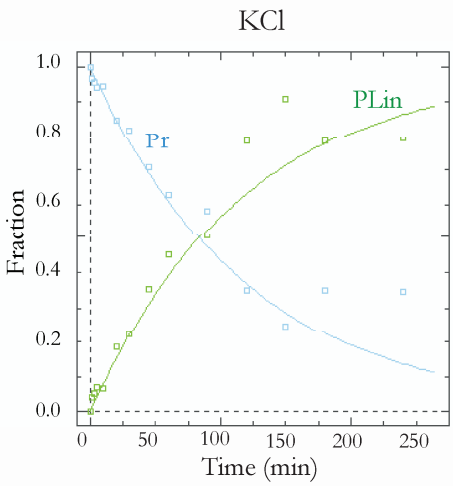

B LT2

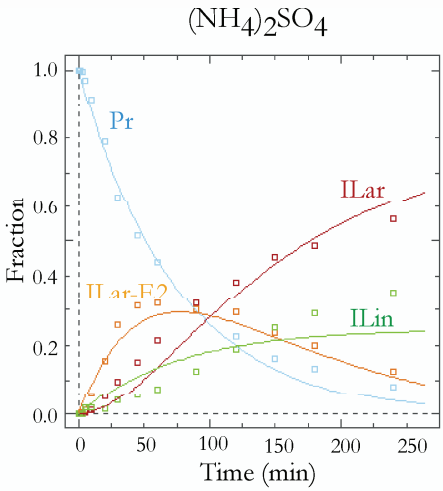

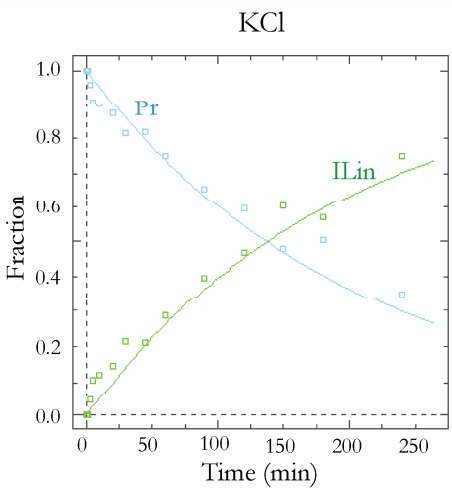

C ST2

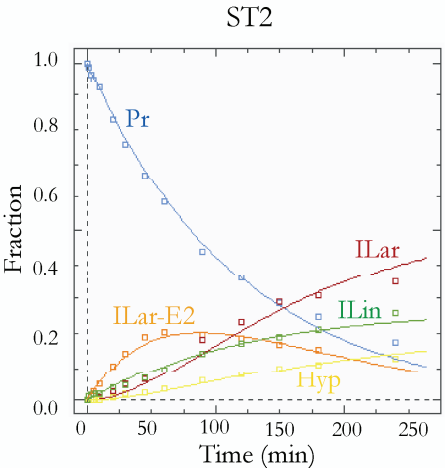

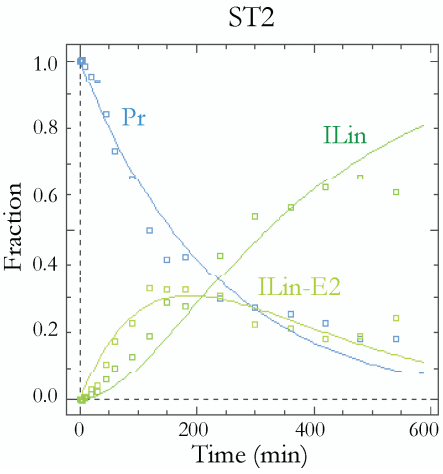

precursor observed was also increased [about 70% *versus* 30% (Costa *et al.*, 2006a) after 7 hours of reaction]. The plot of the overall reaction showed a monophasic behaviour, although the semi-log plot could only be adjust to a straight line as far as 60 minutes of reaction (Figure R4.9 A, green line), which may be caused by more noticeable degradation of the precusor RNA after this time point. Comparing with aI5γ intron, all precursor molecules of RmInt1 intron fell into the "fast" population category (Daniels *et al.*, 1996), although the RmInt1 reaction rate was 2.5-fold lower than that of aI5γ.

In this buffer, the branching pathway predominated over the hydrolytic one (k_{br} = 0.012 min^{-1} *versus* k_{hy} = 0.008 min^{-1}). Relative amounts of lariat and linear intron were 0.571 and 0.4, respectively (Table R4.1). The branching population was dissected as lariat intron and lariat/truncated-3'-exon (Figure R4.8 A, left panel; Scheme1), with relative fractions of (0.259 ± 0.008) and (0.36 ± 0.01), respectively. Partial reaction rates of lariat/truncated-3'-exon and lariat intron were k_1 = (0.0081 ± 0.0006) min^{-1} and k_2 = (0.0047 ± 0.0005) min^{-1}, respectively. The truncated intermediate, therefore, predominated over the lariat intron.

Self-splicing timecourse of LT1 transcript in KCl buffer at 42 ºC (Figure R4.5 B, upper panel) is shown in Figure R4.8 A (right panel). We simplified the model by treating multiple linear products as a single species. As a result, linear products were fitted to a first order single exponential kinetics, in accordance with Scheme 2:

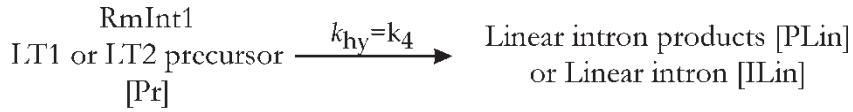

Scheme 2

where $k_T = k_{hy} = k_4 . f_{hy}$ is the sum of all products evolving through the hydrolytic pathway.

The global reaction rate under KCl buffer at 42 ºC was 0.0069 min-1, which is substantially slower than that observed under $(NH_4)_2SO_4$ buffer at 50 ºC. The reaction showed a monophasic behavior, with a single slowly reacting population of molecules. Fractions of linear products at the reaction endpoint was 0.87 (Table R4.1).

TABLE R3.1. Rate constants[1] for self-splicing

Transcript	Ionic reaction conditions[2]	Temp (ºC)	k_T (min^{-1})	k_{br} (min^{-1})	f_{br}	k_{hy} (min^{-1})	f_{hy}
LT1	500 mM $(NH_4)_2SO_4$	50	0.020 ± 0.002	0.012 ± 0.002	0.571 ± 0.009	0.008 ± 0.001	0.4 ± 0.03
LT2	500 mM $(NH_4)_2SO_4$	50	0.0115 ± 0.0005	0.0077 ± 0.0007	0.71 ± 0.02	0.0038 ± 0.0002	0.352[3]
ST2	500 mM $(NH_4)_2SO_4$	50	0,0083 ± 0.0002	0,0054 ± 0.0004	0.641 ± 0.008	0.0029 ± 0.0004	0.35 ± 0.03
LT1	500 mM KCl	42	0.0069 ± 0.0005	0	0	k_T	0.87 ± 0.04
LT2	500 mM KCl	42	0.0045 ± 0.0002	0	0	k_T	0.9 ± 0.1
ST2	500 mM KCl	42	0.0060 ± 0.0002	0	0	k_T	0.83 ± 0.03

[1] Rates reported here are observed rates derived from the plots in Figure R3.6. k_T is the total rate of splicing; k_{br} is the rate of branching; f_{br} is the fraction of molecules that splice through branching; k_{hy} is the rate of hydrolytic splicing and; f_{hy} is the fraction of molecules that splice through hydrolysis. k_T value was determined from the decrease in precursor using Kaleidagraph (Abelbeck Software). The fractional coefficients, f_{br} and f_{hy}, were determined from the fit of product evolution data. From k_T, f_{br} and f_{hy}, k_{br} and k_{hy} were calculated using equations (4) and (5) (see Materials and Methods). Rates and coefficients were also calculated using DynaFit (BioKin Ltd.) and equations (6) to (10), showing a high degree of correspondence. Experimental errors represent the standard error calculated from the fits to rate equations.

[2] In addition to the salts listed, each reaction contained 100 mM MgCl2 and 80 mM Mops (pH 7.5).

[3] This value was fixed based on the linear population observed at long timepoints.

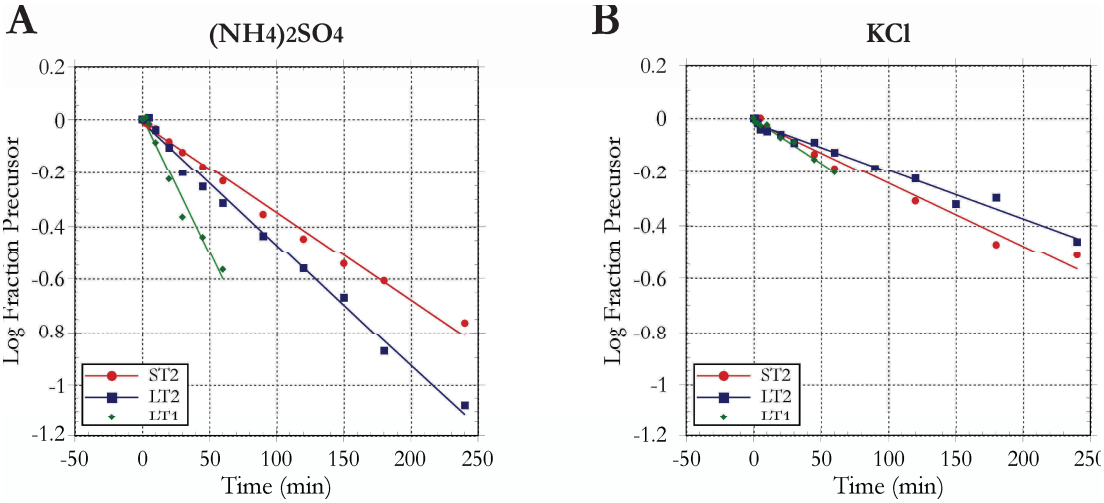

Figure R4.9. Semi-log plots of reaction in LT1, LT2 and ST2 transcripts. Logarithms to base ten of the fractions of precursor from timecourses were plotted against time. LT1 timecourse was reduced to its first 60 minutes of reaction since after that time dataset did not fit well to equation (1). The self-splicing reaction timecourses, carried out in **A** $(NH_4)_2SO_4$ buffer at 50 ºC and **B** KCl buffer at 42 ºC, showed a monophasic kinetic profile for which a single slope was observed.

R.4.6.2 Kinetics of self-splicing in the LT2 transcript

Evolution of precursor and products of self-splicing reactions of LT2 transcript in $(NH_4)_2SO_4$ buffer at 50 ºC conditions is shown in Figure R4.8 B (left panel). Interestingly, in this case we observed the formation of lariat-3'exon intermediate. This suggested that first step of splicing via branching pathway was not rate-limiting for this construct, and we could therefore determine rate constants for both steps of splicing. Surprisingly, this was not the case for the hydrolytic pathway, where the formation of the intermediate was not observed and the first step was still rate-limiting. This behavior can be described by a parallel-sequential kinetic model, as shown in Scheme 3:

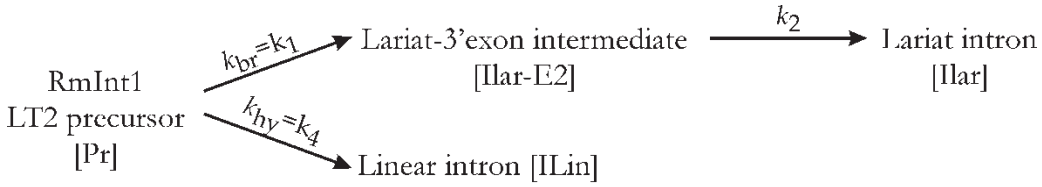

Scheme 3

where $k_T = k_{br} + k_{hy}$. Lariat/3'-exon intermediate and linear intron evolved simultaneously and independently from precursor, while the lariat intron was produced from the intermediate. The sum of product fractions (f_{br} and f_{hy}) equals 1, being the f_{br} the sum of all the products evolving through the branching pathway.

The global reaction rate k_T was 0.0115 min^{-1} (Table R4.1), a value slightly lower but in the range of that observed in LT1 transcript. The fraction of reactive precursor (observed at 7 hours of reaction, for comparing) was 97.5 %, which reacted completely at the end of the timecourse (8 hours). The reaction also showed that all the precursor molecules fell into one homogeneous population with a clear monophasic behavior (Figure R4.9 A, blue line). According to Daniels *et al* (1996), the value of the overall reaction of the LT2 precursor was classified as a fast population of molecules.

The rate constant for the first step of splicing via branching pathway in $(NH_4)_2SO_4$ buffer was 2-fold higher than that of the hydrolytic pathway: 0.0077 min^{-1} *versus* 0.0038 min^{-1}, respectively (Table R4.1). Branched forms predominated over linear ones, with a relative population of 0.71 for the first and 0.352 for the second (Table R4.1). The rate of conversion of lariat/3'-exon intermediate to lariat intron was estimated in (0.0122 ± 0.0008) min^{-1}, slightly higher than the rate for the production of intermediate, which led to the almost complete disappearance of this form at the end of the timecourse. In the hydrolytic pathway, the linear intron was the only product observed, with a relative fraction of 0.352 (Table R4.1). No linear intermediates were detected.

In KCl buffer (Figure R4.8 B, right panel), the only product formed was the linear intron. For that reasons, we considered that LT1 fitted well to a first order single exponential kinetics, in accordance with Scheme 2 (see above). The global reaction rate was 0.0045 min^{-1}. The reaction showed a monophasic behavior, with only one slow population of molecules reacting. The fraction of linear products corresponding to the reaction endpoint was 0.9 (Table R4.1).

R.4.6.3 Kinetics of self-splicing in the ST2 transcript

Self-splicing reaction of ST2 transcript in $(NH_4)_2SO_4$ buffer at 50 ºC (Figure R4.9 A, upper panel) is shown in Figure R4.8 C (left panel). In this case, the pattern of product evolution is more complex. Intron-3'-exon intermediates were observed for both branching and hydrolysis pathways, suggesting that the first step of splicing by either pathway was not rate-limiting. Thus, for each pathway, we could determine the rate

constants for both first and second steps of splicing. In addition, we observed that the lariat-3'-exon intermediate gave rise to a secondary product in addition to the lariat intron. This system can be described by the following parallel-sequential kinetic model (Scheme 4):

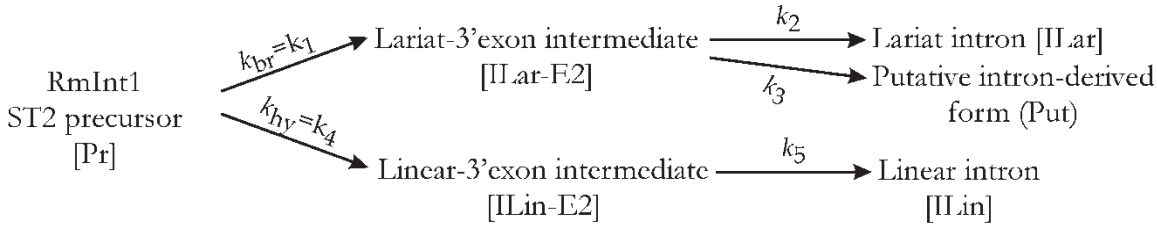

Scheme 4

where $k_T = k_{br} + k_{hy}$. Lariat/3'-exon and linear/3'-exon intermediate forms evolved simultaneously and independently from precursor, while the lariat intron and the putative intron-derived form (Put) were produced from the intermediate. The sum of product fractions (f_{br} and f_{hy}) equals 1, being the f_{br} the sum of all the products evolving through the branching pathway and f_{hy} the sum of all products evolving through the hydrolytic pathway.

The overall observed reaction rate (k_T) was 0.0083 min^{-1} (Table R4.1), the lowest value obtained among the three transcripts studied. The fraction of reactive precursor (observed at 7 hours of reaction, for comparing with LT1 and LT2) was 89 %, and it reacted almost completely at the end of the reaction. Plot of the overall reaction of ST2 showed a monophasic behavior (Figure R4.9 A, red line). According to Daniels *et al* (1996), the value of the reaction rate of the ST2 precursor was classified as belonging to a slow population of molecules.

The branching pathway in $(NH_4)_2SO_4$ buffer was predominant over the hydrolytic one. The relative amounts of lariat and linear forms were f_{br} = 0.641 and f_{hy} = 0.35, respectively (Table R4.1). The rate constants for the first step of branching and hydrolytic splicing were 0.0054 min^{-1} and 0.0029 min^{-1}, respectively (Table R4.1). The rate at which lariat/3'-exon intermediate was converted to lariat intron was (0.0108 ± 0.0004) min^{-1} whereas the rate at which the linear/3'-exon intermediate was converted to linear intron was (0.0065 ± 0.0006) min^{-1}.

In KCl buffer (Figure R4.8 C, right panel), the linear/3'-exon intermediate accumulated, indicating that the first step was not rate limiting. Thus, for each pathway, we

could determine the rate constants for both first and second steps of splicing. Product evolution followed a parallel-sequential kinetic model, according with Scheme 5:

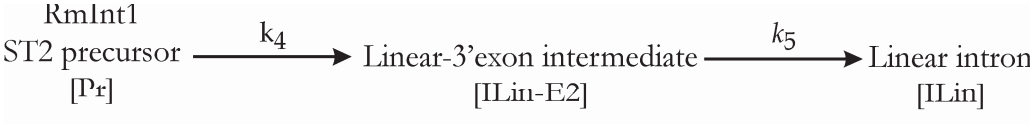

Scheme 5

where $k_T = k_{hy} = k_4$.

The global reaction rate under KCl buffer was 0.0048 min^{-1}. The reaction showed a monophasic behavior, with only one slow population of molecules reacting. The reaction endpoint was 0.83 (Table R4.1).

R4.7 ANALYSIS OF POINT MUTANTS FOR THE STUDY OF SELF-SPLICING MECHANISM IN THE RmInt1 INTRON

In the previous chapter, we analyzed the effect of point mutations on the *in vivo* splicing reaction. Aspects influencing the observed results included not only the secondary structure and tertiary interactions of the ribozyme but also the modulatory effect of the intron-encoded protein (IEP) acting as a maturase in the folding and maintenance of the intron structure as well as a splicing cofactor and; the possible role of host-encoded proteins in the splicing reaction. Of all this factors, the effect of point mutations at conserved positions in the ribozyme active site can be studied in isolation using the self-splicing reaction.

For this purpose, we introduced point mutations and deletions described in the previous chapter (Figure R3.1) in the context of the ST2 transcript (see Materials and Methods, section MX.X). As we recall from Chapter 3, we studied point mutations and deletions in conserved positions in the RmInt1 ribozyme which had been previously reported to affect the first, second or both steps of the splicing reaction, reading it in conjunction with the location of mutated positions in the three-dimensional structure of the intron and the tertiary interactions in which they are involved. Thus, we assayed the ability of each mutant transcript to catalyze the complete splicing reaction by estimating the overall reaction rate and all the reaction constants in each individual step in the process. Besides, in order to examine the two steps of splicing, we calculated relative

A **WT (ST2)**

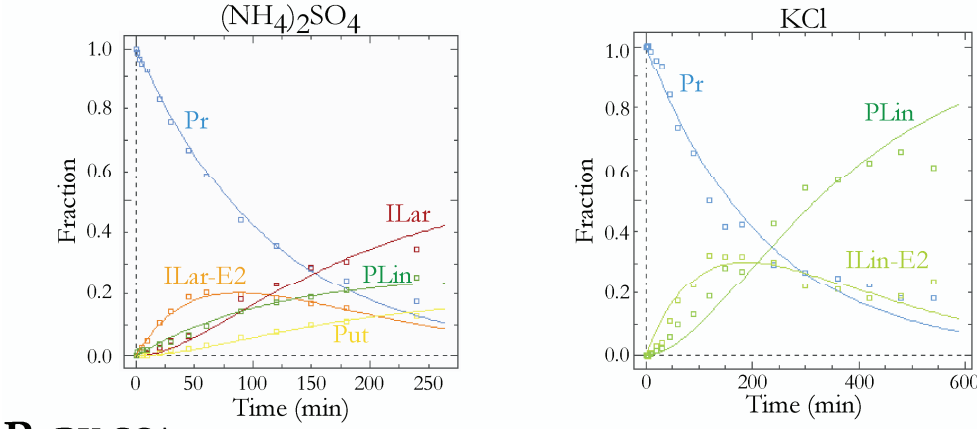

B **DV-CGA**

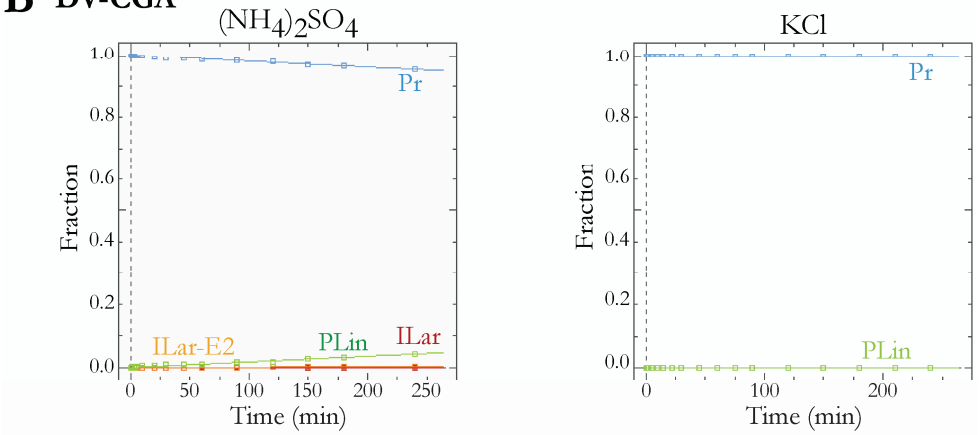

C **J2/3-ΔGA**

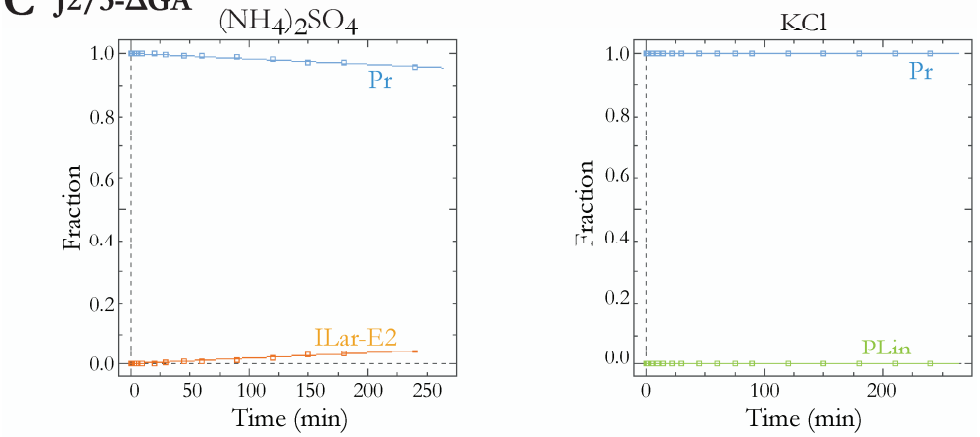

D **Δγ**

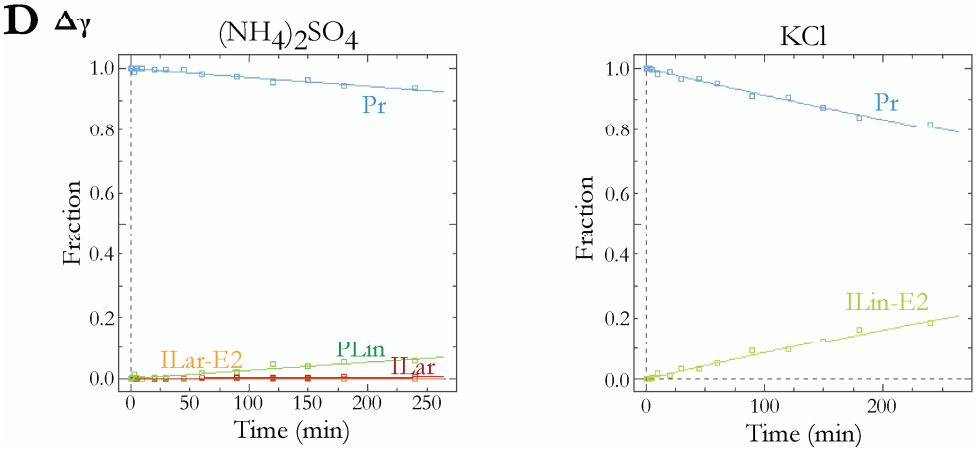

E **Δγ+GEBS3C**

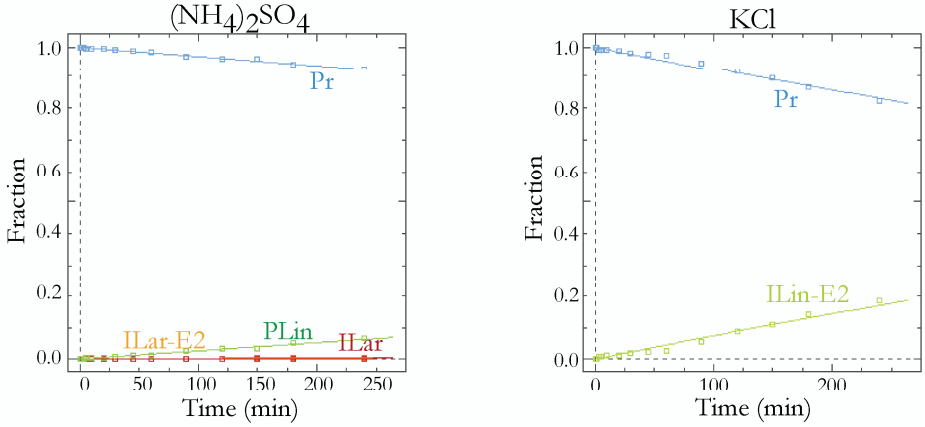

F **GγC**

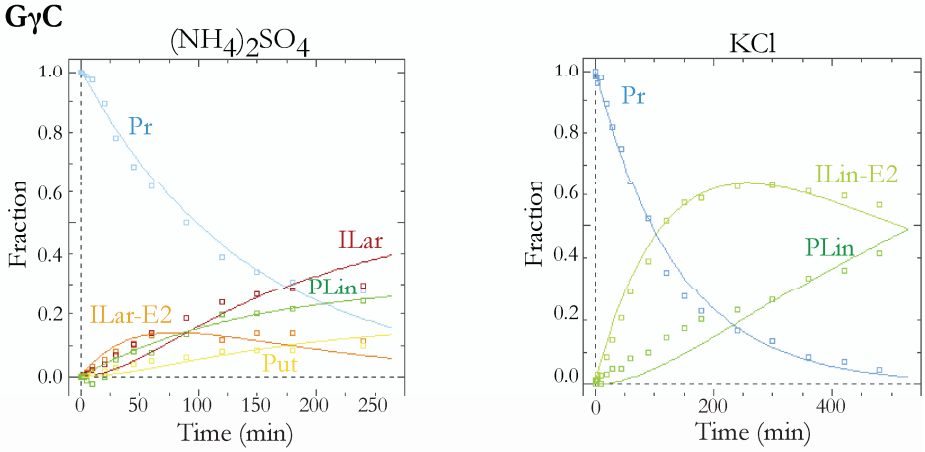

G **GγC-Cγ'G**

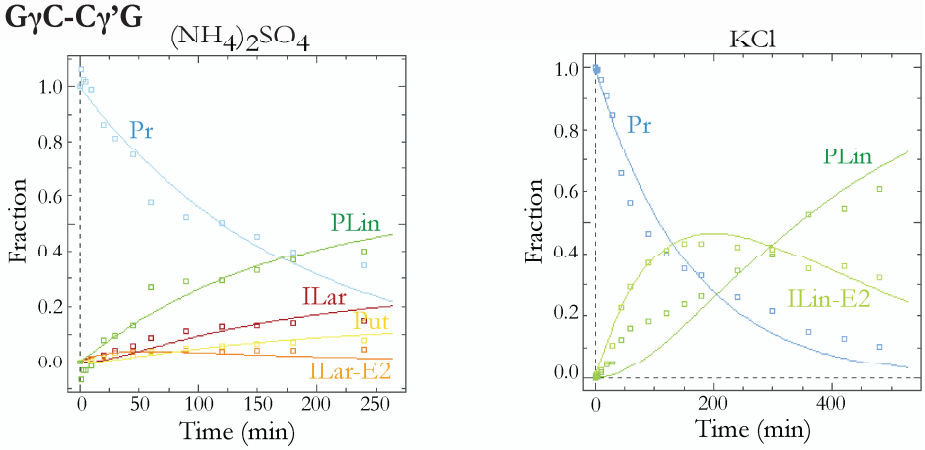

H **Cγ'G**

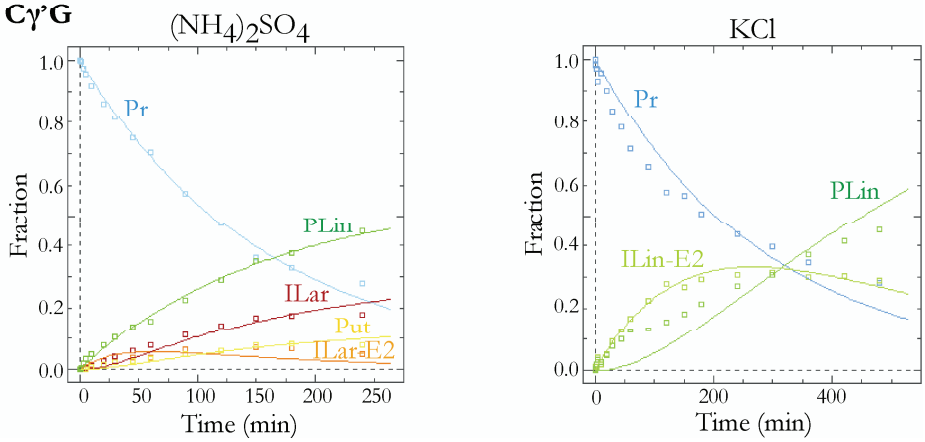

I **C1883A**

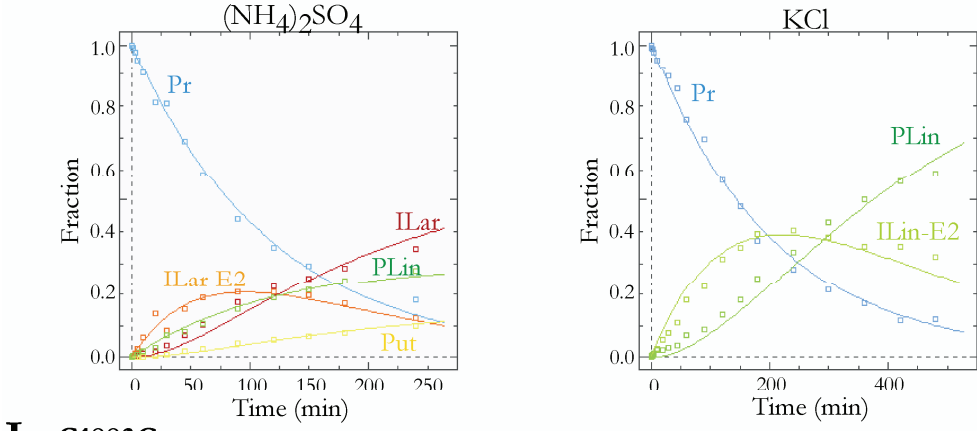

J **C1883G**

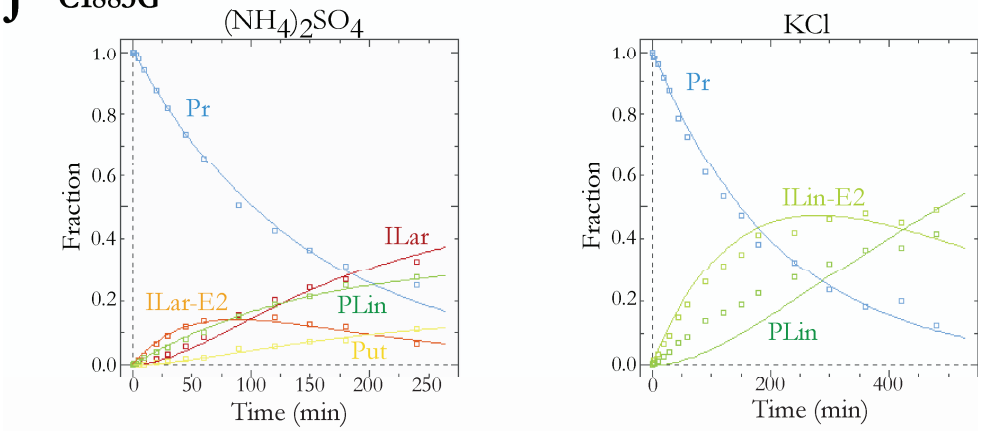

K **C1883U**

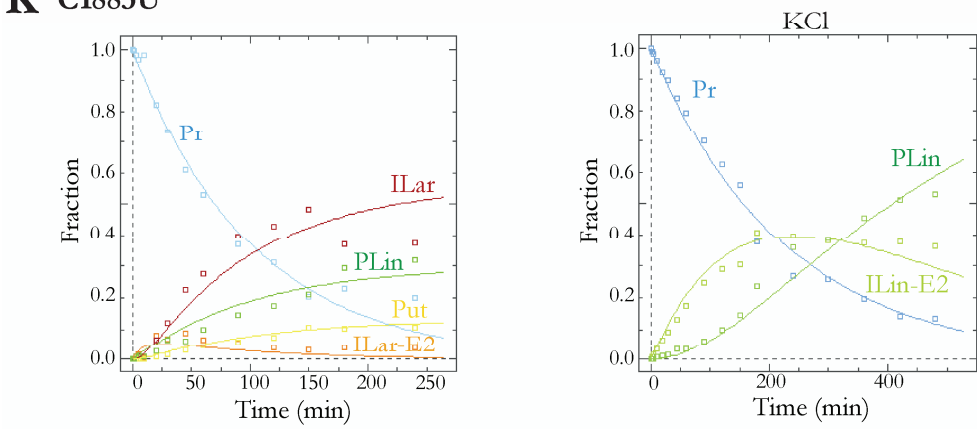

L **GEBS3C**

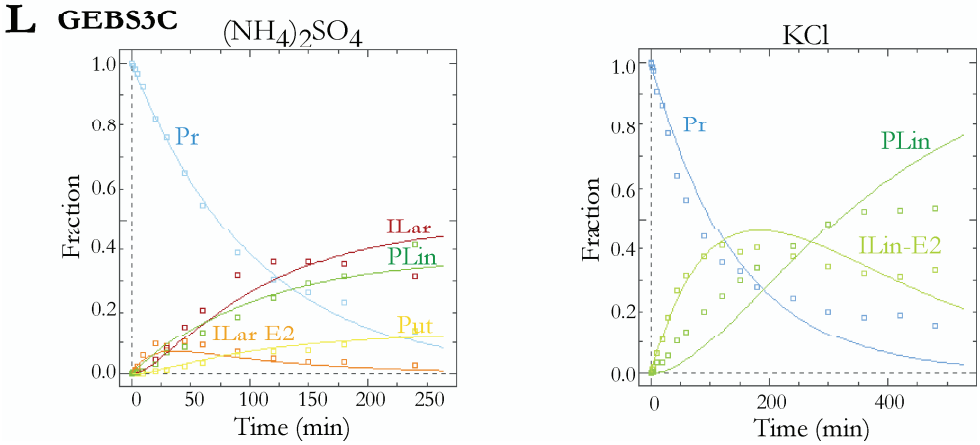

Figure R4.10. Timecourses of RmInt1 splicing mutants under high salt conditions. Splicing reactions from ST2 (WT) (A) precursor and the ST2-derived splicing mutants (B-L) indicated were performed in the presence of either 500 mM $(NH_4)_2SO_4$ buffer (left panels) or 500mM KCl buffer (right panels). Experimental data for the decrease in precursor RNA and the evolution of products were plotted and fitted using DynaFit (BioKin Ltd). Reaction rates are summarized in Table R3.2. Abbreviation used as in Figure R3.9.

efficiencies of the first and second splicing steps of mutants with respect to WT, under $(NH_4)_2SO_4$ and KCl buffers conditions.

As seen in Section R4.5, the wild-type control RNA (WT-ST2) reacted with a rate constant of 0.0086 min^{-1}, in $(NH_4)_2SO_4$ buffer, yielding a predominant intron lariat form (k_2 = 0.0108 min^{-1}) produced through a lariat/3'-exon intermediate via branching pathway (k_1 = 0.0063 min^{-1}). We also observed a putative intron-derived product migrating near the lariat form (k_3 = 0.0028 min^{-1}). The linear forms produced through the hydrolytic pathway reacted with a rate constant of 0.0023 min^{-1} in $(NH_4)_2SO_4$ buffer, and with a rate constant of 0.0044 min^{-1} in KCl buffer. The rate of linear intron formation under the latter buffer conditions was 0.0063 min^{-1}.

Time courses of mutant transcripts carried out under high concentrations of $(NH_4)_2SO_4$ and KCl buffers are shown in figure R4.10. Reaction rates of self-splicing are summarized in Table R4.2. Relative first and second splicing step efficiencies are summarized in Table R4.3.

The mutant DV-CGA, in which positions GUU (1840-2) of the domain V base-pairing with the catalytic triad AGC were substituted by CGA, was severely affected in the first step of splicing under $(NH_4)_2SO_4$ (k_{br} = 17x10^{-6} min^{-1}; k_{hy} = 183x10^{-6} min^{-1}) and KCl buffers, in which the transcript remained unreactive. Notably, this mutant construct was no affected in the second splicing step of the branching pathway (Table R4.3), showing a tiny accumulation of lariat/3'-exon intermediate which rapidly reacted to give lariat intron (k_2 = 0.02).

We observed that the deletion of the dinucleotide GA (453-4) (J2/3-ΔGA mutant), located in the linker region J2/3, dramatically inhibited the first step of the splicing reaction as well (Table R4.2). In addition, J2/3ΔGA did not react through the hydrolytic pathway, and only branching was contributing to the reaction rate (178·10^{-6} min^{-1}). Moreover, the k_2 for lariat formation was not estimated, since there was no possibility of discerning if the accumulation of the unique branched product observed corresponded to

TABLE R4.2. Rate constants for self-splicing in wild-type and mutant transcripts[a]

Transcript[b]	k_T (min^{-1})	$k_{br}=k_1$ (min^{-1})	k_2 (min^{-1})	k_3 (min^{-1})	$k_{by}=k_4$ (min^{-1})	k_5 (min^{-1})	k_6 (min^{-1})
$(NH_4)_2SO_4$ buffer[c]							
WT	0.0086 ± 0.0002	0.0063 ± 0.0001	0.0108 ± 0.0003	0.0038 ± 0.0003	0.0023 ± 0.0001		
DV-CGA	200 ± 10(10^{-6})	17± 5 (10^{-6})[e]	0.02 ± 0.01[e]	–	183 ± 6 (10^{-6})		
J2/3-ΔGA	178 ± 4 (10^{-6})	178 ± 4 (10^{-6})	–	–	–		
Δγ	29 ± 2 (10^{-5})	2 ± 1 (10^{-5})[e]	–	–	27 ± 1 (10^{-5})		
Δγ+GEBS3C	307 ± 9 (10^{-6})	35 ± 5 (10^{-6})	0.004 ± 0.002[e]	–	272 ± 4 (10^{-6})		
GγC	0.0070 ± 0.0003	0.0049 ± 0.0002	0.015 ± 0.001	0.0050 ± 0.0008	0.0021 ± 0.0001		
GγC-Cγ'G	0.0058 ± 0.0004	0.0024 ± 0.0002	0.028 ± 0.009[e]	0.014 ± 0.06[e]	0.0034 ± 0.0002		
Cγ'G	0.0062 ± 0.0002	0.0027 ± 0.0001	0.023 ± 0.003	0.010 ± 0.001	0.0035 ± 0.0001		
C1883A	0.0084 ± 0.0002	0.0059 ± 0.0001	0.0100 ± 0.0004	0.0027 ± 0.0003	0.0025± 0.0001		
C1883G	0.0068 ± 0.0002	0.0045 ± 0.0001	0.0135 ± 0.0005	0.0042 ± 0.0003	0.0023 ± 0.0001		
C1883U	0.0098 ± 0.0005	0.0069 ± 0.0003	0.09 ± 0.02[e]	0.020 ± 0.006[e]	0.0029 ± 0.0002		
GEBS3C	0.0095 ± 0.0004	0.0059 ± 0.0002	0.046 ± 0.08	0.012 ± 0.003	0.0036 ± 0.0002		
KCl buffer[d]							
WT	0.0033 ± 0.0003				0.0033 ± 0.0003	0.0038 ± 0.0005	0.0013 ± 0.0003
DV-CGA	–				–	–	–
J2/3-ΔGA	–				–	–	–
Δγ	0.0009 ± 0.0001				0.0009 ± 0.0001	–	–
Δγ+GEBS3C	0.0008 ± 0.0001				0.0008 ± 0.0001	–	–
GγC	0.0065 ± 0.0001				0.0065 ± 0.0001	0.0010 ± 0.0001	0.0012 ± 0.0001
GγC-Cγ'G	0.0053± 0.0003				0.0053± 0.0003	0.0024 ± 0.0003	0.0016 ± 0.0003
Cγ'G	0.0025 ± 0.0002				0.0025 ± 0.0002	0.0020 ± 0.0005[e]	0.0010 ± 0.0002
C1883A	0.0040 ± 0.0001				0.0040 ± 0.0001	0.0028 ± 0.0002	0.0010 ± 0.0001
C1883G	0.0035 ± 0.0001				0.0035 ± 0.0001	0.0009 ± 0.0001	0.0015 ± 0.0001
C1883U	0.0038 ± 0.0001				0.0038 ± 0.0001	0.0026 ± 0.0002	0.0008 ± 0.0001
GEBS3C	0.0054± 0.0004				0.0054± 0.0004	0.0022 ± 0.0003	0.0022 ± 0.0003

[a] Rates reported here are observed rates. k_T is the total rate of splicing; k_{br} is the rate of branching pathwat; k_2 is the rate of conversion of lariat/3'-exon intermediate to lariat intron; k_3 is the rate of conversion of lariat/3'-exon to the hypothetical intron-derived product; k_{hy} is the rate of hydrolysis; k_5 is the rate of conversion of linear/3'-exon intermediate to linear intron and; k_6 is the rate of linear intron formation directly from the precursor. Rates were estimated using DynaFit (BioKin Ltd). Experimental errors represent the standard error calculated from the fits to rate equations.
[b] All transcripts proceeded form pLM2 and mutant-derived pLM2 plasmids digested with *Bam*HI restriction enzyme. WT = ST2 transcript.
[c] The reaction buffer contained 500 mM $(NH_4)_2SO_4$, 100 mM $MgCl_2$ and 80 mM MOPS (pH 7.5).
[d] The reaction buffer contained 500 mM KCl, 100 mM $MgCl_2$ and 80 mM MOPS (pH 7.5).
[e] Rates followed by an asterisk presented a coefficient of variation higher than 20 %.

lariat/3'-exon intermediate or to the lariat form, although we supposed there was no lariat production (not shown).

Positions involved in the conserved γ-γ' interaction, that is, the G452 in the linker region J2/3 and the last nucleotide of the ribozyme C1884, were subjected to several mutations: deletion of the γ position (Δγ and Δγ-GEBS3C mutants); single substitutions of the G432 by a C (GγC) or the C1884 by a G (Cγ'G mutant), therefore disrupting the γ-γ' interaction and; double substitutions of G432 by a C and C1884 by a G (GγC-Cγ'G), restoring the γ-γ' interaction. The Δγ and Δγ-GEBS3C mutants inhibited the first step of splicing both in $(NH_4)_2SO_4$ and KCl buffers, with rate constants of about 10^{-5} to 10^{-6} (min^{-1}). In addition, the k_2 for lariat formation in the Δγ mutant could not be calculated either, although it seems that all the branched products corresponded to lariat/3'-exon intermediate (Figure SR4.2).

Single Cγ'G and double GγC-Cγ'G mutants in the RmInt1 ribozyme were about 50 % affected in the first step of the branching reaction, whereas GγC was only 20 % reduced in the first step splicing efficiency (Table R4.3). In the GγC mutant, the reduction in the branching rate (k_{br} = 0.0049 min^{-1}) was offset by a 40 % increase in the k_2 rate for the formation of intron lariat (0.015 min^{-1}). Notably, single Cγ'G and double GγC-Cγ'G mutants caused a 2-fold increase in the conversion of lariat/3'-exon intermediate to lariat intron (k_2 = 0.023 min^{-1} and k_2 = 0.028 min^{-1}, respectively). However, the amplitude of lariat formation was still low due to the impairment in the first step (Figure R3.10). In $(NH_4)_2SO_4$ buffer, a 1.5-fold increase in the hydrolytic pathway was observed for Cγ'G and GγC-Cγ'G mutants (k_{hy} = 0.0034 min^{-1} and k_{hy} = 0.0035 min^{-1}, respectively). However, in KCl buffer, GγC and GγC-Cγ'G showed 1.5-fold increase in the hydrolyic pathway, while all three were affected in the second step splicing from slight (GγC-Cγ'G and Cγ'G) to moderate (GγC) (Table R4.2 and R4.3).

TABLE R4.3. Relative self-splicing efficiencies of mutants in the ribozyme of RmInt1 intron[a]

Transcript	Relative active fraction[b]	Branching pathway		Hydrolytic pathway	
		1st step[c] (%)	2nd step[d] (%)	1st step[e] (%)	2nd step[f] (%)
$(NH_4)_2SO_4$ buffer					
WT	100	100	100	100	
DV-CGA	2	0.3	185	8	
J2/3-ΔGA	2	3	0	0	
Δγ	3	0.3	0	12	
Δγ+GEBS3C	4	0.6	37	12	
GγC	81	78	139	91	
GγC-Cγ'G	67	38	259	148	
Cγ'G	72	43	213	152	
C1883A	98	94	93	109	
C1883G	79	71	125	100	
C1883U	114	110	833	126	
GEBS3C	110	94	426	157	
KCl buffer					
WT	100			100	100
DV-CGA	0			0	0
J2/3-ΔGA	0			0	0
Δγ	27			27	0
Δγ+GEBS3C	24			24	0
GγC	197			197	43
GγC-Cγ'G	161			161	78
Cγ'G	76			76	59
C1883A	121			121	75
C1883G	106			106	47
C1883U	115			115	67
GEBS3C	164			164	86

[a] All values are relative to the WT (ST2) transcript.
[b] The fraction of reactive precursor molecules was determined by normalizing values of k_T from mutant samples with respect to WT. It represents the percentage of molecules reacting through branching and hydrolysis pathways.
[c] The relative first splicing step of the branching pathway was determined by normalizing values of k_{br} under $(NH_4)_2SO_4$ buffer conditions from mutant samples with respect to that of WT.
[d] The relative second splicing step of the branching pathway was determined by normalizing values of k_2 under $(NH_4)_2SO_4$ buffer conditions from mutant samples with respect to that of WT.
[e] The relative first splicing step of the hydrolytic pathway was determined by normalizing values of k_{hy} under $(NH_4)_2SO_4$ or KCl buffer conditions from mutant samples with respect to that of WT.
[f] The relative second splicing step of the hydrolytic pathway was determined by normalizing values of k_5+k_6 under KCl buffer conditions from mutant samples with respect to that of WT.

Mutations in the penultimate position (C1883A, C1883G and C1883U), in which a non Watson-Crick interaction with the G1 position has been disrupted, did not affect the first step of splicing neither by branching nor by the hydrolytic pathways (Table R4.2).

Surprisingly, we observed an 8-fold increase in the second splicing step of the branching pathway in the C1883U mutant (k_2 = 0.09 min^{-1}) (Table R4.2 and R4.3). However, a reduction of about 40-60 % in the second step of splicing for the hydrolytic pathway under KCl buffer was observed for C1883U and C1883G, respectively (Table R4.3).

Finally, the mutant GEBS3C, in which the contact between the G329 (EBS3 position) and the first nucleotide of the 3'-exon (IBS3 position) was impaired (EBS3-IBS3 interaction), displayed a rate constant for branching (0.0095 min^{-1}) close to that of a WT, while the rate constant for hydrolysis was about 1.5-fold higher in $(NH_4)_2SO_4$ (0.0036 min^{-1}) and KCl (0.0069 min^{-1}) buffers. An increase in the rate constant for the second step of splicing was only observed for the branching pathway (0.046 min^{-1}).

R.3.7 DISCUSSION

Here, we have designed the RmInt1 intron construct, which can self-splice *in vitro* much more efficiently than the previously described variants, and without the formation of unusual side products. Through the introduction of a set of mutations in the ribozyme of RmInt1 intron we demonstrated the existence of tertiary interaction common to other group IIB introns and identified positions, which affected rate constants of individual steps of the splicing reaction.

*The self-splicing reaction of RmInt1 can be improved by varying the composition of its flanking 3'-exon sequence derived of the IS*Rm2011-2

The *in vitro* self-splicing of RmInt1 intron, as far as it had been analyzed to date (Costa *et al.*, 2006a; Costa *et al.*, 2006b), showed some unconventional characteristics when compared with that of other well-studied group II introns, particularly that of yeast *S.cerevisiae* aI5γ intron (Jacquier and Rosbash, 1986a; Pyle and Green, 1994; Daniels *et al.*, 1996; Chu *et al.*, 1998; Su *et al.*, 2001; Zingler *et al.*, 2010). Unlike the final products commonly described under high salt conditions (Jacquier and Rosbash, 1986b; Peebles *et al.*, 1986; van der Veen *et al.*, 1986; Jarrell *et al.*, 1988b; Daniels *et al.*, 1996), namely lariat and linear intron, ligated and reopened exons, RmInt1 intron showed unusual truncated-3'-exon products derived of the presence of an IBS1-like sequence in the first 10 or 11 nucleotides of the 3' exon, named IBS1*, which simulated the authentic IBS1.

We eliminated the IBS1* sequence of the 3'-exon in the pLM1 construct used in Costa's work which, potentially, was trapping the structure in a misfolded conformation, and subsequently producing the cleavage in the 3' exon of the transcript. We also constructed a pLM1-derivative plasmid, pLM2, in which the RmInt1 3' exon was trimmed to its first 5 nucleotides, while the rest of the 3' exon was replaced by several restriction sites and part of the *lac*Z gene, which were not expected to form long range tertiary interactions with the intron nor with other regions of the exon itself (Figure R3.3). Although it had been proposed that the length of the 3'-exon did not affect the splicing kinetic behavior (Nolte *et al.*, 1998), recent studies showed that shortening both exons resulted in a single population of fast-reacting molecules (Zingler *et al.*, 2010). For that reason, we designed two kinds of transcripts from pLM2 plasmid with different length that shared the same 5' exon: LT2 (long transcript) and ST2 (short transcript).

The analysis of the self-splicing products from LT1, LT2 and ST2 revealed that transcripts obtained using pLM2 as a template (i.e. LT2 and ST2) did not form side products with the truncated 3'-exon neither in $(NH_4)_2SO_4$ nor in KCl buffers (Figures R4.5). By contrast, in ammonium sulfate buffer ST2 transcript produced a stable covalently closed RNA form, which co-migrated with lariat intron on preparative gels. Through DNAzyme and kinetic analysis, we determined that this form, of about 10 nucleotides smaller than lariat intron, was produced from the lariat/3'-exon intermediate. We hypothesize that this intron-derived form could be a "pseudo-lariat form", lacking the 6 nucleotides of its "tail", or an unusual circularized fragment, as previously observed for RmInt1 intron (Costa *et al.*, 2006a), consistent with its higher electrophoretic mobility.

The kinetic analysis indicated that reactions carried out in $(NH_4)_2SO_4$ buffer followed parallel and parallel-sequential kinetic models (Fersht, 1985; Marangoni, 2003). In ammonium sulfate we observed two parallel pathways for the first step of splicing, branching and hydrolysis, which is consistent with previously published works (Daniels *et al.*, 1996; Roitzsch and Pyle, 2009; Stabell *et al.*, 2009). In some cases we observed unusual side products, for example, species containing truncated 3'-exon formed by the LT1 construct, which is consistent with previous studies on this substrate (Costa *et al.*, 2006a). In potassium chloride the reaction followed a sequential kinetic model in the ST2 substrate, in which a linear intron/3'-exon intermediate accumulated, as previously shown by the first group IIA intron form *Podospora anserina* (Schmidt *et al.*, 1990), indicating that the second transesterification reaction of splicing was, in this case, the limiting step, contrary to that previously observed for the ai5γ intron (Chin and Pyle, 1995). By contrast, LT2 substrate in this buffer followed a simple first-order exponential kinetics, with no

intron/3'-exon intermediate accumulation detected, as reported for the aI5γ intron (Jarrell *et al.*, 1988b; Daniels *et al.*, 1996; Zingler *et al.*, 2010).

We found that precursor molecules from the three transcripts were part of a homogeneous population of molecules reacting with a monophasic kinetic behavior. This fact was consistent with the existence of a short 5'-exon in pLM constructs, since it was stated that long 5' exon sequences can induce unfavorable structures which, in turn, can introduce a folding step limiting the rate of *in vitro* self-splicing (Nolte *et al.*, 1998). An example is the ai5γ intron long-exon construct used by Daniels *et al* (1996), in which two conformation of precursor molecules resulted in a slow and a fast population, giving a biphasic kinetic behavior.

From the analysis of reaction rates, it was shown that LT1 and LT2 reacted uniformly as a fast population, with rate constant of 0.020 and 0.0115 (min^{-1}), respectively. The reaction endpoint for the LT1 precursor was only 20%, whereas it reached more than 60 % for the LT2 construct. This finding was consistent with the existence of a kinetic trap in the former (Costa *et al.*, 2006b), which precluded a higher lariat intron population to form (Russell, 2008). ST2 reacted as a slow population (0.0083 min^{-1}), even when this transcript has been shortened in its 5' and 3' exon sequences. In addition, subdenaturing urea concentrations did not increase the rate constant or even diminished it, suggesting that misfolding was not the likely cause for the slow reactivity (Fedorova *et al.*, 2007). It was proposed that the existence of a homogeneous population reacting with a lower rate when compared to a more optimal precursor transcript could be interpreted by the inhibitory structures being in fast equilibrium with the active conformation (Nolte *et al.*, 1998). We hypothesize that any stable structure formed in the 3'-exon of ST2 or some atypical interaction between the 3' exon and other structure of the intron or 5' exon, not occurring in LT2, could be interfering with the splicing process, leading to a reduction in the reaction rate or even resulting in the production of the unconventional intron-derived form described above. In agreement with previous observations (Nolte *et al.*, 1998), rates for hydrolysis were about 2-fold lower than those for branching pathway.

However, the most striking characteristic of RmInt1 intron is the persistence of a lag phase in all transcripts due to the formation of a transient intermediate prior to the excision of the intron form, both in the branching and hydrolytic pathways (Figure R3.5 and R3.8). Unlike aI5 γ intron, RmInt1 forms RNP particles *in vivo*, which could explain the need of protein assistance for a correct splicing of RmInt1. Nevertheless, the

inefficiency of RmInt1 intron *in vitro*, under high-salt conditions, show how the constrains imposed by the RNA structure preclude a productive splicing reaction.

Considered together, our results show that the LT2 construct of RmInt1 intron is better behaved *in vitro* than LT1 RNA, because it does not form unconventional side products and it produces lariat intron with at much higher amplitude. However, RmInt1 is still less efficient that other group II introns studied *in vitro*. For that reason, a further analysis of the secondary and tertiary structures of the RmInt1 intron is necessary in order to elucidate the elements responsible for the defects in the splicing reaction.

Point mutations in the RmInt1 intron affect branching and hydrolytic pathways

Site-directed mutagenesis is a useful and extended tool in the study of self-splicing activity of group II introns. Through different approaches, it has been able to associate specific roles to conserved positions in the ribozyme affecting several aspects of catalysis (Jacquier and Michel, 1990; Jacquier and Jacquesson-Breuleux, 1991; Peebles *et al.*, 1995; Bar-Shalom and Moore, 2000; Costa *et al.*, 2000; Mikheeva *et al.*, 2000; Molina Sanchez *et al.*, 2011). Moreover, recent advances in NMR (Sigel *et al.*, 2000; 2004; Erat *et al.*, 2007) and crystal structure determinations (Zhang and Doudna, 2002; Toor *et al.*, 2008a), have allow the association of known functionalities of conserved positions to defined structural motifs.

Aimed to the determination of critical positions of the RmInt1 ribozyme affecting the first, second or both splicing steps *in vitro*, here we introduced mutations at nucleotides known to participate in tertiary interactions in other group II introns, as previously carried out for the *in vivo* splicing of RmInt1 intron (Figure R3.1, see Chapter 3). We assayed their ability to self-splice *in vitro* and determined their relative efficiencies of first and second steps of the splicing reaction. The effects on the self-splicing reaction could be then explained from the perspective of structure.

Mutations in the conserved catalytic triad 5-AGC-3' at the base of domain V that abolish splicing have been reported repeatedly for the *in vitro* self-splicing of aI5γ intron (Jarrell *et al.*, 1988a; Koch *et al.*, 1992; Dib-Hajj *et al.*, 1993; Peebles *et al.*, 1995). In RmInt1, mutations that disrupted base-pairing with the catalytic triad at positions A1811, G1812 and C1843 (G1840 U1841 U1842 to C1840 G1841 A1842) inhibited the splicing reaction. It has been reported that mutations at positions base pairing with those of the catalytic triad did not lead to severe self-splicing defects *in vitro* (Boulanger *et al.*, 1995; Peebles *et al.*,

1995). However, the same authors observed that base pairings of the A2 and C4 (referred to DV positions) were more important than the identities of the nucleotide bases at those positions and the maintenance of the wobble pair at position G3 was also the responsible of a local distorsion of one helix functionally important, which could influence the loss of activity of the triple mutant (Boulanger *et al.*, 1995; Peebles *et al.*, 1995). Noticeable, according to Boulanger *et al* (1995), the triple mutation at G1840 U1841 U1842 did not lead to a detectable defect in the second step of splicing. As mentioned in Chapter 3, the crystal structure of the *O.i.* group II intron has revealed that only the conserved 5'-AGC-3' nucleotides (and not their pairing partners) form hydrogen bonds with nucleotides of the J2/3 region and the AC bulge in DV, constituting a triple helix (triplex) which is essential for splicing catalysis (Toor *et al.*, 2008a; Toor *et al.*, 2009; Keating *et al.*, 2010)

Mikheeva *et al* (2000) previously reported that the deletion of the dinucleotide G588 A589 (G453 A454 in RmInt1 intron) affected the second splicing step in the yeast aI5γ intron. However, in RmInt1, both the first and the second splicing steps were significantly impaired. This result better matched that of Chanfreau and Jacquier (1996), in which the mutation of the A589 of aI5γ intron affected both steps of the splicing. Photocrosslinking studies initially confirmed these studies, since it was shown that the catalytic domain V interacted with the dinucleotide G588 A589 of ai5γ intron (Podar *et al.*, 1998; de Lencastre and Pyle, 2008), confirming the occurrence of a single active site catalyzing both transesterification reactions (Chanfreau and Jacquier, 1994; de Lencastre *et al.*, 2005). As explained in Chapter 3, recent crystallographic studies have also shown that position G288 and C289 of the *O.i.* group II intron are part of a triple interaction with the G359 U384 and C358 G385 base pairs of DV, respectively, establishing a triple helix (triplex) essential for catalysis (Keating *et al.*, 2010). Moreover, the high correlation observed for self-splicing *in vitro* and splicing *in vivo* of DV and J2/3 region mutant constructs reflects that splicing depends very much on secondary and tertiary structures rather than on an effect of protein co-factors.

The deletion of the G452 (γ position), which also inhibited splicing, is in agreement with the observation of a close proximity of this position with the bulge of the catalytic core through the interaction with the fourth (or fifth in *O.i.* intron) nucleotide of the intron, positioning the 3' splice site for catalysis of the exon junction (de Lencastre and Pyle, 2008; Toor *et al.*, 2008b). Although G452 is also involved in the conserved interaction γ-γ' with the last nucleotide of the intron, it seems that its interactions with the catalytic core could be determinant for the appearance of this phenotype. However, the substitution of the G452 to a C, which is not represented on the nature (Jacquier and

Michel, 1990) did not altered significantly the splicing efficiencies shown for the wild-type strain. It is possible that *in vitro*, the presence of a C nucleotide in the γ position partially substitutes the role of the G in the network of tertiary interactions with the 5' splice site and the active site. This result agrees with the previous observation that substitutions in the γ position did not grossly affect the first step of the splicing reaction (Jacquier and Michel, 1990). By contrast, the same author noted that mismatched combinations accumulated significantly more lariat/3'-exon intermediate (Jacquier and Michel, 1990) while, in RmInt1 intron, a slight increase in the second splicing step was observed. Another possibility could be that a cryptic interaction could occur between the γ' position (C1884) and the G453, located next to the γ position in the wild-type intron, which would restore splicing. *In vivo,* the IEP protein could help to correctly position γ and γ' nucleotides, preventing cryptic interactions to form and so explaining the complete block of splicing observed. On the other hand, simple and double mutations of the γ' position, disrupting or restoring the Watson-Crick interaction, respectively, resulted in a moderate decrease in the first step of splicing and an increase in the second step. Although we did not find any good reason fot these observations, one possibility is that the substitution of the C1884 to a G could lead to a cryptic interaction with the C451 in the J2/3 region, which distorted the complex interactions of that region with elements of the DV triplex (Keating *et al.*, 2010) and the 5'-splice site (de Lencastre and Pyle, 2008), thus enabling the γ-γ' to occur while partially impairing the first step of splicing. However, another possibility could be the formation of a cryptic splice site downstream in the 3' exon, as previously suggested (Schmidt *et al.*, 1996; Molina Sanchez *et al.*, 2011), whereas a novel tertiary interaction in the ribozyme of RmInt1, involving the γ' position, could be affecting the 5'-cleavage efficiency *in vitro.*

It has been previously reported that the penultimate position of group II introns establishes contacts with the first nucleotide of the intron by means of a non Watson-Crick interaction and that substitutions at the penultimate nucleotide of the ribozyme affected the efficiency of the second splicing step *in vitro* (Chanfreau and Jacquier, 1993). We assayed substitutions for the C1883 position to A, C and U. The mutation to adenosine, and in a less extent to guanidine, led to a wild-type phenotype, according with *in vivo* results and in agreement with the presence in the nature of the combination C(first nucleotide)-A(last nucleotide), (Michel *et al.*, 1989; Chanfreau and Jacquier, 1993). The mutation of C to U also showed a wild-type first splicing step, through branching and hydrolysis pathways. However, in $(NH_4)_2SO_4$ buffer, this mutation produced a 9-fold increase of the second step of the splicing reaction. Since there is no available data of intronic 5' and 3' ends in the crystal structure, probably because these regions are

disordered or have been cleaved through secondary reactions (Toor *et al.*, 2010), it is difficult to figure out a structural interpretation for this finding. However, one explanation might be that, *in vitro*, a novel interaction involving the penultimate nucleotide could promote or stabilize the approximation of 5' and 3' exons, leading to a productive second transesterification reaction.

Finally, the disruption of the EBS3-IBS3 interaction through the mutation of the G329 to C caused no effect on the first splicing step of the branching pathway and a moderate increase in that of the hydrolytic pathway. By contrast, a 4-fold increase in the second step of the splicing reaction was observed, as occurred for the mutation of the C1883 to U. The role of the EBS3-IBS3 interaction has been previously shown to be essential for efficient exon ligation *in vitro,* by positioning the 3' splice site in the active site (Costa *et al.*, 2000). In that work, the combination of C(EBS3)−C(+1) assayed here, led to a low second splicing step efficiency, accordingly with the fact that this combination is absence in the nature (Costa *et al.*, 2000). Observations of the crystal structure also reveal that EBS1 and EBS3 form a continuous binding interface which simultaneously recognize both 5' and 3' exon sequences (Toor *et al.*, 2008b). On the basis of structure and previous observations we could not find an explanation which accommodates these findings. However, for an unknown mechanism, this mutation could be stabilizing the interaction between 5' and 3' exons.

Taking all together, we observe an agreement between *in vivo* and *in vitro* results from mutations involved in tertiary interactions with the catalytic core, indicating that splicing rely essentially on the secondary and tertiary intron structures, such as the triple helix between DV and nucleotides within the J2/3 linker. However, some significant differences are observed between *in vitro* and *in vivo* data involving tertiary interactions aimed to approximate 5' and 3' exons (γ-γ' and EBS3-IBS3 interactions) and intron boundaries (G+1 – penultimate nucleotide of the intron), which suggest that trans-acting factor, such as the IEP protein, play an important role in these processes.

This knowledge opens the possibility to go deep into the mechanisms involved in the low splicing efficiency actually observed for RmInt1 intron, which, in turn, could be modulated and used as a biotechnological tool.

CONCLUDING REMARKS

1. The reported system based on the *lac*Z gene, containing the minimal target site for RmInt1 intron insertion, links the splicing of the intron to the strong and constitutive expression of the β-galactosidase protein. The level of expression of β-galactosidase protein can be accurately measured by a Miller assay, which shows a range of detection varying from 60-14000 Miller Units.

2. The wild-type RmInt1 intron excises efficiently from the RNA precursor. The construction in which the intron-encoded protein (IEP) is present *in trans* in a separate plasmid excises at a level similar as that of the full-length intron, whereas the construction with the IEP expressed *in cis* presents a 70 % excision efficiency reduction. RmInt1 excision in *E. coli* was 95% less efficient than excision of the intron in *S. meliloti*, suggesting that host-specific factors may play an important role in the splicing reaction.

3. The lariat form accumulates in the *in vivo* splicing process and this product is free of lariat/3'-exon reaction intermediates. The level of exon ligation observed for RmInt1 intron, in Miller units, is below background levels. By quantitative real-time qRT-PCR the splicing efficiency of RmInt1 intron has been determined *in vivo* in *S. meliloti* (0.07 ± 0.02) % and in *E. coli* (0.016 ± 0.006) %. These findings provide evidence that RmInt1 intron functions more like a retroelement than a spliceosomal intron.

4. The self-splicing reaction efficiency *in vitro* of the RmInt1 intron has been improved by eliminating an IBS1-like sequence present in the first 10 or 11 nucleotides of the 3' exon from the natural target IS*2011-2* insertion sequence. The new construct prevents the formation of unusual truncated side products previously observed, producing an increment of the amplitude of the reaction.

5. The *in vitro* self-splicing reaction of the RmInt1 intron carried out in $(NH_4)_2SO_4$ buffer follows a parallel-sequential kinetic model. In this buffer, two parallel pathways for the first step of splicing, branching and hydrolysis, are observed. The final lariat and linear introns are the result of a sequential reaction in which a transient intron intermediate in formed. In KCl buffer, the RmInt1 intron follows a sequential kinetic model, in which the linear intron is produced from a transient linear-intron intermediate. The transcripts from the RmInt1 intron improved constructs react as a fast and homogeneous population of molecules, showing a monophasic kinetic behavior.

6. The persistence of a lag phase in all transcripts due to the formation of a transient intermediate prior to the excision of the intron form indicates an intrinsic low efficiency of the first-step of splicing of RmInt1 intron *in vitro.*

7. The catalytic core in RmInt1 intron is composed of the triple helix (triplex) between DV and nucleotides within the J2/3 linker common to other group II introns. The disruption of interactions involving components of the catalytic core results in the affectation of both steps of splicing *in vivo* and *in vitro,* indicating that splicing rely essentially on the secondary and tertiary intron structures. This observation also supports the occurrence of an unique active site catalyzing both steps of the splicing reaction.

8. The tertiary interactions aimed to approximate 5' and 3' exons (γ-γ' and EBS3-IBS3 interactions) and intron boundaries (G+1 – penultimate nucleotide of the intron) have been shown to occur for the RmInt1 intron *in vivo.* Significant differences observed *in vitro* indicate that the IEP protein plays an important role helping to correctly position these elements in the RmInt1 ribozyme *in vivo.*

CONCLUSIONES

1. El sistema informador basado en el gen *lac*Z, que contiene la diana mínima de reconocimiento para la inserción del intrón RmInt1, une el proceso de *splicing* del intrón a una expresión fuerte y constitutiva de la proteína β-galactosidasa. El nivel de expresión de la proteína β-galactosidasa puede ser medido con precisión mediante un ensayo Miller, que posee un margen de detección que varía entre 60-14000 unidades Miller.

2. El intrón RmInt1 silvestre se escinde eficientemente de su precursor de ARN. La construcción en la cual la proteína codificada por el intrón (del inglés *I*ntron-*E*ncoded *P*rotein, IEP) está expresada en *trans* desde un plásmido separado se escinde a un nivel similar al del intrón de longitud completa. La construcción con la IEP expresada en *cis* presenta un 70 % de reducción de la escisión. La escisión de RmInt1 en *E.coli* es un 95 % menos eficiente que la misma en *S.meliloti*, lo que sugiere que determinados factores específicos del huésped podrían jugar un papel importante en la reacción de *splicing*.

3. La forma en lazo o *lariat* se acumula durante el proceso de *splicing in vivo* libre de intermediarios de la reacción del tipo intrón en lazo/exón 3'. El nivel de unión de exones observado en el intrón RmInt1, en unidades Miller, se encuentra por debajo del nivel de detección. Mediante PCR cuantitativa (qRT-PCR) se ha determinado que la eficiencia de *splicing in vivo* del intrón RmInt1 es (0.07 ± 0.02) % en *S.meliloti* y (0.016 ± 0.006) % en *E.coli*. Estos hallazgos muestran la evidencia de que el intrón RmInt1 funciona de un modo más parecido a los retroelementos que a los intrones espliceosómicos.

4. La eficiencia de la reacción de *self-splicing in vitro* se ha mejorado mediante la eliminación de una secuencia parecida a IBS1, presente en los primeros 10 u 11 nucleótidos del exón 3' de la diana de inserción natural procedente de la secuencia de inserción IS*2011-2*. La nueva construcción evita la formación de co-productos truncados bastante inusuales, que habían sido observados previamente, produciendo, de este modo, un aumento en la amplitud de la reacción.

5. La reacción de *self-splicing in vitro* del intrón RmInt1 llevada a cabo en tampón $(NH_4)_2SO_4$ sigue un modelo cinético del tipo paralelo-secuencial. En este tampón, se observan dos rutas paralelas durante el primer paso del *splicing* conocidas como *branching* e hidrólisis. Los intrones en lazo y lineal finales son consecuencia de una reacción secuencial a partir de un intermediario transitorio del intrón. En tampón KCl, el intrón RmInt1 sigue un modelo cinético secuencial, en el cual el intrón lineal se produce a partir de un intermediario lineal transitorio. Los transcritos de las construcciones mejoradas del intrón RmInt1 reaccionan rápida y homogéneamente, y muestran un comportamiento cinético monofásico.

6. La persistencia de un retraso en la escisión del intrón, debida a la formación de un intermediario transitorio, indica una baja eficiencia en el primer paso de la reacción de *splicing in vivo* intrínseca del intrón RmInt1.

7. El centro catalítico del intrón RmInt1 se compone de una triple hélice (*triplex*) que se establece entre el DV y los nuclétoidos de la región intermedia J2/3, común a otros intrones del grupo II. La interrupción de interacciones terciarias en las que participan componentes del centro catalítico afectan tanto al primer como al segundo paso de la reacción de *splicing*, tanto *in vivo* como *in vitro*, lo que indica que el *splicing* depende necesariamente de las estructuras secundaria y terciaria del intrón. Esta observación también apoya la existencia de un único sitio activo que catalice ambos pasos de la reacción de *splicing*.

8. Se ha observado que las interacciones terciarias que producen el acercamientos de los exones 5' y 3' (interacciones γ-γ' y EBS3-IBS3) y los extremos del intrón (G+1 – penúltimo nucleótido del intrón) tienen lugar *in vivo* para el intrón RmInt1. También se han encontrado diferencias significativas con los resultados *in vitro*, lo que indica que la proteína IEP juega un papel importante ayudando a disponer correctamente estos elementos en la ribozima de RmInt1 *in vivo*.

BIBLIOGRAPHY

1. Adamidi C, Fedorova O and Pyle AM (2003) A group II intron inserted into a bacterial heat-shock operon shows autocatalytic activity and unusual thermostability. *Biochemistry* 42(12):3409-3418.

2. Alwine JC, Kemp DJ, Parker BA, Reiser J, Renart J, Stark GR and Wahl GM (1979) Detection of specific RNAs or specific fragments of DNA by fractionation in gels and transfer to diazobenzyloxymethyl paper. *Methods Enzymol* 68:220-242.

3. Arnberg AC, Van Ommen GJ, Grivell LA, Van Bruggen EF and Borst P (1980) Some yeast mitochondrial RNAs are circular. *Cell* 19(2):313-319.

4. Augustin S, Muller MW and Schweyen RJ (1990) Reverse self-splicing of group II intron RNAs in vitro. *Nature* 343(6256):383-386.

5. Bachl J and Schmelzer C (1990) Effect of deletions at structural domains of group II intron bI1 on self-splicing in vitro. *J Mol Biol* 212(1):113-125.

6. Bar-Shalom A and Moore MJ (2000) Tri-partite assay for studying exon ligation by the ai5gamma group II intron. *Biochemistry* 39(33):10207-10218.

7. Barrientos-Durán A, Chillon I, Martínez-Abarca F and Toro N (2011) Exon sequence requirements for excision in vivo of the bacterial group II intron RmInt1 *BMC Mol Biol* MS: 7965872549324408.

8. Beauregard A, Curcio MJ and Belfort M (2008) The take and give between retrotransposable elements and their hosts. *Annu Rev Genet* 42:587-617.

9. Belhocine K, Mak A and Cousineau B (2007) Trans-*splicing* of the Ll.ltrB group II intron in *Lactococcus lactis*. *Nucleis Acids Research*:12.

10. Belhocine K, Mak AB and Cousineau B (2008) Trans-splicing versatility of the Ll.LtrB group II intron. *RNA* 14(9):1782-1790.

11. Birnboim HC and Doly J (1979) A rapid alkaline extraction procedure for screening recombinant plasmid DNA. *Nucleic Acids Res* 7(6):1513-1523.

12. Bolivar F (1978) Construction and characterization of new cloning vehicles. III. Derivatives of plasmid pBR322 carrying unique *Eco*RI sites for selection of *Eco*RI generated recombinant DNA molecules. *Genes and Development* 4:16.

13. Bonen L and Vogel J (2001) The ins and outs of group II introns. *Trends Genet* 17(6):322-331.

14. Boorstein WR and Craig EA (1989) Primer extension analysis of RNA. *Methods Enzymol* 180:347-369.

15. Boudvillain M and Pyle AM (1998) Defining functional groups, core structural features and inter-domain tertiary contacts essential for group II intron self-splicing: a NAIM analysis. *EMBO J* 17(23):7091-7104.

16. Boudvillain M, de Lencastre A and Pyle AM (2000) A tertiary interaction that links active-site domains to the 5' splice site of a group II intron. *Nature* 406(6793):315-318.

17. Boulanger SC, Belcher SM, Schmidt U, Dib-Hajj SD, Schmidt T and Perlman PS (1995) Studies of point mutants define three essential paired nucleotides in the domain 5 substructure of a group II intron. *Mol Cell Biol* 15(8):4479-4488.

18. Boulanger SC, Faix PH, Yang H, Zhuo J, Franzen JS, Peebles CL and Perlman PS (1996) Length changes in the joining segment between domains 5 and 6 of a group II intron inhibit self-splicing and alter 3' splice site selection. *Mol Cell Biol* 16(10):5896-5904.

19. Breaker RR and Joyce GF (1994) A DNA enzyme that cleaves RNA. *Chem Biol* 1(4):223-229.

20. Cabanes D, Boistard P and Batut J (2000) Identification of Sinorhizobium meliloti genes regulated during symbiosis. *J Bacteriol* 182(13):3632-3637.

21. Carpousis AJ (2007) The RNA degradosome of Escherichia coli: an mRNA-degrading machine assembled on RNase E. *Annu Rev Microbiol* 61:71-87.

22. Casadaban MJ, Chou J and Cohen SN (1980) In vitro gene fusions that join an enzymatically active beta-galactosidase segment to amino-terminal fragments of exogenous proteins: Escherichia coli plasmid vectors for the detection and cloning of translational initiation signals. *J Bacteriol* 143(2):971-980.

23. Cavalier-Smith T (2009) Predation and eukaryote cell origins: a coevolutionary perspective. *Int J Biochem Cell Biol* 41(2):307-322.

24. Cech TR (1986) The generality of self-splicing RNA: relationship to nuclear mRNA splicing. *Cell* 44(2):207-210.

25. Coros CJ, Landthaler M, Piazza CL, Beauregard A, Esposito D, Perutka J, Lambowitz AM and Belfort M (2005) Retrotransposition strategies of the Lactococcus lactis Ll.LtrB group II intron are dictated by host identity and cellular environment. *Mol Microbiol* 56(2):509-524.

26. Coros CJ, Piazza CL, Chalamcharla VR, Smith D and Belfort M (2009) Global regulators orchestrate group II intron retromobility. *Mol Cell* 34(2):250-256.

27. Costa M and Michel F (1995) Frequent use of the same tertiary motif by self-folding RNAs. *EMBO J* 14(6):1276-1285.

28. Costa M, Deme E, Jacquier A and Michel F (1997) Multiple tertiary interactions involving domain II of group II self-splicing introns. *J Mol Biol* 267(3):520-536.

29. Costa M, Michel F and Westhof E (2000) A three-dimensional perspective on exon binding by a group II self-splicing intron. *EMBO J* 19(18):5007-5018.

30. Costa M, Michel F, Molina-Sánchez M, Martínez-Abarca F and Toro N (2006a) An alternative intron-exon pairing scheme implied by unexpected *in vitro* activities of group II intron RmInt1 from *Sinorhizobium meliloti*. *Biochimie* 88:7.

31. Costa M, Michel F and Toro N (2006b) Potential for alternative intron–exon pairings in group II intron RmInt1 from *Sinorhizobium meliloti* and its relatives. *RNA* 12:4.

32. Cousineau B, Smith D, Lawrence-Cavanagh S, Mueller JE, Yang J, Mills D, Manias D, Dunny G, Lambowitz AM and Belfort M (1998) Retrohoming of a bacterial group II intron: mobility via complete reverse splicing, independent of homologous DNA recombination. *Cell* 94(4):451-462.

33. Cousineau B, Lawrence S, Smith D and Belfort M (2000) Retrotransposition of a bacterial group II intron. *Nature* 404(6781):1018-1021.

34. Cui X, Matsuura M, Wang Q, Ma H and Lambowitz AM (2004) A group II intron-encoded maturase functions preferentially in cis and requires both the reverse transcriptase and X domains to promote RNA splicing. *J Mol Biol* 340(2):211-231.

35. Chanfreau G and Jacquier A (1993) Interaction of intronic boundaries is required for the second splicing step efficiency of a group II intron. *The EMBO Journal* 12(13):8.

36. Chanfreau G and Jacquier A (1994) Catalytic site components common to both splicing steps of a group II intron. *Science* 266:5.

37. Chanfreau G and Jacquier A (1996) An RNA conformational change between the two chemical steps of group II self-splicing. *EMBO J* 15(13):3466-3476.

38. Chen Y, Klein J, McKay L and Dunny G (2005) Quantitative Analysis of Group II Intron Expression and Splicing in *Lactococcus lactis*. *Applied and Environmental Microbiology* 71(5):11.

39. Chin K and Pyle AM (1995) Branch-point attack in group II introns is a highly reversible transesterification, providing a potential proofreading mechanism for 5'-splice site selection. *RNA* 1(4):391-406.

40. Chu VT, Liu Q, Podar M, Perlman PS and Pyle AM (1998) More than one way to splice an RNA: branching without a bulge and splicing without branching in group II introns. *RNA* 4(10):1186-1202.

41. Chu VT, Adamidi C, Liu Q, Perlman PS and Pyle AM (2001) Control of branch-site choice by a group II intron. *EMBO J* 20(23):6866-6876.

42. D'Souza LM and Zhong J (2002) Mutations in the Lactococcus lactis Ll.LtrB group II intron that retain mobility in vivo. *BMC Mol Biol* 3:17.

43. Dai L and Zimmerly S (2002) Compilation and analysis of group II intron insertions in bacterial genomes: evidence for retroelement behavior. *Nucleic Acids Res* 30(5):1091-1102.

44. Dai L, Toor N, Olson R, Keeping A and Zimmerly S (2003) Database for mobile group II introns. *Nucleic Acids Res* 31(1):424-426.

45. Dai L and Zimmerly S (2003) ORF-less and reverse-transcriptase-encoding group II introns in archaebacteria, with a pattern of homing into related group II intron ORFs. *RNA* 9(1):14-19.

46. Dai L, Chai D, Gu S-Q, Gabel J, Noskov S, Blocker F, Lambowitz A and Zimmerly S (2008) A three-dimensional model of a group II intron RNA and its interaction with the intron-encoded reverse transcriptase. *Molecular Cell* 30:14.

47. Daniels D, Michels Jr W and Pyle A (1996) Two competing pathways for *self-splicing* by group II introns: a quantitative analysis of *in vitro* reactions rates and products. *Journal of Molecular Biology* 256(256):19.

48. de Boer HA, Comstock LJ and Vasser M (1983) The tac promoter: a functional hybrid derived from the trp and lac promoters. *Proc Natl Acad Sci U S A* 80(1):21-25.

49. de Lencastre A, Hamill S and Pyle A (2005) A single active-site region for a groupo II intron. *Nature structural & molecular biology* 12(7):2.

50. de Lencastre A and Pyle AM (2008) Three essential and conserved regions of the group II intron are proximal to the 5'-splice site. *RNA* 14(1):11-24.

51. Dib-Hajj SD, Boulanger SC, Hebbar SK, Peebles CL, Franzen JS and Perlman PS (1993) Domain 5 interacts with domain 6 and influences the second transesterification reaction of group II intron self-splicing. *Nucleic Acids Res* 21(8):1797-1804.

52. Ditta G, Stanfield S, Corbin D and Helinski DR (1980) Broad host range DNA cloning system for gram-negative bacteria: construction of a gene bank of Rhizobium meliloti. *Proc Natl Acad Sci U S A* 77(12):7347-7351.

53. Domdey H, Apostol B, Lin RJ, Newman A, Brody E and Abelson J (1984) Lariat structures are in vivo intermediates in yeast pre-mRNA splicing. *Cell* 39(3 Pt 2):611-621.

54. Dunny GM and McKay LL (1999) Group II introns and expression of conjugative transfer functions in lactic acid bacteria. *Antonie Van Leeuwenhoek* 76(1-4):77-88.

55. Edgell DR, Belfort M and Shub DA (2000) Barriers to intron promiscuity in bacteria. *J Bacteriol* 182(19):5281-5289.

56. Eickbush TH (1999) Mobile introns: retrohoming by complete reverse splicing. *Curr Biol* 9(1):R11-14.

57. Engler MJ and Richardson CC (1983) Bacteriophage T7 DNA replication. Synthesis of lagging strands in a reconstituted system using purified proteins. *J Biol Chem* 258(18):11197-11205.

58. Erat MC, Zerbe O, Fox T and Sigel RK (2007) Solution structure of domain 6 from a self-splicing group II intron ribozyme: a Mg(2+) binding site is located close to the stacked branch adenosine. *Chembiochem* 8(3):306-314.

59. Fedorova O, Su LJ and Pyle AM (2002) Group II introns: highly specific endonucleases with modular structures and diverse catalytic functions. *Methods* 28(3):323-335.

60. Fedorova O and Pyle AM (2005) Linking the group II intron catalytic domains: tertiary contacts and structural features of domain 3. *EMBO J* 24(22):3906-3916.

61. Fedorova O, Waldsich C and Pyle AM (2007) Group II intron folding under near-physiological conditions: collapsing to the near-native state. *J Mol Biol* 366(4):1099-1114.

62. Fedorova O and Zingler N (2007) Group II introns: structure, folding and splicing mechanism. *Biol Chem* 388(7):665-678.

63. Fedorova O and Pyle AM (2008) A conserved element that stabilizes the group II intron active site. *RNA* 14(6):1048-1056.

64. Fedorova O, Solem A and Pyle AM (2010) Protein-facilitated folding of group II intron ribozymes. *J Mol Biol* 397(3):799-813.

65. Ferat JL and Michel F (1993) Group II self-splicing introns in bacteria. *Nature* 364(6435):358-361.

66. Ferat JL, Le Gouar M and Michel F (2003) A group II intron has invaded the genus Azotobacter and is inserted within the termination codon of the essential groEL gene. *Mol Microbiol* 49(5):1407-1423.

67. Fernandez-Lopez M, Munoz-Adelantado E, Gillis M, Willems A and Toro N (2005) Dispersal and evolution of the Sinorhizobium meliloti group II RmInt1 intron in bacteria that interact with plants. *Mol Biol Evol* 22(6):1518-1528.

68. Fersht A (1985) *Enzyme structure and mechanism* (W.H. Freeman, New York) 2nd Ed pp xxi, 475 p.

69. Figurski DH and Helinski DR (1979) Replication of an origin-containing derivative of plasmid RK2 dependent on a plasmid function provided in trans. *Proc Natl Acad Sci U S A* 76(4):1648-1652.

70. Garcia-Rodriguez FM, Barrientos-Duran A, Diaz-Prado V, Fernandez-Lopez M and Toro N (2011) Use of RmInt1, a group IIB intron lacking the intron-encoded protein endonuclease domain, in gene targeting. *Appl Environ Microbiol* 77(3):854-861.

71. Giacomini A, Corich V, Ollero FJ, Squartini A and Nuti MP (1992) Experimental conditions may affect reproducibility of the beta-galactosidase assay. *FEMS Microbiol Lett* 79(1-3):87-90.

72. Giacomini A, Ollero F, Squartini A and Nuti M (1994) Construction of multipurpose gene cartridges based on a novel synthetic promoter for high-level gene expression in Gram-negative bacteria. *Gene* 144:8.

73. Gordon PM, Sontheimer EJ and Piccirilli JA (2000) Metal ion catalysis during the exon-ligation step of nuclear pre-mRNA splicing: extending the parallels between the spliceosome and group II introns. *RNA* 6(2):199-205.

74. Gordon PM, Fong R and Piccirilli JA (2007) A second divalent metal ion in the group II intron reaction center. *Chemistry & Biology* 14:6.

75. Gu SQ, Cui X, Mou S, Mohr S, Yao J and Lambowitz AM (2010) Genetic identification of potential RNA-binding regions in a group II intron-encoded reverse transcriptase. *RNA* 16(4):732-747.

76. Guo H, Karberg M, Long M, Jones JP, 3rd, Sullenger B and Lambowitz AM (2000) Group II introns designed to insert into therapeutically relevant DNA target sites in human cells. *Science* 289(5478):452-457.

77. Halbreich A, Pajot P, Foucher M, Grandchamp C and Slonimski P (1980) A pathway of cytochrome b mRNA processing in yeast mitochondria: specific splicing steps and an intron-derived circular DNA. *Cell* 19(2):321-329.

78. Hamill S and Pyle AM (2006) The receptor for branch-site docking within a group II intron active site. *Mol Cell* 23(6):831-840.

79. Hebbar SK, Belcher SM and Perlman PS (1992) A maturase-encoding group IIA intron of yeast mitochondria self-splices in vitro. *Nucleic Acids Res* 20(7):1747-1754.

80. Hensgens LA, Arnberg AC, Roosendaal E, van der Horst G, van der Veen R, van Ommen GJ and Grivell LA (1983) Variation, transcription and circular RNAs of the mitochondrial gene for subunit I of cytochrome c oxidase. *J Mol Biol* 164(1):35-58.

81. Higuchi R, Krummel B and Saiki RK (1988) A general method of in vitro preparation and specific mutagenesis of DNA fragments: study of protein and DNA interactions. *Nucleic Acids Res* 16(15):7351-7367.

82. Higuchi R, Fockler C, Dollinger G and Watson R (1993) Kinetic PCR analysis: Real-Time Monitoring of DNA Amplifications Reactions. *Biotechnology* 11:5.

83. Hollander V and Kuck U (1999a) Group II intron splicing in Escherichia coli: phenotypes of cis-acting mutations resemble splicing defects observed in organelle RNA processing. *Nucleic Acids Res* 27(11):2339-2344.

84. Hollander V and Kuck U (1999b) Group II intron splicing in chloroplasts: identificationof mutations determining intron stability and fate of exon RNA. *Nucleic Acids Res* 27(11):2345-2353.

85. Hong SH, Jeong JS, Lee YJ, Jung HI, Cho KS, Kim CM, Kwon BS, Sullenger BA, Lee SW and Kim IH (2008) In vivo reprogramming of hTERT by trans-splicing ribozyme to target tumor cells. *Mol Ther* 16(1):74-80.

86. Ichiyanagi K, Beauregard A, Lawrence S, Smith D, Cousineau B and M B (2002) Retrotransposition of the Ll.ltrB group II intron proceeds predominantly via *reverse splicing* into DNA targets. *Molecular Microbiology* 46(5):14.

87. Ish-Horowicz D and Burke JF (1981) Rapid and efficient cosmid cloning. *Nucleic Acids Res* 9(13):2989-2998.

88. Jacquier A and Rosbash M (1986a) RNA splicing and intron turnover are greatly diminished by a mutant yeast branch point. *Proc Natl Acad Sci U S A* 83(16):5835-5839.

89. Jacquier A and Rosbash M (1986b) Efficient trans-splicing of a yeast mitochondrial RNA group II intron implicates a strong 5' exon-intron interaction. *Science* 234(4780):1099-1104.

90. Jacquier A and Michel F (1987) Multiple exon-binding sites in class II self-splicing introns. *Cell* 50(1):17-29.

91. Jacquier A and Michel F (1990) Base-pairing interactions involving the 5' and 3'-terminal nucleotides of group II self-splicing introns. *J Mol Biol* 213(3):437-447.

92. Jacquier A and Jacquesson-Breuleux N (1991) Splice site selection and role of the lariat in a group II intron. *J Mol Biol* 219(3):415-428.

93. Jarrell KA, Dietrich RC and Perlman PS (1988a) Group II intron domain 5 facilitates a trans-splicing reaction. *Mol Cell Biol* 8(6):2361-2366.

94. Jarrell KA, Peebles CL, Dietrich RC, Romiti SL and Perlman PS (1988b) Group II intron self-splicing. Alternative reaction conditions yield novel products. *J Biol Chem* 263(7):3432-3439.

95. Jiménez-Zurdo J, García-Rodríguez F, Barrientos-Durán A and Toro N (2003) DNA target site requirements for *homing in vivo* of a bacterial group II intron encoding a protein lacking the DNA endonuclease domain. *Journal of Molecular Biology* 326:11.

96. Karberg M, Guo H, Zhong J, Coon R, Perutka J and Lambowitz AM (2001) Group II introns as controllable gene targeting vectors for genetic manipulation of bacteria. *Nat Biotechnol* 19(12):1162-1167.

97. Keating KS, Toor N, Perlman PS and Pyle AM (2010) A structural analysis of the group II intron active site and implications for the spliceosome. *RNA* 16(1):1-9.

98. Kingsford C, Ayanbule K and Salzberg S (2007) Rapid, accurate, computational discovery of Rho-independent transcription terminators illuminates their relationship to DNA uptake. *Genome Biology* 8:12.

99. Klein JR and Dunny GM (2002) Bacterial group II introns and their association with mobile genetic elements. *Front Biosci* 7:d1843-1856.

100. Klein JR, Chen Y, Manias DA, Zhuo J, Zhou L, Peebles CL and Dunny GM (2004) A conjugation-based system for genetic analysis of group II intron splicing in Lactococcus lactis. *J Bacteriol* 186(7):1991-1998.

101. Koch JL, Boulanger SC, Dib-Hajj SD, Hebbar SK and Perlman PS (1992) Group II introns deleted for multiple substructures retain self-splicing activity. *Mol Cell Biol* 12(5):1950-1958.

102. Koonin EV (2009) Intron-dominated genomes of early ancestors of eukaryotes. *J Hered* 100(5):618-623.

103. Kovach ME, Phillips RW, Elzer PH, Roop RM, 2nd and Peterson KM (1994) pBBR1MCS: a broad-host-range cloning vector. *Biotechniques* 16(5):800-802.

104. Kovach ME, Elzer PH, Hill DS, Robertson GT, Farris MA, Roop RM, 2nd and Peterson KM (1995) Four new derivatives of the broad-host-range cloning vector pBBR1MCS, carrying different antibiotic-resistance cassettes. *Gene* 166(1):175-176.

105. Kwakman JH, Konings D, Pel HJ and Grivell LA (1989) Structure-function relationships in a self-splicing group II intron: a large part of domain II of the mitochondrial intron aI5 is not essential for self-splicing. *Nucleic Acids Res* 17(11):4205-4216.

106. Lambowitz A and Zimmerly S (2004) Mobile group II introns. *Annual Review of Genetics* 38:36.

107. Lambowitz AM, G M and Zimmerly CA (2005) Group II intron homing endonucleases: Ribonucleoprotein complexes with programmable target specifity. *Homing endonucleases and inteins,* Nucleic acids and molecular biology, ed Belfort M (Springer, Berlin ; New York), pp 121-145.

108. Lambowitz AM and Zimmerly S (2010) Group II Introns: Mobile Ribozymes that Invade DNA. *Cold Spring Harb Perspect Biol.*

109. Lee K, Zhan X, Gao J, Qiu J, Feng Y, Meganathan R, Cohen SN and Georgiou G (2003) RraA. a protein inhibitor of RNase E activity that globally modulates RNA abundance in E. coli. *Cell* 114(5):623-634.

110. Lehmann K and Schmidt U (2003) Group II introns: structure and catalytic versatility of large natural ribozymes *Critical reviews in biochemistry and molecular biology* 38(3):55.

111. Liebeg A, Mayer O and Waldsich C (2010) DEAD-box protein facilitated RNA folding in vivo. *RNA Biol* 7(6):803-811.

112. Livak KJ and Schmittgen TD (2001) Analysis of relative gene expression data using real-time quantitative PCR and the 2(-Delta Delta C(T)) Method. *Methods* 25(4):402-408.

113. Marangoni AG (2003) *Enzyme kinetics : a modern approach* (Wiley-Interscience, Hoboken, N.J.) pp xiv, 229 p.

114. Marcaida MJ, Munoz IG, Blanco FJ, Prieto J and Montoya G (2010) Homing endonucleases: from basics to therapeutic applications. *Cell Mol Life Sci* 67(5):727-748.

115. Marques S, Ramos JL and Timmis KN (1993) Analysis of the mRNA structure of the Pseudomonas putida TOL meta fission pathway operon around the transcription initiation point, the xylTE and the xylFJ regions. *Biochim Biophys Acta* 1216(2):227-236.

116. Martinez-Abarca F, Garcia-Rodriguez FM and Toro N (2000) Homing of a bacterial group II intron with an intron-encoded protein lacking a recognizable endonuclease domain. *Mol Microbiol* 35(6):1405-1412.

117. Martínez-Abarca F, Zekri S and Toro N (1998) Characterization and splicing *in vivo* of a *Sinorhizobium meliloti* group II intron associated with particular insertion sequences of the IS*630*-Tc1/IS*3* retroposon superfamily. *Molecular Microbiology* 28(6):12.

118. Martínez-Abarca F, García-Rodríguez F and Toro N (2000) Homing of a bacterial group II intron with an intron-encoded protein lacking a recognizable endonuclease domain. *Molecular Microbiology* 35(6):8.

119. Martínez-Abarca F and Toro N (2000) RecA-independent ectopic transposition *in vivo* of a bacterial group II intron. *Nucleis Acids Research* 28(21):6.

120. Martínez-Abarca F, Barrientos-Durán A, Fernández-López M and Toro N (2004) The RmInt1 group II intron has two different retrohomig pathways for mobility using predominantly the nascent lagging strand at DNA replication forks for priming. *Nucleis Acids Research* 32(9):9.

121. Martinez-Trujillo M, Sanchez-Trujillo A, Ceja V, Avila-Moreno F, Bermudez-Cruz RM, Court D and Montanez C (2010) Sequences required for transcription termination at the intrinsic lambdatI terminator. *Can J Microbiol* 56(2):168-177.

122. Mastroianni M, Watanabe K, White TB, Zhuang F, Vernon J, Matsuura M, Wallingford J and Lambowitz AM (2008) Group II intron-based gene targeting reactions in eukaryotes. *PLoS One* 3(9):e3121.

123. Matsuura M, Saldanha R, Ma H, Wank H, Yang J, Mohr G, Cavanagh S, Dunny GM, Belfort M and Lambowitz AM (1997) A bacterial group II intron encoding reverse transcriptase, maturase, and DNA endonuclease activities: biochemical demonstration of maturase activity and insertion of new genetic information within the intron. *Genes Dev* 11(21):2910-2924.

124. Matsuura M, Noah JW and Lambowitz AM (2001) Mechanism of maturase-promoted group II intron splicing. *EMBO J* 20(24):7259-7270.

125. Mercure S, Cousineau L, Montplaisir S, Belhumeur P and Lemay G (1997) Expression of a reporter gene interrupted by the Candida albicans group I intron is inhibited by base analogs. *Nucleic Acids Res* 25(2):431-437.

126. Michel F, Jacquier A and Dujon B (1982) Comparison of fungal mitochondrial introns reveals extensive homologies in RNA secondary structure. *Biochimie* 64(10):867-881.

127. Michel F, Umesono K and Ozeki H (1989) Comparative and funciotinal anatomy of group II catalytic introns - a review. *Gene* 82:26.

128. Michel F and Ferat JL (1995) Structure and activities of group II introns. *Annu Rev Biochem* 64:435-461.

129. Michel F, Costa M and Westhof E (2009) The ribozyme core of group II introns: a structure in want of partners. *Trends Biochem Sci* 34(4):189-199.

130. Mikheeva S, Murray H, Zhou H, Turczyk B and Jarrel K (2000) Deletion of a conserved dinucleotide inhibits the second step of a group II intron *splicing. RNA* 6:7.

131. Miller JH (1972) *Experiments in molecular genetics* (Cold Spring Harbor Laboratory, Cold Spring Harbor, N.Y.) pp xvi, 466 p.

132. Mills DA, McKay LL and Dunny GM (1996) Splicing of a group II intron involved in the conjugative transfer of pRS01 in lactococci. *J Bacteriol* 178(12):3531-3538.

133. Mohr G, Smith D, Belfort M and Lambowitz AM (2000) Rules for DNA target-site recognition by a lactococcal group II intron enable retargeting of the intron to specific DNA sequences. *Genes Dev* 14(5):559-573.

134. Molina-Sánchez M, Martínez-Abarca F and Toro N (2006) Excision of the *Sinorhizobium meliloti* Group II Intron RmInt1 as Circles *in Vivo. The Journal of Biological Chemistry* 281(39):8.

135. Molina-Sanchez MD, Martinez-Abarca F and Toro N (2010) Structural features in the C-terminal region of the Sinorhizobium meliloti RmInt1 group II intron-encoded protein contribute to its maturase and intron DNA-insertion function. *FEBS J* 277(1):244-254.

136. Molina Sanchez MD, Barrientos-Duran A and Toro N (2011) Relevance of the branch point adenosine, coordination loop and 3' exon binding site for in vivo excision of the Sinorhizobium meliloti group II intron RmInt1. *J Biol Chem*.

137. Morl M and Schmelzer C (1990) Integration of group II intron bI1 into a foreign RNA by reversal of the self-splicing reaction in vitro. *Cell* 60(4):629-636.

138. Müller M, Stocker P, Hetzer M and Schweyen R (1991) Fate of the function phosphate in alternating forward and reverse self-splicing reactions of group II intron RNA. *Journal of Molecular Biology* 122:10.

139. Mullineux ST, Costa M, Bassi GS, Michel F and Hausner G (2010) A group II intron encodes a functional LAGLIDADG homing endonuclease and self-splices under moderate temperature and ionic conditions. *RNA* 16(9):1818-1831.

140. Muñoz-Adelantado E, Villadas P and Toro N (2001) Ectopic transposition of a group II intron in natural bacterial populations. *Molecular Microbiology* 41(3):8.

141. Muñoz-Adelantado E, San Filippo J, Martínez-Abarca F, García-Rodríguez F, Lambowitz A and Toro N (2003) Mobility of the *Sinorhizobium meliloti* group II intron RmInt1 occurs by reverse splicing into DNA, but requires an unknown reverse transcriptase priming mechanism. *Journal of Molecular Biology* 327:23.

142. Murray H, Mikheeva S, Coljee V, Turczyk B, Donahue W, Bar-Shalom A and Jarrel K (2001) Excision of Group II Introns as Circles. *Molecular Cell* 8:11.

143. Nisa-Martínez R, Jiménez-Zurdo J, Martínez-Abarca F, Muñoz-Adelantado E and Toro N (2007) Dispersion of the RmInt1 group II in the *Sinorhizobium meliloti* genome upon acquisition by conjugative transfer. *Nucleis Acids Research* 35(1):9.

144. Noah JW and Lambowitz AM (2003) Effects of maturase binding and Mg2+ concentration on group II intron RNA folding investigated by UV cross-linking. *Biochemistry* 42(43):12466-12480.

145. Nolte A, Chanfreau G and Jacquier A (1998) Influence of substrate structure on in vitro ribozyme activity of a group II intron. *RNA* 4(6):694-708.

146. Nudler E and Gottesman ME (2002) Transcription termination and anti-termination in E. coli. *Genes Cells* 7(8):755-768.

147. Ostersetzer O, Cooke AM, Watkins KP and Barkan A (2005) CRS1, a chloroplast group II intron splicing factor, promotes intron folding through specific interactions with two intron domains. *Plant Cell* 17(1):241-255.

148. Peebles CL, Perlman PS, Mecklenburg KL, Petrillo ML, Tabor JH, Jarrell KA and Cheng HL (1986) A self-splicing RNA excises an intron lariat. *Cell* 44(2):213-223.

149. Peebles CL, Belcher SM, Zhang M, Dietrich RC and Perlman PS (1993) Mutation of the conserved first nucleotide of a group II intron from yeast mitochondrial DNA reduces the rate but allows accurate splicing. *J Biol Chem* 268(16):11929-11938.

150. Peebles CL, Zhang M, Perlman PS and Franzen JS (1995) Catalytically critical nucleotide in domain 5 of a group II intron. *Proc Natl Acad Sci U S A* 92(10):4422-4426.

151. Podar M, Chu VT, Pyle AM and Perlman PS (1998a) Group II intron splicing in vivo by first-step hydrolysis. *Nature* 391(6670):915-918.

152. Podar M, Zhuo J, Zhang M, Franzen JS, Perlman PS and Peebles CL (1998b) Domain 5 binds near a highly conserved dinucleotide in the joiner linking domains 2 and 3 of a group II intron. *RNA* 4(2):151-166.

153. Pyle AM and Green JB (1994) Building a kinetic framework for group II intron ribozyme activity: quantitation of interdomain binding and reaction rate. *Biochemistry* 33(9):2716-2725.

154. Pyle AM, Chu VT, Jankowsky E and Boudvillain M (2000) Using DNAzymes to cut, process, and map RNA molecules for structural studies or modification. *Methods Enzymol* 317:140-146.

155. Pyle AM (2002) Metal ions in the structure and function of RNA. *J Biol Inorg Chem* 7(7-8):679-690.

156. Pyle AM and Lambowitz AM (2006) Group II introns: Ribozymes that splice RNA and invade DNA. *The RNA world : the nature of modern RNA suggests a prebiotic RNA world*, eds Gesteland RF, Cech TR, & Atkins JF (Cold Spring Harbor Laboratory Press, Cold Spring Harbor, NY), 3rd ed. Ed, pp 469-506.

157. Pyle AM, Fedorova O and Waldsich C (2007) Folding of group II introns: a model system for large, multidomain RNAs? *Trends Biochem Sci* 32(3):138-145.

158. Pyle AM (2008) Group II introns: catalyisis for splicing, genomic change and evolution. *Ribozymes and RNA catalysis*, eds Lilley DMJ &Eckstein F (RSC Publishing, Cambridge), pp 201-223.

159. Pyle AM (2010) The tertiary structure of group II introns: implications for biological function and evolution. *Crit Rev Biochem Mol Biol* 45(3):215-232.

160. Qin PZ and Pyle AM (1998) The architectural organization and mechanistic function of group II intron structural elements. *Curr Opin Struct Biol* 8(3):301-308.

161. Rambo RP and Doudna JA (2004) Assembly of an active group II intron-maturase complex by protein dimerization. *Biochemistry* 43(21):6486-6497.

162. Rawsthorne H, Turner KN and Mills DA (2006) Multicopy integration of heterologous genes, using the lactococcal group II intron targeted to bacterial insertion sequences. *Appl Environ Microbiol* 72(9):6088-6093.

163. Robart AR, Montgomery NK, Smith KL and Zimmerly S (2004) Principles of 3' splice site selection and alternative splicing for an unusual group II intron from Bacillus anthracis. *RNA* 10(5):854-862.

164. Robart AR and Zimmerly S (2005) Group II intron retroelements: function and diversity. *Cytogenet Genome Res* 110(1-4):589-597.

165. Roberts AP, Braun V, von Eichel-Streiber C and Mullany P (2001) Demonstration that the group II intron from the Clostridial Conjugative transposon Tn5397 undergoes splicing In vivo. *J Bacteriol* 183(4):1296-1299.

166. Roitzsch M and Pyle AM (2009) The linear form of a group II intron catalyzes efficient autocatalytic reverse splicing, establishing a potential for mobility. *RNA* 15(3):473-482.

167. Rosenberg M and Court D (1979) Regulatory sequences involved in the promotion and termination of RNA transcription. *Annu Rev Genet* 13:319-353.

168. Rozen S and Skaletsky H (2000) Primer3 on the WWW for general users and for biologist programmers. *Methods Mol Biol* 132:365-386.

169. Russell R (2008) RNA misfolding and the action of chaperones. *Front Biosci* 13:1-20.

170. Saldanha R, Chen B, Wank H, Matsuura M, Edwards J and Lambowitz AM (1999) RNA and protein catalysis in group II intron splicing and mobility reactions using purified components. *Biochemistry* 38(28):9069-9083.

171. Sambrook J, Fritsch EF and Maniatis T (1989) *Molecular cloning : a laboratory manual* (Cold Spring Harbor Laboratory, Cold Spring Harbor, N.Y.) 2nd ed. Ed.

172. San Filippo J and Lambowitz AM (2002) Characterization of the C-terminal DNA-binding/DNA endonuclease region of a group II intron-encoded protein. *J Mol Biol* 324(5):933-951.

173. Santoro SW and Joyce GF (1997) A general purpose RNA-cleaving DNA enzyme. *Proc Natl Acad Sci U S A* 94(9):4262-4266.

174. Scharf SJ, Horn GT and Erlich HA (1986) Direct cloning and sequence analysis of enzymatically amplified genomic sequences. *Science* 233(4768):1076-1078.

175. Schmelzer C and Schweyen RJ (1986) Self-splicing of group II introns in vitro: mapping of the branch point and mutational inhibition of lariat formation. *Cell* 46(4):557-565.

176. Schmidt U, Riederer B, Morl M, Schmelzer C and Stahl U (1990) Self-splicing of the mobile group II intron of the filamentous fungus Podospora anserina (COI I1) in vitro. *EMBO J* 9(7):2289-2298.

177. Schmidt U, Sagebarth R, Schmelzer C and Stahl U (1993) Self-splicing of a Podospora anserina group IIA intron in vitro. Effects of 3'-terminal intron alterations on cleavage at the 5' and 3' splice site. *J Mol Biol* 231(3):559-568.

178. Schmidt U, Podar M, Stahl U and Perlman PS (1996) Mutations of the two-nucleotide bulge of D5 of a group II intron block splicing in vitro and in vivo: phenotypes and suppressor mutations. *RNA* 2(11):1161-1172.

179. Sharp PA (1985) On the origin of RNA splicing and introns. *Cell* 42(2):397-400.

180. Sharp PA (1991) "Five easy pieces". *Science* 254(5032):663.

181. Shearman C, Godon JJ and Gasson M (1996) Splicing of a group II intron in a functional transfer gene of Lactococcus lactis. *Mol Microbiol* 21(1):45-53.

182. Sigel RK, Vaidya A and Pyle AM (2000) Metal ion binding sites in a group II intron core. *Nat Struct Biol* 7(12):1111-1116.

183. Sigel RK, Sashital DG, Abramovitz DL, Palmer AG, Butcher SE and Pyle AM (2004) Solution structure of domain 5 of a group II intron ribozyme reveals a new RNA motif. *Nat Struct Mol Biol* 11(2):187-192.

184. Silverman SK (2005) In vitro selection, characterization, and application of deoxyribozymes that cleave RNA. *Nucleic Acids Res* 33(19):6151-6163.

185. Simon DM, Kelchner SA and Zimmerly S (2009) A broadscale phylogenetic analysis of group II intron RNAs and intron-encoded reverse transcriptases. *Mol Biol Evol* 26(12):2795-2808.

186. Singh RN, Saldanha RJ, D'Souza LM and Lambowitz AM (2002) Binding of a group II intron-encoded reverse transcriptase/maturase to its high affinity intron RNA binding site involves sequence-specific recognition and autoregulates translation. *J Mol Biol* 318(2):287-303.

187. Smith D, Zhong J, Matsuura M, Lambowitz AM and Belfort M (2005) Recruitment of host functions suggests a repair pathway for late steps in group II intron retrohoming. *Genes Dev* 19(20):2477-2487.

188. Solem A, Zingler N, Pyle AM and Li-Pook-Than J (2009) Group II introns and their protein collaborators. *Non-protein coding RNAs*, eds Walter NG, Woodson SA, & Batey RT (Springer, Berlin), pp 167-182.

189. Southern EM (1975) Detection of specific sequences among DNA fragments separated by gel electrophoresis. *J Mol Biol* 98(3):503-517.

190. Southern EM (1979) Analysis of restriction-fragment patterns from complex deoxyribonucleic acid species. *Biochem Soc Symp* 44:37-41.

191. Spaink H, Okker R, Wijffelman C, Pees E and Lugtenberg B (1987) Promoters in the nodulation region of the *Rhizobium leguminosarum* Sym plasmid pRL1JI. *Plant Molecular Biology* 9:13.

192. Stabell FB, Tourasse NJ and Kolsto AB (2009) A conserved 3' extension in unusual group II introns is important for efficient second-step splicing. *Nucleic Acids Res* 37(10):3202-3214.

193. Stern DB, Goldschmidt-Clermont M and Hanson MR (2010) Chloroplast RNA metabolism. *Annu Rev Plant Biol* 61:125-155.

194. Studier FW (1991) Use of bacteriophage T7 lysozyme to improve an inducible T7 expression system. *J Mol Biol* 219(1):37-44.

195. Su LJ, Qin PZ, Michels WJ and Pyle AM (2001) Guiding ribozyme cleavage through motif recognition: the mechanism of cleavage site selection by a group ii intron ribozyme. *J Mol Biol* 306(4):655-668.

196. Su LJ, Waldsich C and Pyle AM (2005) An obligate intermediate along the slow folding pathway of a group II intron ribozyme. *Nucleic Acids Res* 33(21):6674-6687.

197. Swisher JF, Su LJ, Brenowitz M, Anderson VE and Pyle AM (2002) Productive folding to the native state by a group II intron ribozyme. *J Mol Biol* 315(3):297-310.

198. Toor N, Hausner G and Zimmerly S (2001) Coevolution of group II intron RNA structures with their intron-encoded reverse transcriptases. *RNA* 7(8):1142-1152.

199. Toor N and Zimmerly S (2002) Identification of a family of group II introns encoding LAGLIDADG ORFs typical of group I introns. *RNA* 8(11):1373-1377.

200. Toor N, Robart AR, Christianson J and Zimmerly S (2006) Self-splicing of a group IIC intron: 5' exon recognition and alternative 5' splicing events implicate the stem-loop motif of a transcriptional terminator. *Nucleic Acids Res* 34(22):6461-6471.

201. Toor N, Keating K, Taylor S and Pyle A (2008a) Crystal structure of a self-spliced group II intron. *Science* 320:6.

202. Toor N, Rajashankar K, Keating K and Pyle A (2008b) Structural basis for exon recognition by a group II intron. *Nature structural & molecular biology*:2.

203. Toor N, Rajashankar K, Keating KS and Pyle AM (2008c) Structural basis for exon recognition by a group II intron. *Nat Struct Mol Biol* 15(11):1221-1222.

204. Toor N, Keating KS and Pyle AM (2009) Structural insights into RNA splicing. *Curr Opin Struct Biol* 19(3):260-266.

205. Toor N, Keating KS, Fedorova O, Rajashankar K, Wang J and Pyle AM (2010) Tertiary architecture of the Oceanobacillus iheyensis group II intron. *RNA* 16(1):57-69.

206. Toro N, Jiménez-Zurdo J and García-Rodríguez F (2007) Bacterial group II introns: not just splicing. *FEMS Microbiol Rev* 31:17.

207. van der Veen R, Arnberg AC, van der Horst G, Bonen L, Tabak HF and Grivell LA (1986) Excised group II introns in yeast mitochondria are lariats and can be formed by self-splicing in vitro. *Cell* 44(2):225-234.

208. van der Veen R, Kwakman JH and Grivell LA (1987) Mutations at the lariat acceptor site allow self-splicing of a group II intron without lariat formation. *EMBO J* 6(12):3827-3831.

209. Vogel J and Borner T (2002) Lariat formation and a hydrolytic pathway in plant chloroplast group II intron splicing. *EMBO J* 21(14):3794-3803.

210. Waldsich C and Pyle AM (2008) A kinetic intermediate that regulates proper folding of a group II intron RNA. *J Mol Biol* 375(2):572-580.

211. Wank H, SanFilippo J, Singh RN, Matsuura M and Lambowitz AM (1999) A reverse transcriptase/maturase promotes splicing by binding at its own coding segment in a group II intron RNA. *Mol Cell* 4(2):239-250.

212. Wartell RM and Reznikoff WS (1980) Cloning DNA restriction endonuclease fragments with protruding single-stranded ends. *Gene* 9(3-4):307-319.

213. Watanabe K and Lambowitz AM (2004) High-affinity binding site for a group II intron-encoded reverse transcriptase/maturase within a stem-loop structure in the intron RNA. *RNA* 10(9):1433-1443.

214. Yao J, Zhong J, Fang Y, Geisinger E, Novick RP and Lambowitz AM (2006) Use of targetrons to disrupt essential and nonessential genes in Staphylococcus aureus reveals temperature sensitivity of Ll.LtrB group II intron splicing. *RNA* 12(7):1271-1281.

215. Zhang L and Doudna JA (2002) Structural insights into group II intron catalysis and branch-site selection. *Science* 295(5562):2084-2088.

216. Zhong J, Karberg M and Lambowitz AM (2003) Targeted and random bacterial gene disruption using a group II intron (targetron) vector containing a retrotransposition-activated selectable marker. *Nucleic Acids Res* 31(6):1656-1664.

217. Zhou L, Manias DA and Dunny GM (2000) Regulation of intron function: efficient splicing in vivo of a bacterial group II intron requires a functional promoter within the intron. *Mol Microbiol* 37(3):639-651.

218. Zhuang F, Karberg M, Perutka J and Lambowitz AM (2009a) EcI5, a group IIB intron with high retrohoming frequency: DNA target site recognition and use in gene targeting. *RNA* 15(3):432-449.

219. Zhuang F, Mastroianni M, White TB and Lambowitz AM (2009b) Linear group II intron RNAs can retrohome in eukaryotes and may use nonhomologous end-joining for cDNA ligation. *Proc Natl Acad Sci U S A* 106(43):18189-18194.

220. Zingler N, Solem A and Pyle AM (2010) Dual roles for the Mss116 cofactor during splicing of the ai5gamma group II intron. *Nucleic Acids Res* 38(19):6602-6609.

221. Zuker M (2003) Mfold web server for nucleic acid folding and hybridization prediction. *Nucleic Acids Res* 31(13):3406-3415.